Arborescent Polypeptides for Sustained Drug Delivery Applications

by

Mosa Alsehli

A thesis
presented to the University of Waterloo
in fulfillment of the
thesis requirement for the degree of
Doctor of Philosophy
in
Chemistry

Waterloo, Ontario, Canada, 2017

Examining Committee Membership

The following individuals served on the Examining Committee for this thesis. The decision of the Examining Committee is by majority vote.

External Examiner	Elizabeth Gillies Professor
Supervisor(s)	Mario Gauthier Professor
Internal Member	Jean Duhamel Professor
Internal-external Member	Michael Tam Professor
Other Member(s)	Xiaosong Wang Associate Professor

Author's Declaration

I hereby declare that I am the sole author of this thesis. This is a true copy of the thesis, including any required final revisions, as accepted by my examiners.

I understand that my thesis may be made electronically available to the public.

Abstract

This Ph.D. dissertation describes the synthesis of arborescent copolymers of generations G1 and G2 designed to serve as drug delivery nanocarriers for cancer treatment. Poly(γ-benzyl L-glutamate) (PBG) building blocks were generated by ring-opening polymerization of γ-benzyl L-glutamic acid *N*-carboxyanhydride (Glu-NCA) initiated with *n*-hexylamine. Partial or full deprotection of the benzyl ester groups followed by coupling with PBG chains yielded a comb-branched (arborescent polymer generation zero or G0) PBG structure. Additional cycles of deprotection and grafting yielded G1 and G2 arborescent polypeptides. Optimization of the arborescent PBG synthesis was carried out in terms of the reaction temperature, solvent composition, reaction time, and mole ratio of reactants and coupling agents. Side chains of poly(ethylene oxide) (PEO) were then grafted either randomly or at the chain ends of the arborescent PBG substrates to produce amphiphilic arborescent copolymers denoted as PBG-*g*-PEO and PBG-*eg*-PEO, respectively.

The branching density of the G0PBG substrates was controlled by varying the length and the deprotection level of the linear PBG substrates used in their synthesis. Three G0PBG cores with branching densities varying from a compact and dense to a loose and porous structure were thus synthesized. The arborescent PBG-*g*-PEO amphiphilic copolymers formed mostly unimolecular micelles with small amounts of aggregation in aqueous media, whereas arborescent PBG-*eg*-PEO were completely devoid of aggregation. The hydrodynamic diameter of the copolymers varied from 13 to 39 nm, depending on their generation number and the branching density of the G0PBG cores.

The ability of these unimolecular micelles to encapsulate and release doxorubicin (DOX), an anticancer drug, was correlated with their generation number and the branching density of the hydrophobic cores. Both the drug loading content (DLC) and the drug loading efficiency (DLE) increased with the generation number of the copolymers as a result of increasing the PBG content in the micelles. For each generation, slightly higher values of DLE and DLC were observed for micelles with a denser core structure. The release profiles indicated that the drug release rate could be modulated by the generation number of the copolymers or by controlling the branching density, and thereby the porosity of the cores: Micelles with more densely branched cores decreased the diffusion rate of the drug. Three different strategies were examined to load DOX into G1PBG-*eg*-PEO and G2PBG-*eg*-PEO. The DOX was either physically entrapped (PBG-*eg*-PEO/DOX), loaded via electrostatic interactions (PGA-*eg*-PEO-DOX), or covalently conjugated to the unimolecular micelles via a pH-sensitive hydrazone bond (PGA-*eg*-PEO-Hyd-DOX). While all these systems had a good drug loading capacity, encapsulation via electrostatic interactions yielded the highest DLC and DLE. All these systems exhibited sustained and pH-responsive drug release behavior, with slower release at physiological pH (7.4) than at pH 5.5, but PGA-*eg*-PEO-Hyd-DOX had the best overall pH-responsive release behavior. The versatile encapsulation and release properties of these unimolecular micelles show that they could be useful as nanocarriers for a broad range of drug release applications.

Acknowledgements

I deeply appreciate and acknowledge the help of my supervisor, Professor Mario Gauthier, for his expert guidance, constant encouragement and support throughout my Ph.D. research.

I would like to thank my supervisory committee members: Professor Jean Duhamel, Professor Michael K.C. Tam, and Professor Xiaosong Wang, for their time and valuable suggestions throughout the course of the program.

I would also like to take the opportunity to thank Dr. Greg Whitton for the guidance which he provided at the beginning of this project, and Aklilu Worku for his help with the AFM and TEM work.

In addition, I would like to thank my coworkers at the University of Waterloo for their friendship and useful discussions: Ala Alturk, Yahya Alzahrany, Ryan Amos, Daisuke Aoki, Dr. Toufic Aridi, Paul Dymond, Joanne Fernandez, Victoria Hisko, Dr. Eda Güngör, Dr. Hemali Lad, Dr. Ilias Mahmud, Dr. Firmin Moingeon, Mehdi Neqal, Dr. Olivier Nguon, Dr. An Nguyen, Dr. Deepak Vishnu, Liying Wang, and all other past and current coworkers from the Gauthier and Duhamel laboratories.

I am at total loss of words in expressing the depth of my emotion to my family for their love, support, and confidence they always give me. My special thanks go to my wife Ashwaq Alsehli for her love, patience and colossal support.

Last but not least, I would like to acknowledge the financial support of Taibah University, Saudi Arabia, and the Natural Science and Engineering Research Council of Canada (NSERC) for this work.

Dedication

I dedicate this work to my loving mother and late father for their unconditional love, support, and encouragement.

"The first essential in chemistry is that thou shouldest perform practical work and conduct experiments, for he who performs not practical work nor makes experiments will never attain to the least degree of mastery."

Jabir Ibn Hayyan (721-815 A.D.)

Table of Contents

List of Figures

List of Tables

List of Schemes

List of Abbreviations and Symbols

2VP	2-Vinylpyridine
10HCPT	10-Hydroxycamptothecin
AA	α-Amino acid
AFM	Atomic force microscopy
AM	Activated monomer
ATRP	Atom transfer radical polymerization
b	Block
BBEMA	2-(2-Bromoisobutyryloxy)ethyl methacrylate
BEMA	2-Bromoethyl methacrylate
b.p.	Boiling point
BPLP	Photoluminescent polymer
Bz	Benzyl
Bz-Glu	γ-Benzyl L-glutamic acid
C_e	Coupling efficiency
CMC	Critical micelle concentration
CMM	Couple-monomer methodology
CPT	Camptothecin
D	Dendritic branching units
d	Deuterated
DB	Degree of branching
DBCO	Dibenzocyclooctyne
DCC	*N*,*N*'-Dicyclohexylcarbodiimide
DCM	Dichloromethane
DDS	Drug delivery system
DHBA	3,5-Dihydroxybenzyl alcohol
DIC	*N*,*N*'-Diisopropylcarbodiimide
DLC	Drug loading content
DLE	Drug loading efficiency
DLS	Dynamic light scattering
DMA	*N*,*N*-Dimethylacetamide
DMF	*N*,*N*-Dimethylformamide
DMM	Double-monomer methodology
DMSO	Dimethyl sulfoxide
dn/dc	Refractive index increment
DOX	Doxorubicin

DOX·HCl	Doxorubicin hydrochloride
DPE	1,1-Diphenylethylene
DPMK	Diphenylmethylpotassium
DRI	Differential refractometer index
DVB	Divinylbenzene
eg	Chain end-grafted
EDC·HCl	1-Ethyl-3-(3-dimethylaminopropyl)carbodiimide hydrochloride
EO	Ethylene oxide
EtOAc	Ethyl acetate
EPR	Enhanced permeability and retention effect
eq	Equivalent
FA	Folic acid
FDA	Food and Drug Administration
f_n	Number-average branching functionality
f_{NH2}	Primary amine functionality level
FPT	Freeze-pump-thaw
f_{tBu}	Mole fraction of *tert*-butyl ester protecting groups
G	Generation
g	Graft
Glu-NCA	γ-Benzyl L-glutamic acid *N*-carboxyanhydride
$(OtBu)_2$-PBG	$Glu(OtBu)_2$-terminated poly(γ-benzyl L-glutamate)
G_y	Grafting yield
h	Hour(s)
HA	Hexyl acrylate
HBMI	Hyperbranched macroinitiator
HBr	Hydrogen bromide
HCl	Hydrogen chloride or hydrochloric acid
HF	Hydrofluoric acid
HOAt	1-Hydroxy-7-azabenzotriazole
HOBt	1-Hydroxybenzotriazole
HPAH	Polyacylhydrazone
HVT	High-vacuum technique
HYPAM	Hyperbranched PAMAM
IR	Infrared
L	Linear chain segment
LiCl	Lithium chloride
$LiAlH_4$	Lithium aluminum hydride

KNaph	Potassium naphthalene
MALDI	Matrix-assisted laser desorption ionization
MALLS	Multi-angle laser light scattering
M_0	Number-average molecular weight of the primary chains
M/I	Monomer to initiator molar concentration ratio
MG	Number-average molecular weight of graft polymer
M_n	Number-average molecular weight
MP	6-Mercaptopurine
MPS	Mononuclear phagocytic system
MTX	Methotrexate
MW	Molecular weight
M_w	Weight-average molecular weight
MWCO	Molecular weight cut-off
MWD	Molecular weight distribution
n	Refractive index
NCA	α-Amino acid *N*-carboxyanhydride
NMR	Nuclear magnetic resonance
P2VP	Poly(2-vinylpyridine)
PAH	Polycyclic aromatic hydrocarbon
PAMAM	Polyamidoamine
PB	Polybutadiene
PBG	Poly(γ-benzyl L-glutamate)
PBS	Phosphate-buffered saline
PDI	Polydispersity index
PEA	Poly(esteramine)
PEG	Poly(ethylene glycol)
PEGMA	poly(ethylene glycol) methacrylate
PEHAM	Poly(etherhydroxylamine)
PEI	Polyethyleneimine
PEO	Poly(ethylene oxide)
PGA	Poly(L-glutamic acid)
PGly	Polyglycidol
PGlyAc	Poly(glycidol acetal)
PHEA	Poly(2-hydroxyethyl acrylate)
PhMgCl	Phenylmagnesium chloride
PLA	Poly(lactic acid)
PLGA	Poly(lactic-*co*-glycolic acid)

PMMA	Poly(methyl methacrylate)
PPLG	Poly(γ-propargyl L-glutamate)
PS	Polystyrene
PtBuGlu	Poly(γ-*tert*-butyl L-glutamate)
PTP	Proton transfer polymerization
RAFT	Reversible addition-fragmentation chain transfer copolymerization
RBF	Round-bottomed flask
ROMBP	Ring-opening multi-branching polymerization
ROP	Ring-opening polymerization
SANS	Small-angle neutron scattering
SCROP	Self-condensing ring-opening polymerization
SCVP	Self-condensing vinyl polymerization
SEC	Size exclusion chromatography
SMM	Single-monomer methodology
sec-BuLi	*sec*-Butyllithium
T	Terminal branching units
tBu	*tert*-Butyl
tBuGlu	γ-*tert*-Butyl L-glutamic acid
TEA	Triethylamine
TEM	Transmission electron microscopy
TFA	Trifluoroacetic acid
TFBA	4-Trifluoromethylbenzaldehyde
THF	Tetrahydrofuran
TBBPE	1,1,1-*tris*(4-(2-Bromoisobutyryloxy)phenyl)ethane
UV	Ultraviolet
WHO	World Health Organization
X	Degree of polymerization
X_n	Number-average degree of polymerization
Z	Number of surface groups

Chapter 1 **Foreword**

1.1 Opening Remarks

Dendritic polymers are a unique and versatile type of macromolecules characterized by a highly branched tree-like architecture, incorporating multiple branching levels, resulting from coupling reactions of either small molecule monomers (hyperbranched polymers and dendrimers), or macromolecular building blocks (dendrigraft polymers).[1] Amphiphilic dendritic polymers are particularly interesting because they can display micelle-like properties and provide excellent *in vivo* colloidal stability which makes them ideal for applications in drug delivery.[2] Dendrigraft polymers (referring collectively to arborescent and dendrimer-like star polymer structures) are the most recently reported subset of dendritic polymers.[3,4] Due to the vast array of architectures that can be obtained for these systems, dendrigraft polymers are an excellent alternative in the design of unimolecular micelles.[5-7] In contrast to the other dendritic polymers, high molecular weight polymers can be obtained for these systems in relatively few steps, while maintaining fairly narrow molecular weight distributions ($M_w/M_n < 1.1$).[1]

The encapsulation and release properties of arborescent copolymers were investigated using various polycyclic aromatic hydrocarbon probes as well as indomethacin and lidocaine as model drugs.[5,6] Unfortunately, the system used (based on polystyrene and poly(2-vinylpyridine) building blocks) lacked the biocompatibility necessary for biomedical applications. Biocompatible arborescent copolymers were recently synthesized and evaluated as unimolecular micelles,[7] but the ability of these copolymers to encapsulate and control the release of hydrophobic drugs has not yet been explored.

1.2 Research Objectives and Thesis Outline

The design of drug delivery nanocarriers that can encapsulate hydrophobic drug molecules efficiently, transport their cargo to specific target sites and release it in a sustained and controlled manner is of great interest for cancer chemotherapy. This Dissertation focuses on the synthesis and the micellar properties of two families of amphiphilic arborescent copolymers, namely arborescent poly(γ-benzyl L-glutamate) (PBG) substrates grafted either randomly or at the end of the PBG chain segments with poly(ethylene oxide) (PEO) chain segments (denoted PBG-*g*-PEO and PBG-*eg*-PEO, respectively). The main goals of the work were to study their aqueous solution behavior and to investigate the ability of these biocompatible copolymers to encapsulate and control the release rate of hydrophobic drugs in aqueous media. For each system, the influence of varying the generation number and the branching density of the core on micelle properties such as the drug loading capacity and the release kinetics was investigated. Three different strategies were used to load doxorubicin (DOX), an anticancer drug, into G1PBG-*eg*-PEO and G2PBG-*eg*-PEO. The DOX was either physically entrapped (PBG-*eg*-PEO/DOX), loaded via electrostatic interactions (PGA-*eg*-PEO-DOX), or covalently conjugated to the unimolecular micelles via a pH-sensitive hydrazone bond (PGA-*eg*-PEO-Hyd-DOX).

This dissertation is comprised in seven chapters. Following this Foreword, a literature review is presented (Chapter 2) that is divided into two sections: The first part reviews different families of polymeric micelles used as drug carriers including amphiphilic block copolymer micelles, unimolecular micelles and cross-linked micelles; the second part provides an overview of methods currently available for the synthesis, modification, and

drug delivery applications of dendritic polymers with various structures. Chapter 3 reports on the synthesis and the optimization of well-defined dendritic graft (arborescent) polypeptides from amine-terminated poly(γ-benzyl L-glutamate) (PBG) chains. The influence of reaction conditions such as the temperature, solvent, reaction time, and the mole ratio of reactants and coupling agents was investigated. The design and synthesis of biocompatible arborescent poly(γ-benzyl L-glutamate) (PBG) substrates *randomly grafted* with linear poly(ethylene oxide) (PEO) are discussed in Chapter 4, whereas the use of *chain end-grafted* PBG substrates is discussed in Chapter 5. In both Chapter 4 and Chapter 5, arborescent copolymers with PBG cores of generations G1 and G2, derived from G0PBG substrates with different branching densities, were examined as drug nanocarriers. The effects of the branching density on the micelle size, the drug loading capacity, the drug loading efficiency, and the drug release rate were investigated. Different strategies to load doxorubicin (DOX), an anticancer drug, into these unimolecular micelles are compared in Chapter 6. DOX was either physically entrapped, loaded via electrostatic interactions, or covalently conjugated to the unimolecular micelles via a pH-sensitive hydrazone bond. Chapter 7 provides overall concluding remarks drawn from the Thesis work, a summary of original contributions to knowledge, and suggestions for future work.

In agreement with the University of Waterloo Thesis guidelines, Chapters 2-6 are organized as individual manuscripts for publication in scientific journals. Included within each chapter are an abstract, an introductory section providing relevant background information on the subject matter, experimental methods, discussion of the results, and conclusions. An extended abstract for the whole Thesis is also provided in the preliminary

pages of this Dissertation, and a single list of references is given at the very end of the document, organized and numbered according to each individual chapter.

Chapter 2 Introduction:

Background and Literature

Review

2.1 Background: Cancer and Its Treatment

Cancer is a group of diseases characterized by the uncontrolled growth and spread of abnormal cells.[1] Cancer is usually caused by genetic changes (mutations) in cells. It is presently a major public health problem throughout the world in many forms including leukemia, myeloma, carcinoma, lymphoma and sarcoma, and is one of the leading causes of death. A recent report from the World Health Organization (WHO) stated that there were 14.1 million new cancer cases and 8.2 million cancer deaths in 2014.[2] With an increasing global population, the number of new cancer cases has also grown from 12.7 million in 2008 to 14.1 million in 2014. It is estimated by the World Health Organization that new cancer incidence will rise from 14.1 million in 2014 to 19 million by 2025, and to 24.4 million by 2035 as shown in Figure 2.1. As a result, much effort in research has focused on new cancer treatments over the past few years.

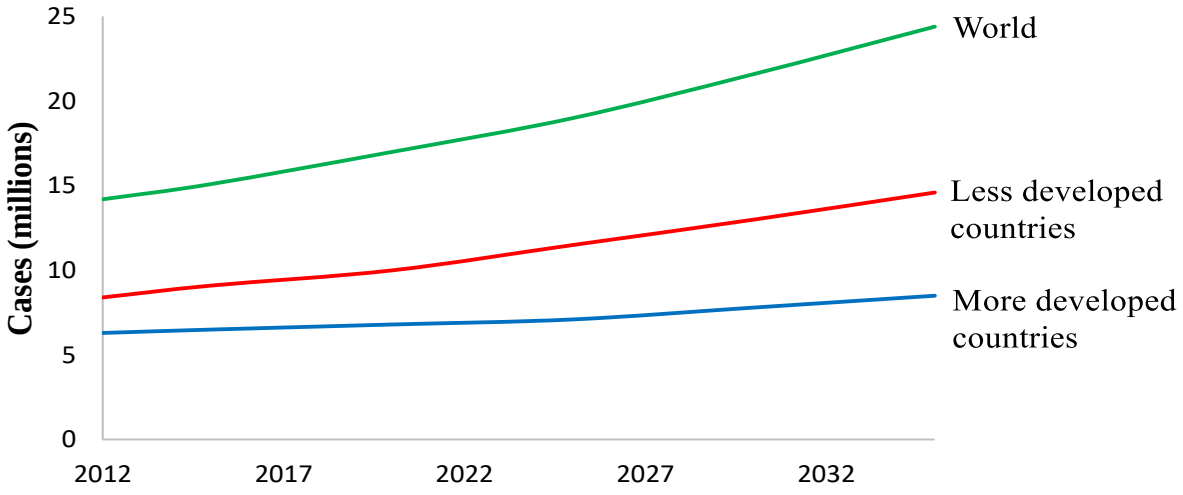

Source: WHO GloboCan

Figure 2.1. Estimated global cancer incidence, 2012-2035.[2]

Most cancers are treated by radiation therapy, surgery and/or chemotherapy.[1] Radiation therapy uses high energy electromagnetic waves to kill or damage cancer cells. It is one of the most common treatments for cancer, either by itself or along with other treatments. The radiation may come from outside the body or from radioactive materials inserted into the tumor. Surgery is the oldest known method and is often the first treatment option if the tumor can be removed from the body. Surgery can be used to diagnose or even help prevent cancer in some cases. Sometimes surgery may leave residual cancer cells that can change their growth rate and trigger a faster metastatic process. Therefore chemotherapy, radiation, or both methods may be used to make the tumor shrink before or after surgery.

Chemotherapy is an effective method using therapeutic agents to treat cancers that have spread, since the small size of anticancer drugs allows them to travel easily through the entire body. Chemotherapy conventionally involves small molecule drugs to kill rapidly dividing cancer cells by damaging their RNA or DNA. Although conventional cancer treatment options have progressed significantly over the last few years, chemotherapy is still far from optimal due to a few problems, namely: The non-specific distribution of anticancer drugs throughout the body; most of the drugs used for chemotherapy have a low solubility in water, and thus are not solubilized properly in the bloodstream to provide sustained therapeutic efficacy; and the fact that repeated doses of anticancer drugs are required for therapeutic efficacy. Consequently, there has been increased interest in developing drug delivery carriers for the effective transportation of anticancer drugs to specifically target tumor tissues and kill mainly cancer cells.[1,3]

In the first section of this Chapter, we provide an overview of polymeric drug delivery systems in cancer chemotherapy. Special attention is given to polymeric micelles based on polypeptides that are coated with poly(ethylene glycol) (PEG). We first briefly describe amphiphilic block copolymers micelles as nanocarriers for drug delivery applications. We then discuss two approaches that can be used to produce more stable micelles, either by constructing unimolecular micelles or by crosslinking block copolymer micelles.

2.1.1 Drug Delivery Systems

A drug delivery system (DDS) is defined as a device or a formulation that enables the introduction of therapeutic agents in the body to overcome the limitations of traditional chemotherapy, by improving its efficacy and safety through controlling the rate, time, and place of release of the drugs. A wide range of nanometric drug delivery systems have been designed, including liposomes, polymeric micelles, nanoparticles, dendrimers, silica nanoparticles, carbon nanotubes, and metallic particles (Figure 2.2).[4]

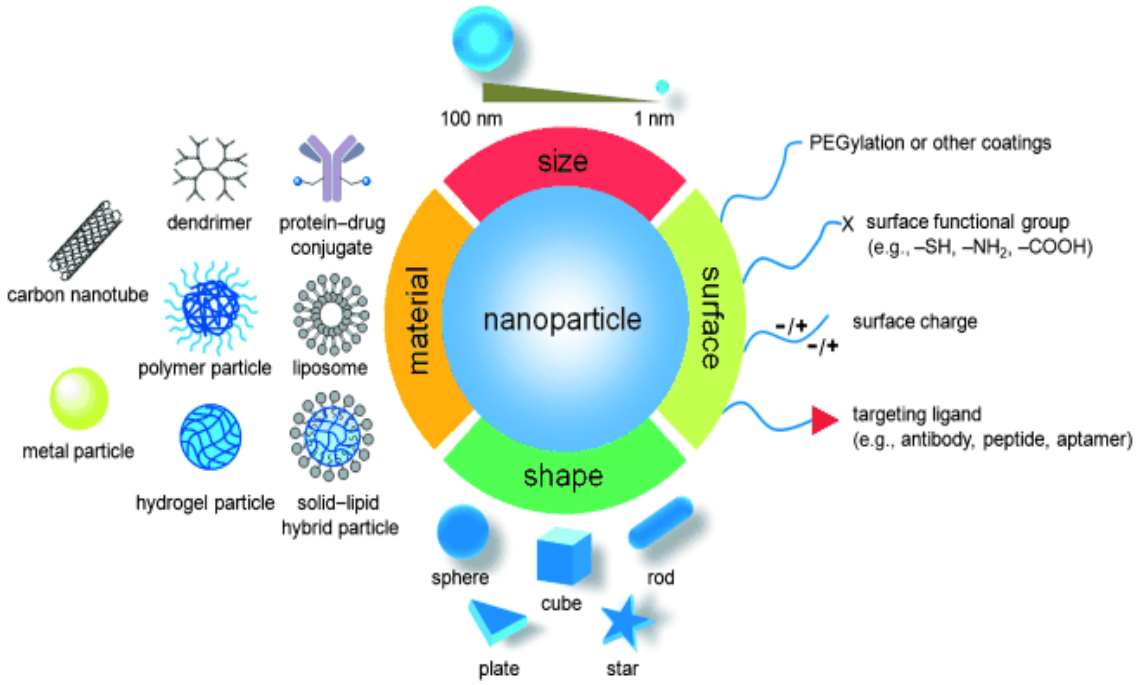

Figure 2.2. Some examples of nanometric drug delivery systems explored for applications in cancer therapy.

Reprinted from ref. 4, with permission from John Wiley & Sons, Inc.

Drug delivery systems have multiple advantages: (A) they can increase significantly the solubility of hydrophobic drugs in aqueous environments, by encapsulation or incorporation of the drugs within amphiphilic materials; (B) they can improve the pharmaceutical properties of drugs, potentially without the need to alter them; (C) they can carry drugs to their site of action, thereby limiting their toxicity and enhancing the therapeutic efficacy; (D) it is possible to achieve a high carrying or loading capacity for a drug within a single macromolecular entity or assembly; and (E) since nanocarriers can escape quick clearance and elimination, the circulation time of the drug-loaded carrier in the blood is increased (ranging from hours to days) in comparison to the free drug.[5] As a

result, cancer chemotherapy using drug delivery systems is expected to increase treatment efficacy with fewer side-effects.

Drug-loaded carriers can passively accumulate in tumors through the enhanced permeation and retention (EPR) effect.[6,7] Nanocarriers can be designed to be large enough to escape premature elimination in the kidneys *via* glomerular filtration, but small enough to participate in the EPR effect and passively accumulate in tumor tissues (Figure 2.3).[8] Blood vessels surrounding tumor tissues are "leaky" in comparison to normal blood vessels, and thus drug-loaded carriers can effectively travel across the fenestrations to reach and accumulate in tumor tissues, thereby exerting their therapeutic effect as the drug is being released. In contrast, free small molecule drugs diffuse non-specifically to tissues. Through passive targeting of tumor tissues by drug-loaded carriers, the side-effects of the drugs can be minimized since normal tissues will be less affected.

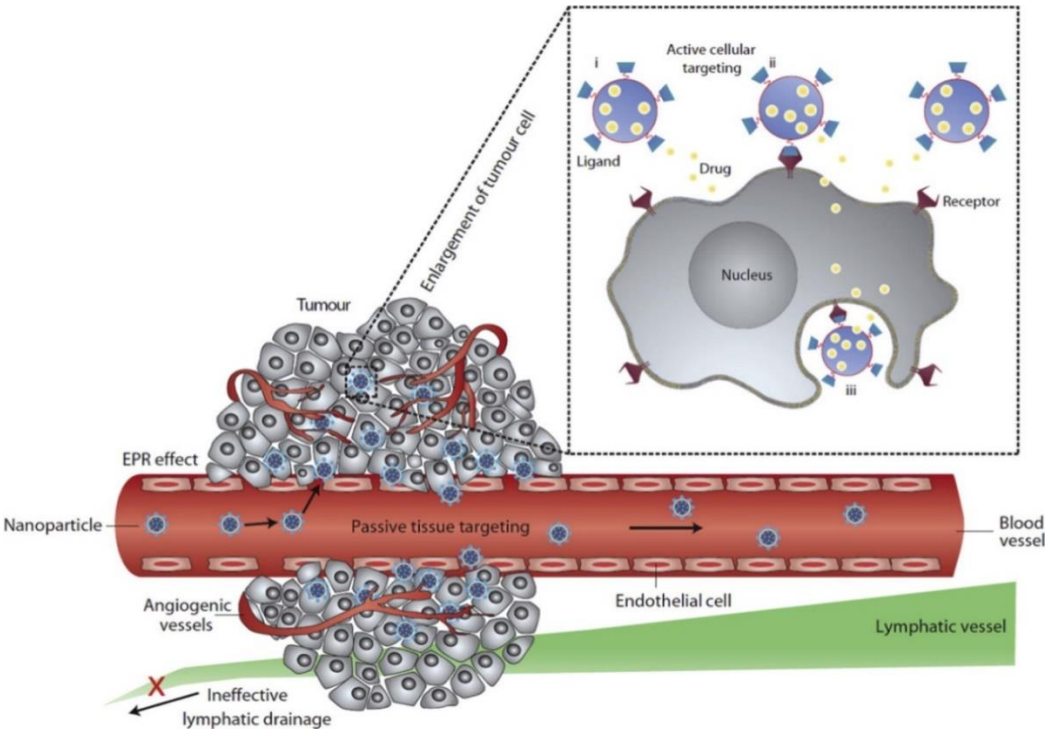

Figure 2.3. The EPR effect, describing the mechanism of enhanced macromolecule accumulation in tumor tissues.

Reprinted by permission from Macmillan Publishers Ltd: Nature Nanotechnology, from ref. 8, copyright 2007.

To date some drug delivery systems have been clinically approved, and several more are under clinical investigation and development (Table 2.1). The first drug-loaded carrier Doxil®, approved in 1995, uses poly(ethylene glycol)- (PEG)-modified liposomes to encapsulate doxorubicin (DOX).[9] Doxil® was prepared with a 100 nm diameter to target specifically tumor tissues while leaving healthy tissues unaffected. The serious side-effects due to the toxicity of free DOX were reduced 3-fold by encapsulating DOX into these nanocarriers.[10]

Table 2.1. Nanocarrier-based therapeutics in clinical use and undergoing clinical trials.

Trade name	Formulation	Drug	Phase of development	Ref.
Doxil	liposomes	doxorubicin	approved	[11]
Abraxane	albumin-bound nanoparticles	paclitaxel	approved	[12]
Genexol-PM	polymeric micellar nanoparticles	paclitaxel	approved	[13]
Myocet	liposomes	doxorubicin	approved	[14]
NK105	micellar nanoparticles	paclitaxel	phase III	[15]
BIND-014	polymer matrix	docetaxel	phase II	[16]
Genexol-PM	methoxy PEG-PLA	paclitaxel	phase II	[17]
AuroLase	gold nanoparticles	_	phase I	[18]
DEP^{TM}-Docetaxel	dendrimers	docetaxel	phase I	[19]

Among all the nanocarrier systems available, this literature review will focus on polymeric micellar systems as drug carriers including amphiphilic block copolymers micelles, unimolecular micelles and crosslinked micelles.

2.1.2 Polymeric Micelles as Drug Carriers

Recent developments in the knowledge of the human body have opened the door to the identification and understanding of the mechanisms underlying many challenging diseases. Many of these diseases cannot be treated using conventional small molecule drugs.[20] It has been recognized that enhancing one or more of the intrinsic adsorption, excretion, distribution, and metabolism characteristics of a small molecule drug is a crucial step in developing more effective drug therapies. This requires multidisciplinary collaboration between researchers with expertise in chemistry, biology, and engineering to manufacture new drug delivery systems for effective treatment.[21] Over the last couple of decades, a considerable number of new drug delivery systems have been developed to improve the bioavailability of drugs, enhance their aqueous solubility, increase their circulation time in the bloodstream, and specifically deliver them to target tissues. In this context, polymeric micelles (e.g. amphiphilic block copolymers micelles, unimolecular micelles and crosslinked micelles) with tunable properties have shown great promise and are in the front line of development for drug delivery systems.[22,23]

Among drug carriers, polymeric micelles show great potential due to their higher loading capacity and great stability in the bloodstream. Furthermore, the physicochemical properties of the polymers can be tuned to meet specific requirements. In addition,

polymeric micelles may be coated with hydrophilic polymers such as poly(ethylene glycol) (PEG), which helps the micelles escape recognition by the mononuclear phagocytic system and thus prolongs their circulation time in the bloodstream.[24] The size of polymeric micelles usually falls within the range of 10-100 nm in diameter, which is above the threshold for filtration by the kidneys, and therefore polymeric micelles have the ability to carry many drugs with prolonged circulation times. Ligands or/and antibodies can be attached to the surface of polymeric micelles to specifically target certain parts of the body.[22] Some polymeric nanoparticles can achieve high drug loading, which maximizes the drug/excipient ratio. In addition, the incorporation of drugs in polymeric matrices controls their release rate, which can be sustained or stimuli-responsive.[25] The use of a specific stimuli-sensitive delivery system allows the release of the encapsulated drug only when one or more stimuli are present. For instance, the pH around tumor tissues in the body tends to be more acidic (5.4 to 6.5) relatively to the physiological pH (7.4).[26] Furthermore, the small size of polymeric micelles allows them to accumulate passively in tumors, through the so-called enhanced permeation and retention effect (EPR).[6]

Despite the remarkable therapeutic potential of polymeric micelles as drug nanocarriers, the availability of well-defined water-soluble synthetic polymers of uniform dimensions, that are nontoxic and biocompatible, and therefore suitable for *in vivo* applications, is still limited.[27] Degradable polymeric biomaterials are preferable for therapeutic devices such as sustained release drug delivery nanocarriers. Biodegradable polymers can be defined as polymers that are degradable *in vivo*, either enzymatically or non-enzymatically, to produce biocompatible or nontoxic by-products.[28] Therefore, it is

possible to implant these materials into the body without subsequent removal by surgery or other procedures. For example, poly(lactic-*co*-glycolic acid) (PLGlyA), poly(amino acid) (PAA), poly(glycolic acid) (PGlyA), poly(ethylene glycol) (PEG), poly(methyl methacrylate) (PMMA) and poly(lactic acid) (PLA) (Figure 2.4) have been approved by the US Food and Drug Administration (FDA) for use in humans. If a polymer is not totally biodegradable, it should be completely eliminated from the body within a reasonable time period.

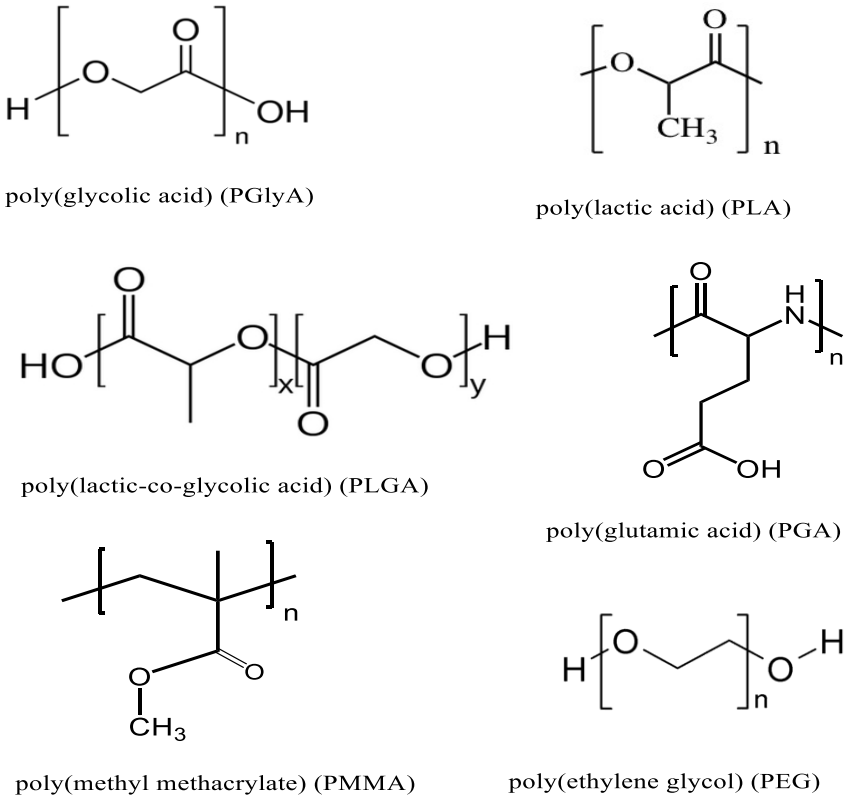

Figure 2.4. Chemical structure of polymers commonly used in drug delivery applications.

The biodegradable polymers used in the fabrication of nanocarriers for drug delivery applications can be categorized, according to their origin, into natural, synthetic or semisynthetic. Natural polymers include proteins (e.g. collagen, gelatin and albumin) and polysaccharides (e.g. dextran, hyaluronic acid, pullulan, cellulose and inulin). Natural polymers are generally more biocompatible and biodegradable, as most of them are present within structural tissues of living organisms. In comparison to natural polymers, synthetic biodegradable polymers have a high mechanical strength but a low degradation rate. In addition, these materials can be tailored to meet absorption time requirements, which potentially facilitates dosage reproducibility and scale-up, without concerns about disease transmission, that can be a problem with naturally occurring polymers.[32] Examples of synthetic polymers used in the construction of nanocarriers include aliphatic polyesters, polypeptides, polyanhydrides, polyorthoesters and polycyanoacrylates.

Polypeptides are increasingly receiving attention as building blocks for the construction of biological nanostructures for biomedical applications. Poly(amino acid)s, especially poly(L-glutamic acid), poly(L-lysine) and poly(L-aspartic acid) and their derivatives, are widely used as components of nanocarriers for drug delivery because of their remarkable characteristics such as their high biocompatibility, easy biodegradability and relatively low cost, in addition to the presence of versatile functional groups such as hydroxyl, carboxyl and amino functionalities useful for a variety of chemical modification reactions.[29] In addition, polypeptides have the ability to form well-defined secondary structures (α-helices and β-sheets) that contribute to the self-assembling of polypeptide chains, leading to novel nanostructured materials. All these features make poly(amino acid)s and their derivatives

excellent polymers for drug delivery applications. Several micellar formulations based on polypeptides are currently undergoing clinical testing or preclinical evaluation (Table 2.2).

Table 2.2. Various polypeptide-based materials currently undergoing clinical testing or preclinical evaluation for drug delivery.

Polymer	Drug	Phase completed	Ref.
PEG-b-PGA	Doxorubicin	Phase II	[30]
mPEG-b-P(PGA-co-Phe)	Doxorubicin	Phase I	[31]
PEG-b-PBLA	Doxorubicin	Phase I	[32]
PGA	Paclitaxel	Phase III	[33]
γ-PGA-b-PLLA	Paclitaxel	Phase I	[34]

PEG-b-PGA: poly(ethylene glycol)-*b*-poly(L-glutamic acid); (mPEG-b-P(PGA-co-Phe)): poly(ethylene glycol)-*b*-poly(L-glutamic acid-*co*-L-phenylalanine); PEG-b-PBLA: poly(ethylene glycol)-*b*-poly(β-benzyl-L-aspartate); PGA: poly(γ-glutamic acid); γ-PGA-*b*-PLLA: poly(γ-glutamic acid)-*b*-poly(lactide).

Traditionally, amino acids have been polymerized by solid-phase peptide synthesis, but the synthesis of peptides with more than 100 residues often results in undesired by-products due to incomplete deprotection and coupling steps. As a result, a number of alternate approaches have been developed to prepare poly(amino acid)s. The synthetic technique

most commonly used to that end is the ring-opening polymerization of *N*-carboxyanhydride (NCA) derivatives of α-amino acids initiated by primary amines.[35]

The polymerization of *γ*-benzyl-L-glutamate *N*-carboxyanhydride (Glu-NCA) initiated by primary amines is subject to termination by end group cyclization, which prohibits further growth of the poly(*γ*-benzyl-L-glutamate) (PBG) chain. Chain end cyclization can be practically eliminated, thus preserving the terminal amine group on the chain, by lowering the reaction temperature (Scheme 2.1).[36] This technique is economical and can lead to large quantities of polymer in good yield.

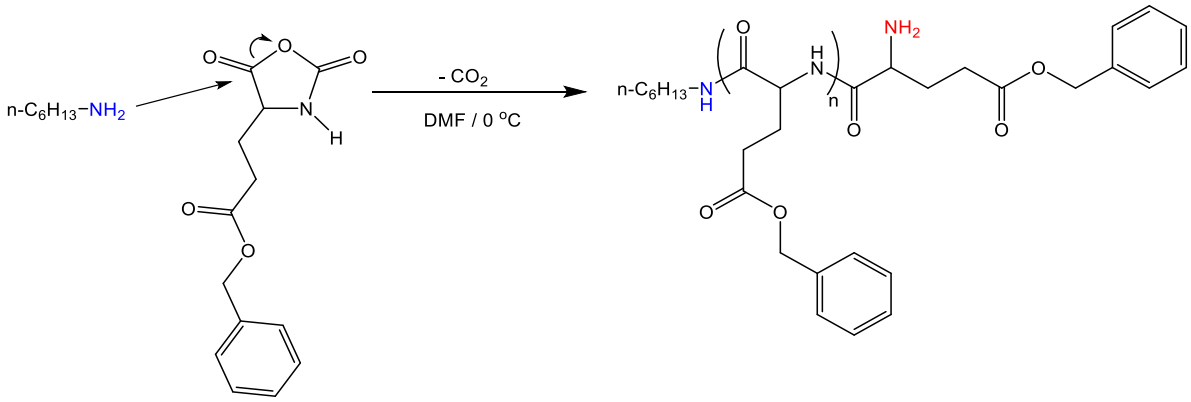

Scheme 2.1. Synthesis of poly(γ-benzy-L-glutamate) by ring-opening polymerization of the corresponding NCA monomer.

Poly(ethylene glycol) (PEG), a polymer of either ethylene glycol or ethylene oxide, is a biocompatible, hydrophilic and non-toxic polymer approved by the FDA for internal use in drug delivery applications. It is the polymer most successfully used to coat nanoparticles (a procedure called PEGylation) to avoid the interaction of nanoparticles with components

of biological fluids and prevent the adsorption of plasma proteins, thus avoiding recognition by the mononuclear phagocytic system (MPS) and subsequent clearance by the kidneys. PEGylation also increases the blood circulation time for polymeric nanoparticles, while providing steric hindrance and protection for cargoes that are sensitive towards particular environments.[37]

There has been extensive research in designing polymeric nanocarriers of different types, sizes, morphologies and stabilities for drug delivery applications. In the following section, amphiphilic block copolymers micelles, unimolecular micelles and crosslinked micelles developed to that end will be briefly reviewed.

2.1.2.1 Amphiphilic Block Copolymer Micelles

Amphiphilic copolymer micelles have recently emerged as colloidal drug carriers formed in aqueous media through the self-assembly of amphiphilic copolymers with different architectures (e.g. block and graft), albeit block copolymers are most common.[22] Micellar solutions of amphiphiles are an effective way to deliver drugs to their targets. Block copolymer micelles are usually spherical, have a size in the range of 10-200 nm and a core-corona structure as shown in Figure 2.5.[23] Copolymers that form micelles in aqueous environments consist of two segments with different affinities for water: one is hydrophobic, while the other is hydrophilic. The major driving force behind the self-assembly of amphiphilic copolymers is the decrease in free energy of the system as the hydrophobic segments withdraw from the aqueous medium to minimize their unfavorable interaction with water. The formation of polymeric micelles, or self-assembly, starts only

when a certain minimum concentration of the amphiphile in water, called the critical micelle concentration (CMC), is exceeded. The hydrophilic segment of the block copolymer then forms the corona or shell of the micelles, while the hydrophobic segment forms the core. Polymeric micelles of amphiphilic block copolymers with low CMC values exhibit enhanced stability. Therefore, increasing the hydrophobicity of the nonpolar component reduces the CMC and thus micelle stability increases.[38]

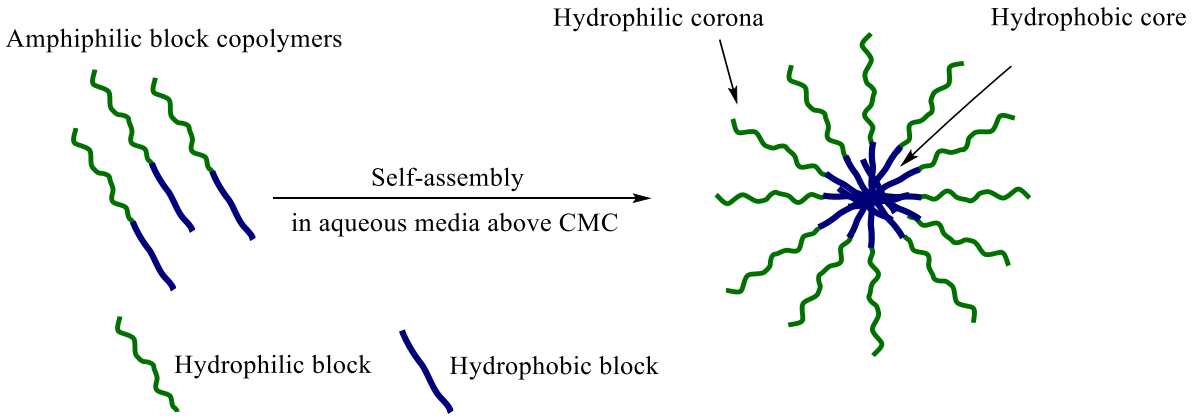

Figure 2.5. Polymeric micelle formed by the self-assembly of amphiphilic block copolymer molecules in aqueous media.

Polymeric micelles are great nanocarriers for drug delivery applications in cancer treatment due to their remarkable core-shell structure that gives them many advantages. One of the most important properties of polymeric micelles is their ability to solubilize hydrophobic or poorly water soluble anti-cancer drugs within their core, and thus enhance their bioavailability. The hydrophobic core offers a good microenvironment for the solubilization of hydrophobic drugs. For instance, polymeric micelles of poly(lactic acid)-

b-poly(ethylene glycol) (PLA-*b*-PEG) increased the aqueous solubility of the anticancer drugs paclitaxel and doxorubicin 5,000-fold and 12,000-fold, respectively.[39,40] Polymeric micelles not only solubilize hydrophobic drugs but also protect them from inactivation in the biological milieu, control their release, decrease their side effects and protect them against degradation, thus increasing their overall therapeutic efficacy.[22] In addition, the small size of polymeric micelles allows them to circulate in the bloodstream for extended periods of time, since their size is large enough to prevent fast renal clearance. The hydrophilic shell of the polymeric micelles confers them aqueous solubility, reduces their uptake by cells of the immune system, and provides an effective steric barrier maintaining colloidal stability and increasing their circulation time. This, in turn, gives the polymeric micelles a better chance of accumulating in tumor tissues through passive targeting via the EPR effect.[41]

Polymeric micelles have been prepared from various amphiphilic copolymers including diblock (A-B), triblock (A-B-A) and graft copolymers. A number of different polymers have been used as core-forming segments including poly(L-amino acids), polyesters (e.g. PLA, PCL, PLGA) and polyethers (e.g. poly(propylene oxide)).[22] Poly(ethylene glycol) is the most commonly used shell-forming segment of polymeric micelles, although other hydrophilic polymers such as poly(*N*-vinyl-2-pyrrolidone), poly(acrylic acid) (PAA), poly(*N*-isopropylacrylamide) and poly(carboxybetaine)s have also been used.[37] Poly(amino acid)s or their derivatives, especially hydrophobic forms of poly(L-glutamic acid), poly(L-lysine) and poly(L-aspartic acid), are widely used as core-forming segments in polymeric micelles due to their remarkable characteristics.[29] Some examples of

polymeric micelle-based anticancer drug formulations having passed the experimental stages and currently undergoing clinical trials are provided in Table 2.3.

Table 2.3. Polymeric micelle-based formulations currently undergoing clinical trials.

Trade name	Polymer	Drug	Phase completed	Ref.
NK-105	PEG-PPBA	Paclitaxel	Phase I	[42]
Genexol®-PM	PEG-PDLLA	Paclitaxel	Phase II	[43]
NK-012	PEG-PGA	SN-38	Phase I	[44]
SP-1049C	PEG-PPO-PEG	Doxorubicin	Phase I	[45]
NK-911	PEG-PAsp-DOX	Doxorubicin	Phase I	[46]

PEG: poly(ethylene glycol); PAsp: poly(aspartic acid); PDLLA: poly(D,L-lactide); PPBA: poly(4-phenyl-1-butanoate)-L-aspartamide; PGA: poly(glutamic acid); SN-38: 7-ethyl-10-hydroxycamptothecin.

Although the stability of amphiphilic block copolymer micelles has been enhanced, they remain sensitive to solvents and different experimental parameters such as concentration and temperature. Most importantly, these self-assembled systems may dissociate upon dilution in the human body, which leads to uncontrolled drug release and reduces the efficacy of the treatment. Polymeric micelles can be stabilized via crosslinking

of either the core or the corona, or by constructing unimolecular structures that remain stable regardless of their environment. These approaches to stabilizing micellar structures will be considered next.

2.1.2.2 Unimolecular Micelles

Unimolecular micelles are single-molecule micelles with distinct core and shell components that are covalently bonded. In contrast to conventional block copolymer micelles obtained via noncovalent interactions, unimolecular micelles do not dissociate upon dilution and are very stable regardless of their concentration, as shown in Figure 2.6.[47] Their size and morphology can also be precisely controlled. Moreover, different numbers and types of functional groups can be attached to every single-molecule micelle. As a result, different tasks can be achieved simultaneously. For instance, multiple drugs and/or diagnosing agents can be delivered at the same time to the same site in the body. All the above features make unimolecular micelles especially attractive as nanocarriers for drug delivery applications. Examples of these unique structures include dendrimers, dendrigraft polymers and star polymers.

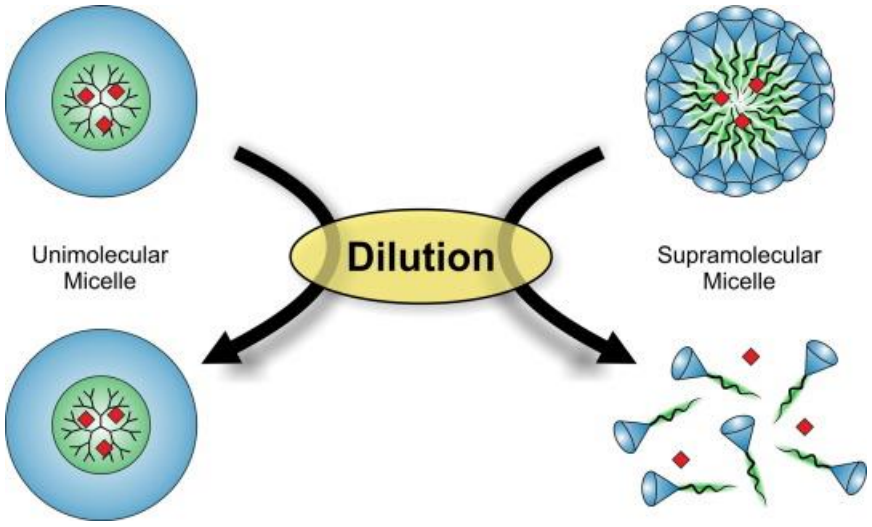

Figure 2.6. Different behaviors of unimolecular and supramolecular micelles under dilution.

Reprinted from Biotechnology Advances 33, Lukowiak, M. C., Thota, B. N. S. and Haag, R., Dendritic core–shell systems as soft drug delivery nanocarriers, 1327, Copyright 2015, with permission from Elsevier.

Dendritic polymers are a type of branched macromolecules characterized by a highly branched tree-like architecture incorporating multiple branching levels, resulting from coupling reactions of either small molecule monomers (hyperbranched polymers and dendrimers), or macromolecular building blocks (dendrigraft polymers). In solution (e.g. water and organic solvents), amphiphilic dendritic polymers exist either as unimolecular species or form multimolecular aggregates.[47] Dendritic polymer properties can be fine-tuned to suit certain therapeutic needs, and the possibility to construct them with specific functional groups that can be used to attach drugs, targeting moieties or imaging agents. makes them ideal carriers for drug delivery applications (Figure 2.7).[48] In these dendritic unimolecular micellar systems, the bioactive compounds can be physically entrapped within the dendritic scaffold and/or covalently conjugated to the terminal functional

groups. Their release behavior can be controlled and/or tuned in the biological environment, for example via pH, enzymatic, redox, irradiation or temperature-triggered cleavage.[49]

Despite the desirable characteristics of dendritic polymers, their use in biological systems is limited due to toxicity issues associated with some of them. For instance, polyamidoamine (PAMAM) dendrimers are cytotoxic for *in vivo* applications. The cytotoxicity of these dendrimers can be greatly reduced by modifying their surface with hydrophilic polymers such as PEG.[37] Thus coating PAMAM dendrimers with PEG (PEGylation) not only decreased their cytotoxicity, but also improved their stability and increased their circulation time in the bloodstream.

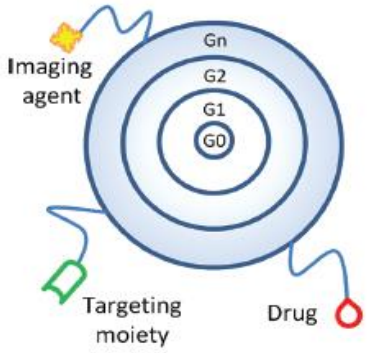

Figure 2.7. Schematic illustration of multifunctional nanocarriers as bearers for drugs, imaging agents, and/or targeting moieties.

Reprinted with permission from "Larson, N. and Ghandehari, H., Chemistry of Materials, 2012, 24, 840-853". Copyright 2012 American Chemical Society.

Dendritic polymers have been used as delivery vehicles for various hydrophobic drugs, to improve their aqueous solubility and enhance their therapeutic efficacy. Various

dendritic platforms such as polyamidoamine (PAMAM), poly(propylene imine) (PPI), poly(L-lysine), poly(ether hydroxylamine) (PEHAM), poly(ester amine) (PEA) and polyglycerol have been synthesized and explored as drug delivery vehicles.[50] Some dendritic polymer-based products are currently being evaluated in clinical trials.[51] For example, Starpharma have been granted authorization by the FDA for Phase III clinical trials of Vivagel®, a dendrimer-based treatment for bacterial vaginosis.[52]

2.1.2.3 Crosslinked Micelles

Regular polymeric micelles, obtained by the self-assembly of amphiphilic copolymers, have attracted much attention over recent years as they are very useful to solubilize hydrophobic drugs, thus increasing their overall therapeutic efficacy. Unfortunately, polymeric micelles are always at equilibrium with non-associated single polymer chains. When applied *in vivo*, polymeric micelles face several difficulties, primarily related to their dilution in the body, which shifts the micellar equilibrium toward the unimer state (Figure 2.8).[53] As a result, there has been significant interest in the stabilization of polymeric micelle structures. In recent years, an easy technique developed to stabilize polymeric micelles is crosslinking. Covalently connecting the polymer chains within polymeric micelles can successfully prevent self-assembled micelles from dissociating, can control the drug release rate, and may provide nanocarriers for stimuli-responsive drug release.[53]

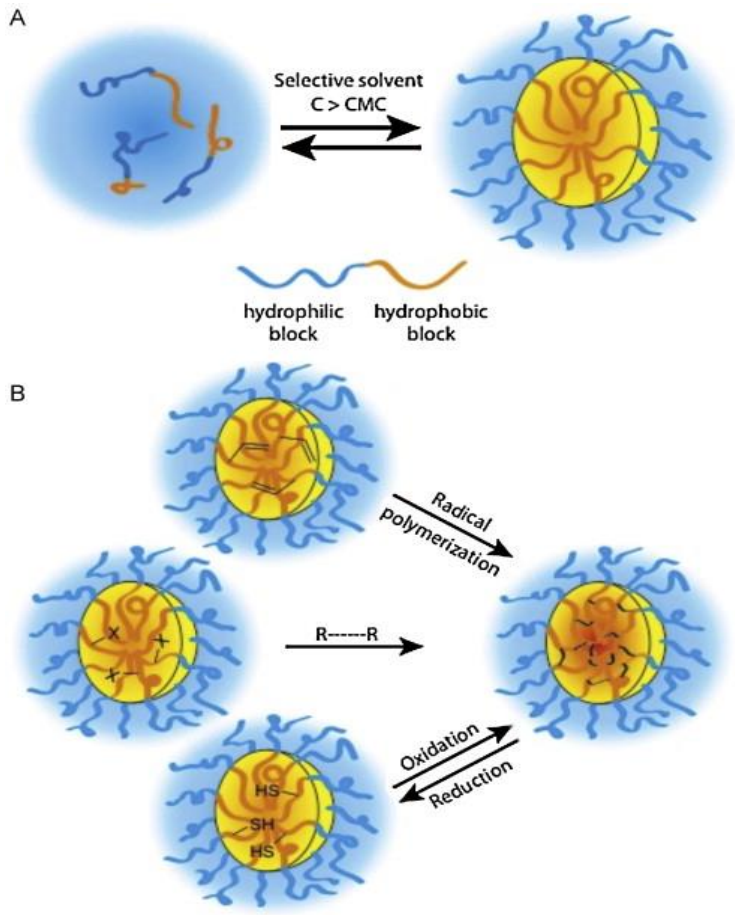

Figure 2.8. Micelle formation: (A) Self-assembly of amphiphilic copolymers above the critical micelle concentration (CMC), and (B) Different methods applied for core-crosslinking of polymeric micelles: radical polymerization, bifunctional agents (R—R), and the oxidation of thiols.

Reprinted from Nano Today 10, Talelli, M., Barz, M., Rijcken, C. J. F., Kiessling, F., Hennink, W. E. and Lammers, T., Core-crosslinked polymeric micelles: Principles, preparation, biomedical applications and clinical translation, 93, Copyright 2015, with permission from Elsevier.

In crosslinked micelles the assembly of the building blocks (unimers) is based on hydrophobic interactions, but is stabilized *via* the formation of crosslinks either within the core or the shell of the micelles. This can be done by incorporating stable bonds between the unimers after self-assembly, to keep the micellar structures together during their

circulation in the bloodstream. Crosslinked micelles are very interesting as nanocarriers for drug delivery, mainly because of their improved *in vivo* stability but also to control their drug release kinetics, and thereby to improve their therapeutic efficacy.

In general, side chain or end group functionalized block copolymers are required to covalently core-crosslink the structure after micelle formation. Core-crosslinked micelles can be obtained by different techniques such as through the addition of bifunctional reagents when the core of the micelles carries reactive functional groups, by radical polymerization when double bonds are present, or via disulfide bridges derived from thiol groups. The latter method is interesting in that it provides an option for stimuli-responsive drug release, since disulfides are intrinsically biodegradable in reducing environments such as the cytosol of cells. For instance, Cheng and coworkers[54] developed camptothecin-conjugated, reduction-sensitive, core-crosslinked micelles with built-in disulfide bonds. Camptothecin (CPT) was reacted with 2-hydroxyethyl disulfide to yield CPT-S-S-OH, which initiated the ROP of tyrosine(alkynyl)-O-carboxyanhydride to afford CPT-SS-poly(tyrosine(alkynyl)-OCA). Core-crosslinking was achieved via azide-alkyne click chemistry, by the co-precipitation of CPT-S-S-poly(tyrosine(alkynyl)-OCA), mPEG-poly(tyrosine(alkynyl)-OCA), and a diazide crosslinker to obtain micelles that could undergo disassembly and concurrent drug release upon redox triggering. The study showed that core-crosslinked polymeric micelles had enhanced stability over non-crosslinked micelles under physiological conditions, while exhibiting rapid degradation and drug release in a reductive environment. Shell-crosslinked polymeric micelles were also

prepared to physically encapsulate the hydrophobic drug camptothecin as therapy against the hepatitis C virus.[55] Lower cytotoxicity was observed as compared to the free drug.

Despite the great advantages of crosslinking micelles to obtain nanocarriers with high *in vivo* stability, this can cause very slow drug release and/or reduce the biodegradability of the nanocarriers, and thus reduce their therapeutic efficacy. In contrast, due to the vast array of architectures that can be obtained, unimolecular micelles obtained from dendritic polymers are an ideal alternative in the design of nanocarriers. In addition, the properties of these unimolecular micelles can be easily fine-tuned to suit certain therapeutic needs, and the possibility to construct them with many functional groups to attach drugs, imaging agents, targeting moieties, etc. makes them highly desirable nanocarriers for drug delivery applications. These dendritic polymer micelles will be reviewed next.

2.2 Dendritic Polymer Micelles for Drug Delivery

Branched polymers have physical properties distinct from their linear analogues. For example high-density polyethylene, a linear polymer without any branches, has a high degree of crystallinity making it a tough material. On the other hand, the multiple short branches present along the backbone of low-density polyethylene lead to a lower degree of crystallinity and increased ductility.[56,57] By controlling the degree of branching, it is thus possible to obtain polymers with properties tailored for specific applications.

Dendritic polymers are a class of macromolecules characterized by a tree-like architecture (Figure 2.9), with multiple branching levels resulting from coupling reactions

of either small molecule monomers (hyperbranched polymers and dendrimers) or macromolecular building blocks (dendrigraft polymers).[58-61] These materials can be synthesized with good control over their molecular size, branching functionality, and the chemical functionality of the chain ends.[62] These molecules have a unique combination of features including a compact globular topology and diameters ranging from 1 to over 100 nm, the presence of internal cavities, and a large number of functional groups at their periphery. Due to these remarkable features, a broad spectrum of applications are being developed for these materials in areas including microencapsulation, drug delivery, nucleic acid therapy, diagnostic agents, light harvesting, and catalysis.

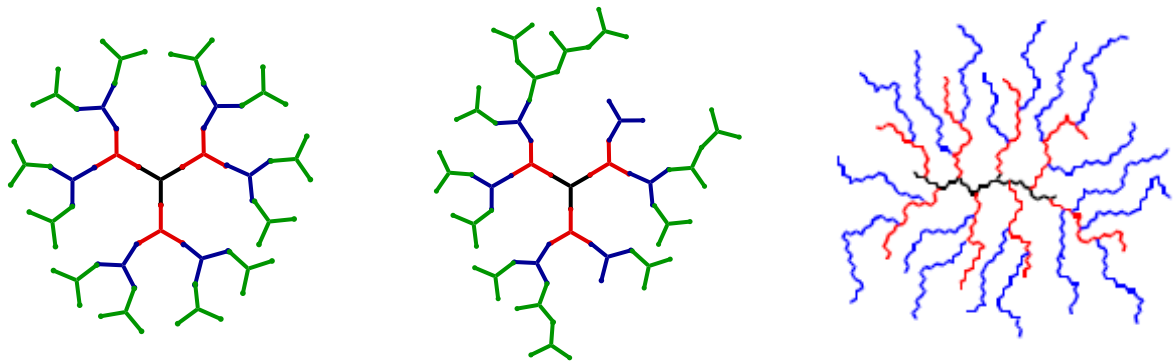

Figure 2.9. Schematic representation of dendritic polymers: (a) dendrimer, (b) hyperbranched polymer, and (c) dendrigraft polymer.

Dendrimers, the first family of dendritic polymers reported in the literature, ideally have a perfectly branched, defect-free structure. Their synthesis involves successive cycles of protection, condensation, and deprotection steps to obtain each branching level

(generation). This stepwise synthesis leads to strictly controlled branching and a very narrow molecular weight distribution ($M_w/M_n < 1.01$).[61] However many synthetic steps are required to produce high molecular weight materials due to the use of low molecular weight monomers as building blocks. On the other hand, high molecular weight hyperbranched polymers can be obtained in one pot self-condensation reactions of AB_n–type monomers without protecting groups, but generally with poor control over their structure. The completely random branching process used in the synthesis of hyperbranched polymers provides the least defined structures, and results in broad molecular weight distributions ($M_w/M_n > 2$) in most cases.[63,64] The third family of dendritic polymers is dendrigraft polymers, typically obtained in a generation-based scheme analogous to dendrimers, but with cycles of polymerization and grafting reactions.[65,66] The use of polymeric chain segments rather than small molecules as building blocks leads to very rapid growth, such that high molecular weights are obtained in only a few steps. In contrast to dendrimers, the random distribution of coupling sites over the substrate makes arborescent polymer growth less sensitive to side reactions, since the structural defects are also randomly distributed over the whole molecule. Under appropriate conditions very high molecular weights can be achieved quickly for these systems, while maintaining narrow molecular weight distributions ($M_w/M_n < 1.1$).

The unique structure and interfacial properties of dendritic polymers make them suitable as nanocarriers for applications such as drug and gene delivery, and as diagnostic agents.[67-70] While polymeric micelles obtained by the self-assembly of amphiphilic block copolymers have been widely investigated for the encapsulation of drugs within their

hydrophobic core, they can be very sensitive to variations in their environment. For example, self-assembled nanocarriers can become unstable and dissociate into free chains when subjected to pH or temperature variations, or upon dilution in the bloodstream. In contrast, dendritic polymers can be designed to behave like unimolecular micelles, namely single molecules with an amphiphilic, covalently bonded core-shell morphology. They are stable irrespective of their concentration or the solvency conditions, which makes them especially attractive as nanocarriers for drug delivery. The numerous advantages of dendritic polymers in drug delivery have been discussed in several papers.[68,69,71-75] Beyond providing a hydrophobic microenvironment that can greatly increase the solubility limit of the free drug in aqueous environments, these can provide a high loading capacity,[68] are able to cross biological barriers,[47,76-79] have tunable surface charges,[77] and can improve the pharmaceutical and pharmacological properties of drugs, potentially without the need to alter the drug but rather through suitable design of the molecular architecture of the carrier.[50,80] Their small size allows them to passively accumulate in tumors through the enhanced permeation and retention (EPR) effect.[77,79] Active targeting can be achieved by introducing ligands on the carrier that can interact with overexpressed cell receptors,[80,81] and the protection they afford minimizes drug degradation and loss.[82,83] In these nanocarrier systems, the bioactive compound can either physically interact with the dendritic scaffold or be covalently conjugated with functional groups located on the branching or terminal units, and their release can be triggered and/or tuned in the biological environment through pH, enzymatic, redox, irradiation, or temperature-dependent processes.[49,71,73]

In this section, an overview is provided for the methods currently available for the synthesis, modification, and drug delivery application of dendritic polymers with various structures. The following section is divided according to the three main subclasses of dendritic polymers, namely dendrimers, hyperbranched polymers, and dendrigraft polymers, respectively. For each dendritic polymer type, well-established and more recent synthetic routes are described. Some of these approaches are illustrated using either seminal articles or examples that illustrate well that particular strategy. Specific dendritic polymers showing promise as nanocarriers for drug delivery applications are then discussed. While many systems have potential applications in drug delivery, only selected examples will be discussed here. Special attention is provided to the different modification methods proposed to achieve desirable nanocarrier properties. This approach is expected to spark new ideas and to motivate continued investigations in this emerging research area.

2.2.1 Dendrimers

The most extensively investigated subset of dendritic polymers, dendrimers, were first synthesized in a so-called divergent (core-first) fashion and were termed "cascade molecules" by Vögtle in 1978.[84] The word "dendrimer", coined by Tomalia in 1985 from the Greek words *dendri* (tree-branch-like) and *meros* (part), was first used in his paper on polyamidoamine (PAMAM) molecules.[85] Since this first report, many compositions and surface modifications have been reported for dendrimeric materials. The two most widely studied dendrimer families are the Tomalia-type PAMAM dendrimers and the Fréchet-type polyether compositions.

2.2.1.1 Dendrimer Synthesis: Divergent and Convergent Methods

Dendrimers have a core–shell structure with three distinct architectural components: a central core, an interior shell composed of repeating units, and terminal functional groups forming the outer shell. The strictly controlled structure of dendrimers results from the layered assembly of repeating units surrounding the core, which is obtained through sequential reaction cycles. This can be achieved in two different ways, namely by divergent (core-first) or convergent (arms-first) strategies as shown in Scheme 2.2. These syntheses involve repetitive stepwise growth and deprotection/activation protocols with careful purification steps for each generation.

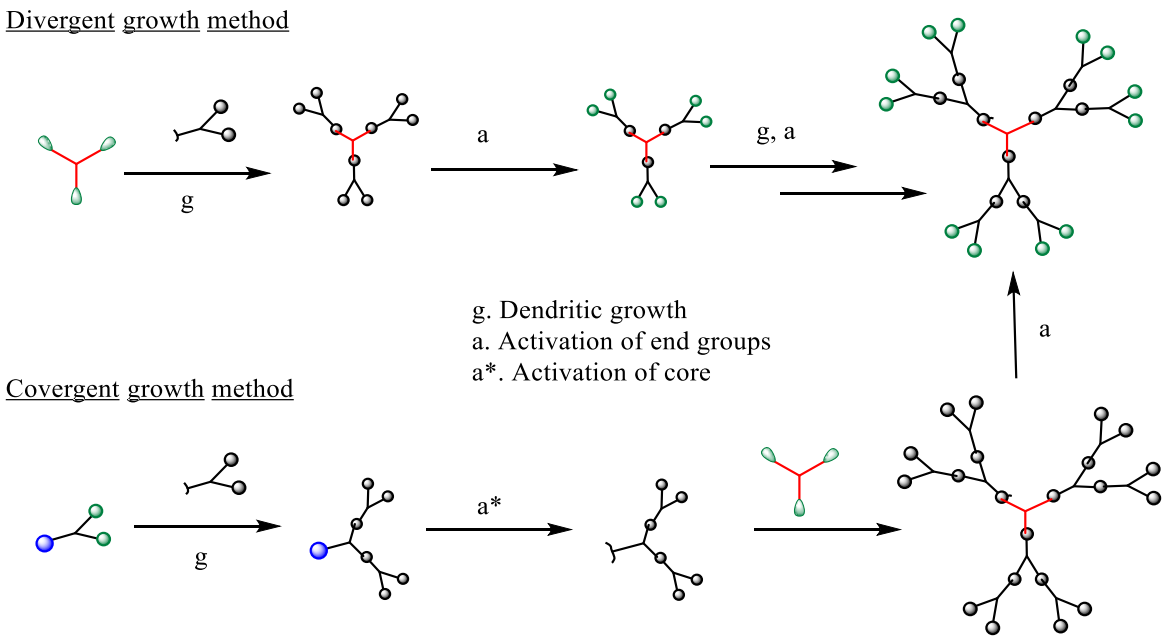

Scheme 2.2. Divergent *vs*. convergent growth schemes for the synthesis of dendrimers.

In the divergent growth method a multifunctional core is coupled with an excess of reagent containing at least two protected branching sites, followed by purification and removal of the protecting groups. The synthesis of PAMAM dendrimers by the condensation of amines with acrylates is provided in Scheme 2.3 to illustrate this strategy. An initiating core containing two or more amine functionalities is first reacted with an excess of methyl acrylate in a Michael addition, resulting in an alkyl ester branch for each amine proton. Amidation of the ester groups with a large excess of ethylenediamine yields the primary amine terminal groups of a 'generation zero' (G0) dendrimer. Each amino group in this branched molecule is again reacted sequentially with methyl methacrylate and ethylenediamine to yield the first-generation (G1) PAMAM dendrimer, and so on. Each reaction cycle yields dendrimers of successive generation numbers, with increasing size and molecular weight.

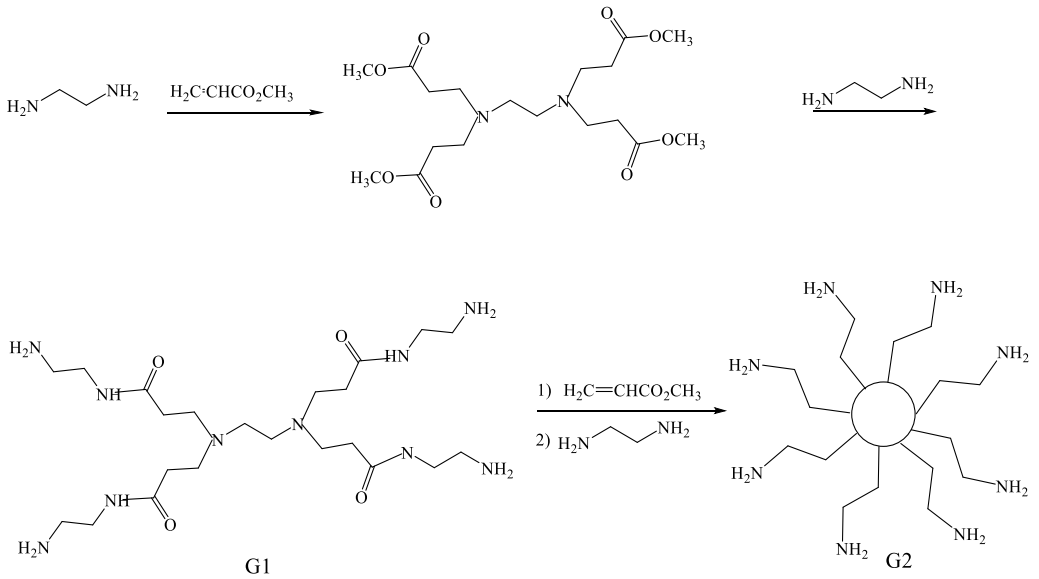

Scheme 2.3. Divergent PAMAM dendrimer synthesis from an ethylenediamine (EDA) core.

Polyamidoamine or PAMAM dendrimers were the first dendritic materials commercialized, under the trade name Starburst®, and are likely the dendritic polymers most widely investigated to date. Dendrimers synthesized by the divergent approach require extensive purification at each reaction step, since a large excess of reagents is necessary to avoid defects in the structure due to incomplete reactions. This can be achieved by ultrafiltration or column chromatography. The divergent approach is currently the preferred strategy for the commercial production of dendrimers.

In the convergent growth method, individual dendrons or dendrimer wedges are first synthesized by protection/coupling/deprotection strategies analogous to the divergent approach described above, but starting from the periphery of the molecules. When the growing dendrons have reached the desired size (generation), they are coupled with a multifunctional core to give a complete dendrimer. In convergent growth, a small number of reactive sites are involved at each step, which restricts the number of possible side reactions. Another advantage of this method over the divergent strategy is that the growth of the dendrons can be more easily monitored and controlled, since the dendrons are structurally simpler. Furthermore there is a larger difference in molecular weight between the starting material and the product, which enables straightforward separation of the reactants and the product.

Newkome first reported a convergent dendron synthesis scheme in 1985 for the preparation of so-called arborol molecules, but the generation number and the molecular weight attained initially were very limited.[86] Hawker and Fréchet subsequently developed another convergent approach in 1990,[87] whereby they achieved the synthesis of polyether

dendrimers by coupling benzyl bromide with 3,5-dihydroxybenzyl alcohol (DHBA) to create dendrons (dendritic fragments) as shown in Scheme 2.4. Conversion of the G1 dendritic benzyl alcohol to a benzylic bromide and further cycles of DHBA monomer coupling led to the following dendron generations. The dendritic fragments thus obtained, carrying a bromide functionality at their focal point, were finally coupled with a multifunctional core such as l,l,l-tris(4′-hydroxypheny1)ethane to obtain a symmetrical dendrimer. One of the most interesting advantages of the convergent method is the ability to obtain bifunctional dendrimers (e.g. Janus micelles) if dendrons containing functional groups of different types are coupled.[88]

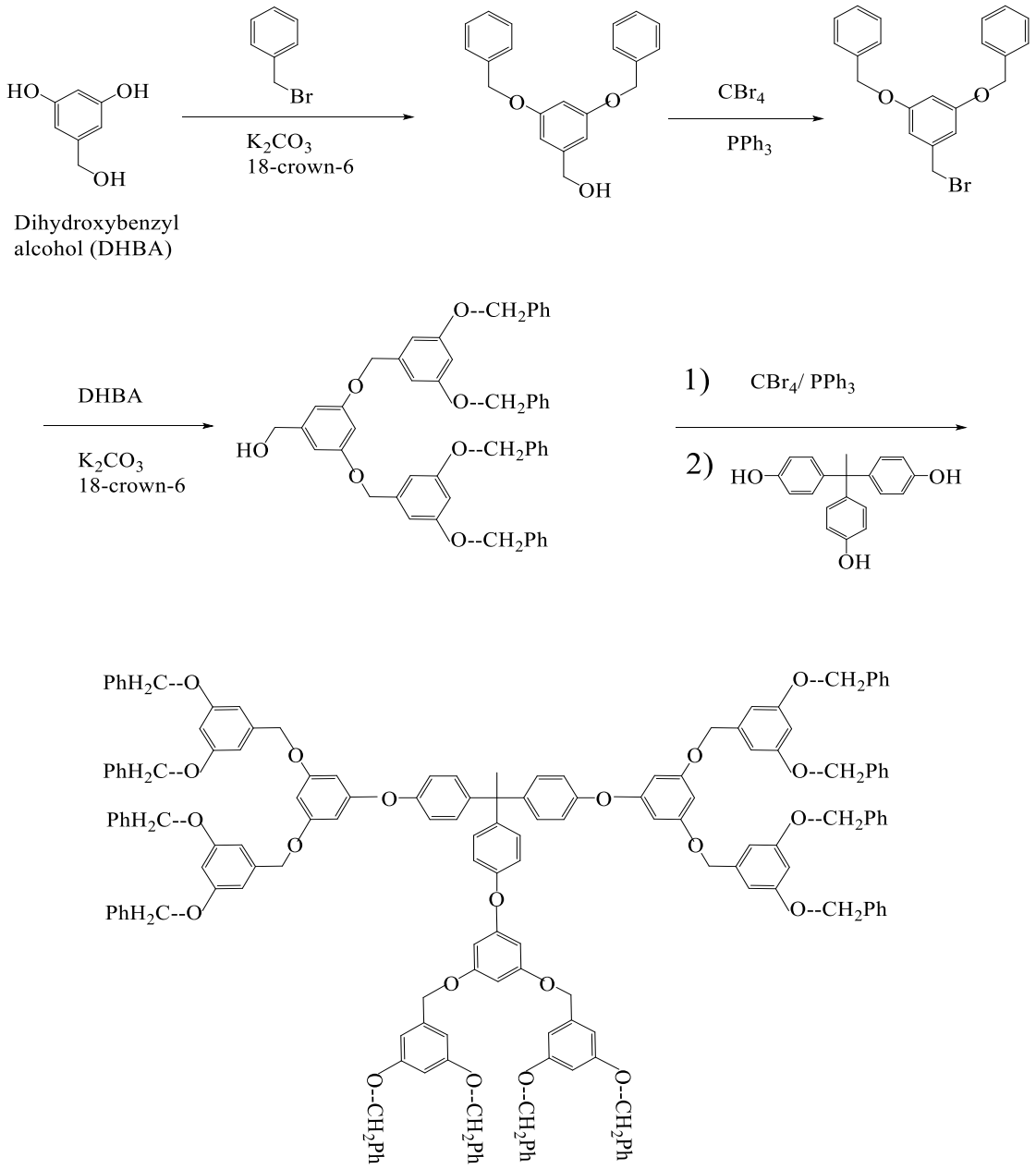

Scheme 2.4. Synthesis of a Fréchet-type benzyl ether dendrimer by a convergent approach.

The main drawbacks of both the divergent and convergent dendrimer synthesis schemes described above is that they are tedious and time-consuming. Fortunately, several

improvements have been suggested for these methodologies over the past years.[89] The necessity for deprotection or activation steps was thus eliminated by introducing the concept of orthogonality, namely the use of functional groups reacting under different conditions.[90] For example, an orthogonal coupling strategy was applied to the synthesis of a G6 dendrimer from AB_2 monomer units containing two pairs of complementary coupling functionalities in just three steps.[91] The most commonly employed reaction for that purpose is the copper(I)-catalyzed Huisgen 1,3-dipolar cycloaddition (click reaction) between azides and primary acetylenes (CuAAC), selectively forming 1,4-disubstituted 1,2,3-triazole rings as shown in Scheme 2.5.[92,93]

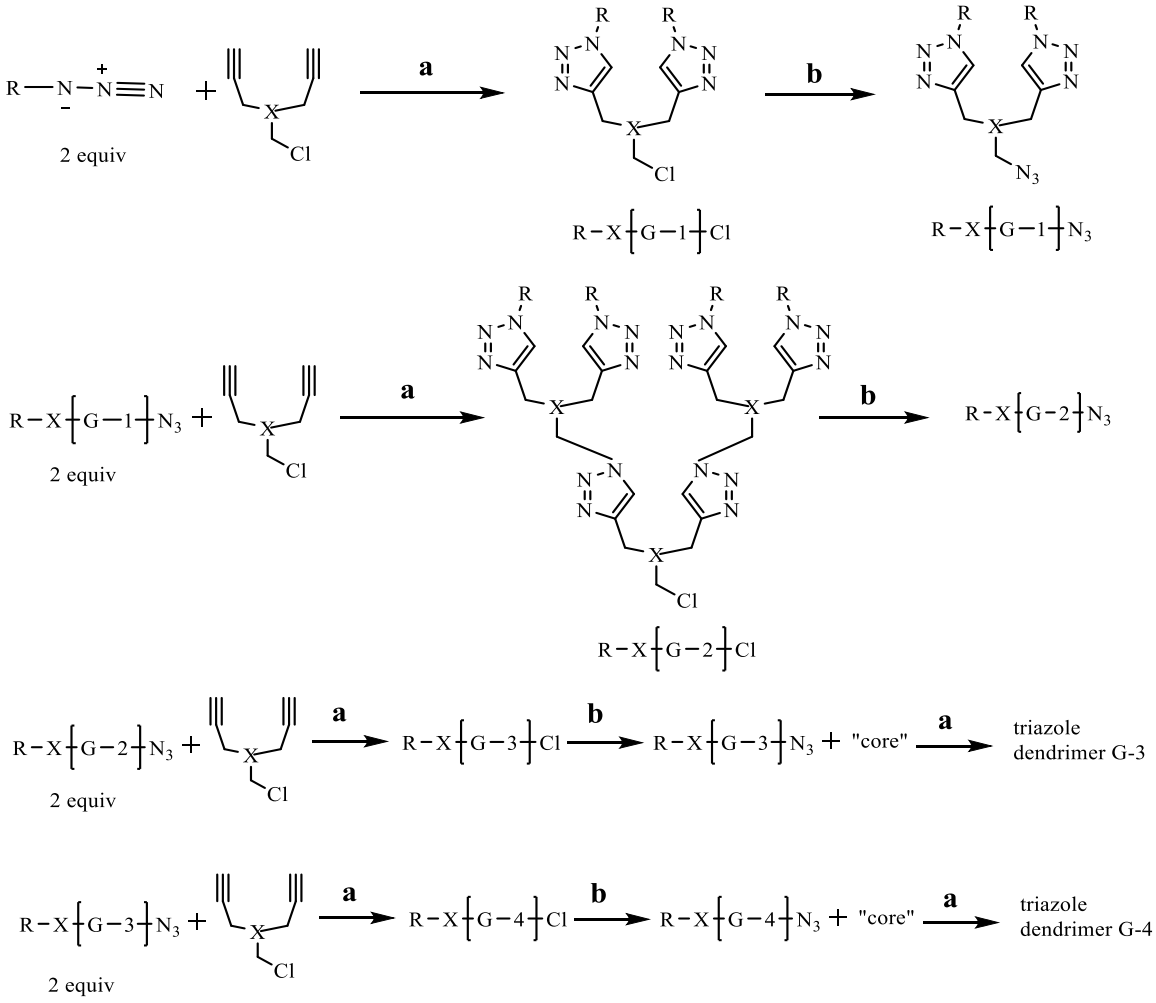

Scheme 2.5. Convergent approach toward triazole dendrimers. a) $CuSO_4$ (5 mol %), sodium ascorbate (10 mol %), H_2O/tBuOH (1:1); b) 1.5 equiv NaN_3, CH_3COCH_3/H_2O (4:1).

Unfortunately, complete removal of the copper (I) catalyst from the CuAAC reaction can be difficult, especially in the synthesis of dense (upper generation) dendrimers. Recently, Gonzaga et al. achieved the synthesis of upper-generation dendrimers in high yield, and with only water-soluble salt byproducts.[94] The strategy was based on the metal-

free cycloaddition of alkynes to azides with electron-deficient alkynes such as derivatives of acetylene dicarboxylate. The reaction between acetylenedicarboxylic acid and 2-bromopropanol yielded an activated monomer that coupled with azides in a metal-free click reaction. More recently, click reactions were combined with orthogonal reactions to further improve dendrimer syntheses. For example, a combination of thiol–ene click addition (a reaction between a thiol and an alkene to form an alkyl sulfide) with esterification led to G5 dendrimers in only 5 steps.[95] Furthermore, a combination of thiol–ene click chemistry (radical-mediated addition of thiols across double bonds) with S_N2 nucleophilic substitution reactions was employed to synthesize multifunctional dendrimers from carbohydrate building blocks.[96,97] In this approach (Scheme 2.6) Roy and coworkers reacted a glucose-based AB_4 monomer (**8**), possessing four allyl groups and a *N*-(2-(glucosyloxy)ethyl)-2-chloroacetamide group, with thioacetylated **16** in the presence of a slight excess of 1 M MeONa–MeOH solution, to obtain dendrimer **17** (containing 24 allyl groups) in high yield. A subsequent thiol–ene reaction between **17** and thiogalactoside **18** provided glycodendrimer **19**, with 24 sugar residues. The uniformity of the structure was confirmed by gel permeation chromatography, which clearly showed a symmetrical Gaussian pattern with a low PDI of 1.064. Very recently, the same group reported the synthesis of G3 dendrimers with 108, 180, and 252 hydroxyl surface groups using AB_3, AB_5 and AB_7 hypermonomers, respectively.[98] The dendrimers were constructed using a combination of microwave-assisted highly efficient CuAAC and thiol–ene reactions not requiring protection and deprotection steps. Low polydispersity indexes (PDI) of 1.03-1.08 confirmed the nearly monodisperse nature of the products.

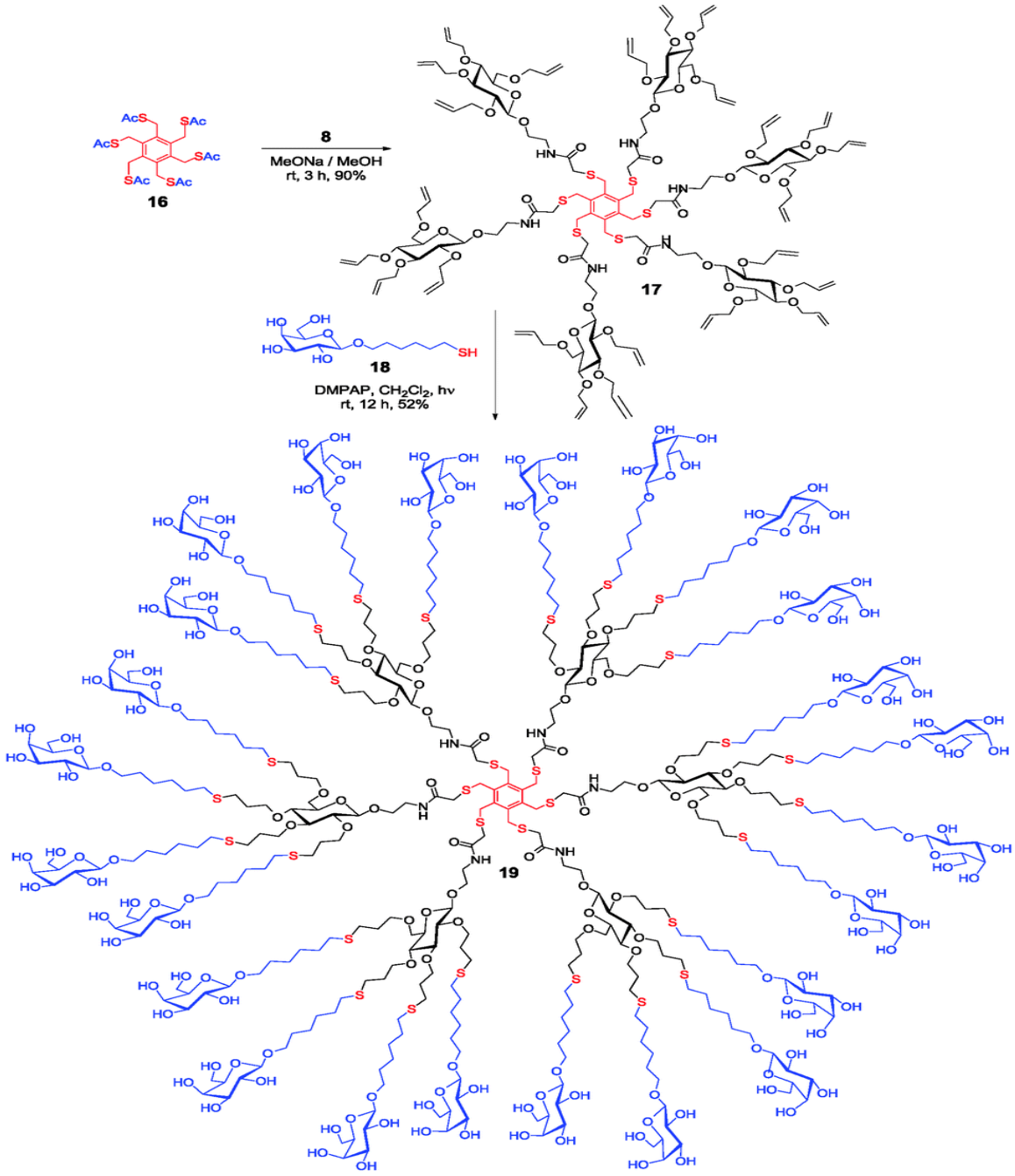

Scheme 2.6. Synthesis of a dendrimer containing 24 galactoside groups.

Reproduced from ref. 96, with permission from the Royal Society of Chemistry.

Dendrimers possess several features making them attractive as nanocarriers for drug delivery applications, among which the presence of open cavities allowing the encapsulation of poorly water-soluble drugs.[99] For example, dendrimers based on glycerol and succinic acid were used to encapsulate 10-hydroxycamptothecin (10HCPT), a poorly water-soluble anticancer drug.[100] The study showed that encapsulation not only increased cellular uptake of the drug 16-fold as compared to the free drug, but it also improved the cellular retention of 10HCPT. The inability of nanocarriers acting by simple physical entrapment to precisely control the rate of drug release has led to a shift in attention toward the covalent conjugation approach. In this case, the release kinetics of the drug from the dendrimer are governed by the nature of the chemical linkage used to couple the drug with the dendrimer. A wide range of linking strategies have been reported for that approach. For example, drugs can be linked to the dendritic scaffold through amide, hydrazone, ester, imine, carbamate or disulfide groups, as well as enzymatically cleavable peptide sequences.[49] As a result, many researchers have attempted to develop new dendrimer systems taking advantage of their high density of functional groups for ease of drug conjugation. For instance, Kurtoglu et al. investigated the drug release properties of G4 polyamidoamine (PAMAM) dendrimer–ibuprofen conjugates with ester, amide, and peptide linkers. The amide-linked conjugates were relatively stable against hydrolysis, whereas the ester-linked conjugates displayed pH-dependent release behavior.[75]

The development of targeted drug delivery is urgently required to further increase therapeutic efficacy and reduce toxicity. This was addressed, for example, using multifunctional dendrimers conjugated with drugs, targeting moieties, and imaging agents

as drug delivery nanocarriers.[101] A PAMAM G5 dendrimer possessing 128 primary amino groups on its surface was thus used to covalently attach fluorescein isothiocyanate (FITC, an imaging agent), folic acid (FA) to target folate receptors overexpressed in cancer cells, and methotrexate (MTX), an anticancer drug conjugated through an ester bond. The results demonstrated that the PAMAM dendrimers were suitable for the targeted delivery of chemotherapeutic molecules capable of killing cancerous cells. Stimuli-responsive drug nanocarriers are another approach to promote therapeutic efficacy and reduce toxicity by controlling drug release at target sites. Different stimuli have been considered in the development of smart dendrimers for drug delivery including specific enzymes, pH, temperature, and light. For instance, Zhang et al. prepared novel enzyme-sensitive dendrimer–doxorubicin conjugates for ovarian cancer therapy.[102] They obtained PEGylated peptide dendrimer–DOX conjugate nanocarriers through a two-step copper-catalyzed click reaction. The surface of the peptide dendrimer was modified with alkynyl groups twice. Azido-terminated PEG chains were first conjugated with a dendrimer via a click reaction, and then coupled with glycylphenylalanyl-leucylglycine tetra-peptide (Gly–Phe–Leu–Gly, GFLG)-modified DOX on the surface of the dendrimer through a click reaction as shown in Scheme 2.7. The GFLG spacer served as an enzyme-responsive linker to connect the anticancer drug DOX to the PEGylated peptide dendrimer, to be cleaved by cathepsin B, overexpressed in tumor cells. The study showed higher antitumor activity for the PEGylated peptide dendrimer–DOX conjugate as compared to free DOX.

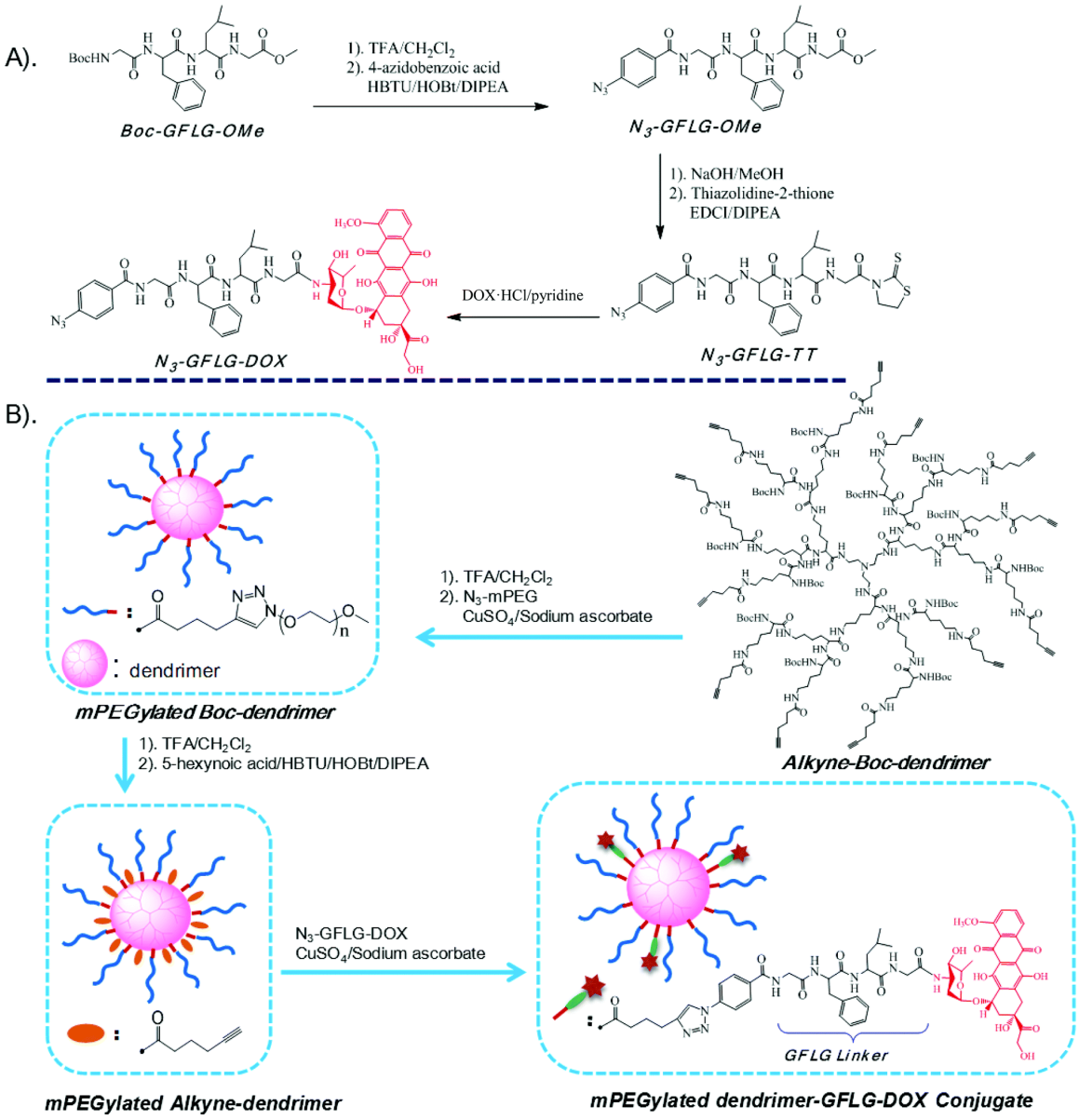

Scheme 2.7. Synthesis of a PEGylated dendrimer–GFLG–DOX conjugate.

Reproduced from ref. 101, with permission from the Royal Society of Chemistry.

Another study compared the anticancer activity of G4−paclitaxel dendrimers and PEG−paclitaxel conjugates. The data provided evidence that the G4−paclitaxel conjugate

enhanced the activity of the drug as compared to PEG−paclitaxel.[103] These results further demonstrate the great potential of dendritic polymers as drug carriers.

2.2.2 Hyperbranched Polymers

As early as 1952, Flory developed a theory concluding that highly branched polymers could be synthesized by the polycondensation of an AB_n-type monomer ($n \geq 2$) for which only the A and B functional groups can react with each other.[104] However it is only in 1988 that the first experimental example of a hyperbranched polymer was reported by Gunatillake et al.[105] Since then, hyperbranched polymers also gained much attention in both academia and industry due to their unique properties and ease of preparation. They are obtained in a single reaction step (Scheme 2.8), and hence are more readily available than other dendritic polymers such as dendrimers.

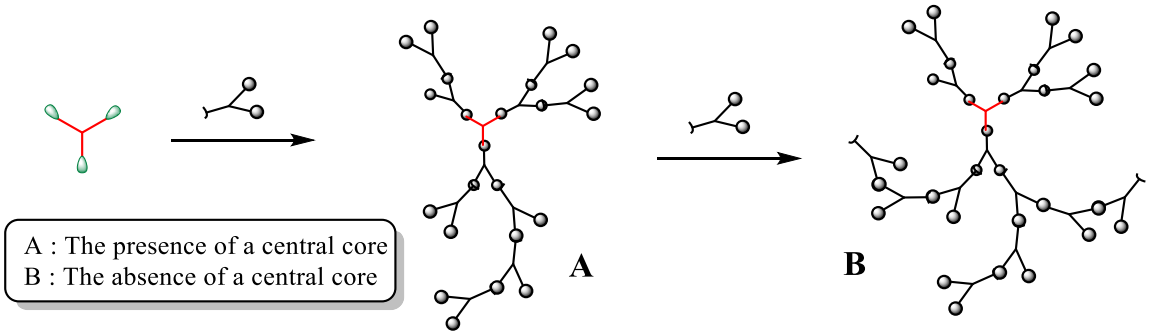

Scheme 2.8. Core (I) and non-core (II) methods for the synthesis of hyperbranched polymers.

The synthetic strategies used for hyperbranched polymers fall into two main categories. In the single-monomer methodology (SMM), hyperbranched polymers are directly synthesized by the polymerization of an AB_n-type monomer, while in the double-monomer methodology (DMM), either two types of AB_n monomers or an $A_2 + B_3$ monomer pair serves to generate the molecules. The SMM includes at least four specific approaches, depending on the reaction mechanism involved: The step-growth polycondensation of AB_n monomers, self-condensing ring-opening polymerization (SCROP), self-condensing vinyl polymerization (SCVP), and proton transfer polymerization (PTP). The DMM can be further divided into two main subclasses based on the monomer pair and reaction pathway selected, namely the '$A_2 + B_3$' approach and the couple-monomer methodology (CMM), which is a combination of the SMM and '$A_2 + B_3$' schemes.[64] Hyperbranched polymers are closer to conventional polymers than dendrimers in terms of molecular weight distribution, which can even be broader than for linear polymers. Furthermore, for hyperbranched polymers the addition of each monomer takes place randomly, and thus a large number of geometrical isomers can be formed for a given molecular weight.[64]

The synthesis of hyperbranched polymers carried out as one-pot reactions offers limited control over the molecular weight of the products, and ultimately leads to gelation. Another problem is that intramolecular side reactions such as cyclization resulting from "backbiting" processes are common in these systems. One technique developed to minimize the occurrence of side reactions is a slow monomer addition protocol, whereby the monomer is added throughout the reaction. This method was termed "concurrent slow addition".[106,107] Polyfunctional initiators used in batch reactions have also shown promise

in controlling the molecular weight and reducing the polydispersity index (PDI = M_w/M_n) of the product.[106,108]

Kim and Webster reported the first example of a single-monomer polycondensation technique, using 3,5-dibromophenylboronic acid and aqueous sodium carbonate in the presence of a Pd catalyst.[109] A representation of this reaction and the resulting hyperbranched structure obtained are shown in Scheme 2.9.

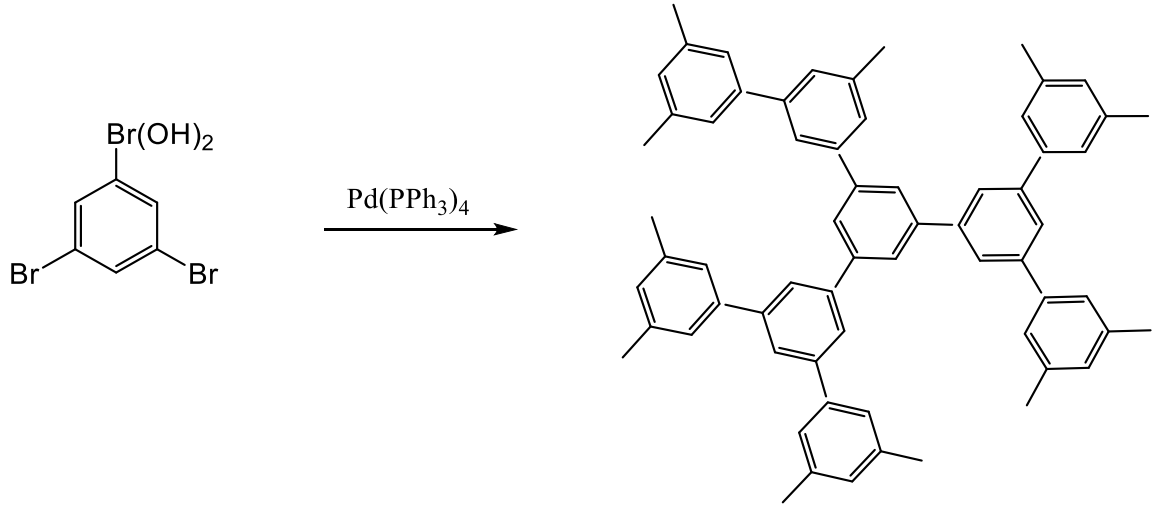

Scheme 2.9. Hyperbranched polyphenylene synthesis by the single-monomer polycondensation method.

The most versatile approach to hyperbranched polymer synthesis is likely the DMM, due to the wide range of monomers and chemical functionalities to which it can be applied. A hyperbranched analogue of the commercially available PAMAM dendrimers (HYPAM) was thus synthesized by a one-pot method as shown in Scheme 2.10.[110] This approach can

be described as an A_6 + B_6 reaction of tris(2-aminoethyl)amine with tris(2-di(methyl acrylate)aminoethyl)amine.

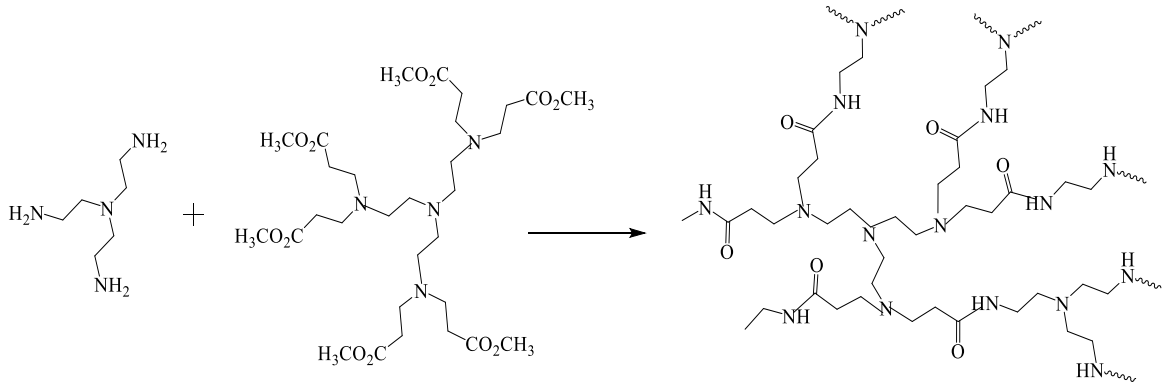

Scheme 2.10. Synthesis of hyperbranched PAMAM (HYPAM).

In 1995, Fréchet et al.[111] first reported the radical polymerization of monomers by the so-called self-condensing vinyl polymerization (SCVP) technique to synthesize hyperbranched polymers with numerous reactive groups. This technique uses vinyl monomers also containing a pendant group that can be converted into an initiating moiety (represented as AB*), and thus can introduce branches in the polymer structure. Chain extension of the branched polymer with linear polymer chains can also be achieved by the atom transfer radical polymerization (ATRP) technique. The combination of these techniques can be used to produce hyperbranched polymers with various architectures and compositions, some of which may be promising as nanocarriers for drug delivery applications. For instance, Porsch et al. reported the synthesis of high molecular weight hyperbranched dendritic-linear polymer (HBDLP) hybrids in a two-step process via a

combination of self-condensing vinyl (co)polymerization (SCV(C)P) and atom transfer radical polymerization (ATRP; Scheme 2.11).[102] A hydrophobic hyperbranched macroinitiator (HBMI) was first produced by SCV(C)P utilizing ATRP, with 1,1,1-tris(4-(2-bromoisobutyryloxy)phenyl)ethane (TBBPE) as trifunctional ATRP initiator, and the inimer 2-(2-bromoisobutyryloxy)ethyl methacrylate (BBEMA) in combination with hexyl acrylate (HA). The active end groups were subsequently used to chain-extend the hyperbranched macroinitiators (HBMIs) with linear, hydrophilic poly(ethylene glycol) methacrylate (PEGMA) segments via ATRP, to form a high molecular weight amphiphilic HBDLP. The chain-extension reactions proceeded in a controlled manner, resulting in polymers with reasonably uniform GPC traces and low polydispersity indices (PDI = 1.3-1.7).

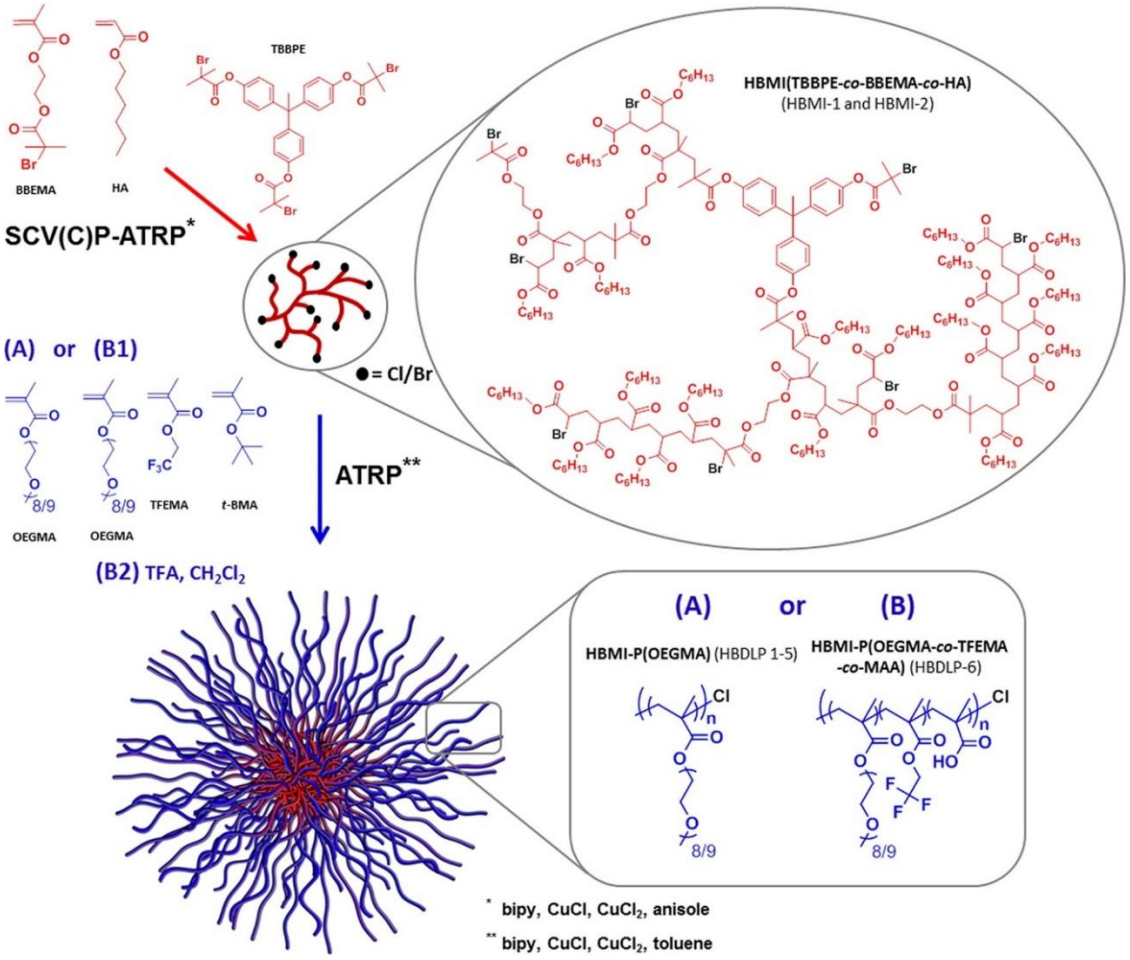

Scheme 2.11. Synthesis of hyperbranched dendritic-linear polymers by sequential SCV(C)P-ATRP and ATRP techniques.

Reprinted with permission from "Porsch, C.; Zhang, Y.; Ducani, C.; Vilaplana, F.; Nordstierna, L.; Nyström, A. M.; Malmström, E. Biomacromolecules 2014, 15, 2235". Copyright 2014 American Chemical Society.

The HBDLP served to encapsulate doxorubicin to achieve sustained delivery. In addition, one of the HBMIs was chain-extended with a fluorine-containing copolymer, so that the unimolecular micelles would have potential as theranostic nanoagents.

The therapeutic efficacy of many anticancer drugs is limited by their poor penetration into tumors; targeted drug delivery is needed to address this challenge. Hyperbranched polymers are potentially useful as carriers for active drugs and, when coupled with targeting ligands, may further enhance the therapeutic efficacy and reduce the toxicity of the drugs. For example, arginylglycylaspartic acid (RGD) peptides are one of the promising ligands for targeting αvβ3 integrin, overexpressed in various cancer cells. Seleci et al.[112] fabricated a tumor-targeting amphiphilic star-hyperbranched block copolymer derived from a hyperbranched substrate, namely hyperbranched poly(methyl methacrylate)-*block*-poly(2-hydroxyethyl methacrylate) (PMMA-*b*-PHEMA), as a targeted drug delivery nanocarrier. The copolymer was prepared via sequential visible light-induced self-condensing vinyl polymerization (SCVP) and conventional vinyl polymerization. This involved a manganese-based visible light photoinitiator system ($Mn_2(CO)_{10}$) in the copolymerization of methyl methacrylate (MMA) with 2-bromoethyl methacrylate (BEMA), possessing both polymerizable and initiating sites within its structure. The subsequent visible light-induced polymerization of HEMA in the presence of the hyperbranched PMMA macroinitiator resulted in the formation of amphiphilic PMMA-*b*-PHEMA copolymers, possessing a hydrophobic hyperbranched PMMA core and hydrophilic PHEMA chains. DOX was successfully encapsulated within these copolymer micelles. It was concluded that the RGD-mediated amphiphilic star-hyperbranched block copolymers were more efficiently internalized by cells than star polymers without the targeting moiety on their surface.

While the physical entrapment of drugs by hyperbranched polymers has been successfully demonstrated, some limitations still exist for efficient drug encapsulation and controlled release by these systems. The major limiting issue is the relatively rapid and uncontrollable release of the drug from the hyperbranched polymer core. The preparation of covalently bonded hyperbranched polymer-drug conjugates stable in buffer solutions is the most obvious solution to this problem, and thus much research has focused on covalent drug attachment. Several types of covalent linker groups have been used to regulate drug release from HBP nanocarriers,[49] as well as co-delivery systems based on HBP designed to promote therapeutic efficiency through synergistic effects. For example, Zhu and coworkers reported the covalent conjugation of a polyacylhydrazone (HPAH) hyperbranched polymer with DOX through acid-sensitive acylhydrazone bonds.[113] Subsequently, the autophagy inhibitor LY was loaded into the HPAH−DOX micelles core to yield an effective chemotherapeutic system for oral squamous cell carcinoma. The hyperbranched polymer HPAH was synthesized by the polycondensation of 2,3-butanedione (BD) and 1-(2-aminoethyl)piperazine tripropionylhydrazine ($AEPNHNH_2$), yielding a weight-average molecular weight (M_w) of 4.0×10^3 g/mol and a polydispersity index (PDI) of 1.6 (Scheme 2.12).[114] Then HPAH−DOX was prepared by conjugation of DOX onto the surface of HPAH, through further condensation of its ketone functionality with the acylhydrazine groups. The study showed that DOX and LY were released in a controlled manner. Furthermore, the *in vitro* investigation revealed that, as compared to the HPAH−DOX micelles and a physical mixture of HPAH−DOX with LY, the LY-loaded HPAH−DOX micelles resulted in synergistic inhibition of tumor cell proliferation. This HBP-based stimulus-responsive co-delivery system for chemotherapy drugs and

autophagy inhibitors provides a promising platform for clinically applicable combination therapies.

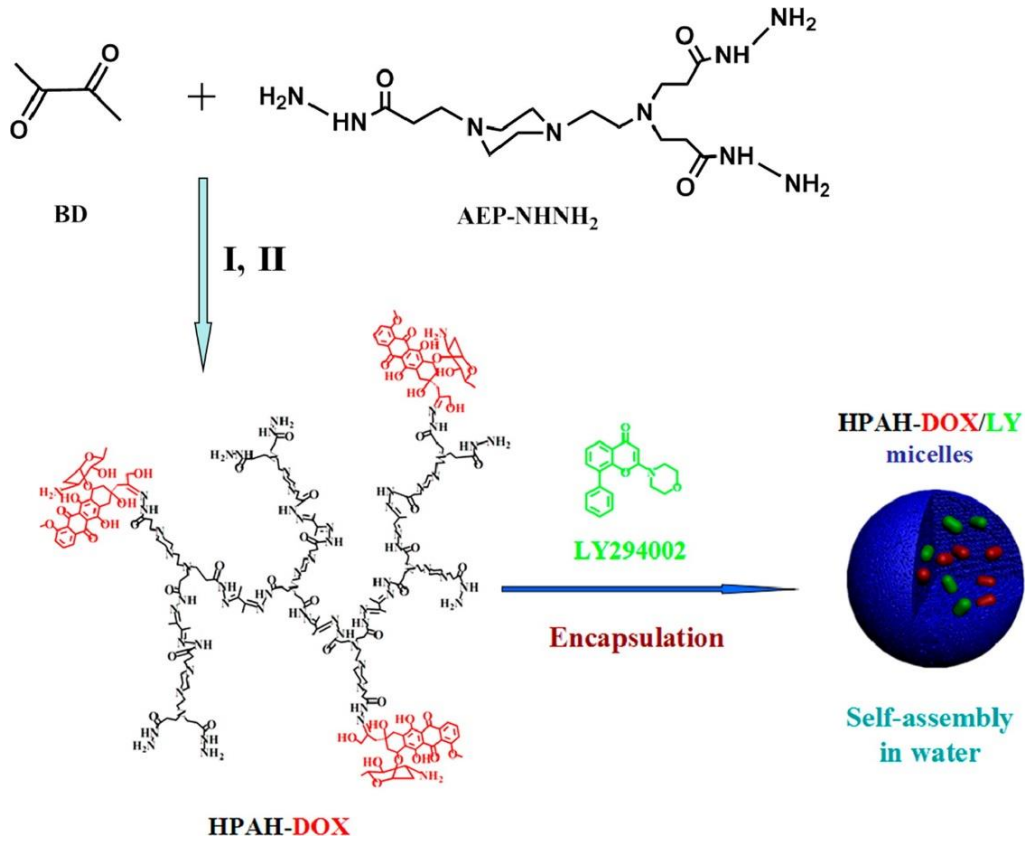

Scheme 2.12. Synthesis of HPAH–DOX and autophagy inhibitor LY-loaded HPAH-DOX micelles.

Reprinted with permission from "Saiyin, W.; Wang, D.; Li, L.; Zhu, L.; Liu, B.; Sheng, L.; Li, Y.; Zhu, B.; Mao, L.; Li, G.; Zhu, X. Molecular Pharmaceutics 2014, 11, 1662". Copyright 2014 American Chemical Society.

Very recently, the same group synthesized redox-responsive hyperbranched polymer–drug conjugates by coupling a thiol-functionalized hyperbranched polymer with thiol-containing drugs.[115] The HBP poly((*S*-(4-vinyl) benzyl *Ś*-propyltrithiocarbonate)-*co*-(poly(ethylene glycol) methacrylate)) or poly(VBPT-*co*-PEGMA), with multiple thiol

groups, was synthesized by a one-pot reaction via reversible addition-fragmentation chain transfer (RAFT) copolymerization (Scheme 2.13). The branched poly(VBPT-*co*-PEGMA) substrate was obtained by RAFT copolymerization of a vinyl-containing trithiocarbonate RAFT agent and PEGMA with a weight-average molecular weight of 1.8×10^4 g/mol and a PDI around 2.0. The trithiocarbonate worked as both monomer and RAFT chain transfer agent. The trithiocarbonate terminal groups of poly(VBPT-*co*-PEGMA) were easily transformed into thiol groups using propylamine, to be coupled with the hydrophobic thiol-containing anticancer drug 6-mercaptopurine (MP) by a thiol−disulfide exchange reaction, resulting in the formation of the poly(VBPT-*co*-PEGMA)-S-S-MP conjugate.

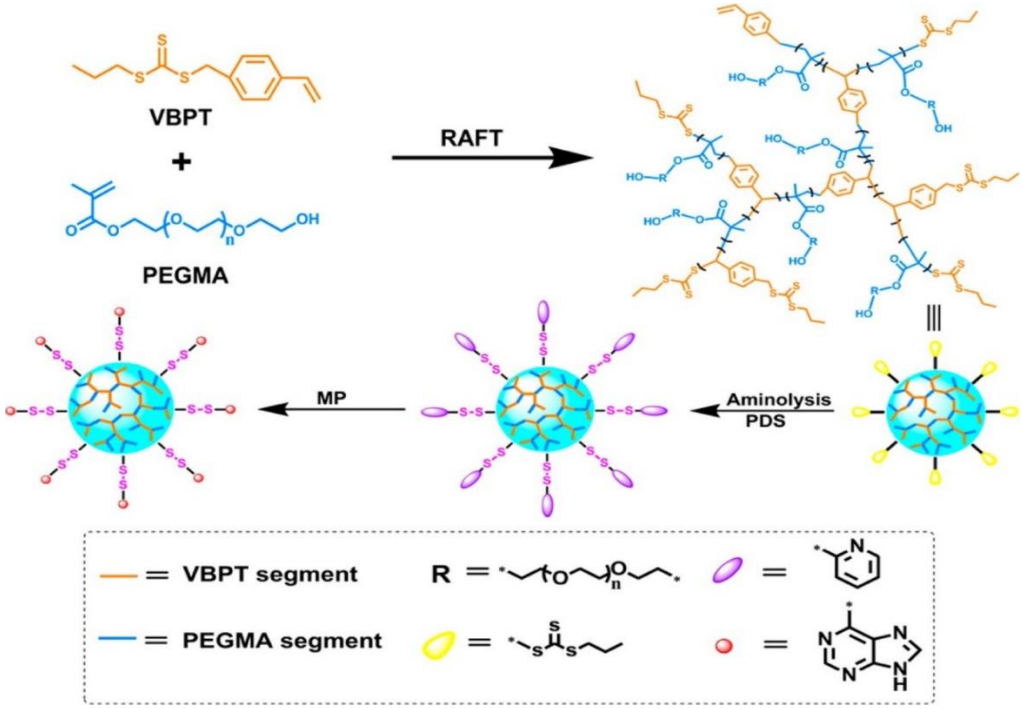

Scheme 2.13. Synthetic route to poly(VBPT-*co*-PEGMA)-S-S-MP.

Reprinted with permission from "Zhuang, Y.; Su, Y.; Peng, Y.; Wang, D.; Deng, H.; Xi, X.; Zhu, X.; Lu, Y. Biomacromolecules 2014, 15, 1408.". Copyright 2014 American Chemical Society.

Since the concentration of glutathione (GSH), a thiol-containing tripeptide capable of reducing disulfide bonds in biological environments, is much higher in tumors than in normal tissues, the redox-responsive HBP–drug conjugate selectively released the drug at tumor sites and thus increased the anticancer drug efficacy. This redox-responsive HBP–drug conjugate provides a promising platform for the delivery and controlled release of thiol-containing drugs or biological molecules.

Given the broad range of synthetic techniques and potential applications reported for hyperbranched polymers, the reader is referred to excellent reviews for more details on the synthetic strategies, characterization, properties, functionalization, and potential applications of hyperbranched polymers as therapeutic agents.[77,80,116]

2.2.3 Dendrigraft Polymers

Dendrigraft polymers, referring collectively to arborescent and dendrimer-like star polymer structures, are the third and most recently reported subset of dendritic polymers.[65,66] Whereas monomers are invariably employed in constructing dendrimers, reactive polymers serve as building blocks in successive grafting reactions for the synthesis of dendrigraft systems. Since a large number of coupling sites are randomly distributed on the grafting substrates, a rapid increase in molecular weight is observed per arborescent polymer generation and high molecular weight species are obtained in a few steps, while narrow molecular weight distributions ($M_w/M_n < 1.1$) are maintained in most cases. The closely related dendrimer-like star polymers, in contrast, have a terminally branched structure achieved through coupling sites strictly located at the chain ends of the previous

generation.[117] As a result, a lower rate of molecular weight increase per generation is observed in these systems. Dendrigraft polymers have been synthesized by divergent (core first) approaches, including both *grafting onto* and *grafting from* methodologies, and by convergent (arms first) approaches, that are essentially *grafting through* methodologies. In the following section it is not intended to present a comprehensive overview of all the synthetic strategies developed to date, but rather to provide examples illustrating the potential of these materials in drug delivery applications. For a more detailed overview of the synthesis and properties of dendrigraft polymers, the reader is directed to a review by Teertstra and Gauthier.[60]

2.2.3.1 Divergent *Grafting Onto* Strategy

The divergent approach relies upon successive grafting reactions starting from a linear substrate (equivalent to the core in dendrimer syntheses) as illustrated in Scheme 2.14. The first examples of dendrigraft polymer syntheses, using *grafting onto* strategies, were reported independently by Gauthier and Möller[65] and by Tomalia et al.[66] in 1991. Gauthier and Möller achieved the synthesis of branched polystyrenes, denominated arborescent polymers, by anionic grafting, while Tomalia et al. used cationic grafting to obtain branched polyethylenimines called Comb-burst® polymers. The synthesis of these materials starts with grafting linear side chains onto a linear polymer substrate functionalized with coupling sites to yield a comb-branched (generation zero or G0) polymer. The introduction of further coupling sites on the G0 polymer and grafting with side chains leads to a generation one (G1) polymer, and so on for subsequent generations.

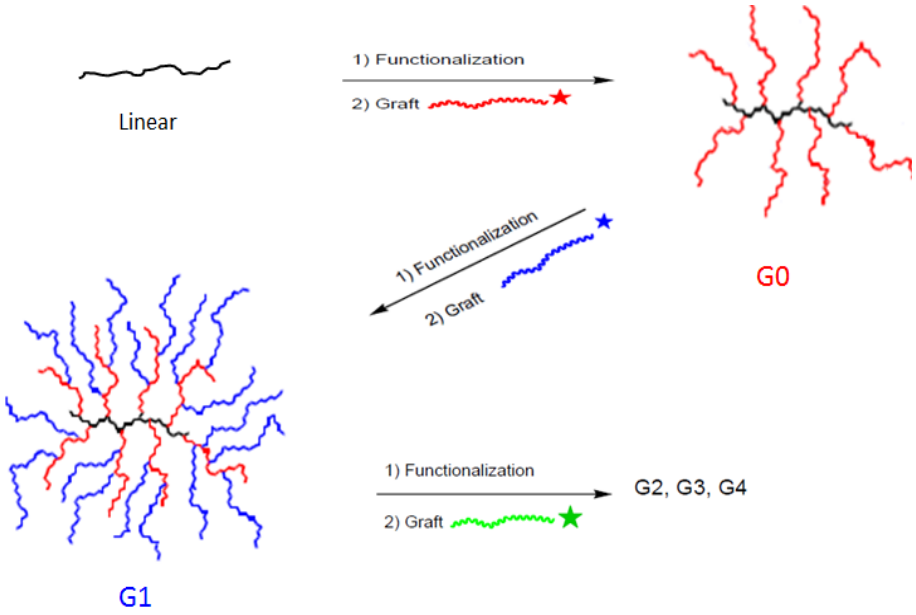

Scheme 2.14. General *grafting onto* scheme for the synthesis of arborescent polymers.

The first example of the synthesis of arborescent polystyrene used chloromethyl coupling sites on the polystyrene substrates, and "living" polystyryllithium as side chains.[65] Repetition of the functionalization and grafting reactions as shown in Scheme 2.15 led to arborescent polymers of generations up to G3. To achieve a high grafting yield, it was necessary to "cap" the polystyryl anions with a single 1,1-diphenylethylene unit to suppress metal-halogen exchange reactions competing with coupling. To avoid the use of chloromethyl methyl ether, a potent carcinogen, a modified coupling method using acetyl coupling sites was subsequently developed by Li and Gauthier.[118] It was also necessary to cap the polystyryl anions with a few 2-vinylpyridine units in that case, to minimize side reactions of the macroanions and increase the grafting yield. Repetition of acetylation and anionic grafting cycles led to generations of arborescent polymers with a low PDI (1.07-1.09).

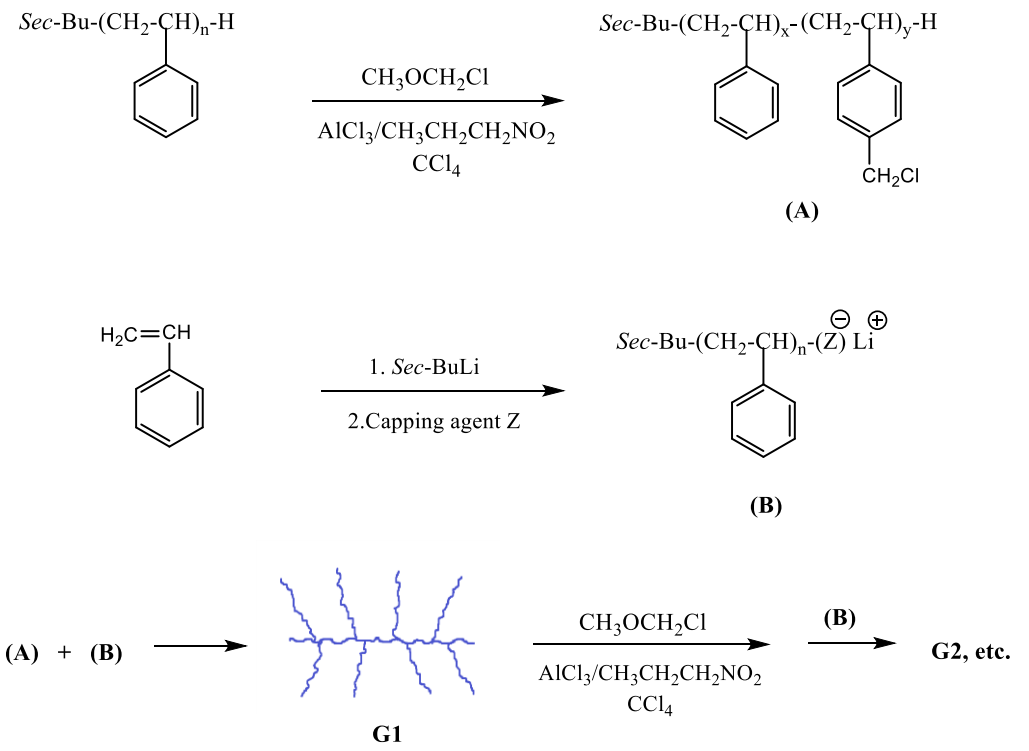

Scheme 2.15. Arborescent polystyrene synthesis by grafting onto chloromethylated polystyrene substrates.

The *grafting onto* strategy developed for arborescent polystyrene was subsequently extended to the synthesis of different arborescent homopolymers of polyisoprene[119] and polybutadiene,[120] but also to graft copolymers potentially useful as drug nanocarriers such as arborescent polystyrene-*graft*-poly(2-vinylpyridine)[121] and polystyrene-*graft*-poly(methacrylic acid).[122] Fully biocompatible arborescent polymers constructed from poly(γ-benzyl L-glutamate) (PBG) side chains were also synthesized recently via successive grafting reactions (Scheme 2.16).[123] In this case linear PBG building blocks were obtained by the ring-opening polymerization of γ-benzyl L-glutamate *N*-carboxyanhydride initiated by *n*-hexylamine. A fraction of the benzyl groups on a linear

PBG substrate were deprotected and coupled with linear PBG using *N*,*N*'-diisopropylcarbodiimide and 1-hydroxybenzotriazole as coupling agents to give a generation zero (G0) arborescent PBG. Further partial deprotection and grafting cycles led to arborescent PBG reaching $M_n > 10^6$ g/mol and $M_w/M_n = 1.06$ for a G3 polymer. Amphiphilic PBG-based arborescent copolymers incorporating a hydrophilic shell of poly(ethylene oxide), polyglycidol or poly(glutamic acid), potentially very useful for drug release, have also been reported.[124] Very recently, doxorubicin hydrochloride (DOX·HCl) was loaded into hydrophilic arborescent poly(L-glutamic acid)-*g*-poly(ethylene oxide) copolymers via electrostatic interactions between the anionic polypeptide core and the cationic drug, to achieve a loading content of 14% w/w and a loading efficiency of 83%. Drug release from the loaded micelles was sustained over 1 month at 37 °C. The release rate was slow at physiological pH (7.4) but significantly increased at pH 5.5, mimicking the endosomal environment, suggesting pH-responsive release of DOX from the micelles.[125]

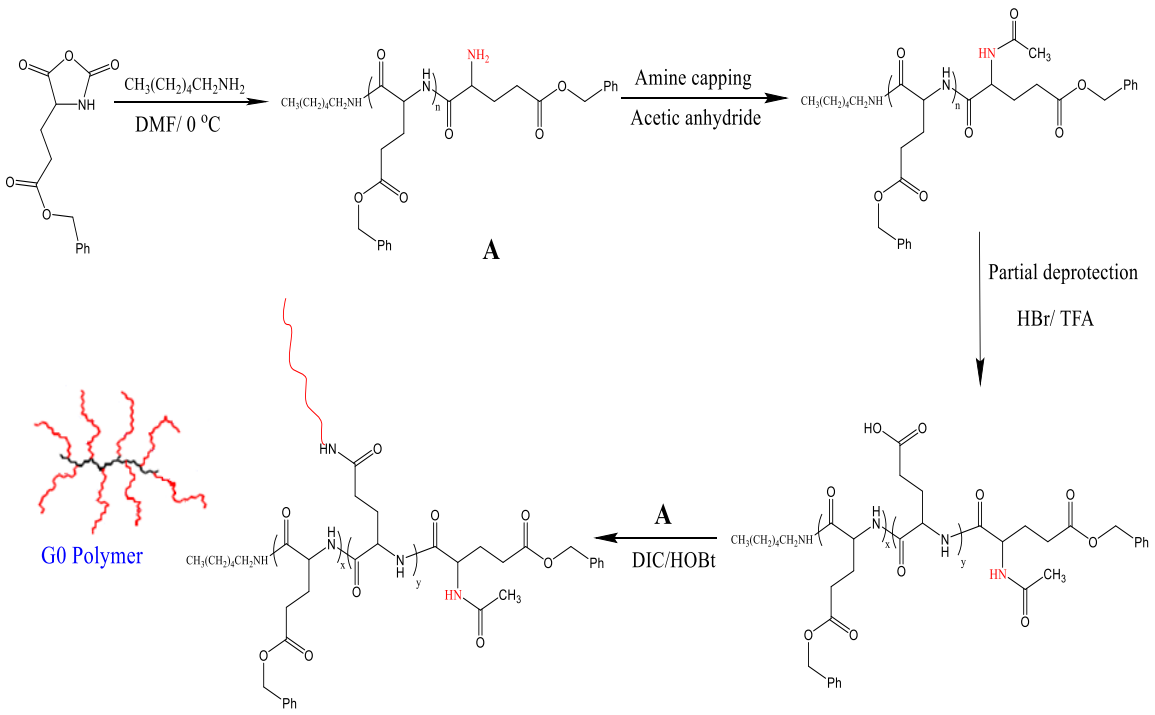

Scheme 2.16. Synthesis of G0 arborescent PBG with a comb-branched structure.

The arborescent polystyrene-*graft*-poly(2-vinylpyridine) copolymers were also tested as model drug delivery systems. Njikang et al. thus investigated the encapsulation in aqueous solutions of various polycyclic aromatic hydrocarbon (PAH) probes within the hydrophobic core of arborescent polystyrene-*graft*-poly(2-vinylpyridine) (PS-*g*-P2VP) unimolecular micelles with different structures.[126] The study showed that the copolymers with a high polystyrene content were far better sorbents, albeit the capacity difference was less important for the less hydrophobic probes such as naphthalene. Variations in the structure of the unimolecular micelles also had a significant influence on the solubilization process: The highly hydrophobic probes were solubilized mostly in the hydrophobic core, while those of higher polarity remained in the ionic shell and the core-shell interfacial

region. The solubilization capacity of copolymers of similar composition was also lower for the higher generation samples, presumably due to their increased structural rigidity. In a subsequent study, the release characteristics of these systems loaded with indomethacin and lidocaine as model drugs were investigated.[127] The *in vitro* release of indomethacin and lidocaine in dilute HCl solutions was sustained, with an initial burst followed by slower release. The arborescent PS-*g*-P2VP copolymers used in this investigation were obviously not biocompatible, and the *in vitro* test conditions were different from real biological systems. These results were nevertheless useful in showing that the solubilization and release characteristics of arborescent copolymers could be controlled through variations in their structure and composition, and to understand the influence of branching on the release profile.

The efforts dedicated initially to the synthesis of dendrigraft polymers, namely the arborescent and Comb-burst® polymers, inspired many researchers to develop other strategies for the synthesis of related materials in recent years. A broad range of branched polymer architectures have been reported in the literature as a result of this, and the naming of these polymers likewise varied extensively. Selected examples of the different architectures reported, and a discussion of their potential as drug nanocarriers are provided below.

Dendrigraft polymers can be designed to have a core-shell morphology, to behave like covalently bonded unimolecular micelles. These can be designed to have therapeutic drug carrying ability, to act as imaging agents, and may be functionalized with targeting ligands for a wide range of biomedical applications. For example, drug nanocarriers that also act

as imaging agents can be easily monitored *in vivo* to determine their biodistribution by fluorescence microscopy.[70] Different strategies have been proposed to obtain fluorescent drug nanocarriers including the encapsulation or conjugation of organic dyes, and the use of inorganic fluorescent nanocarriers or other metallic nanoparticles.[128] Yang et al. thus reported novel biodegradable photoluminescent polymers (BPLPs)[129] that were used by Gong et al. to construct fluorescent multi-arm star amphiphilic block copolymer drug nanocarriers.[130] This was achieved by first reacting citric acid with 1,8-octanediol, followed by condensation with L-cysteine via their carboxyl group to yield a hydrophobic fluorescent BPLP segment as shown in Scheme 2.17. In a second step, an amphiphilic linear block copolymer BPLP-PEG-cRGD was synthesized by conjugating the hydrophilic PEG segment with cRGD peptide, and then with the BPLP. Finally, fluorescent unimolecular micelles H40-BPLP-PEG-cRGD were obtained with a weight-average molecular weight of 1.6×10^5 g/mol and PDI of 1.43 by conjugating the BPLP-PEG-cRGD block copolymer with Boltorn® H40 (a 4th generation hyperbranched polymer) core through an esterification reaction. The successful encapsulation of DOX within the hydrophobic core was demonstrated by achieving a drug loading of 15.7 wt %. The multi-arm star amphiphilic block copolymer H40-BPLP-PEG-OCH_3/cRGD thus not only proved to be a promising candidate as a tumor-targeting drug nanocarrier, but also as a bioimaging probe.

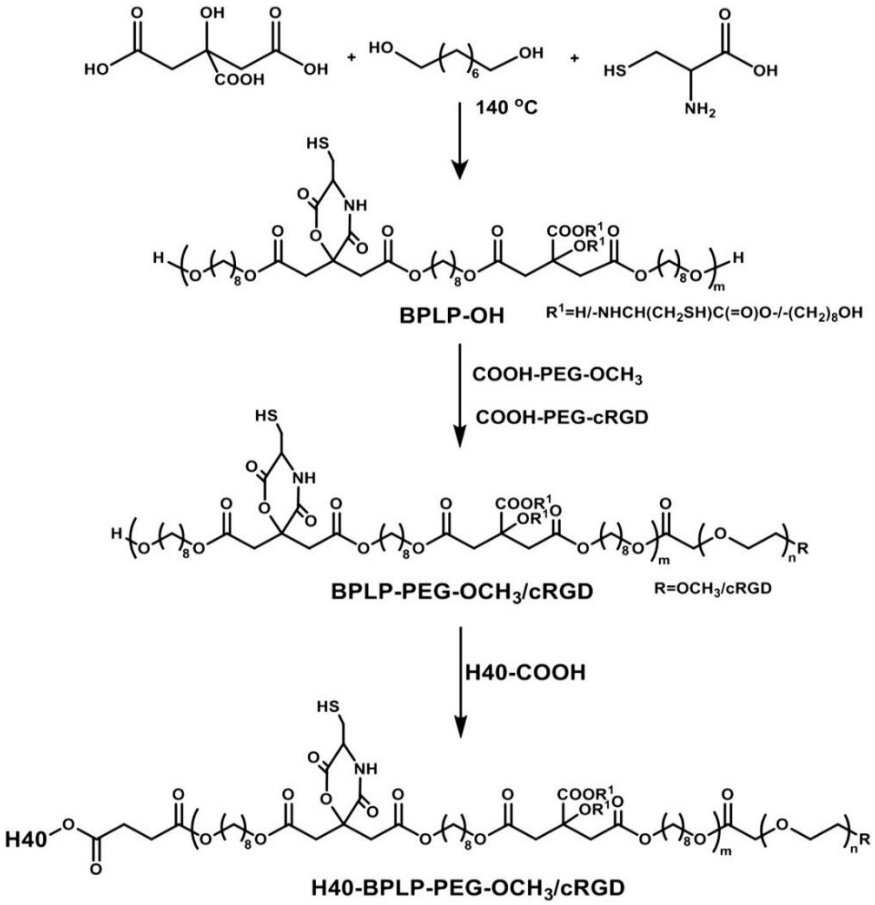

Scheme 2.17. Synthesis of fluorescent multi-arm star amphiphilic block copolymer H40-BPLP-PEG-OCH3/cRGD.

Reprinted from ref. 129, with permission from John Wiley & Sons, Inc.

One major limitation to the simple physical entrapment of a drug within the core of dendritic polymers is that it is difficult to precisely control the rate of drug release. This may lead to rapid drug release before the dendritic polymers reach their designated targets, and thus result in low therapeutic efficacy, apart from eliciting severe side effects.[73] As mentioned earlier, much attention has been paid to covalent drug conjugation to further improve drug delivery efficacy. However, the covalent conjugation chemistry must be

carefully selected to allow bond cleavage and release of the drug molecules under specific biological conditions. For instance, water-soluble and pH-responsive star polymers analogous to the dendrimer-like systems, including imaging probes, were obtained for the treatment and/or visualization of solid tumors.[131] The star polymer nanocarriers were prepared by coupling semitelechelic or heterotelechelic *N*-(2-hydroxypropyl)methacrylamide copolymers containing thiazolidin-2-thione end groups with the terminal amino groups of PAMAM dendrimers. Controlled radical RAFT polymerization was used for the synthesis of a multivalent copolymer of *N*-(2-hydroxypropyl)methacrylamide with a Boc-protected hydrazide group-bearing monomer (copolymers 1 and 2 in Scheme 2.18). The anticancer drug DOX was then attached via pH-sensitive hydrazine linkages. Finally dibenzocyclooctyne (DBCO), a fluorescent dye, was conjugated with the star polymer by a copper-free click reaction. The study demonstrated that the nanocarriers were able to effectively deliver DOX to solid tumors in a controlled manner.

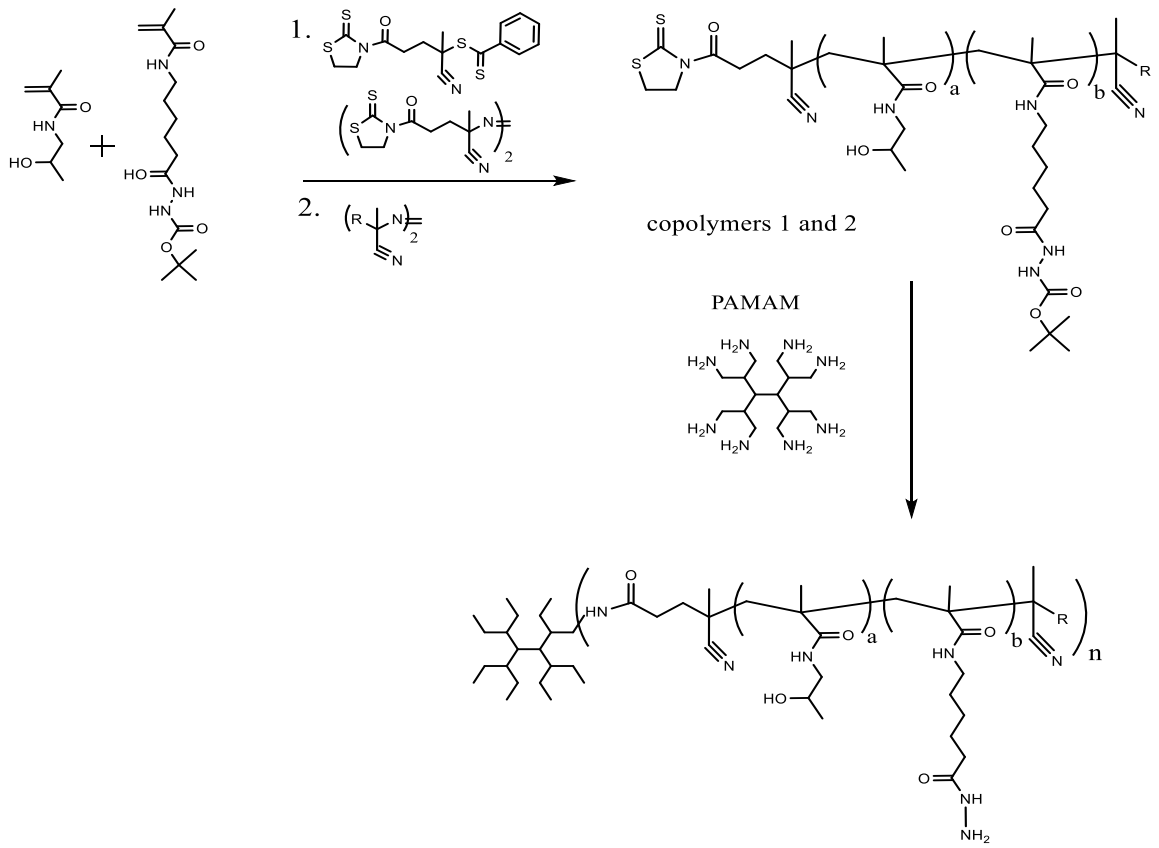

Scheme 2.18. Synthesis of star copolymers prepared by RAFT polymerization.

2.2.3.2 Divergent *Grafting From* Strategy

The divergent *grafting from* method starts with a substrate acting as a multifunctional initiator, from which polymer chains are grown. Unfortunately, in most cases it is difficult to characterize the structure of the graft polymers generated by this approach, and the molecular weight distribution of the products is generally broad; thus this method has received less attention than the *grafting onto* strategy. In spite of these limitations, this approach has allowed the synthesis of novel dendritic polymers inaccessible by other methods. The first example of this methodology was reported in 1995 by Six and Gnanou for the synthesis of dendrimer-like star poly(ethylene oxide) through a strictly controlled

terminal branching process.[132] This involved the synthesis of a star polymer, and conversion of the terminal groups to a difunctional initiator to allow chain extension for the synthesis of the next generation. They also obtained amphiphilic and water-soluble dendrimer-like star polymers by similar strategies.[133-135] The preparation of a dendrimer-like star polymer incorporating three poly(ethylene oxide) and six poly(acrylic acid) side chains by a combination of living anionic polymerization of ethylene oxide (EO) and subsequent atom transfer radical polymerization (ATRP) of *tert*-butyl acrylate, followed by hydrolysis, is provided in Scheme 2.19 to illustrate this strategy.

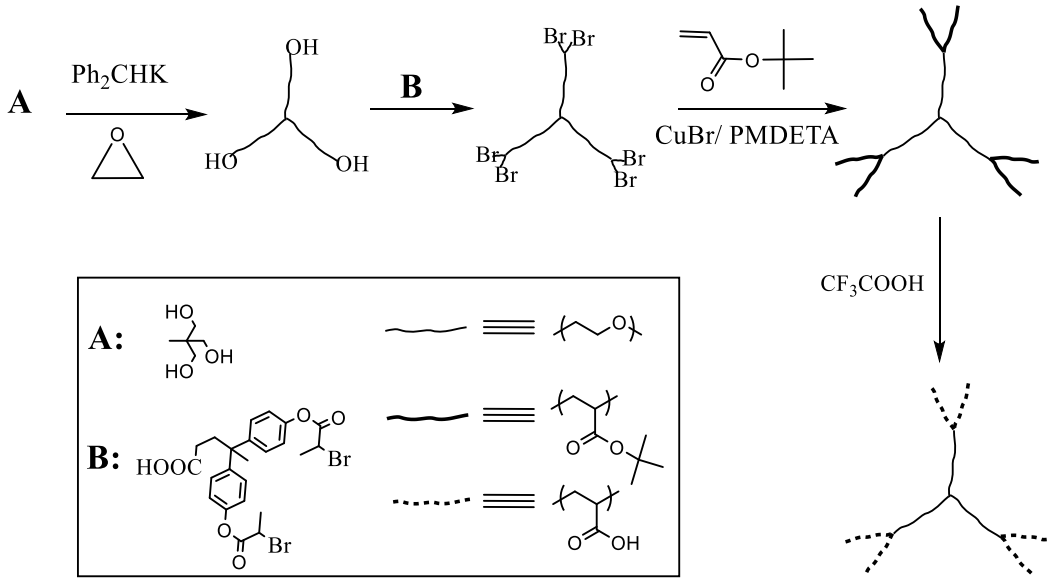

Scheme 2.19. Synthesis of a dendrimer-like star copolymer with a poly(ethylene oxide) core and poly(acrylic acid) side chains.

In comparison to traditional linear polymers, dendritic polymers have a large number of functional groups – on the surface of the dendritic core, along or at the end of the polymer-forming arms – which can be used for two, or even more different tasks such as

to deliver a drug, to serve as a targeting agent, and as a probe for imaging. Thus the construction of multifaceted dendritic polymers – also called Janus micelles – with different types of peripheral groups to perform multiple functions is in high demand for biomedical applications. Recently, Gnanou and coworkers constructed Janus-type dendrimer-like poly(ethylene oxide) molecules (PEOs) of three generation carrying terminal hydroxyl groups on one side and cleavable ketal groups on the other, that were conjugated with folic acid (FA) to target folate receptors, and subsequently used to encapsulate camptothecin (CPT) as a therapeutic agent (Figure 2.10).[136] The conjugation of both small molecules was accomplished by click chemistry based on 1,3-dipolar cycloaddition.

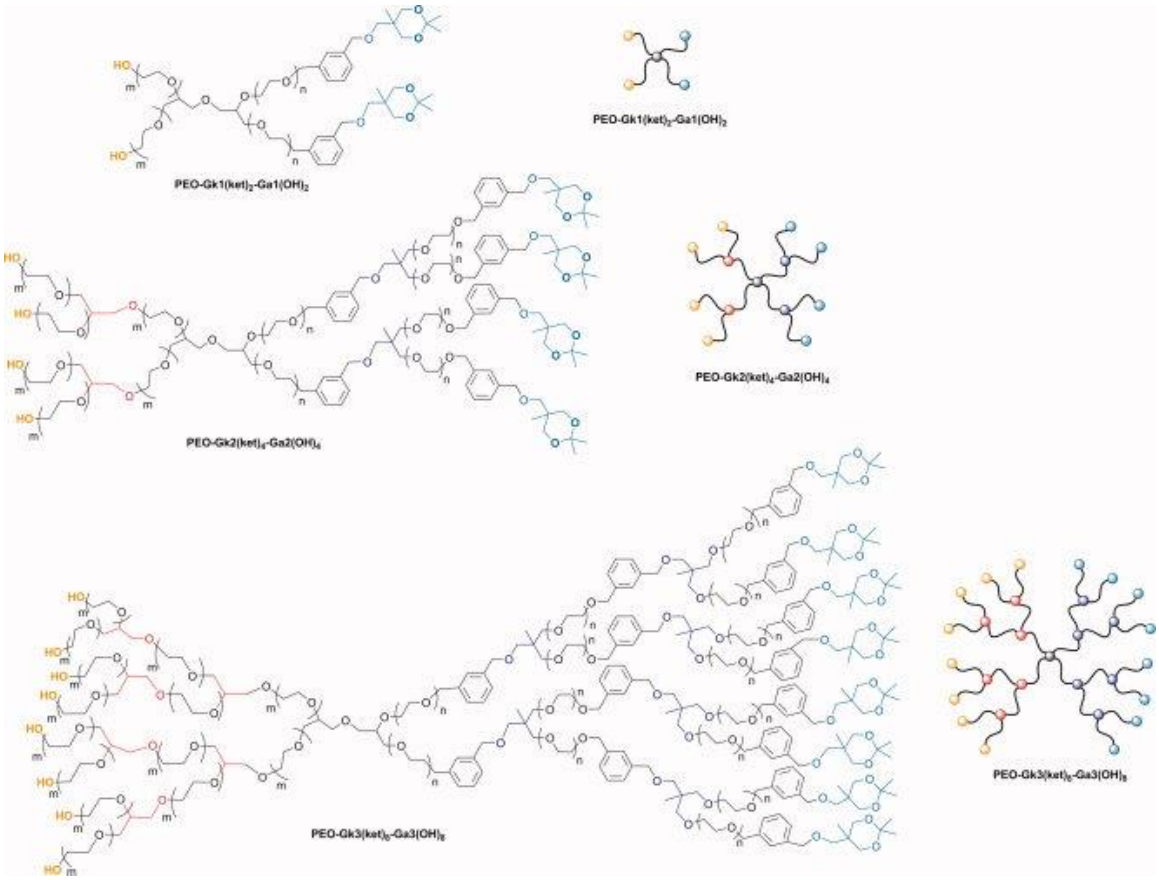

Figure 2.10. Structure of three Janus-type dendrimer-like PEOs used for conjugation.

Reprinted from ref. 135, with permission from John Wiley & Sons, Inc.

Structural variables such as the size and porosity of dendrigraft polymers can be designed to meet specific requirements for drug delivery applications. For example, the loading and release properties of these materials can be tailored by adjusting the composition, the branching density and the size of the side chains in the core and the corona. Very recently, Libera et al. evaluated the effects of macromolecular composition and structure on the encapsulation efficiency. They synthesized dendritic copolymers containing a hydrophobic core of poly(*tert*-butyl glycidyl ether) of controllable density,

and a hydrophilic polyglycidol shell with a comparable molar mass and number of hydroxyl groups by anionic sequential polymerization.[137] The poorly water-soluble ruthenium complex $Ru(NH_3)_3Cl_3$, a potential anticancer drug, was either encapsulated within the hydrophobic core of the nanoparticles by entrapment from a suspension in water or water/methanol mixtures, or bound to the polymer shell by complexation with the hydroxyl groups. The solubilization capacity of two dendritic copolymers with different core densities did not differ significantly, but interestingly, the copolymer with the lower molar mass and smaller hydrodynamic radius core had a higher encapsulation efficiency in both encapsulation methods.

One advantage of dendritic nanocarriers is that they can be designed as delivery systems for combined drugs, to maximize their therapeutic effect on tumors. Thus He et al. prepared a unimolecular micelle-like multilayered nanocarrier (PPDP) based on polyamidoamine (PAMAM) dendrimers as dual drug (paclitaxel and doxorubicin) containers, by combining a layer of hydrophobic oligo(3-caprolactone) (PCL) with hydrophilic PEGylated amidoamine dendrons within each molecule (Scheme 2.20).[138] Two nanocarrier variations were examined, either by encapsulating DOX and PTX in the different layers of the carrier (PPDP-enc-DOX + PTX), or by conjugating DOX through a pH-sensitive linkage on the exterior and encapsulating PTX in the core of the nanocarrier (PPDP-coj-DOX-enc-PTX) as shown in Scheme 2.20. The study showed that for both systems, the release of PTX was achieved in a sustained manner over 48 h *in vitro*. The DOX release profile displayed a burst for the PPDP-enc-DOX + PTX system, while for the PPDP-coj-DOX-enc-PTX system the DOX release profile was sustained. Both systems displayed higher cytotoxicity

towards MCF-7/ADR and MCF-7 cells than free DOX and PTX alone, due to the synergistic effect of the drugs.

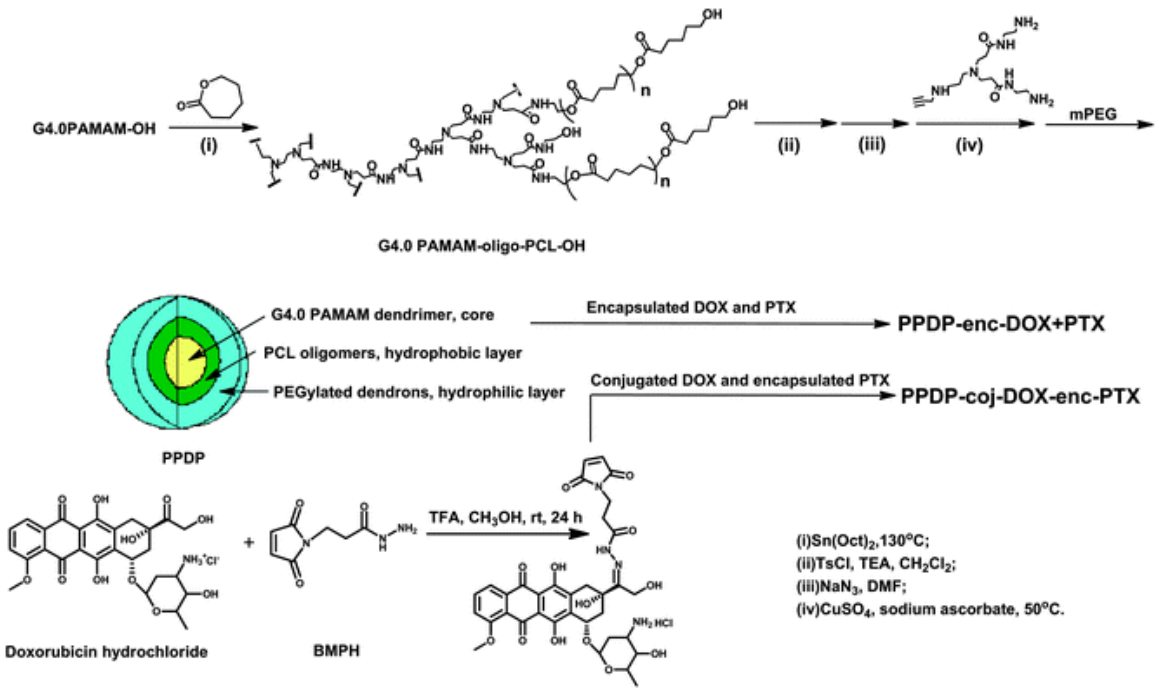

Scheme 2.20. Synthesis of PAMAM dendrimer-based multilayered drug delivery systems.

Reproduced from ref. 137, with permission from Royal Society of Chemistry.

Dendrimer-like star polymers are typically composed of a hydrophobic star polymer core and a shell of hydrophilic arms, which makes them very attractive for drug delivery applications. Their large number of surface functional groups can serve not only to conjugate drugs, but also ligand molecules for targeted delivery. For instance, a folate-functionalized degradable amphiphilic dendrimer-like star polymer (FA-DLSP) incorporating a well-defined poly(L-lactide) (PLLA) star polymer as hydrophobic core and six hydrophilic polyester dendrons based on 2,2-bis(hydroxymethyl)propionic acid

forming a hydrophilic shell was successfully synthesized by a combination of living ring-opening polymerization (ROP) of L-lactide and dendrimer synthesis.[139] To further enhance the water solubility of the unimolecular micelles, their surface was functionalized with carboxylic acid groups that were coupled with PEG segments (Scheme 2.21), and then with folate groups. The hydrophobic anticancer drug DOX was successfully encapsulated into the hydrophobic core of the micelles, with a drug loading of 4 wt% as determined by spectroscopic analysis. The *in vitro* release study showed that release of the encapsulated DOX was strongly pH-dependent: DOX was released more rapidly at pH 5.3 than that at pH 7.4, because of the higher solubility of DOX in water at lower pH. Cellular uptake studies showed that the FA-DLSP micelles had greater cellular uptake than FA-deficient DLSP. The above results suggest that the FA-DLSP unimolecular micelles may be promising nanocarriers for targeted cancer therapy.

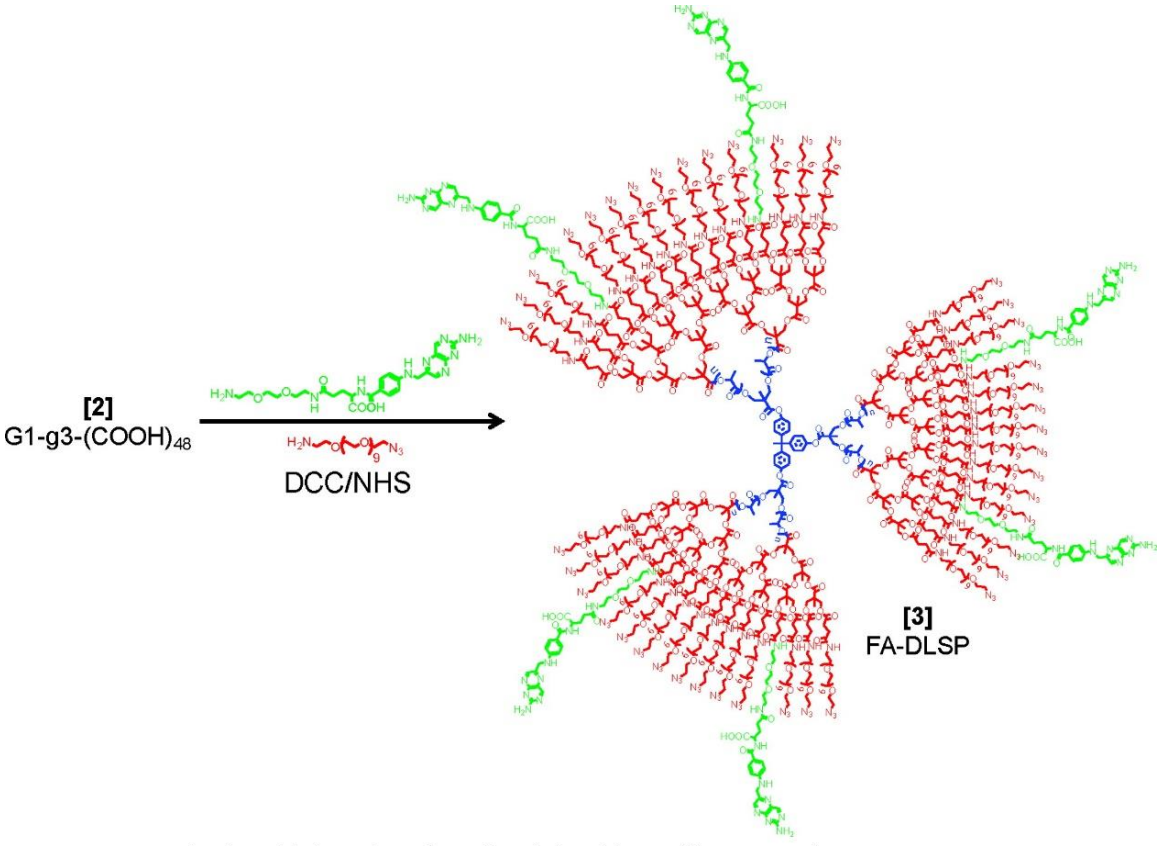

Scheme 2.21. Synthesis of a folate-functionalized dendrimer-like star polymer, FA-DLSP.

Reprinted with permission from "Cao, W.; Zhou, J.; Mann, A.; Wang, Y.; Zhu, L. Biomacromolecules 2011, 12, 2697". Copyright 2011 American Chemical Society.

2.2.3.3 Convergent *Grafting Through* Strategy

Puskas et al.[140] developed the first convergent cationic polymerization strategy to synthesize arborescent isobutylene homopolymers in a single reaction pot. This was achieved by the cationic copolymerization of isobutylene with a small amount of an inimer such as 4-(2-methoxyisopropyl) styrene to yield a "living" branched polymer structure with multiple cationic active sites at the chain ends, which were subsequently used to initiate the polymerization of styrene as shown in Scheme 2.22.[141]

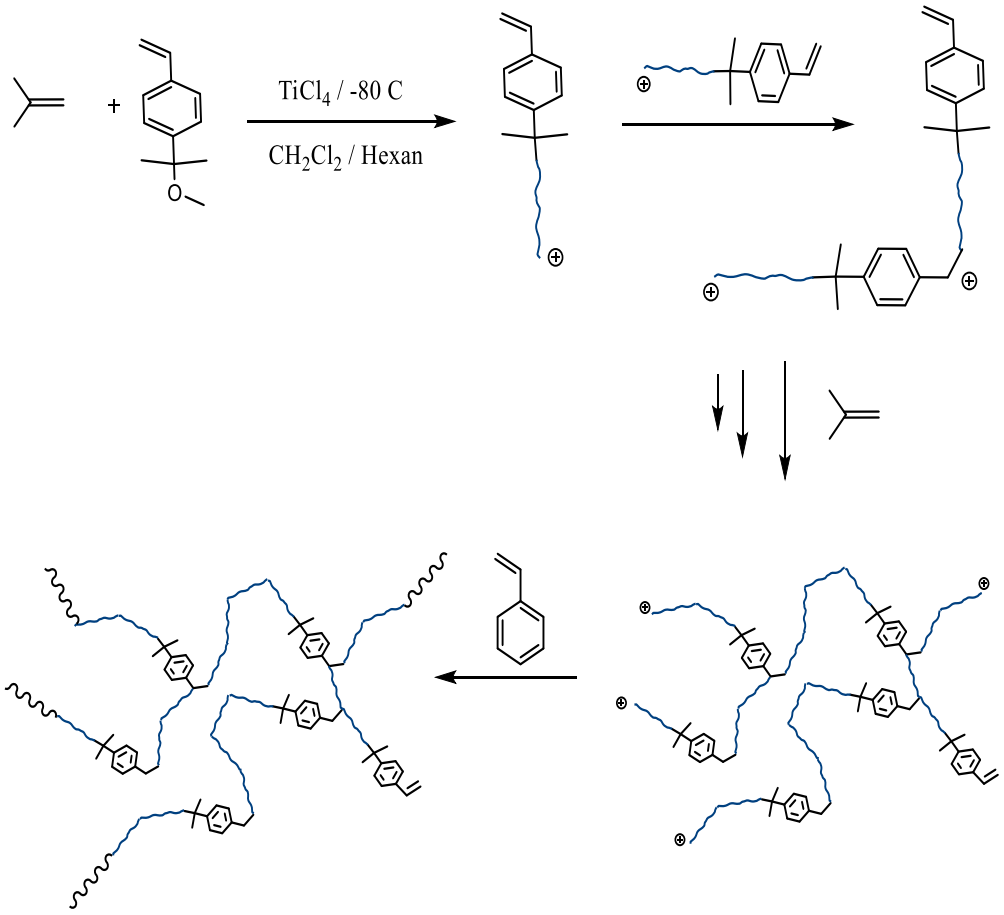

Scheme 2.22. One-pot synthesis of hyperbranched polyisobutylene with polystyrene end-blocks.

The approval of polystyrene-*b*-polyisobutylene-*b*-polystyrene linear triblock copolymers by the Food and Drug Administration (FDA) as a coating material on the Taxus® coronary stent has opened a new door for polyisobutylene-based biomaterials. For instance, Puskas and Hoerr also studied drug release from arborescent polyisobutylene with polystyrene end blocks. ElectroNanospray™, a proprietary technology for coating materials on the surface of medical devices, was used to coat coronary stents with arborescent polyisobutylene-*b*-polystyrene loaded with Dexamethasone, a model drug. The

study showed that the drug release profiles were influenced by both the molecular weight of the dendritic polyisobutylene-*b*-polystyrene scaffold and by the spraying conditions used for the polymer-drug mixture.[142]

Characteristics such as the size and porosity of amphiphilic dendrigraft copolymers can be designed to meet specific requirements for drug delivery applications by adjusting their composition, branching functionality, generation number, and the size of the side chains in their core and corona. Internal functionality can be introduced easily within the repeating units in many cases. Furthermore, as mentioned earlier, dendrigraft copolymers can be produced in one-pot reactions in some cases with very high molecular weights and relatively narrow molecular weight distributions. As a result, dendrigraft polymers seem to represent a good compromise solution between achieving a low dispersity comparable to dendrimers and maintaining a reasonably low production cost. We therefore believe that these materials have great potential in drug delivery applications.

2.3 Conclusions

Drug delivery systems overcome the limitations of traditional chemotherapy by improving its efficacy and safety through controlling the rate, time, and place of release of drugs in the body. A broad range of drug delivery systems have been developed over the last 10 years. Among these systems, polymeric micelles including amphiphilic block copolymers micelles, unimolecular micelles and crosslinked micelles have been shown to improve drug bioavailability, enhance their aqueous solubility, increase the circulation time of drugs in the blood, and allow their delivery to a specific target. In this context,

polymeric micelles with tunable properties have shown a great promise and are in the front line of development for drug delivery systems.

Dendritic polymers are a unique and versatile class of branched polymers ideal for a number of high value applications, and particularly for drug delivery. Numerous methods have been reported to synthesize dendritic polymers while achieving control over the characteristics of the polymers, to achieve desirable properties or functionality. While the commercialization of dendrimers has been restricted by their tedious and costly synthesis, the one-pot syntheses reported for hyperbranched and dendrigraft polymers make these materials more viable for (large scale) commercial production and applications. The field of dendritic drug delivery nanocarriers has rapidly evolved over the past decade, with an increasing number of candidates currently being under clinical evaluation. A wide range of dendritic polymer architectures and chemistries are currently being developed specifically for drug delivery applications. The collaboration between polymer chemists, medicinal and pharmaceutical scientists, and clinicians is critical for the development of clinical applications for practical uses of these nanocarriers.

Chapter 3 Synthesis Optimization of Arborescent Polypeptides

3.1 Overview

Polypeptides are receiving increasing attention as building blocks to create nanostructures for biomedical applications. The goal of this investigation was to explore the influence of the reaction conditions in the synthesis of well-defined dendritic graft (arborescent) polypeptides from amine-terminated poly(γ-benzyl L-glutamate) (PBG) chains. The ring-opening polymerization of γ-benzyl L-glutamate *N*-carboxyanhydride (Glu-NCA) was initiated by different initiators to yield linear PBG building blocks. Cleavage of a fraction of the benzyl groups on a linear PBG substrate and coupling with linear PBG side chains using a carbodiimide reagent yielded a comb-branched or generation zero (G0) arborescent PBG. The optimization was carried out in terms of the reaction temperature, solvent, reaction time, and mole ratio of reactants and coupling agents. Two carbodiimide reagents, namely *N,N′*-diisopropylcarbodiimide (DIC) and 1-ethyl-3-(3-dimethylaminopropyl)carbodiimide hydrochloride (EDC·HCl) in combination with 1-hydroxybenzotriazole (HOBt) as a coupling additive were used to increase the reactivity of the carboxyl groups. The graft polymers were characterized by size exclusion chromatography (SEC) and NMR spectroscopy analysis. Size exclusion chromatography served to evaluate the grafting reaction in terms of grafting yield (fraction of side chains coupled with the substrate) and coupling efficiency (fraction of coupling sites consumed on the substrate). The maximum grafting yield and coupling efficiency achieved under the optimized conditions were 67% and 74%, respectively.

3.2 Introduction

Dendritic polymers are a type of macromolecules characterized by a highly branched tree-like architecture, incorporating multiple branching levels, resulting from coupling reactions of either small molecule monomers (hyperbranched polymers and dendrimers), or macromolecular building blocks (dendrigraft polymers).[1,2] The unique structure and interfacial features of dendritic polymers make them suitable for biomedical applications such as nanocarriers for drugs, genes and diagnostic agents.[3-5] Dendrigraft polymers (referring collectively to arborescent and dendrimer-like star polymer structures) are the third and most recently reported subset of dendritic polymers.[6,7] Whereas monomers are invariably employed in constructing dendrimers, reactive polymers serve as building blocks in successive grafting reactions for the synthesis of dendrigraft molecules. Since a large number of coupling sites are randomly distributed on the grafting substrates, a rapid increase in molar mass is observed for each arborescent polymer generation while a narrow molar mass distribution ($M_w/M_n < 1.1$) is maintained.

Polypeptides are receiving increasing attention as building blocks to construct nanostructures for biomedical applications such as micelles.[8] The development of synthetic polypeptides with tunable dendritic topologies and well-defined structures is therefore of great interest. Peptides are commonly synthesized by sequential coupling of the carboxylic group of one amino acid with the amino group of another amino acid as shown in Scheme 3.1.[9] A wide range of methods have been developed for that purpose.[9-11]

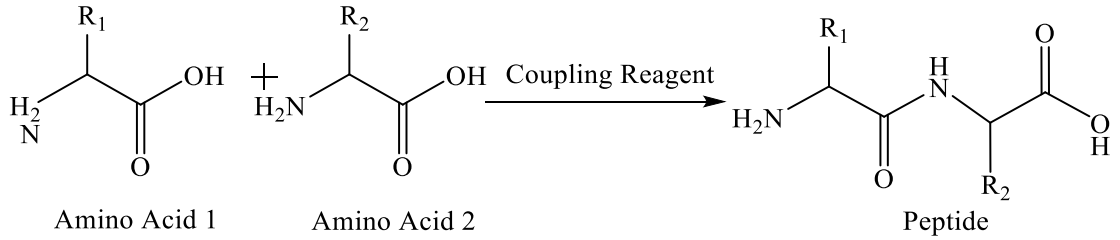

Scheme 3.1. General peptide coupling reaction.

Peptide coupling is performed in the presence of coupling reagents, which allows the reaction to occur under mild conditions while minimizing side reactions. Carbodiimide reagents such as *N,N*'-dicyclohexylcarbodiimide (DCC) and *N,N*′-diisopropylcarbodiimide (DIC) have been widely used, and are still in use today to activate the carboxylic acid group of amino acids.[12] Some of the reagents commonly used in peptide coupling are shown in Figure 3.1.[10]

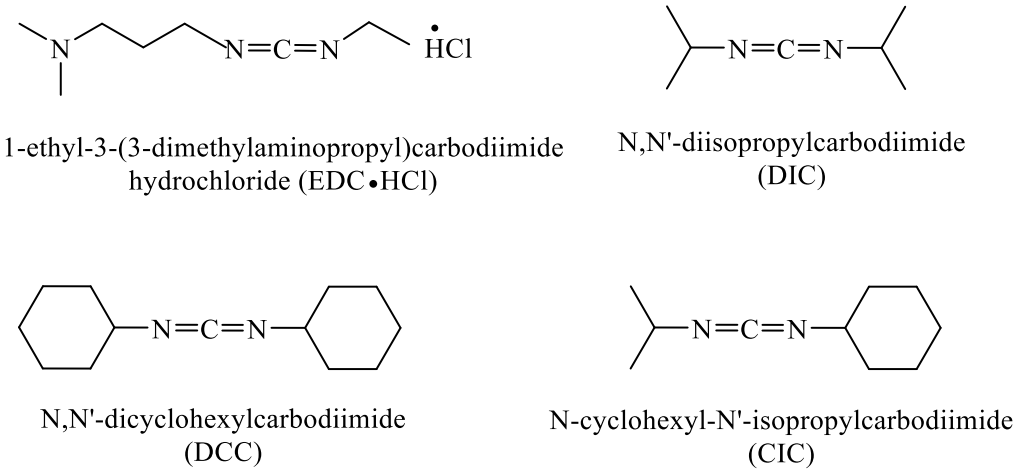

Figure 3.1. Commonly used carbodiimide reagents.

The general mechanism of activation by carbodiimides is shown in Scheme 3.2. The initial step is the addition of the carboxylic group of the amino acid to the carbodiimide to form an *O*-acylisourea, a species that rapidly reacts with amine groups to yield a peptide bond and produces the corresponding urea as a by-product (path A, Scheme 2.3). The *O*-acylisourea may also undergo attack by a second acid group to give the symmetrical anhydride, if an excess of carboxylic acid is used (path B, Scheme 2.3). The anhydride can also react with the amine to give the peptide. Furthermore, an undesirable rearrangement of the highly reactive *O*-acylisourea may occur (path C, Scheme 2.3) to give a highly stable *N*-acylurea. The high reactivity of carbodiimides allows fast reactions, however its use alone as a coupling reagent decreases the coupling efficiency due to the side reactions described above.[11,13]

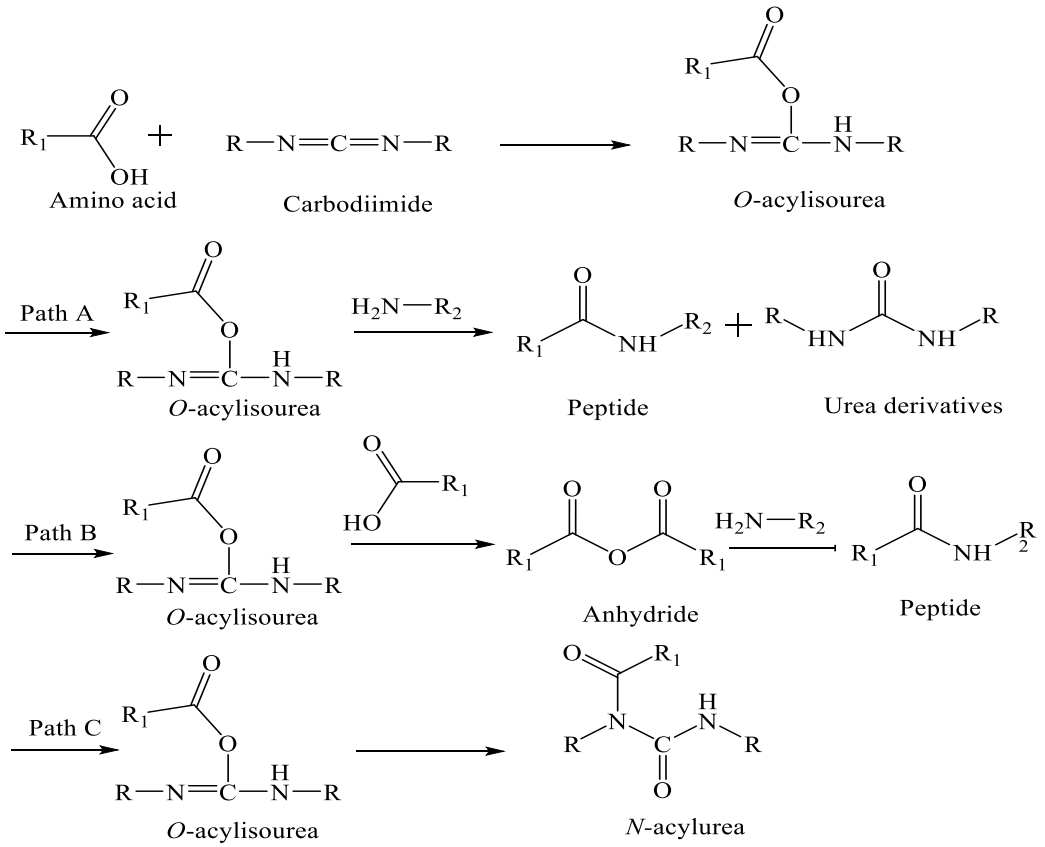

Scheme 3.2. Activation of an amino acid by a carbodiimide and side product formation.

Nowadays, most peptide bond-forming reactions are done in the presence of additives such as 1-hydroxybenzotriazole (HOBt) or 1-hydroxy-7-azabenzotriazole (HOAt) to inhibit side reactions.[14-16] These additives react with the *O*-acylisourea to form the corresponding active esters that are less reactive than *O*-acylisourea. These additives also increase the efficiency of carbodiimide-mediated reactions by preventing the formation of the *N*-acylurea, and thus increase the coupling yield as shown in Scheme 3.3.[10]

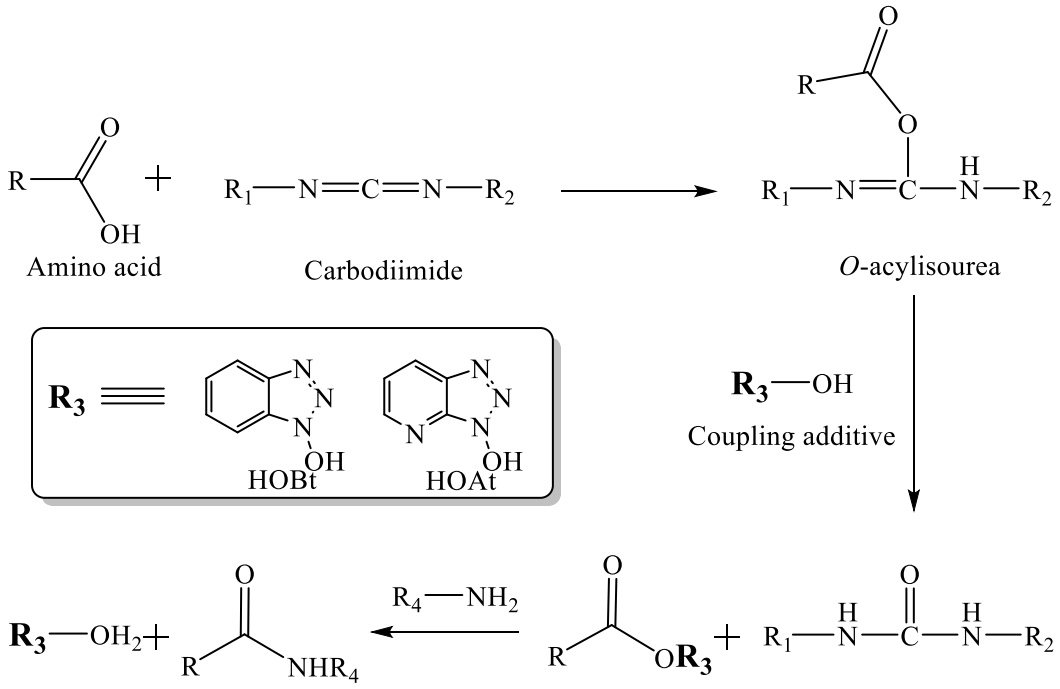

Scheme 3.3. Activation of an amino acid by onium reagents such as HOBt and HOAt.

One of the most facile routes to the preparation of polypeptides is through the polymerization of α-amino acid *N*-carboxyanhydrides (NCAs). Our laboratory used this latter approach for the synthesis of well-defined (M_w/M_n<1.07) arborescent polypeptides using poly(γ-benzyl L-glutamate) (PBG) building blocks. Molar masses reaching 1.1×10^6 were thus obtained, but the grafting yield (fraction of side chains reacted) and the coupling efficiency (fraction of coupling sites reacted) for this system were limited to 62% and 41%, respectively.[17] Considering that every peptide is susceptible to different side reactions, it is impossible to develop a universal procedure for the synthesis of these materials.

One of our goals was to further optimize the grafting yield and the coupling efficiency in the synthesis of arborescent polypeptides derived from PBG. Different carbodiimide coupling reagents and additives were investigated to promote the availability of the amino termini and/or to increase the reactivity of the carboxyl groups in the coupling reaction. The optimization was also carried out in terms of the reaction temperature, solvent, reaction time, and mole ratio of reactants and coupling agents. Size exclusion chromatography (SEC) analysis served to evaluate the grafting reaction in terms of grafting yield and coupling efficiency. The arborescent polypeptides thus obtained can serve as intermediates in the preparation of unimolecular micelles, potentially useful for controlled drug delivery applications.

3.3 Experimental Procedures

3.3.1 Characterization and Sample Preparation

Proton nuclear magnetic resonance (^{1}H NMR) spectroscopy was used to estimate the degree of polymerization of linear poly(γ-benzyl L-glutamate) (PBG), and to determine the deprotection level of the PBG substrates. The instrument used was a Bruker 300 MHz spectrometer. Fluorine Nuclear Magnetic Resonance ^{19}F NMR spectroscopy on the same instrument was used to determine the chain end primary amine functionality level, f_{NH2}, of the polymers used in the grafting reactions.

Analytical SEC was used for the characterization of the PBG substrates, the PBG side chains, the crude reaction products, and the purified graft polymers. The analytical SEC

system consisted of a Waters 510 HPLC pump, a 50 μL injection loop, a Waters 2410 differential refractometer (DRI) detector, and a MiniDAWN laser light scattering detector operating at a wavelength of 690 nm, to allow the determination of the absolute molecular weight of the samples. A Jordi DVB Mixed-bed Linear column (500 mm × 10 mm, molecular weight range 10^2 – 10^7 g/mol) was used for the separation. The system was operated at a flow rate of 1 mL/min at room temperature (25 ˚C), using *N*,*N*-dimethylformamide (DMF) with LiCl (1 g/L) as the mobile phase.

Preparative SEC was carried out on a system consisting of a Waters M45 HPLC pump, a 2 mL sample injection loop, a Waters R401 differential refractometer detector, and a Jordi Gel DVB 1000 Å, 250 mm × 22 mm preparative SEC column. *N*,*N*-Dimethylformamide with 0.2 g/L LiCl served as the mobile phase. The concentration of the crude polymer injected was around 25 mg/mL. The system was operated at a flow rate of 3 mL/min at room temperature (25 ˚C).

3.3.2 Solvent and Reagent Purification

Dimethyl sulfoxide and *n*-hexylamine were purified by stirring overnight with CaH_2 and distillation under reduced pressure. *N*,*N'*-Dimethylformamide serving in the polymer synthesis (DMF; Aldrich, >99%), 3-amino-1-propanol and 5-amino-1-pentanol were purified by distillation under reduced pressure. Ethyl acetate (Fisher, 99.9%) was distilled from $LiAlH_4$ under nitrogen. γ-Benzyl L-glutamic acid (Bz-Glu; Bachem, >99%), diethyl ether (EMD Millipore OmniSolv), HBr solution (Aldrich, 33% in acetic acid), *N*,*N*'-diisopropylcarbodiimide (DIC; Aldrich, 99%), triphosgene (Aldrich, 98%), 1-ethyl-3-(3-

dimethylaminopropyl)carbodiimide hydrochloride (EDC·HCl), 1-hydroxybenzotriazole (HOBt; Fluka, water content ca. 15% w/w), tetrahydrofuran (THF, EMD Millipore OmniSolv), methanol (EMD Millipore OmniSolv), trifluoroacetic acid (TFA, Caledon, 99.9%), $LiAlH_4$ (Aldrich, 95%), acetic anhydride (Caledon, 97%), deuterated DMSO (DMSO-d_6, Cambridge isotopes, 99.9% D), and triethylamine (TEA, EMD) were used as received from the suppliers.

3.3.3 Synthesis of γ-Benzyl L-Glutamic Acid *N*-Carboxyanhydride (Glu-NCA)

The monomer was synthesized from γ-benzyl L-glutamic acid and triphosgene as described in the literature.[18] γ-Benzyl L-glutamic acid (Bz-Glu) (10.0 g; 42.0 mmol) was dissolved in 300 mL of freshly distilled ethyl acetate in a 1-L round-bottomed flask fitted with a reflux condenser and a N_2 bubbler. After heating to reflux, triphosgene (4.8 g, 16 mmol) was added at once and refluxing was continued for 3.5 h longer. The reaction was allowed to cool to room temperature, and then stored in a refrigerator (5 ˚C) for 2 h. The cold reaction mixture was transferred to a cold separatory funnel, washed with 100 mL of distilled water chilled to 0 ˚C, and 100 mL of chilled 0.5% aqueous $NaHCO_3$ solution. The ethyl acetate layer was dried over anhydrous $MgSO_4$, filtered by gravity, and concentrated to 100–120 mL on a rotary evaporator. An equal volume of cold hexane was then added to induce crystallization of the monomer. After chilling to -5 ˚C overnight, the monomer crystals were collected by filtration in a Schlenk funnel under N_2. For further purification, in some cases, the obtained monomer was recrystallized twice from *n*-hexane and ethyl acetate (*n*-hexane/ethyl acetate v/v: 2/1), to remove the last traces of HCl and remaining

impurities. The product was dried under vacuum and stored under N_2 in a freezer until used. Yield = 9.7 g (88 %); ^{1}H NMR (300 MHz, $CDCl_3$): 7.55–7.22 (s, 5H), 6.72 (s, 1H), 5.09 (s, 2H), 4.35–4.31 (t, 1H), 2.57–2.51 (t, 2H), 2.33–2.19 (m, 1H), 2.18–2.00 (m, 1H).

3.3.4 Synthesis of Poly(γ-benzyl L-glutamate) PBG Serving as Side Chains

A linear polymer serving as side chain material was synthesized as described previously.[17] Briefly, γ-benzyl L-glutamate *N*-carboxyanhydride (Glu-NCA, 12.5 mmol) was dissolved in dry DMF (8 mL) at 0 ˚C. *n*-Hexylamine (0.50 mmol, for a target X_n = 25) was then added to the monomer and the reaction was allowed to proceed for 3 days at 0 ˚C. The linear polymer was recovered by precipitation in cold methanol, centrifugation, and drying under vacuum overnight before characterization. Yield = 83%, M_w/M_n = 1.09. ^{1}H NMR (300 MHz, DMSO-d_6): X_n = 24.0, δ: 8.01 (b, 1H), 7.45–7.18 (s, 5H), 5.01–4.88 (s, 2H), 4.09–3.87 (b, 1H), 2.32–1.88 (b, 4H), 1.31–1.15 (b, 0.4H), 0.76–0.74 (s, 0.12H).

3.3.5 Synthesis of Poly(γ-benzyl L-glutamate) PBG Serving as Substrate

The Glu-NCA monomer (8.00 mmol) was dissolved in dry DMF (6.00 mL) and *n*-hexylamine (0.16 mmol, for a target X_n = 50) was added. The reaction was allowed to proceed for 4 h at room temperature. Then the reaction was quenched with acetic anhydride (310 μL, 3.26 mmol) to deactivate the terminal amine moiety. After 1 h the product was precipitated in cold methanol, centrifuged and dried under vacuum overnight before characterization. Yield = 90%, M_w/M_n = 1.19. ^{1}H NMR (300 MHz, DMSO-d_6): X_n = 49.0, δ: 8.01 (b, 1H), 7.45–7.18 (s, 5H), 5.01–4.88 (s, 2H), 4.09–3.87 (b, 1H), 2.32–1.88 (b, 4H), 1.31–1.15 (b, 0.2H), 0.76–0.74 (s, 0.06H).

3.3.6 Synthesis of Partially Deprotected Linear PBG Substrate

A linear PBG sample with X_n = 49 (1.10 g, 5.02 mmol Bz-Glu units) was dissolved in TFA (11 mL) and 0.31 mL of 33% (w/w) HBr solution in acetic acid was added. The reaction was stirred for 3 hours before the polymer was precipitated in diethyl ether and recovered by suction filtration, to yield a polymer with 29 mol % of free glutamic acid moieties. Yield = 0.65 g (69%).

3.3.7 Synthesis of G0 Arborescent PBG

In a typical coupling reaction, the partially deprotected polymer substrate (0.21 g, 0.312 mmol -CO_2H) and the polymer serving as side chains (1.67 g, 0.31 mmol chains) were dissolved in 15 mL of dry DMSO. The peptide coupling reagents DIC (0.24 mL, 1.56 mmol) and HOBt (0.21 g, 1.56 mmol) were then added to the reaction with TEA (0.22 mL, 1.56 mmol) as a base. The reaction was allowed to proceed for 36 h at room temperature before adding *n*-hexylamine (0.19 mL, 1.87 mmol), to deactivate residual activated carboxylic acid sites. After 3 h, the product was precipitated in cold methanol and recovered by suction filtration. Unreacted side chain material was removed from the G0 crude polymer by preparative size exclusion chromatography (SEC).

3.3.8 Quantification of Primary Amines by ^{19}F NMR Analysis

^{19}F NMR spectroscopy was used to determine the chain end primary amine functionality level, f_{NH2}, of the linear polymers used in the grafting reactions as described in literature.[19] The PBG sample (0.10 g, 1.72×10^{-5} mol chains) was first dissolved in 3 mL of deuterated DMSO (DMSO-d_6). A solution of 4-trifluoromethylbenzaldehyde (TFBA,

0.0901 g, 5.17×10^{-4} mol) and benzotrifluoride (α,α,α-trifluorotoluene, BTF, 0.0756 g, 6.16×10^{-4} mol) in 2 g of DMSO-d_6 was then prepared, and 0.1706 g of that reagent solution (4.563×10^{-5} mol TFBA, 4.531×10^{-5} mol BTF) was added to the PBG solution which was stirred for 2 h before it was transferred to an NMR tube for analysis.

3.4 Results and Discussion

3.4.1 Synthesis of Monomer (Glu-NCA)

The synthesis of α-amino acid *N*-carboxyanhydrides (NCAs) is a key step in the synthesis of the polypeptides used in this work. This requires a high monomer purity, in addition to a good yield in this first synthetic step. There are three main procedures for the synthesis of NCAs in the literature, namely the Leuchs and the Fuchs-Farthing methods. The Leuchs technique is based on the cyclization of *N*-alkoxycarbonyl amino acid halides, while the Fuchs-Farthing approach, based on the direct phosgenation of unprotected α-amino acids, is most convenient due to the ease of removal of by-products.[20,21] Phosgene, a highly toxic gas, was the reagent initially used in that protocol, but triphosgene was subsequently suggested as an alternative, economically viable, and solid material much safer to manipulate.[22] The preferred approach to prepare the Glu-NCA monomer in the current investigation was using triphosgene in ethyl acetate, with monomer purification as suggested by Poché et al. and as shown in Scheme 3.4.[18] The initially turbid solutions became clear during the reaction, due to the conversion of the poorly soluble amino acid into the more soluble Glu-NCA monomer. The Glu-NCA monomer thus obtained was

purified by repeated recrystallizations from *n*-hexane and ethyl acetate, to remove the last traces of HCl and remaining impurities, yielding a white crystalline material.

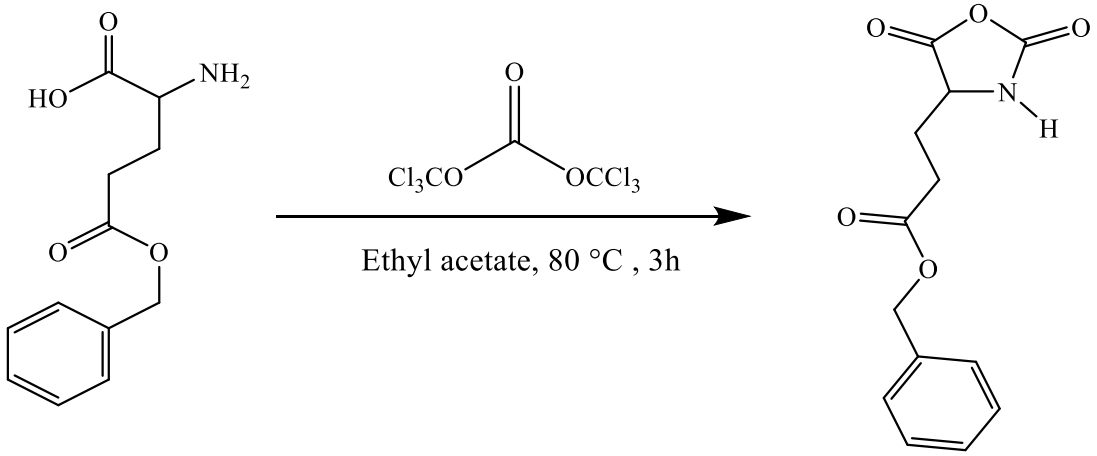

Scheme 3.4. Synthesis of γ-benzyl L-glutamic acid *N*-carboxyanhydride (Glu-NCA).

Figure 3.2 shows the ^{1}H NMR spectrum obtained for Glu-NCA in $CDCl_3$, with characteristic resonances at 2.57, 4.36, 5.11 and 7.35 ppm assigned.

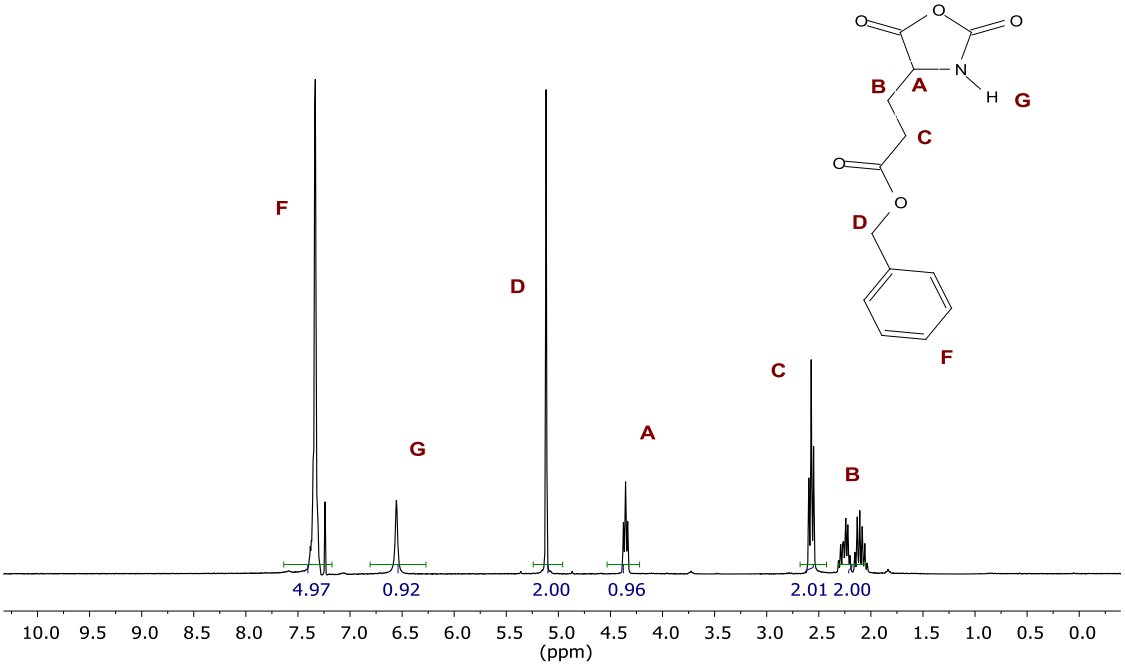

Figure 3.2. **^{1}H NMR spectrum for Glu-NCA.**

3.4.2 Synthesis of PBG Serving as Side Chains

The polymerization of Glu-NCA monomers has been widely investigated in recent years. The polymers are usually prepared through amine-initiated ring-opening polymerization (ROP) of the corresponding monomers at room temperature.[23] Unfortunately, PBG synthesized by this method is sensitive to chain termination through chain end cyclization resulting from the intramolecular nucleophilic attack of the terminal amino group on the benzyl ester functionality (Scheme 3.5). This can lead to uncontrollable molecular weights, broad molecular weight distributions, and most importantly for the current investigation, to the loss of the primary amine end group.[24-26] The amine terminus

on the PBG side chains should be preserved not only during the ring-opening polymerization of Glu-NCA, but also during sample workup and storage. It was reported that side reactions in the polymerization of NCAs could be eliminated, while also preserving the primary amine chain end of PBG, by lowering the reaction temperature.[27,28] Recently, Whitton and Gauthier reported the synthesis of well-defined (M_w/M_n<1.07) PBG with high amine functionality levels (f_{NH2} reaching 98%), using *n*-hexylamine as initiator at 0 ˚C.[17] End group cyclization in the polymerization reaction was also investigated to some extent.

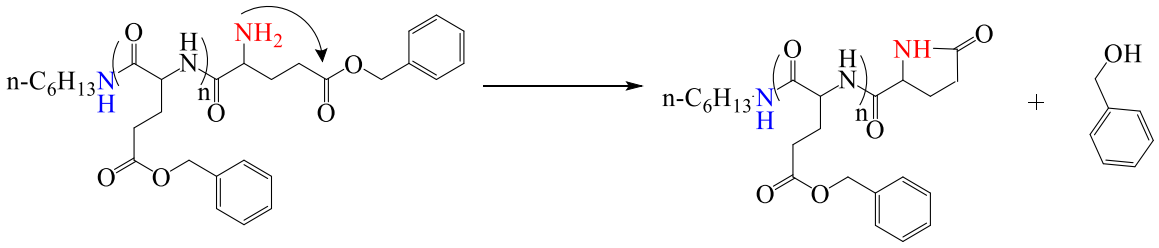

Scheme 3.5. Chain termination of linear PBG by end group cyclization.

In the current investigation, PBG with a "living" amino end group was synthesized by the ring-opening polymerization of Glu-NCA in *N*,*N*-dimethylformamide (DMF) at 0 ˚C or at 25 ˚C, using different primary amine initiators. Confronted to the difficulty of achieving a high grafting yield and coupling efficiency in the preparation of arborescent polypeptides using the peptide coupling reaction, an initiating system was sought that would provide control over the ROP of Glu-NCA and include both a primary amine (for initiation) and an alcohol functional group (for coupling via an esterification reaction), in

addition to *n*-hexylamine used previously. Steglich esterification is a widely used method under mild conditions, resulting in the condensation reaction of carboxylic acids and alcohols to form esters.[29] The reaction usually utilizes *N*,*N*′-dicyclohexylcarbodiimide (DCC) as a coupling reagent and 4-dimethylaminopyridine (DMAP) as a catalyst (Scheme 3.8B). Three different amine initiators were therefore investigated for the polymerization of Glu-NCA, namely *n*-hexylamine, 3-amino-1-propanol and 5-amino-1-pentanol (Scheme 3.6). Despite the presence of the –OH group in the amino alcohol initiators, the nucleophilicity of the primary amine in the ring-opening polymerization of the Glu-NCA monomers should be comparable, and thereby the initiation of the ring-opening reaction should proceed similarly. The polymerization of Glu-NCAs with 3-amino-1-propanol and 5-amino-1-pentanol was conducted under conditions identical to *n*-hexylamine. As shown in Table 3.1 the initiators, under identical conditions, exhibited different behaviors in the ROP of Glu-NCA. Among these, *n*-hexylamine gave the best control over the polymerization reaction by yielding PBG with the expected molecular weight and the lowest polydispersity index (PDI) at 0 ˚C (Table 3.1).

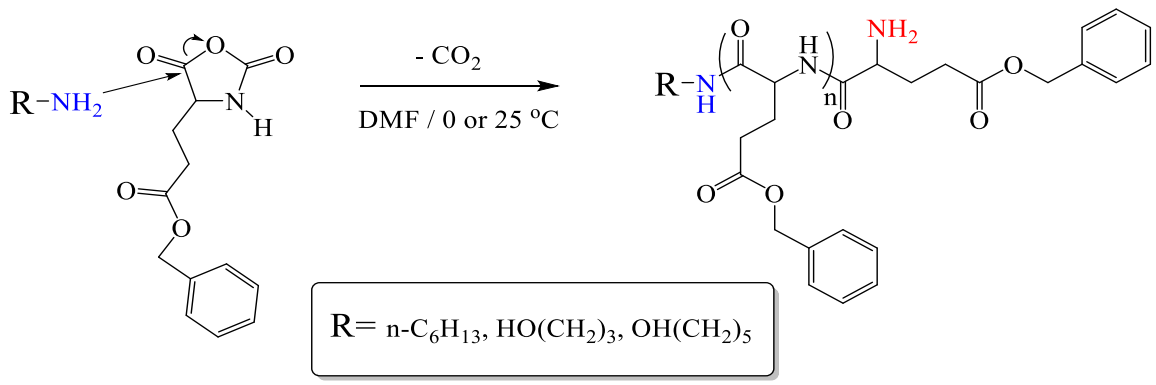

Scheme 3.6. Polymerization of γ-benzyl L-glutamic acid *N*-carboxyanhydride (Glu-NCA) using primary amine initiators.

Table 3.1. Synthesis of PBG using different initiators.

Initiator	X_n (NMR)	M_n (NMR)	M_n^{app} (SEC)	PDI	f_{NH2}
n-hexylamine	20	4,900	4,880	1.11	97
3-amino-1-propanol	18	4,200	4,700	1.18	87
5-amino-pentanol	18	4,300	3,500	1.22	83

All polymerizations carried out at 0 ˚C with a target $X_n = 20$.

Indeed, the polymerization initiated by *n*-hexylamine yielded PBG with a degree of polymerization $X_n = 20$ for a monomer/initiator ratio $M/I = 20$, in excellent agreement with the targeted $X_n = 20$. Furthermore, *n*-hexylamine yielded PBG with a low polydispersity index (PDI = 1.11) and a high amine functionality level (f_{NH2} = 97%, Figure 3.3). The ^{19}F NMR spectroscopy technique used to determine the chain end primary amine functionality,

f_{NH2}, will be discussed further in Section 3.4.3. Control of polymerization can be achieved only when the polymer end group is the only initiating species and termination is insignificant. In contrast to *n*-hexylamine, 3-amino-1-propanol and 5-amino-1-pentanol yielded PBG with higher PDI values (suggesting slower initiation) and uncontrolled molecular weights (with X_n lower than the target value), possibly due to chain termination through end group cyclization leading to the loss of the primary amine end group. Consequently, in the current investigation, arborescent polypeptide synthesis was only investigated using PBG building blocks with an amine terminus, obtained with the *n*-hexylamine initiator (Scheme 3.8A), and the exploration of esterification as an alternate coupling technique was abandoned.

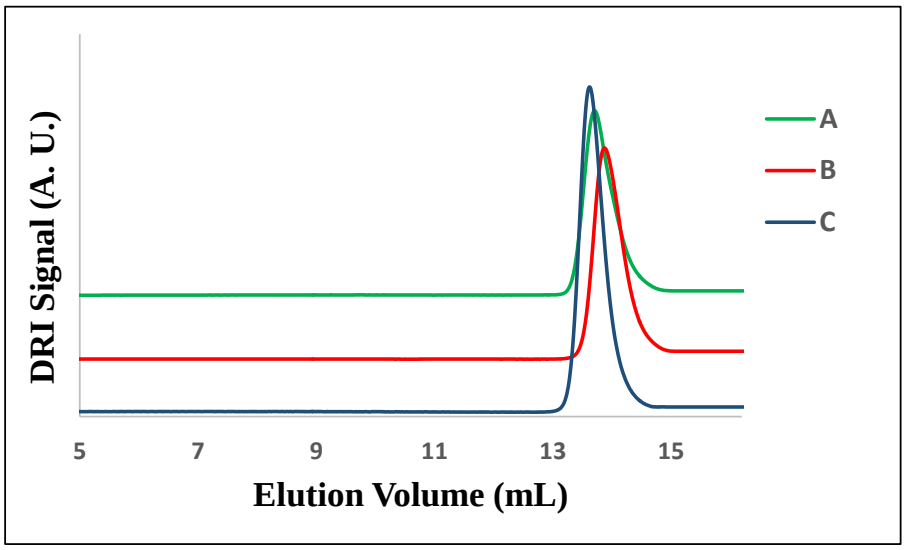

Figure 3.3. SEC Analysis of PBG polymers obtained by ROP of Glu-NCA using (A) 3-amino-1-propanol, (B) 5-amino-1-pentanol and (C) *n*-hexylamine initiators.

To further investigate initiation by *n*-hexylamine, the effects of the molar ratio of monomer to initiator (*M*/*I*) and of the reaction temperature were investigated. The polymerizations were conducted with ratios of *M*/*I* = 20, 25 and 50 at 0 ˚C in DMF. As shown in Table 3.2, *n*-hexylamine consistently yielded low dispersities (PDI = 1.08-1.11) under these conditions.

Table 3.2. Synthesis of linear PBG using different monomer to initiator (*M*/*I*) molar ratios.

Target X_n	Time (day)	X_n^{NMR}	M_n^{NMR}	M_n^{app}(SEC)	PDI	f_{NH2}
20	2.5	21	4,900	5,200	1.11	97
25	2.5	25	5,800	5,700	1.08	98
50	4	49	11,000	12,700	1.10	95

All polymerizations carried out at 0 ˚C for 2.5-4 days.

The reaction temperature is an important parameter in the ROP of Glu-NCA monomers. The relationship between the amine functionality level f_{NH2} and the reaction temperature is shown in Table 3.3. As the reaction temperature was increased from 0 to 25 ˚C, f_{NH2} decreased from about 98% to 68%. M_n also decreased slightly, while PDI increased. These results clearly demonstrated the non-living and uncontrolled behavior of the Glu-NCA polymerization even at room temperature, while higher M_n and lower polydispersities were

obtained at 0 ˚C, which is consistent with decreased chain end cyclization at low temperature (Figure 3.4).

Table 3.3. Synthesis of linear PBG using *n*-hexylamine as initiator at different temperatures.

T (^{0}C)	Target X_n	X_n^{NMR}	M_n^{NMR}	M_n^{app}(SEC)	PDI	f_{NH2}
0	25	25	5,800	5,700	1.08	98
25	25	23	5,400	5,200	1.17	68

Consequently, the PBG building blocks used in the subsequent work were synthesized by ring-opening polymerization of Glu-NCA in *N*,*N*-dimethylformamide (DMF) at 0 ˚C, using *n*-hexylamine as initiator. That initiator not only ensured reproducible batch-to-batch results but also scalability (from 1- to 10-g scale syntheses). Another advantage of that initiator is that it provides a well-defined signal for the terminal methyl group facilitating the determination of the degree of polymerization (X_n) of the product. The absolute values of M_n and X_n were determined by ^{1}H NMR analysis of the linear PBG samples as shown in Figure 3.5, by comparing the integrated peak intensities for the benzylic methylene protons in the repeating units (ca. 4.9 ppm) and the terminal methyl group signal from the *n*-hexylamine initiator around 0.75 ppm. The X_n for the sample of Figure 3.5 was calculated as (2.00/2H) / (0.12/3H) = 25.0 by that approach.

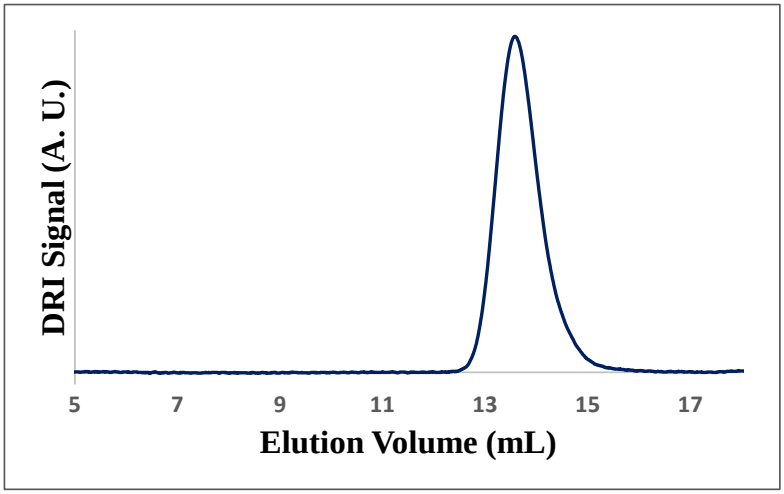

Figure 3.4. SEC Analysis of PBG obtained at 0 ˚C.

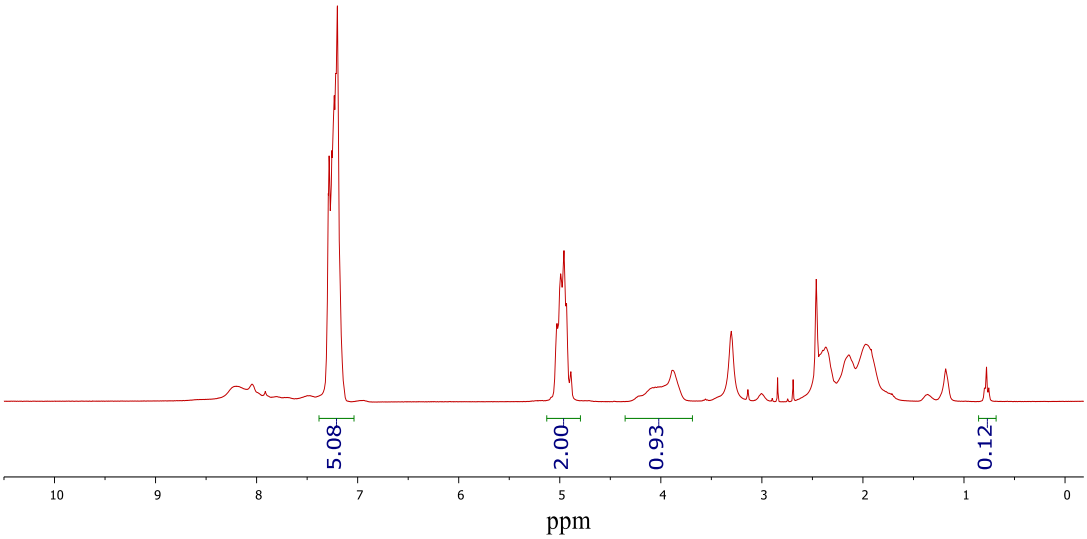

Figure 3.5. ^{1}H NMR spectrum for linear PBG with X_n = 25 obtained at 0˚C.

3.4.3 Synthesis and Deprotection of PBG Serving as Substrate

A linear PBG substrate was synthesized by ring-opening polymerization (ROP) of the corresponding Glu-NCA monomer as described above for the side chains with X_n = 49, but

quenching the reaction with acetic anhydride to deactivate the terminal amine moiety as shown in Scheme 3.7. The linear PBG with X_n = 49 was partially deprotected to serve as substrate in the synthesis of a G0 polymer. Coupling sites (carboxyl groups) for the grafting reaction were thus randomly introduced on the substrate through deprotection of a portion (ca. 30%) of the benzyl ester groups. This corresponds to around 15 coupling sites on the substrate. The PBG side chains in the synthesis of the arborescent polymers had X_n = 25 in all cases. Steric crowding of the chains should be minimized during the grafting reaction under these conditions. Better resolution of the SEC peaks for the graft polymer and unreacted side chain material is also expected, enabling more accurate calculation of the grafting yield and the coupling efficiency.

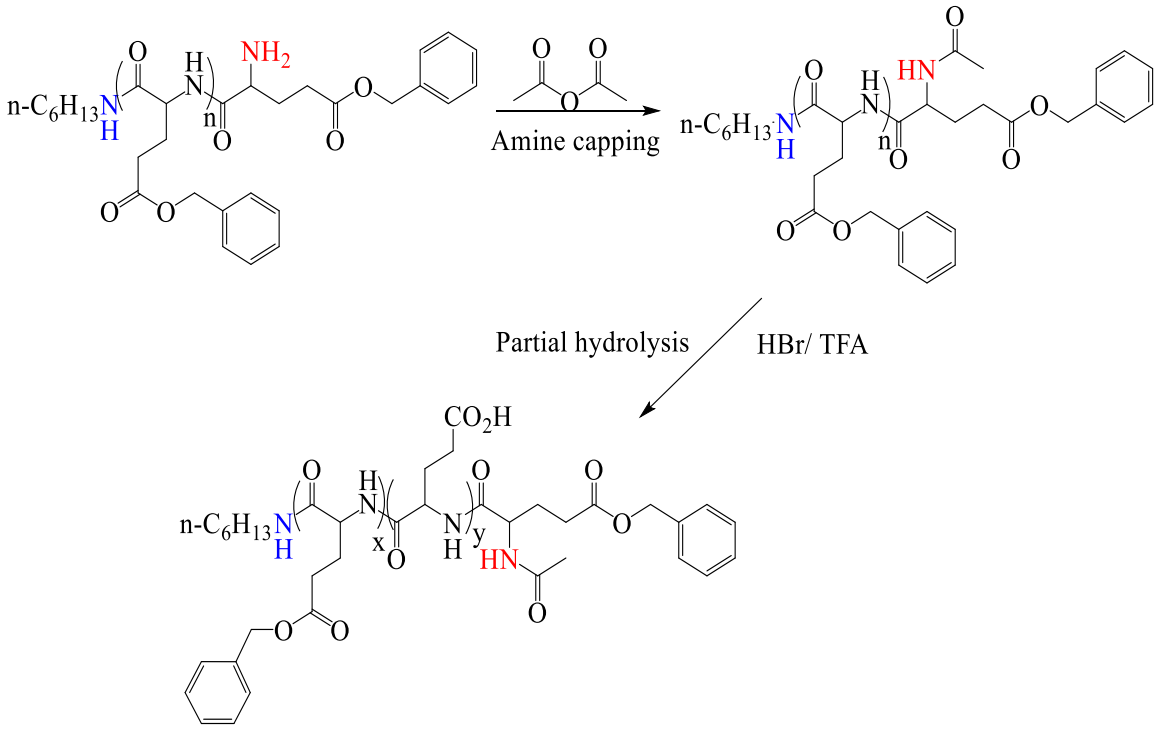

Scheme 3.7. Synthesis and deprotection of linear PBG substrate.

The treatment of linear PBG with a mixture of HBr/TFA allowed the cleavage of a controlled fraction of benzyl ester protecting groups under mild conditions to generate the coupling sites. The functionalization (deprotection) level of the PBG substrates was determined by ^{1}H NMR analysis as shown in Figure 3.6. The ratio of intensities for the benzylic methylene protons (2H at 4.9 ppm) on the remaining protected structural units and for the methine protons (1H at 3.9 ppm), respectively, was used to determine the deprotection level. Taking Figure 3.6 as an example, dividing the methylene protons integral (1.00/2H) by the methine protons integral (0.70/1H) gives the fraction of repeat units still protected as 0.70, or 70%. The corresponding deprotection level is therefore 30%.

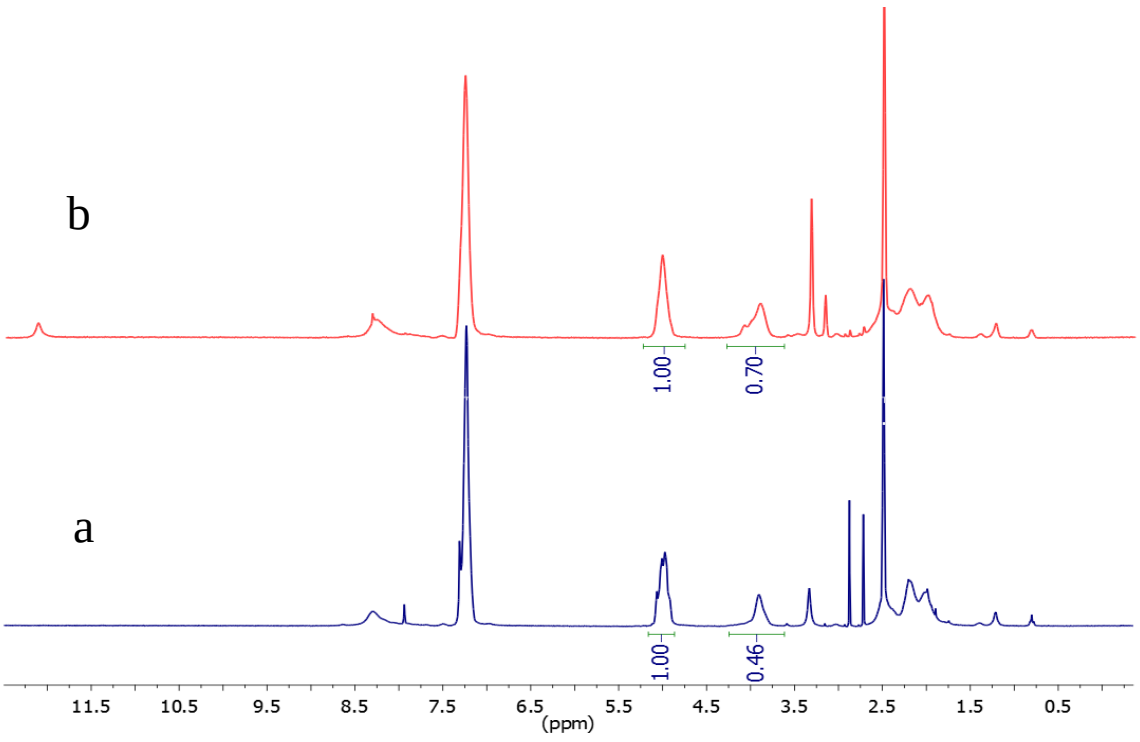

Figure 3.6. ^{1}H NMR spectra for PBG (a) before and (b) after partial deprotection with HBr.

To ensure that no degradation occurred during deprotection, the stability of PBG under acidic conditions was investigated using SEC analysis. The SEC profiles overlaid in Figure 3.7 for PBG and partially deprotected PBG-COOH display a small decrease in molecular weight corresponding to the deprotection of a fraction of the benzyl ester moieties, but no significant change in the breadth of the molecular weight distribution (PDI = 1.05 and 1.07 before vs. after deprotection, respectively). This clearly confirms that HBr/TFA deprotection is suitable for the PBG chains.

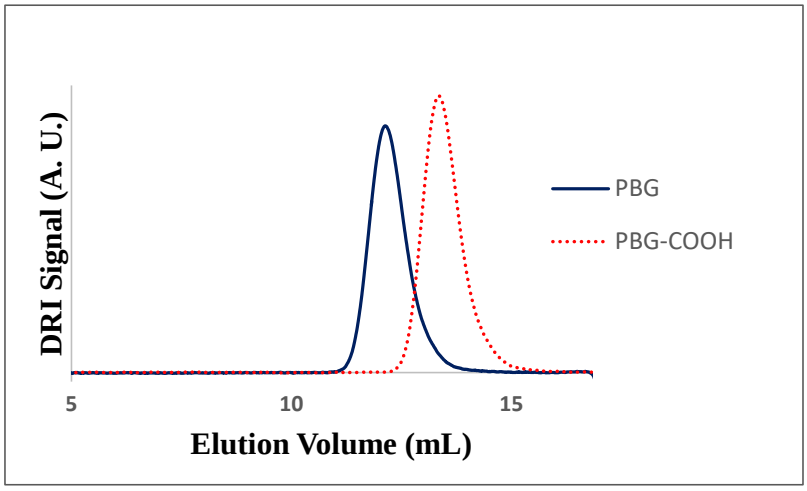

Figure 3.7. SEC Analysis of a PBG polymer before and after partial deprotection with HBr.

3.4.4 Optimization of the Grafting Reaction

Some of the methods described in the literature to improve the coupling yield were evaluated for the synthesis of arborescent polymers. The successful coupling of amino acids in the synthesis of peptides depends on the reactivity of the carboxyl group on the peptide substrate, and on the accessibility of the primary amine on the amino acid to be

added.[9] Activation of the carboxyl group is a prerequisite for the synthesis of an amide bond. While many activation procedures have been developed to this end, the use of dicyclohexylcarbodiimide (DCC) is still widespread. In this study however, other carbodiimides such as diisopropylcarbodiimide (DIC) were preferred because they yield urea coupling by-products that are more soluble than the dicyclohexylurea formed by DCC.[16] The synthesis of arborescent G0 polypeptides from amine-terminated poly(γ-benzyl L-glutamate) (PBG) chains and a carboxyl-functionalized PBG substrate is shown in Scheme 3.8A.

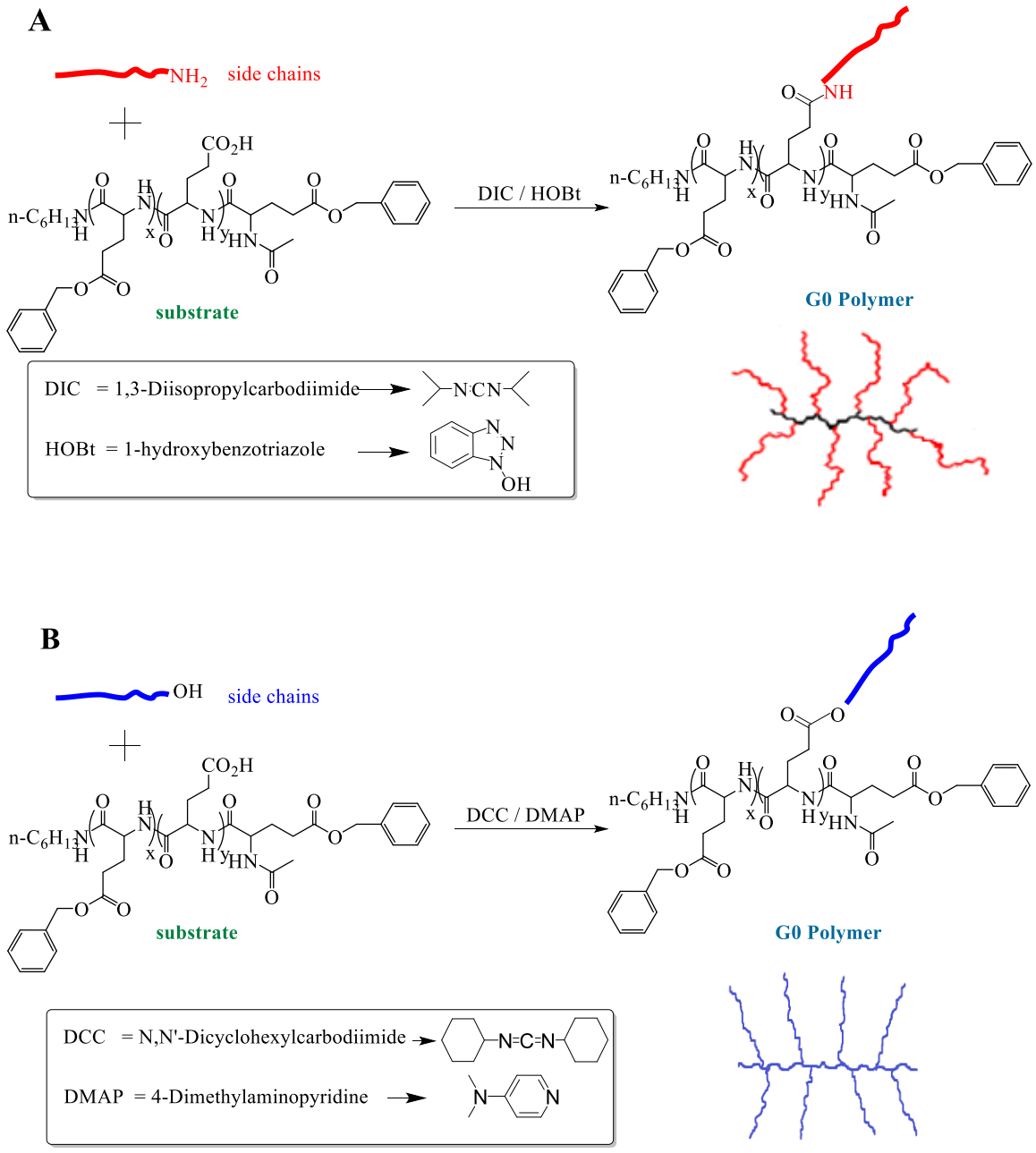

Scheme 3.8. Synthesis of a branched arborescent G0 polypeptide from PBG building blocks using peptide coupling (A) and esterification (B).

Since the main goal of this investigation was to optimize the grafting reaction of PBG side chains onto a partially deprotected PBG-CO_2H substrate, it was necessary to determine

the “living” characteristics of the primary amine end groups in the PBG side chains before the optimization of grafting. Deactivation of the primary amine end groups not only leads to linear PBG chains incapable of coupling with the substrate, but also to errors in the estimation of the grafting yield and coupling efficiency. For these reasons, a method developed by Ji et al.[19] was used to determine the functionality level of the “living” primary amines in the PBG side chains. This method used the reaction of 4-trifluoromethylbenzaldehyde (TFBA) with the primary amine to produce an imine functionality at the chain end of the polymer as shown in Scheme 3.9. ^{19}F NMR spectroscopy was employed to observe the chemical shift of the fluorine atoms when the imine was formed, to be compared with the signal for benzotrifluoride (BTF) serving as internal standard.

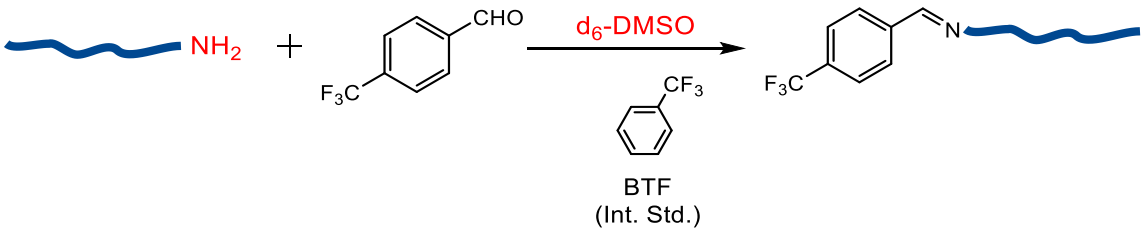

Scheme 3.9. Reaction of 4-trifluoromethylbenzaldehyde (TFBA) with the primary amine end group in a PBG chain.

The ^{19}F NMR spectrum obtained for a PBG sample (Table 3.2, sample with X_n=25), synthesized at 0° C using *n*-hexylamine as initiator, is shown in Figure 3.8. The amine functionality level f_{NH2} of the PBG side chains was calculated by integrating the peaks in the ^{19}F NMR spectrum as shown in Equation 3.1. The number of moles of chains present

in the reaction was determine by comparing the integration value for the imine fluorides (0.374) to the integration value for the internal standard BTF fluorides (1.000). An amine functionality level f_{NH2} > 98% was thus obtained.

$$f_{NH2} = \frac{mol\ imine}{mol\ polymer\ chains} = \frac{mol\ BTF \times \left(\frac{Imine\ integration}{BTF\ integration}\right)}{\left(\frac{g\ of\ polymer}{M_n\ of\ polymer}\right)} = \frac{4.53 \times 10^{-4}\ mol \times \left(\frac{0.374}{1.00}\right)}{\frac{0.100\ g}{5800\ g/mol}}$$

$$= 0.983 \qquad (3.1)$$

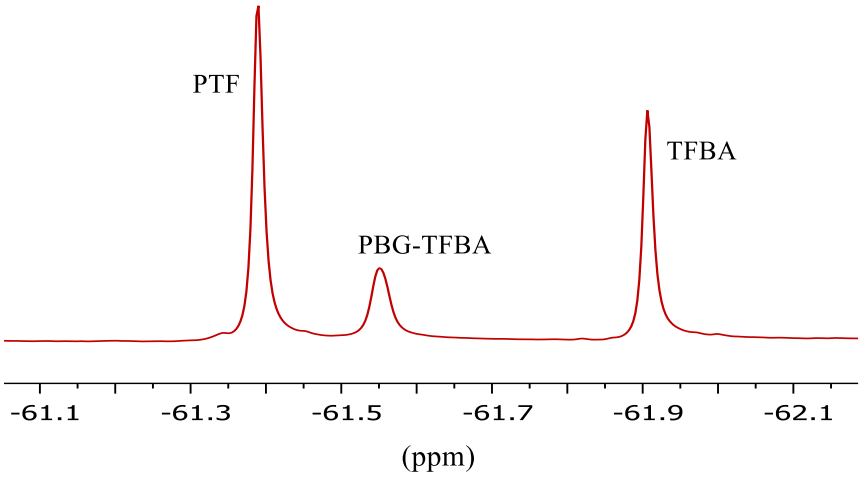

Figure 3.8. ^{19}F NMR spectra for linear PBG synthesized at 0° C with primary amine end groups, after treatment with 4-trifluoromethylbenzaldehyde (TFBA).

Since *n*-hexylamine initiation of the ROP of Glu-NCA in DMF at 0 ˚C led to better controlled polymerization reactions, with lower dispersities and a high primary amine functionality level f_{NH2} > 98%, all the PBG serving as side chain material subsequently used in the optimization of the grafting reaction was synthesized under these conditions.

Variations in the reaction temperature and time, solvent, and in the mole ratio of reactants and coupling reagents were used to maximize the grafting yield. For each reaction, short (M_n ~ 5,800 g/mol, X_n = 25) PBG side chains were grafted onto a partially (30%) deprotected, M_n ~ 11,000 g/mol (X_n = 49) linear PBG substrate with 15 coupling sites on average. This approach should provide better resolution of the SEC peaks for the graft polymer and unreacted side chain than when using components of equal molecular weight, and thus more accurate calculation of the grafting yield and coupling efficiency. The grafting yield, defined as the fraction of side chains becoming coupled with the substrate in a grafting reaction, was determined from the relative areas of the peaks for the graft polymer and the side chains in SEC analysis of the crude product. For Sample 3 in Figure 3.9, for example, the peak on the left (graft polymer) and the right (unreacted side chain material) have areas (in arbitrary units) of 35.8 and 15.0, respectively. The weight fraction of the substrate in the graft polymer was 13%, and therefore the corrected peak area for the graft polymer was 35.8 × 0.87 = 30.7. A grafting yield of 30.7 / (30.7+ 15.0) = 0.67 (67%) was thus calculated. The fraction of coupling sites consumed in a grafting reaction, defined as the coupling efficiency, was estimated by comparing the number of side chains grafted with the number of coupling sites present on the substrate.[17] Thus for a G0 sample having a branching functionality f_n of 10.9 side chains, derived from a substrate having 14.7 coupling sites (Sample 3, Table 3.7), the coupling efficiency was 10.9 / 14.7 = 0.745 or 74%.

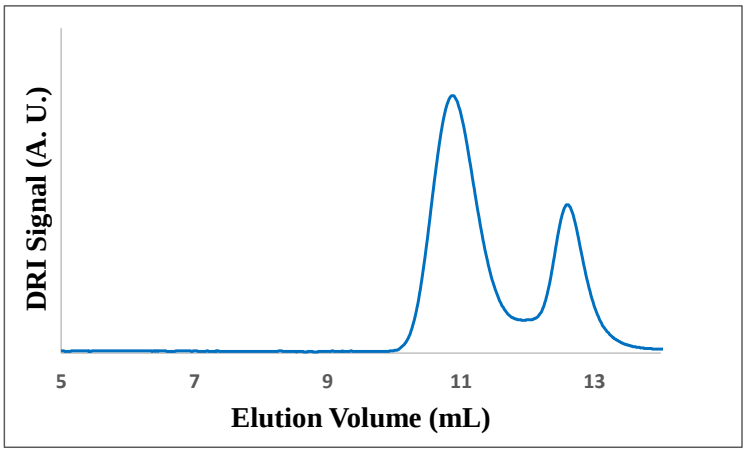

Figure 3.9. **SEC analysis of crude Sample 3 in Table 3.7.**

Two carbodiimide reagents, namely *N*,*N*′-diisopropylcarbodiimide (DIC) and 1-ethyl-3-(3-dimethylaminopropyl)carbodiimide hydrochloride (EDC·HCl), in combination with 1-hydroxybenzotriazole (HOBt) as coupling additive, were used to increase the reactivity of the carboxyl groups. The two coupling reagents (DIC and EDC·HCl) with HOBt, at room temperature with a 1:1 side chain:substrate molar ratio, yielded no significant difference in grafting yield nor coupling efficiency (Table 3.4). Thus DIC was selected as the coupling reagent for the rest of the investigation due to its lower cost.

Table 3.4. **Influence of the coupling agents on the coupling reaction.**

Solvent	Coupling agent	MALLS M_n	MALLS M_w/M_n	Grafting yield (%)	Coupling efficiency (%)
DMF	DIC	65,800	1.02	55	64
Acetonitrile/DMF	EDC·HCl	67,100	1.02	51	66

The coupling protocol was further optimized in terms of the reaction temperature and time in DMF, using DIC/HOBt as coupling agents with a 1:1 molar ratio of side chains to $–CO_2H$ groups on the substrate (Table 3.5). A lower coupling rate was observed at 0 ˚C as expected. Starting the reaction at 0 ˚C and then allowing it to proceed at room temperature increased the grafting yield when using DMF as solvent. Increasing the reaction temperature and/or time apparently favored the coupling reaction more than competing chain end cyclization, which increased the grafting yield and the coupling efficiency. The results in Table 3.5 clearly show that increasing the reaction temperature enhanced the rate of the coupling reaction. While only 28% of the side chains were coupled with the substrate after 32 h in DMF at 0 ˚C, the yield increased to 53% after only 12 h in DMF at 25 ˚C. Further increase in reaction temperature to 40 ˚C led to no significant difference in grafting yield nor coupling efficiency. As a result, all subsequent coupling reactions were carried out at 25 ˚C.

Table 3.5. Influence of the reaction temperature and time on the coupling reaction in DMF.

Temperature (˚C)	Time (h)	MALLS M_n	MALLS M_w/M_n	Grating yield (%)	Coupling efficiency (%)
0	12	-		7	-
0	32	-		28	-
25*	24	59,500	1.02	57	56
10	12	-		12	-
10	32	-		27	-
10	64	53,400	1.03	52	47
25	12	-		53	-
25	32	-		53	-
25	64	65,800	1.02	55	64
40	12	-		55	-
40	32	-		55	-
40	64	63,100	1.06	54	61

* The reaction was started at 0 ˚C for 32 h and then allowed to proceed at 25 ˚C for 24 h.

The influence of the solvent composition and the reaction time on the grafting yield and the coupling efficiency, using DIC/HOBt as coupling agents with a 1:1 molar ratio of side chains to substrate, was also examined (Table 3.6). When the reaction was carried out in DMF, the grafting yield was maximized after 12 h, without further improvements even

after 64 h. As the reaction proceeds, the accessibility of the remaining coupling sites on the substrate is expected to decrease, thus making further grafting reactions more difficult. When the reaction was carried out in DMSO the coupling rate was slower, but the grafting yield and the coupling efficiency were much improved after 64 h. Low grafting yields were observed in a DCM/DMF mixture, probably due to its lower polarity favoring side reaction in the activation process. DMSO therefore yielded the best results.

Table 3.6. Influence of the solvent composition and the reaction time on the coupling reaction.

Solvent	Time (h)	MALLS		Grating yield (%)	Coupling efficiency (%)
		M_n	M_w/M_n		
DMF	12	-		53	-
-	64	65,800	1.02	55	64
DMSO	12	-		46	-
-	64	78,400	1.03	59	79
DCM/DMF	12	-		47	-
-	64	59,500	1.02	50	55

We then evaluated the effects of the CO_2H:NH_2 (substrate:side chain) stoichiometry on the grafting yield and the coupling efficiency. Given the inaccessibility of some of the CO_2H coupling sites on the substrate, using a slight excess of substrate was investigated as a means to maximize the grafting yield without sacrificing the coupling efficiency (Table 3.7). The reactions carried out in DMSO at 25 ˚C for at least 36 h, using a 1.25 : 1 ratio of CO_2H:NH_2, were deemed optimal because they provided a reasonable grafting yield (67%)

and a coupling efficiency of 74%, close to the maximum efficiency observed in the equimolar reactions (78%). Interestingly, using a 1.25:1 ratio of CO_2H:NH_2 groups led to a 13% (as opposed to 25%) increase in grafting yield, from 59% to 67%. This result suggests that steric hindrance was not the only limiting factor in these grafting reactions, but that other side reactions may have occurred that led to deactivation of the carboxylic acid moieties on the substrates during the grafting reaction. It is important to mention that we did not correct any of the grafting yields reported by taking into consideration the fraction of active chains (f_{NH2}), because side chains with a amine functionality level (f_{NH2} > 98%) were used in all the reactions.

Table 3.7. Influence of the CO_2H:NH_2 molar ratio on the coupling reaction.

Sample	Molar ratio CO_2H : NH_2	MALLS		Grating yield (%)	Coupling efficiency (%)
		M_n	M_w/M_n		
1	1 : 1.25	75,300	1.04	47	75
2	1 : 1	76,200	1.02	59	76
3	1.25 : 1	74,600	1.04	67	74
4	1.5 : 1	68,300	1.04	76	66
5	2 : 1	48,000	1.05	86	43

The CO_2H:NH_2 ratio of 1.25, while increasing the coupling efficiency for Sample 3, only led to a small decrease in the total number of side chains added in the reaction (Table

3.7 and Figure 3.10). This approach was therefore deemed to be optimal, although larger stoichiometric ratios could also be considered if the goal were to minimize the presence of side chain contaminant in the product while sacrificing the coupling efficiency.

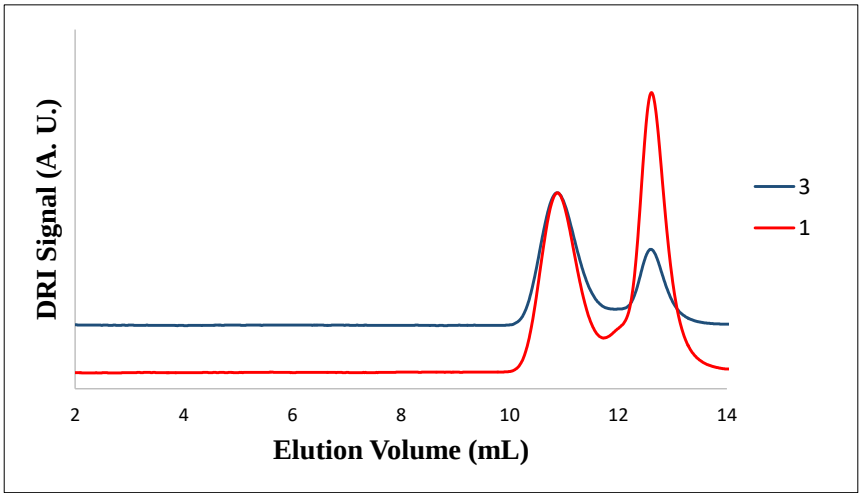

Figure 3.10. SEC analysis of crude Samples 1 and 3 (Table 3.7) showing the influence of the CO_2H:NH_2 stoichiometry on the grafting yield.

To minimize the amount of coupling agents used in the reaction, while maximizing the grafting yield and the coupling efficiency, the effects of the DIC/HOBt:CO_2H (coupling agents:substrate) stoichiometry was investigated while the DIC/HOBt ratio was kept constant at 1. The grafting reaction was also carried out with a 2-fold excess molar ratio of carboxyl groups to primary amines, to determine whether carboxyl group deactivation during the grafting reaction could be a significant factor (along with steric hindrance of the substrate) contributing to lowering the grafting yield and coupling efficiency in these reactions. For Sample 6 (Table 3.8), a stoichiometric amount (DIC/HOBt:CO_2H = 1) was used. Samples 7, 5 and 8 were obtained with DIC/HOBt:CO_2H ratios of 2, 5 and 10,

respectively, to maximize the activation of the carboxyl groups, and thus the grafting yield and the coupling efficiency. As mentioned earlier, the initial step in amide bond formation is the activation of the carboxyl group by addition of the carbodiimide to form an intermediate *O*-acylisourea species. If activation of the carboxylic acid is inefficient, an excess of coupling reagents should help to maximize carboxyl group activation.

Table 3.8. Influence of the CO_2H:coupling agents molar ratio on the coupling reaction. The reactions were carried out in DMSO at 25 ˚C for at least 36 h, using a 2:1 ratio of CO_2H:NH_2.

Sample	Molar ratio coupling agents: coupling sites	MALLS		Grating Yield (%)	Coupling efficiency (%)
		M_n	M_w/M_n		
6	1	38000	1.07	76	31
7	2	40500	1.04	79	34
5	5	48000	1.05	86	43
8	10	46000	1.05	84	41

As shown in Table 3.8, a 1:1 molar ratio of coupling agents (DIC/HOBt) to CO_2H groups (Sample 6) led to a grafting yield of 76% and a coupling efficiency of 31%. When a 5-fold molar ratio of coupling agents was used (Sample 5), the grafting yield and coupling efficiency were maximized at 86% and 43%, respectively. Further increasing the

stoichiometric amount of coupling agents to a 10-fold ratio (Sample 8) yielded no significant differences in grafting yield nor coupling efficiency. Thus a 5:1 molar ratio of coupling agents (DIC/HOBt) to CO_2H groups was selected as optimal, as it reduced the amounts of chemicals to be used and disposed, and simplified sample purification. Since a 2-fold excess of coupling sites was added in the reactions relatively to the side chains, the coupling efficiency (defined as the fraction of coupling sites consumed on the substrate) could only reach a maximum value of 50% if all the side chain material were consumed. Despite the excess of coupling sites used, only 86% of the side chains reacted, which means that 14% of the chain ends were deactivated during the coupling reaction (Sample 5, Table 3.8). It is therefore clear that not only steric hindrance was a limiting factor in these coupling reactions, but also deactivation of the amino chain ends during the grafting reaction, as it is unlikely that over 50% of the carboxyl coupling sites were deactivated. Another factor may nevertheless also have contributed to lowering the grafting yield and coupling efficiency in the G0PBG synthesis, namely the distribution of carboxylic acid moieties on the substrate. We assumed that the partial deprotection of PBG would lead to randomly distributed coupling sites on the substrate, but the deprotection of adjacent structural units is certainly possible. In that case, the grafting yield and coupling efficiency may decrease due to increased steric crowding for coupling on adjacent carboxylic acid moieties. The SEC analysis results for crude Samples 6 and 5 are compared in Figure 3.11 to show the influence of the CO_2H:coupling agents molar ratio on the coupling reaction.

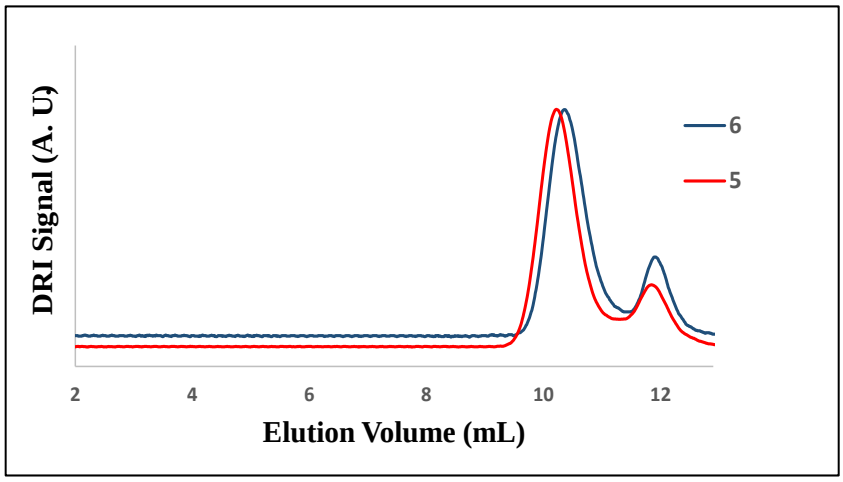

Figure 3.11. Comparison of the SEC analysis of crude Samples 6 and 5 (Table 3.8) to show the influence of the CO_2H:coupling agents molar ratio on the coupling reaction.

3.4.5 Purification of Arborescent Polymers

All the crude graft polymer samples were contaminated with linear side chain material that did not react in the coupling reaction. Since it was impossible to remove these side chains by precipitation or fractionation, it was necessary to use preparative size exclusion chromatography (SEC) for that purpose. The purified G0 polymer, recovered by evaporation of the solvent under vacuum, dissolution in TFA and precipitation in methanol, was obtained free of linear PBG contaminant, as shown in Figure 3.12.

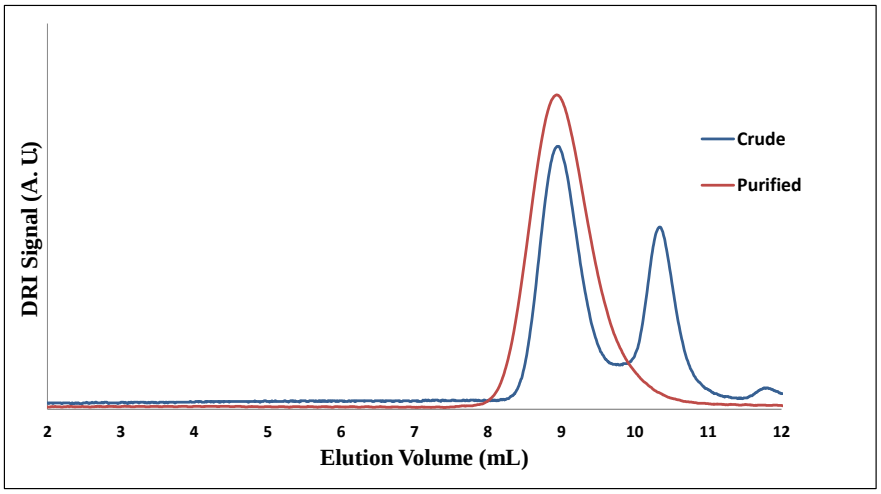

Figure 3.12. Comparison of SEC curves for G0 PBG, crude and purified by preparative SEC.

3.5 Conclusions

Since the main goal of this investigation was to optimize the grafting reaction of poly(γ-benzyl L-glutamate) (PBG) side chains onto partially deprotected PBG substrates, a series of reactions was planned in a systematic fashion to allow direct comparisons. After determining that *n*-hexylamine as initiator yielded the best results for the ring-opening polymerization of Glu-NCA in DMF at 0 ˚C, yielding narrow molecular weight distributions and high primary amine functionality levels (f_{NH2} > 98%), "living" PBG side chains were synthesized under these conditions to be used in the optimization of the grafting reaction in the synthesis of G0 PBG. For each reaction, short (M_n ~ 5,800 g/mol) PBG side chains were grafted onto a partially (30%) deprotected, M_n ~ 11,000 linear PBG substrate.

It was demonstrated that the efficiency of the polypeptide coupling reactions used to synthesize arborescent PGB could be optimized by varying the solvent, temperature, reaction time, and reactant stoichiometry used. Different carbodiimide coupling agents had no influence on the grafting yield nor the coupling efficiency; thus DIC was preferred on the basis of its lower cost. Starting the reaction at 0 ˚C and then allowing it to proceed at room temperature increased the grafting yield when using DMF as solvent. Allowing the temperature to increase to room temperature apparently favored the grafting reaction more than chain end cyclization, as it increased both the grafting yield and coupling efficiency. Further increase to 40 ˚C led to no significant difference in grafting yield nor coupling efficiency however. When the reaction was carried out in DMF the grafting yield was maximized after 12 h, with no further improvement even after 64 h. As the reaction proceeded, the accessibility of the remaining coupling sites on the substrate likely decreased, thus making further grafting reactions more difficult.

When the reaction was carried out in DMSO the coupling rate was slower, but the grafting yield and the coupling efficiency were significantly improved after 64 h. Low grafting yields were observed in a DCM/DMF mixture, probably due to its lower polarity favoring side reactions in the activation process. DMSO therefore yielded the best results. Reactant stoichiometry optimization not only increased the grafting yield, but it also reduced the total number of side chains added in the reaction. The reactions carried out in DMSO at 25 ˚C for at least 36 h, using a slight excess of substrate (CO_2H:NH_2 ratio of 1.25) were optimal. A 5:1 molar ratio of coupling agents (DIC/HOBt) to CO_2H groups on the substrate also maximized the grafting yield and the coupling efficiency.

By utilizing the optimized reaction conditions mentioned above, namely by carrying out the reactions in DMSO at 25 ˚C for at least 36 h, using a 1.25:1 ratio of CO_2H:NH_2 and a 5:1 molar ratio of coupling agents (DIC/HOBt) to CO_2H groups on the substrate, well-defined (PDI < 1.04) G0 arborescent or comb-branched polypeptides were obtained with a grafting yield and coupling efficiency reaching 67% and 74%, respectively. These optimized reaction conditions were used to synthesize arborescent PBG of generations G1 and G2 in the subsequent chapters of this Thesis. The PBG arborescent polypeptides constructed also served as intermediates in the preparation of unimolecular micelles useful for sustained drug delivery applications.

Chapter 4 Unimolecular Micelles from Randomly Grafted Arborescent Copolymers with Different Core Branching Densities: Encapsulation of Doxorubicin and *In Vitro* Release Study

4.1 Overview

A series of amphiphilic arborescent copolymers of generations G1 and G2 with an arborescent poly(γ-benzyl L-glutamate) (PBG) core and poly(ethylene oxide) (PEO) chain segments in the shell, PBG-*g*-PEO, were synthesized and evaluated as drug delivery nanocarriers. The PBG building blocks were generated by ring-opening polymerization of γ-benzyl L-glutamic acid *N*-carboxyanhydride (Glu-NCA) initiated with *n*-hexylamine. Partial or full deprotection of the benzyl ester groups followed by coupling with PBG chains yielded a comb-branched (arborescent polymer generation zero or G0) PBG structure. Additional cycles of deprotection and grafting yielded G1 and G2 arborescent polypeptides. Side chains of poly(ethylene oxide) were then randomly grafted onto the arborescent PBG substrates to produce amphiphilic arborescent copolymers. Control over the branching density of G0PBG was investigated by varying the length and the deprotection level of the linear PBG substrates used in their synthesis. Three G0PBG cores with different branching densities varying from a compact and dense to a loose and more porous structure were thus synthesized. The copolymers were characterized using ^{1}H NMR, size exclusion chromatography (SEC), dynamic light scattering (DLS), transmission electron microscopy (TEM), and atomic force microscopy (AFM). These amphiphilic copolymers behaved like unimolecular micelles in aqueous solutions in most cases. It was demonstrated that these biocompatible copolymers can encapsulate hydrophobic drugs such as doxorubicin (DOX) within their hydrophobic core with a high efficiency. Sustained and pH-responsive DOX release was observed from the unimolecular micelles, which suggests that they could be useful as drug nanocarriers for cancer therapy.

4.2 Introduction

Amphiphilic block copolymer micelles have recently attracted much attention in biomedical fields such as for drug delivery.[1-3] One of the most important characteristics of polymeric micelles in drug delivery applications is their ability to solubilize hydrophobic or poorly water soluble drugs within their core, and thus enhance their bioavailability.[4] Polymeric micelles obtained by the self-assembly of linear block copolymers are always at dynamic equilibrium with non-associated (unimer) polymer chains. The self-assembly of isolated polymer chains to form micelles only starts when a minimum concentration is reached, known as critical micelle concentration (CMC).[5] As a consequence, when applied *in vivo*, polymeric micelles based on linear block copolymers face a difficulty related to their dilution in the body, which shifts the micellar equilibrium toward the unimer state and causes drug leaching, thus reducing the efficacy of drug delivery.[6-9]

Amphiphilic dendritic polymer micelles are an interesting alternative to conventional amphiphilic block copolymer micelles, in that each micelle is formed by a single molecule with amphiphilic properties (unimolecular micelles), with a covalently bound core-shell morphology. In contrast to block copolymer micelles, unimolecular micelles are stable irrespective of their concentration or the solvency conditions.[8,10-15] Due to these remarkable features, the past decade has witnessed a surge of interest in the synthesis and characterization of unimolecular micelles, particularly in relation to biomedical applications. To date, the polymers most widely investigated to form unimolecular micelles for various applications are dendrimers and hyperbranched polymers. Unfortunately

dendrimers are time-consuming and tedious to synthesize, while hyperbranched polymers are easier to synthesize but only with limited control over their structure.[16-18]

In contrast to dendrimers and hyperbranched polymers, dendrigraft (arborescent) polymers are a subset of dendritic polymers derived from reactive polymer building blocks in successive grafting reactions rather than small molecule monomers.[19,20] A schematic representation of the step-wise grafting procedure used for the synthesis of arborescent polymers is shown in Scheme 4.1. Due to the presence of a large number of coupling sites randomly distributed on the grafting substrates, a rapid increase in molecular weight is observed over successive arborescent polymer generations and high molecular weight species are obtained in a few steps, while narrow molecular weight distributions (M_w/M_n < 1.1) are maintained in most cases.[21] Arborescent unimolecular micelles can be obtained by the addition of hydrophilic segments in the last grafting cycle. For example, arborescent polystyrene-*graft*-poly(2-vinylpyridine) (PS-*g*-P2VP) copolymers were synthesized by grafting poly(2-vinylpyridine) side chains onto arborescent PS substrates of different generations. These copolymers were freely soluble in acidic aqueous solutions, behaving like unimolecular micelles that were able to solubilize various polycyclic aromatic hydrocarbon probes within their hydrophobic core.[22] In a subsequent study, the release properties of these systems loaded with indomethacin and lidocaine as model drugs were also investigated.[23] Unfortunately, the arborescent PS-*g*-P2VP copolymers used in this investigation were not biocompatible and only water-soluble at low pH due to protonation of the P2VP side chains, and thus the conditions of these *in vitro* investigations were very different from real biological systems. The synthesis of fully biocompatible arborescent

polymers from poly(γ-benzyl L-glutamate) (PBG) side chains therefore represents a significant advancement in that area.[24] We are now planning to investigate these materials as micellar drug delivery vehicles.

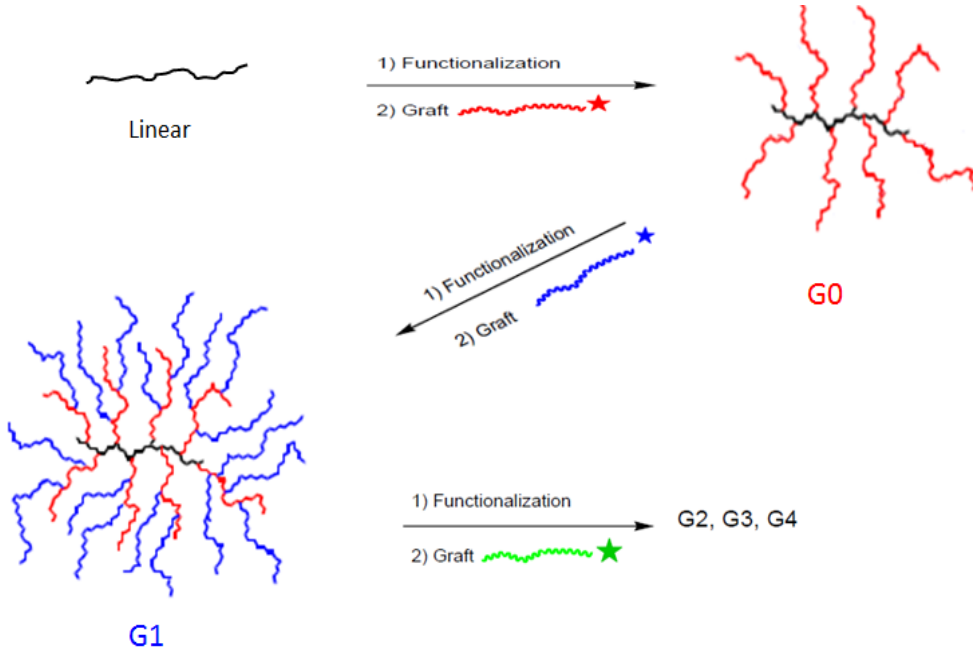

Scheme 4.1. Generation-based synthesis of arborescent polymers.

Structural variables such as the size and branching density of arborescent copolymers can be designed to meet specific requirements for various applications. For example, the properties of these materials can be tailored by adjusting the composition and the size of the side chains used in their core and corona. Since the core structure of dendritic micelles is expected to be a critical parameter controlling their drug solubilization ability, clarifying the relationship between the core structure of arborescent copolymers and micellar properties such as the drug loading capacity and release kinetics would be useful in

tailoring the properties of these materials for drug delivery applications. Our group previously reported the synthesis of arborescent PBG substrates grafted either randomly or at their chain ends with linear poly(ethylene oxide), polyglycidol, and poly(glutamic acid) to form a hydrophilic shell.[25]

Despite the remarkable potential of arborescent micelles as drug nanocarriers, the use of fully biocompatible arborescent copolymers in drug delivery has yet to be explored. We herein expand the design and synthesis of biocompatible amphiphilic arborescent copolymers as drug nanocarriers. Arborescent copolymers with poly(γ-benzyl L-glutamate) (PBG) cores of generations G1 and G2, derived from G0PBG substrates with different branching densities, and a shell of poly(ethylene oxide) (PEO) chain segments were examined. The effects of the PBG core branching density on the micellar size, drug loading capacity, drug loading efficiency, and drug release rate were investigated. The copolymers were characterized in solution by dynamic light scattering (DLS), proton nuclear magnetic resonance (^{1}H NMR) and size exclusion chromatography (SEC) measurements, and in the solid state with transmission electron microscopy (TEM) and atomic force microscopy (AFM). The encapsulation and release properties were investigated by UV spectroscopy using doxorubicin (DOX) as a model hydrophobic drug.

4.3 Experimental Procedures

4.3.1 Characterization and Sample Preparation

4.3.1.1 Nuclear Magnetic Resonance (NMR) Spectroscopy

Proton nuclear magnetic resonance (^{1}H NMR) spectroscopy was used to estimate the degree of polymerization of the linear poly(γ-benzyl L-glutamate) PBG chains, to determine the deprotection level of the PBG substrates, and to investigate the ability of randomly grafted arborescent copolymers to form micelles. The instrument used was a Bruker 300 MHz spectrometer. Fluorine nuclear magnetic resonance (^{19}F NMR) spectroscopy was also performed on the Bruker 300 MHz instrument to determine the chain end primary amine functionality, f_{NH2}, of the polymers used in the grafting reactions.

4.3.1.2 Size Exclusion Chromatography (SEC) Analysis

Analytical SEC was used for the characterization of the arborescent PBG substrates of generations G0-G2 and of the copolymers. The analytical SEC system consisted of a Viscotek GPCmax unit equipped with a VE 2001 GPC Solvent/Sample Module, a Viscotek double detector array equipped with refractive index and dual-angle light scattering detectors, and two Agilent Technologies PLgel 5 μm MIXED-C and PLgel 10 μm MIXED-B organic mixed bed columns, with dimensions of 7.5 mm (ID) × 300 mm (L). The system was operated at a flow rate of 0.5 mL/min at 70 ˚C, using dimethyl sulfoxide (DMSO) with LiBr (0.05 M) as the mobile phase. Analysis of the chromatograms was performed with the OmniSEC 4.6.1 software package.

Preparative SEC was carried out on a system consisting of a Waters M45 HPLC pump, a 2-mL sample injection loop, a Waters R401 differential refractometer detector, and a Jordi Gel DVB 1000 Å 250 mm × 22 mm preparative SEC column. *N*,*N*-Dimethylformamide (DMF) with 0.2 g/L LiCl was used as the mobile phase. The concentration of polymer injected was 25 mg/mL. The system was operated at a flow rate of 3 mL/min at room temperature (25 ˚C).

4.3.1.3 Dynamic Light Scattering (DLS) Measurements

Light scattering measurements were performed on a Zetasizer Nano ZS90 (Malvern Instruments) equipped with a 4 mW He–Ne laser operating at 633 nm and 25.0 ˚C, at a scattering angle of 90°. The polymers were dissolved in phosphate buffered saline (PBS), DMF, or water at least 12 h before analysis. The concentration of the solutions was around 0.5 $mg{\cdot}mL^{-1}$, 0.2 $mg{\cdot}mL^{-1}$, and 0.1 $mg{\cdot}mL^{-1}$ for the G0, G1 and G2 copolymers, respectively. All the solutions were filtered with either PTFE or cellulose acetate membrane filters having a nominal pore size of 0.45 μm prior to the measurements. Each sample was measured in triplicate. The light scattering data were analyzed with the Zetasizer 7.11 Software (Malvern Instruments).

4.3.1.4 UV-visible (UV-vis) Spectroscopy

Absorption spectra were obtained on a Cary 100 Bio UV-Vis spectrophotometer with a spectral bandwidth (SBW) of 2 nm, operated with the Cary Varian UV Scan Application (v3.001339). The absorption peak at 483 nm for doxorubicin was used to calculate the

doxorubicin loading in the DOX-polymer samples. Absorbance measurements were performed in the 200–800 nm range and baseline correction was applied for PBS.

4.3.1.5 Transmission Electron Microscopy (TEM)

The dendritic micelles were imaged with a Philips CM10 electron microscope operated at 60 kV accelerating voltage. The images were recorded with an Advance Microscopy Techniques 11 megapixel digital camera and the Image Capture Software Engine version 5.42.558. The feature sizes and size distributions were measured with the open source processing program ImageJ (version 1.46r).[26] Either automatic selection or manual analysis of the features was used, depending on the contrast and the resolution of the images. In either case, a minimum of 15 measurements were taken for each sample to provide adequate average size information. In some cases, contrast adjustment was necessary to improve visualization and help with measurement of the features. The samples for TEM measurements were prepared by the following method: one drop of solution (0.05 $mg \cdot mL^{-1}$) was cast onto a 300 mesh Formvar® carbon-coated copper TEM grid (Electron Microscopy Sciences, FCF300-Cu) placed onto filter paper and the excess solution was wicked off with filter paper. After 1 min, one drop of 2% (w/v) phosphotungstic acid was added to the grid and the excess staining solution was wicked off with filter paper. Finally the grid was transferred onto a new piece of filter paper in a Petri dish and left to dry overnight at room temperature.

4.3.1.6 Atomic Force Microscopy (AFM)

Muscovite mica discs were adhered onto steel substrates using double-sided adhesive tape to allow securing of the sample on the magnetic spin coater. Immediately prior to film casting, a fresh surface was exposed by cleavage with a strip of Scotch® MultiTask tape. The polymer solutions were prepared at concentrations ranging from 0.01 to 0.05 $mg.mL^{-1}$. A 20 μL aliquot of the solution was deposited on the mica substrate and spun at about 3000 revolutions per minute (rpm) for 60 s under ambient conditions. Atomic force microscopy (AFM) images were recorded in the tapping mode on a Nanoscope III instrument (Digital Instruments, model MMAFM-2, scan stage J) housed in a NanoCube acoustic isolation cabinet and mounted on a Halcyonics Micro 40 vibration isolation table. The measurements were performed using Si probes (VistaProbes, T300) having a spring constant of 40 N/m, a resonance frequency of 300 kHz, and the following characteristics: length 125 μm, width 40 μm, tip height 14 μm, and tip radius < 10 nm. The images were analyzed using the Nanoscope v 1.40 software. The scan rate was typically between 0.7 and 1.2 Hz, at a scan angle of 0°, acquiring 512 samples/line.

4.3.2 Solvent and Reagent Purification

Dimethyl sulfoxide and *n*-hexylamine were purified by stirring overnight with CaH_2 and distillation under reduced pressure. *N,N'*-Dimethylformamide serving in the polymer synthesis (DMF; Aldrich, >99%) was purified by distillation under reduced pressure. Ethyl acetate (Fisher, 99.9%) was distilled from $LiAlH_4$ under nitrogen. γ-Benzyl L-glutamic acid (Bz-Glu; Bachem, >99%), diethyl ether (EMD Millipore OmniSolv), HBr solution (Aldrich, 33% in acetic acid), *N,N*'-diisopropylcarbodiimide (DIC; Aldrich, 99%), 1-ethyl-

3-(3-dimethylaminopropyl)carbodiimide hydrochloride (EDC·HCl; Aldrich, 98%), 1-hydroxybenzotriazole (HOBt; Fluka, water content ca. 15% w/w), tetrahydrofuran (THF, EMD Millipore OmniSolv), methanol (EMD Millipore OmniSolv), triphosgene (Aldrich, 98%), trifluoroacetic acid (TFA, Caledon, 99.9%), $LiAlH_4$ (Aldrich, 95%), acetic anhydride (Caledon, 97%), deuterated DMSO (DMSO-d_6, Cambridge isotopes, 99.9% D), deuterated H_2O (D_2O; Aldrich, 99.9 atom % D) and triethylamine (TEA, EMD) were used as received from the suppliers. Doxorubicin hydrochloride (DOX·HCl) was obtained from Sigma-Aldrich (USA). Dialysis bags Spectra/Por® 7 (MWCO 3.5 kDa) were purchased from Spectrum Laboratories Inc. (USA).

4.3.3 Synthesis

4.3.3.1 Synthesis of γ-Benzyl L-Glutamic Acid *N*-Carboxyanhydride (Glu-NCA)

The monomer was synthesized from γ-benzyl L-glutamic acid and triphosgene as described in the literature.[27] γ-Benzyl L-glutamic acid (Bz-Glu) (10.0 g; 42.0 mmol) was dissolved in 300 mL of freshly distilled ethyl acetate in a 1-L round-bottomed flask fitted with a reflux condenser and a N_2 bubbler. After heating to reflux, triphosgene (4.8 g, 16 mmol) was added at once and refluxing was continued for 3.5 h longer. The flask was allowed to cool to room temperature, and then stored in a refrigerator (5 ˚C) for 2 h. The cold reaction mixture was transferred to a cold separatory funnel, washed with 100 mL of distilled water chilled to 0 ˚C, and then with 100 mL of chilled 0.5% aqueous $NaHCO_3$ solution. The ethyl acetate layer was dried over anhydrous $MgSO_4$, filtered by gravity, and concentrated to 100–120 mL on a rotary evaporator. An equal volume of cold hexane was

then added to induce crystallization of the monomer. After chilling to -5 ˚C overnight, the monomer crystals were collected by filtration in a Schlenk funnel under N_2. For further purification, in some cases, the monomer was recrystallized twice from *n*-hexane and ethyl acetate (*n*-hexane/ethyl acetate v/v: 2/1), to remove the last traces of remaining impurities. The product was dried under vacuum and stored under N_2 in a freezer until used. Yield = 9.7 g (88 %); ^{1}H NMR (300 MHz, $CDCl_3$): 7.55–7.22 (s, 5H), 6.72 (s, 1H), 5.09 (s, 2H), 4.35–4.31 (t, 1H), 2.57–2.51 (t, 2H), 2.33–2.19 (m, 1H), 2.18–2.00 (m, 1H).

4.3.3.2 Synthesis of Poly(γ-benzyl L-glutamate) PBG Serving as Side Chains

A linear polymer serving as side chains was synthesized as described previously.[24] Briefly, Glu-NCA (8 g, 30.4 mmol) was dissolved in dry DMF (20 mL) at 0 ˚C. *n*-Hexylamine (182 μL, 1.38 mmol, for a target X_n = 22) was then added to the monomer and the reaction was allowed to proceed for 2.5 days at 0 ˚C. The linear polymer was recovered by precipitation in cold methanol, centrifugation, and drying under vacuum overnight before characterization. Yield = 82%, M_n = 5,100, M_w/M_n = 1.09. ^{1}H NMR (300 MHz, DMSO-d_6): X_n = 22.0, δ: 8.01 (b, 1H), 7.45–7.18 (s, 5H), 5.01–4.88 (s, 2H), 4.09–3.87 (b, 1H), 2.32–1.88 (b, 4H), 1.31–1.15 (b, 0.4H), 0.76–0.74 (s, 0.14H).

4.3.3.3 Synthesis of Linear PBG Serving as Substrates

Three linear PBG substrates with either 15, 30 or 68 repeating units were synthesized. The number of PBG repeating units was controlled by the amount of Glu-NCA and *n*-hexylamine used in the reaction. The Glu-NCA (4 g, 15.2 mmol) was dissolved in dry DMF (10 mL) and *n*-hexylamine (134 μL, 1.01 mmol, 67 μL, 0.50 mmol and 29.5 μL, 0.22 mmol

for target X_n = 15, 30 and 68, respectively) was then added. The reaction was allowed to proceed at room temperature for 3, 4 and 5 h, respectively, before quenching with acetic anhydride (780 μL) to deactivate the terminal amine moiety. After 1 h the product was precipitated in cold methanol, centrifuged and dried under vacuum overnight before characterization.

The different linear PBG substrates are identified in the form PBG_x, where X denotes the experimental number of PBG repeating units in the chains.

(PBG with target X_n = 15) Yield = 89%, M_w/M_n = 1.17. ^{1}H NMR (300 MHz, DMSO-d_6): δ: 8.01 (b, 1H), 7.45–7.18 (s, 5H), 5.01–4.88 (s, 2H), 4.09–3.87 (b, 1H), 2.32–1.88 (b, 4H), 1.31–1.15 (b, 0.2H), 0.76–0.74 (s, 0.20H). X_n = 15.0 (PBG_{15})

(PBG with target X_n = 30) Yield = 90%, M_w/M_n = 1.18. ^{1}H NMR (300 MHz, DMSO-d_6): δ: 8.01 (b, 1H), 7.45–7.18 (s, 5H), 5.01–4.88 (s, 2H), 4.09–3.87 (b, 1H), 2.32–1.88 (b, 4H), 1.31–1.15 (b, 0.2H), 0.76–0.74 (s, 0.10H). X_n = 29.0 (PBG_{29})

(PBG with target X_n = 68) Yield = 92%, M_w/M_n = 1.19. ^{1}H NMR (300 MHz, DMSO-d_6): δ: 8.01 (b, 1H), 7.45–7.18 (s, 5H), 5.01–4.88 (s, 2H), 4.09–3.87 (b, 1H), 2.32–1.88 (b, 4H), 1.31–1.15 (b, 0.2H), 0.76–0.74 (s, 0.05H). X_n = 65.0 (PBG_{65})

4.3.3.4 Synthesis of Partially Deprotected Linear PBG Substrates

A linear polymer PBG_{29} (3.05 g, 13.9 mmol Bz-Glu units) was dissolved in a mixture of TFA (33 mL) and 33% (w/w) HBr solution in acetic acid (0.88 mL, 4.17 mmol). The reaction was stirred for 3 hours at room temperature before the polymer was precipitated

in diethyl ether and recovered by suction filtration to give a product with 31% of free glutamic acid moieties. Yield = 64%.

PBG_{29}-CO_2H. ^1H NMR (300 MHz, DMSO-d_6): δ: 8.01 (b, 1H), 7.45–7.18 (s, 5H), 5.01–4.88 (s, 2H), 4.09–3.87 (b, 1H), 2.32–1.88 (b, 4H), 1.31–1.15 (b, 0.2H), 0.76–0.74 (s, 0.1H). X_n = 29.0

The partially deprotected linear PBG_{65} substrate was synthesized by the same procedure described above to give a product with 31% of free glutamic acid moieties. Yield = 68%.

PBG_{65}-CO_2H. ^1H NMR (300 MHz, DMSO-d_6): δ: 8.01 (b, 1H), 7.45–7.18 (s, 5H), 5.01–4.88 (s, 2H), 4.09–3.87 (b, 1H), 2.32–1.88 (b, 4H), 1.31–1.15 (b, 0.2H), 0.76–0.74 (s, 0.05H). X_n = 65.0

4.3.3.5 Synthesis of Fully Deprotected Linear PBG Substrate

Sample PBG_{15} (2.90 g, 13.2 mmol Bz-Glu units) was dissolved in a mixture of TFA (30 mL) and 2.8 mL (13 mmol) of 33% (w/w) HBr solution in acetic acid. The reaction was allowed to stir for 3 h at room temperature before the polymer was precipitated in diethyl ether. After drying under vacuum the precipitate was dissolved in and dialyzed against distilled water, and subsequently freeze-dried, yielding a polymer with fully deprotected glutamic acid moieties as a white solid. Yield = 43%.

PBG_{15}-CO_2H. ^1H NMR (300 MHz, DMSO-d_6): δ: 8.01 (b, 1H), 4.09–3.87 (b, 1H), 2.32–1.88 (b, 4H), 1.31–1.15 (b, 0.2H), 0.76–0.74 (s, 0.2H). X_n = 15.0

4.3.3.6 Synthesis of G0 Arborescent PBG

In a typical coupling reaction used for the synthesis of $G0PBG_{29}$ and $G0BPG_{65}$, the partially (31 %) deprotected polymer serving as substrate (1.10 g, 1.78 mmol $-CO_2H$) and the polymer serving as side chains (5.39 g, 1.05 mmol chains) were dissolved in 50 mL of dry DMSO. The peptide coupling reagents DIC (2.37 mL, 15.2 mmol) and HOBt (2.05 g, 15.2 mmol) were then added to the reaction with TEA (0.73 mL, 5.2 mmol). The reaction was allowed to proceed for 36 h at room temperature before adding *n*-hexylamine (1.84 mL, 18.2 mmol) to deactivate residual activated carboxylic acid sites. After 3 h the product was precipitated in cold methanol and recovered by suction filtration. Unreacted side chains were removed from the G0 crude polymer by preparative size exclusion chromatography (SEC).

In a typical coupling reaction for $G0PBG_{15}$, the fully deprotected polymer serving as substrate (0.14 g, 1.08 mmol $-CO_2H$) and the polymer serving as side chains (5.07 g, 0.98 mmol chains) were dissolved in 45 mL of dry DMSO. The peptide coupling reagents DIC (0.93 mL, 6.0 mmol) and HOBt (0.81 g, 6.0 mmol) were then added to the reaction with TEA (0.69 mL, 4.9 mmol). The reaction was allowed to proceed for 36 h at room temperature before adding *n*-hexylamine (0.72 mL, 7.2 mmol) to deactivate residual activated carboxylic acid sites. After 3 h the product was precipitated in cold methanol and recovered by suction filtration. Unreacted side chains were removed from the G0 crude polymer by preparative size exclusion chromatography (SEC).

4.3.3.7 Synthesis of G1 and G2 Arborescent PBG

The G1 and G2 arborescent PBG substrates were synthesized as described in the previous chapter. Briefly, G0PBG (2.2 g, 10.0 mmol Bz-Glu units) was first partially deprotected by dissolution in a mixture of TFA (20 mL) and 0.64 mL (3.0 mmol) of 33% (w/w) HBr solution in acetic acid. The reaction was allowed to stir for 3 hours at room temperature before the polymer was recovered by precipitation in diethyl ether, suction filtration, and drying under vacuum. The product was recovered with 53% yield with 31 mol % of free glutamic acid moieties. In a typical coupling reaction for the synthesis of G1PBG, the partially deprotected G0PBG substrate (0.3 g, 0.48 mmol $-CO_2H$) and the polymer serving as side chains (2.27 g, 0.44 mmol chains) were dissolved in 15 mL of dry DMSO. The peptide coupling reagents DIC (0.42 mL, 2.7 mmol) and HOBt (0.36 g, 2.7 mmol) were then added to the reaction with TEA (0.31 mL, 2.2 mmol). The reaction was allowed to proceed for 36 h at room temperature before adding *n*-hexylamine (0.32 mL, 3.2 mmol) to deactivate residual carboxylic acid sites. After 3 h the product was recovered by precipitation in cold methanol, suction filtration, and drying under vacuum. Unreacted side chains were removed from the crude polymer by preparative SEC. The G2 arborescent PBG samples were synthesized and purified as described for the G1 sample.

4.3.3.8 Quantification of Primary Amine Functionality Level by ^{19}F NMR Analysis

^{19}F NMR spectroscopy was used to determine the chain end primary amine functionality level, f_{NH2}, of the linear polymers used in the grafting reactions as described in the literature.[28] The PBG sample (0.10 g, 1.72×10^{-5} mol chains) was first dissolved in 3 mL of deuterated DMSO (DMSO-d_6). A solution of 4-trifluoromethylbenzaldehyde

(TFBA, 0.0901 g, 5.17×10^{-4} mol) and benzotrifluoride (BTF, 0.0756 g, 6.16×10^{-4} mol) in 2 g of DMSO-d_6 was then prepared, and 0.1706 g of that reagent solution (4.563×10^{-5} mol TFBA, 4.531×10^{-5} mol BTF) was added to the PBG solution which was stirred for 2 h before it was transferred to an NMR tube for analysis.

4.3.3.9 Synthesis of Diphenylmethylpotassium

Diphenylmethylpotassium (DPMK) was prepared as described in the literature.[29] Briefly, in a flame-dried 3-neck round-bottom flask (RBF) with a magnetic stirring bar, attached to a high-vacuum line, 150 mL of dry THF was introduced followed by potassium metal (4.2 g, 107 mmol, 2 eq) cut into small pieces. Naphthalene (6.89 g, 53.7 mmol, 1 eq) was added, at which point the solution turned dark green. After stirring for 30 min, diphenylmethane (18.1 mL, 107 mmol, 2 eq) was added to the flask with a syringe. All these additions were performed under nitrogen atmosphere. The reaction was allowed to proceed overnight to give a dark red DPMK solution.

4.3.3.10 Determination of the Concentration of the DPMK Solution

In a flame-dried 3-neck RBF with a magnetic stirring bar and purged with nitrogen, attached to a high-vacuum line, 30 mL of dry THF were introduced followed by a few drops of DPMK solution, until the solution retained a pale yellow coloration. Acetanilide (50 mg, 0.37 mmol) was then added to the solution, at which point the solution became colorless. The DPMK solution was then slowly added (0.75 mL) to obtain the same pale yellow color present initially. The concentration of DPMK was determined to be 0.49 M.

4.3.3.11 Ethylene Oxide Purification

Ethylene oxide (EO) is very toxic in both its liquid and gas forms. Therefore it must be handled with special care in a well-ventilated fume hood. A vacuum manifold was connected to the EO tank line, and a thick-wall (double-thickness) ampoule with a PTFE stopcock, a magnetic stirring bar, and approximately 2 g of calcium hydride as drying agent. The apparatus was thoroughly flamed to remove adsorbed water before the manifold was sealed, the ampoule was cooled in liquid nitrogen, and EO was introduced slowly and condensed in the ampoule. The ampoule was then removed and mounted on a vacuum manifold with a RBF containing a magnetic stirring bar and another ampoule with a PTFE stopcock. The EO was degassed with three successive freeze-pump-thaw cycles. After closing the ampoule containing the EO the rest of the manifold was evacuated, flame-dried and purged with nitrogen. Then phenylmagnesium chloride solution (PhMgCl, 10 mL, 2.0 M in THF) was added to the RBF. After removing the THF under vacuum the EO was recondensed to the RBF, stirred with the PhMgCl in an ice bath for 1 h, and slowly recondensed to the empty ampoule, which was subsequently removed and stored in the fume hood.

4.3.3.12 Polymerization of EO

Poly(ethylene oxide) (PEO) with a primary amine end group was synthesized using a vacuum manifold with a 5-neck RBF containing a magnetic stirring bar and the sealed ampoule containing the purified EO monomer (17.4 g, 0.395 mol). After the RBF was flame-dried under vacuum and purged with nitrogen, dry THF (200 mL) was added. The DPMK solution was introduced drop-wise through one neck until a faint yellow color

persisted, followed by 3-aminopropanol (0.138 mL, 1.75 mmol). Additional DPMK solution (4.7 mL, 2.3 mmol) was then added to deprotonate the alcohol. The EO monomer (17.4 g, 0.395 mol, for a target X_n = 226, M_n = 10000 g/mol) was added to the reaction, transferred to the ampoule and sealed carefully. The reaction was allowed to proceed for 9 days at 45 ˚C in an oil bath, after which acidified methanol (0.5 mL, 1/10 v/v HCl/methanol) was added to the dark brown solution to terminate the reaction. The solution was concentrated by rotary evaporation and precipitated in diethyl ether. The brownish powder recovered by filtration was redissolved in methanol and precipitated again in diethyl ether. The polymer, recovered by suction filtration and drying under vacuum, was obtained as a white powder. Yield: 12.8 g (73%). SEC (THF): M_n^{app} = 10,100 g/mol, M_w/M_n = 1.12. ^{1}H NMR: (300 MHz, $CDCl_3$): δ: 3.87-3.35 (m, 912H), 3.1 (br, 2H), 1.96 (br, -OH), X_n = 228 (M_n = 10,100 g/mol).

4.3.3.13 Synthesis of Arborescent Copolymers

The arborescent copolymers were synthesized and purified similarly to the arborescent PBG samples. The synthesis of G1PBG$_{15}$-*g*-PEO is described below as an example. The partially deprotected G1PBG$_{15}$ substrate (30 mol % of free glutamic acid moieties, 0.040 g, 0.063 mmol –CO_2H) and the PEO serving as side chains (0.58 g, 0.057 mmol chains) were dissolved in 5 mL of dry DMSO. The peptide coupling reagents DIC (0.055 mL, 0.35 mmol) and HOBt (0.047 g, 0.35 mmol) were then added to the reaction with TEA (0.040 mL, 0.29 mmol) as a base. The reaction was allowed to proceed for 36 h at room temperature before adding *n*-hexylamine (0.042 mL, 0.42 mmol) to deactivate residual activated carboxylic acid sites. After 3 h the product was precipitated in cold methanol and

recovered by suction filtration. Unreacted side chains were removed from the G1PBG$_{15}$-*g*-PEO crude product by preparative size exclusion chromatography (SEC) in DMF and the sample was recovered by precipitation in cold diethyl ether, suction filtration, and drying under vacuum: Grafting yield = 27%, M_n =1.2×10^6, M_w/M_n = 1.07 (MALLS).

4.3.3.14 Preparation of DOX-Loaded Unimolecular Micelles

All the DOX-loaded micelles were prepared by dialysis. DOX·HCl was first neutralized with two equivalents of triethylamine (TEA) in DMSO to obtain the drug it its free base (hydrophobic) form. The arborescent copolymer (10 mg) was dissolved in 1 mL of DMSO and stirred for 2 hours. Then 0.5 mL of DOX solution in DMSO (4 mg/mL) was added to the micellar solution and the mixture was stirred overnight in the dark. The organic solvent and free drug were removed by dialysis (MWCO 3500) against deionized water (1 L) for 24 h (the dialysis medium was changed three times) and the solution was either lyophilized in the dark or used directly for measurements. For the determination of the drug loading content (DLC) and the drug loading efficiency (DLE), the lyophilized DOX-loaded micelles were dissolved in deionized water and the absorbance was measured on a UV-Vis spectrometer at 483 nm. The DLC and DLE were calculated according to the following equations:

$$\mathrm{DLC} = \frac{\text{mass of drug in micelles}}{\text{mass of micelles and drug}} \times 100\% \qquad (4.1)$$

$$\mathrm{DLE} = \frac{\text{mass of drug in micelles}}{\text{total mass of drug in feed}} \times 100\% \qquad (4.2)$$

4.3.3.15 *In Vitro* Release of DOX

To determine the release profiles of DOX, a 3 mg sample of the freeze-dried DOX-loaded unimolecular micelles was suspended in 1 mL of phosphate buffered saline (release medium, 10 mM phosphate, 137 mM NaCl and 2.7 mM KCl, pH 7.4 or 5.5; the pH was adjusted by addition of 6 M HCl) and transferred into a dialysis bag (MWCO 3500). The release experiment was initiated by placing the sealed dialysis bag into 3 mL of release medium at the same pH and 37 ˚C, with constant shaking at 100 rpm. At selected time intervals, the release medium was completely withdrawn and replaced with 3 mL of fresh medium. The amount of DOX released was calculated based on the absorbance measured on a UV-Vis spectrometer at 483 nm and a molar extinction coefficient ε = 10,240 $M^{-1} \cdot cm^{-1}$. The drug release studies were performed in triplicate for each sample.

4.4 Results and Discussion

4.4.1 Synthesis of Linear PBG Substrates

The characteristics of arborescent copolymers can be tailored to meet specific requirements for different applications through variations in the synthetic procedure. For instance, the molecular weight of the linear substrate serving in the synthesis of the G0 polymer, the functionalization level of the substrate, and the number of grafting cycles used in their synthesis can be varied. In the current investigation, the length and the deprotection level of the linear PBG substrate used in the synthesis of G0PBG were varied, while the length of the PBG side chains (core building blocks) had $M_n \approx 5000$ g/mol in all cases. Linear PBG substrates with three different length were synthesized with X_n = 15, 29, and

65 as shown in Table 4.1. The number of benzyl glutamate repeating units was controlled by varying the ratio of monomer (Glu-NCA) to initiator (*n*-hexylamine) used in the polymerization reaction. Initially, linear PBG substrates were used with different lengths and the deprotection level of the substrates employed in the synthesis of G0PBG was varied with the hope that the shape of the molecules could be controlled. Unfortunately, the TEM and AFM images indicated that they were all spherical. This approach nevertheless allowed us to vary the branching density in the cores, which seemed to correlate very well with the release properties of the micelles, as discussed in Section 4.4.7.

Table 4.1. Synthesis of linear PBG substrates with different molecular weights.

Sample	Target X_n	^{1}H NMR X_n	$M_n^{H\ NMR}$	M_n^{app}(SEC)	PDI
PBG_{15}	15	15	3,600	3,880	1.11
PBG_{29}	30	29	6.600	6,900	1.10
PBG_{65}	68	65	14,500	15,700	1.12

The different linear PBG substrates are identified in the form PBG_x, where X denotes the experimental number of PBG repeating units in the chains. The arborescent G0PBG molecules obtained by coupling the amine-terminated PBG side chains with the different carboxyl-functionalized PBG substrates are likewise identified in the form $G0PBG_{x,}$ where X denotes the number of PBG repeating units that were used as substrate for the synthesis

of G0PBG. For example, G0PBG$_{29}$ describes an arborescent polymer derived from the PBG substrate with X_n = 29. Similar sample notation is used for the G1 and G2 samples.

All the PBG substrates used in this work were synthesized by the ring-opening polymerization of Glu-NCA in *N*,*N*-dimethylformamide (DMF) at 25 ˚C, using *n*-hexylamine as initiator, and quenching with acetic anhydride to deactivate the terminal amine moiety as shown in Scheme 4.2.

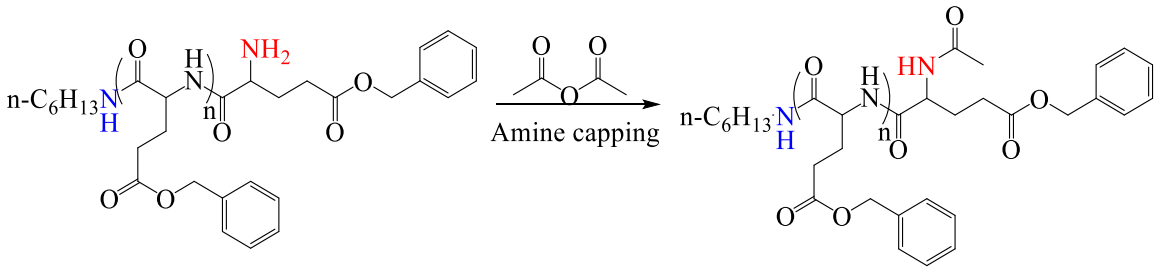

Scheme 4.2. Deactivation of the terminal amine moiety on the linear PBG substrates.

As shown in Figure 4.1, the absolute values of M_n and X_n were determined from ^{1}H NMR analysis of the linear PBG samples, by comparing the integrated peak intensities for the benzylic methylene protons in the repeating units (4.9 ppm) and the terminal methyl group signal from the *n*-hexylamine initiator (0.77 ppm). For example, since the integrals for the peaks at 4.9 ppm and 0.77 ppm were 0.9 and 0.09, respectively, the X_n for PBG$_{15}$ was calculated as (0.9/2H)/ (0.09/3H) = 15.0 by that approach.

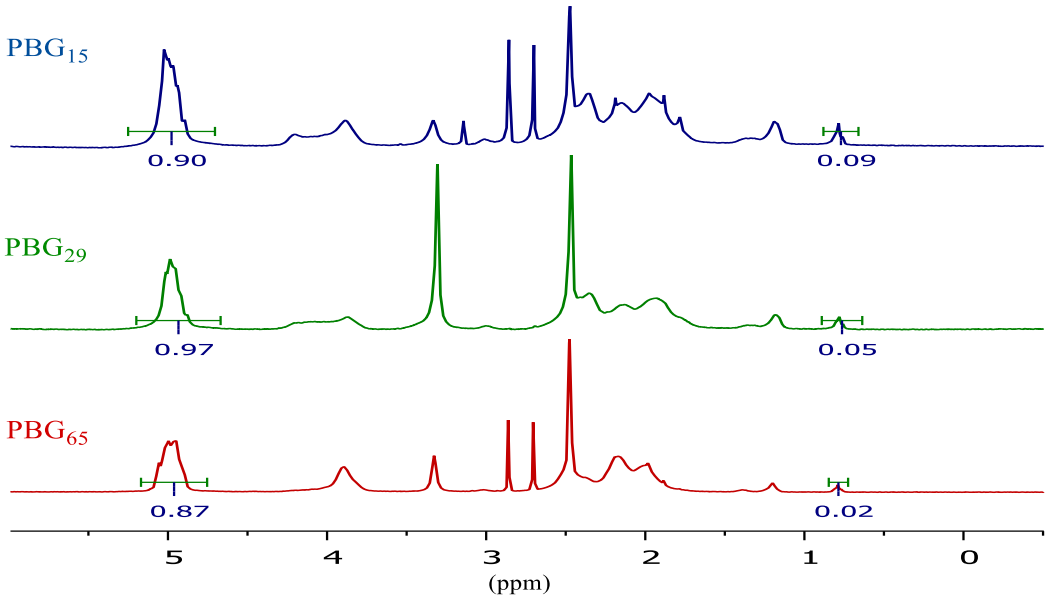

Figure 4.1. Comparison of ^{1}H NMR spectra for the different linear PBG samples.

4.4.2 Deprotection of Linear PBG Substrates

The branching functionality f_n of arborescent polymer molecules can be varied through the functionalization (deprotection) level of the substrate. In the current investigation, only the deprotection level of the linear PBG substrate serving in the G0 polymer synthesis was varied (Scheme 4.3).

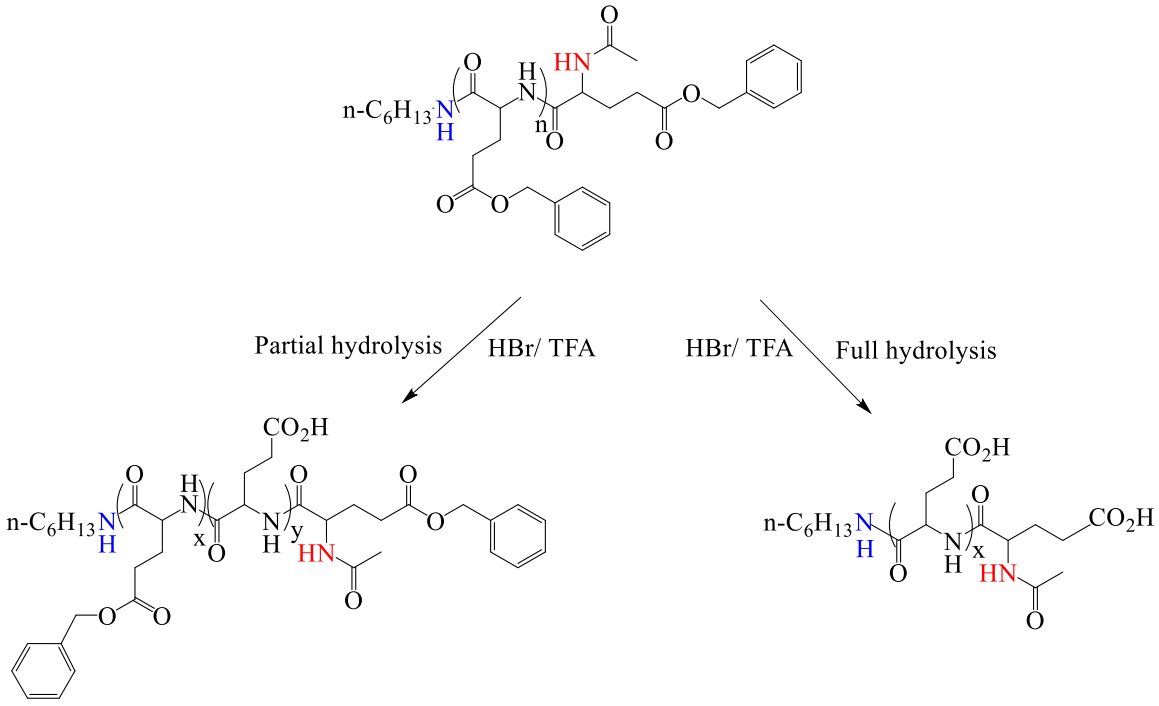

Scheme 4.3. Partial and complete deprotection of the PBG substrates.

The treatment of linear PBG with a mixture of HBr/TFA allowed the cleavage of a controlled fraction of benzyl ester protecting groups under mild reaction conditions, to generate coupling sites (carboxyl groups) for the grafting reaction. A target deprotection level of 31 % was used for PBG_{29} and PBG_{65}, while 100 % deprotection was used for PBG_{15} as shown in Table 4.2. The deprotection level was controlled by varying the molar ratio of HBr added with respect to the benzyl ester moieties.

Table 4.2. Deprotected linear PBG serving as substrates.

Sample	Target X_n	^{1}H NMR X_n	Target deprotection level (%)	^{1}H NMR deprotection level (%)
PBG_{15}	15	15	100	100
PBG_{29}	30	29	30	31
PBG_{65}	68	65	30	31

The deprotection level of the PBG substrates was determined by ^{1}H NMR analysis as described in Chapter 3 (Section 3.4.2). The ^{1}H NMR spectra for partly deprotected PBG_{29} and PBG_{65}, and for fully deprotected PBG_{15} are shown in Figure 4.2. The ratio of integrated intensities for the benzylic methylene protons (2H at 4.9 ppm) of the remaining protected structural units to the methine protons (1H at 3.9 ppm) was used to determine the deprotection level of PBG_{29} and PBG_{65}. For example, dividing the methylene protons integral (2.00/2H) by the methine protons integral (1.45/1H) gave a fraction of repeat units still protected of 0.69 or 69%. The corresponding deprotection level was therefore 31% for both PBG_{29} and PBG_{65} (Figure 4.2b and Figure 4.2c). The disappearance of the benzylic methylene (2H at 4.9 ppm) and phenyl protons (5H at 7.3 ppm) confirmed the complete deprotection of the glutamic acid units in the PBG_{15} substrate (Figure 4.2a).

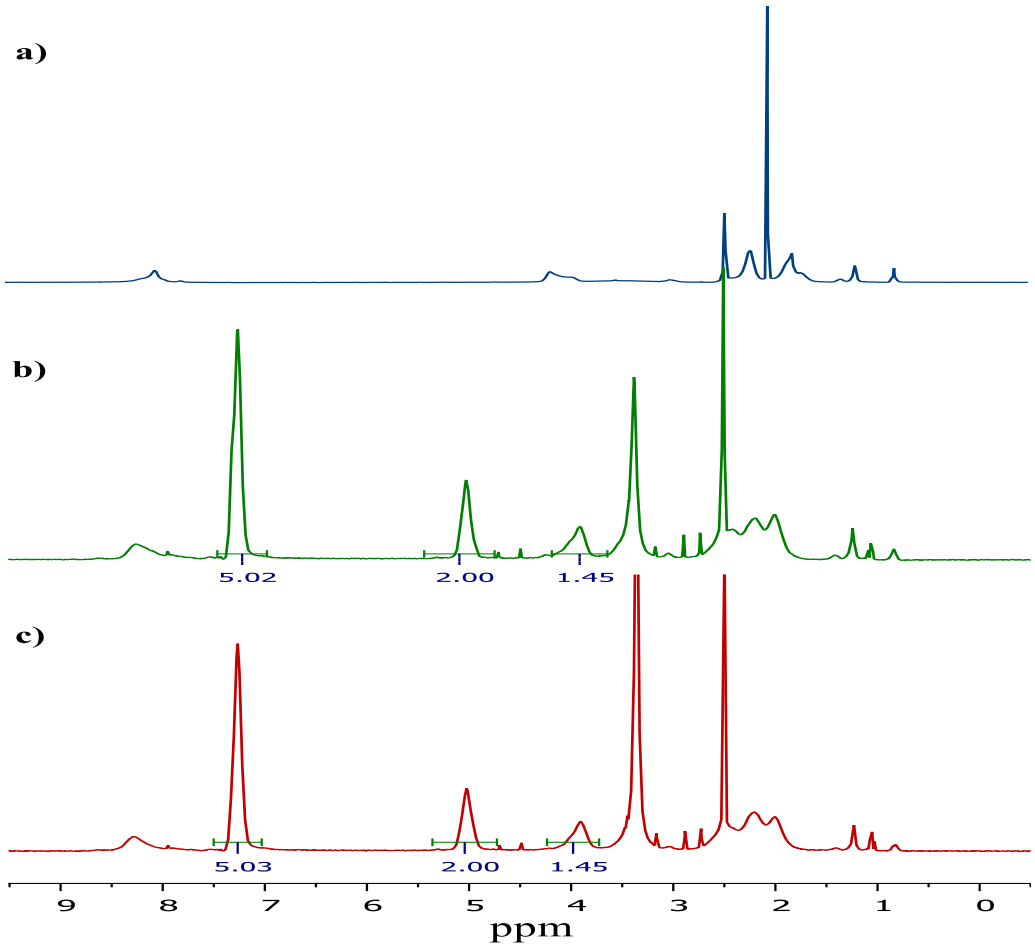

Figure 4.2. ^{1}H NMR spectra for (a) fully deprotected linear PBG$_{15}$, (b) partially deprotected linear PBG$_{29}$, and (c) partially deprotected linear PBG$_{65}$.

4.4.3 Synthesis of G0PBG with Different Branching Densities

The synthesis of arborescent G0PBG from amine-terminated PBG side chains and carboxyl-functionalized PBG substrates of different lengths and deprotection levels was achieved using the optimized coupling reaction conditions determined in Chapter 3. The coupling reagents *N*,*N*′-diisopropylcarbodiimide (DIC) and 1-hydroxybenzotriazole (HOBt) were used to activate the carboxyl groups. All the reactions were carried out in

DMSO at 25 ˚C, using a 5:1 molar ratio of coupling agents (DIC/HOBt) to CO_2H groups on the substrate to maximize the grafting yield and the coupling efficiency. These optimized conditions were also subsequently used to synthesize the G1 and G2 arborescent PBG. The general coupling reaction for the synthesis of arborescent PBG is shown in Scheme 4.4, using a G0 polymer synthesis as an example.

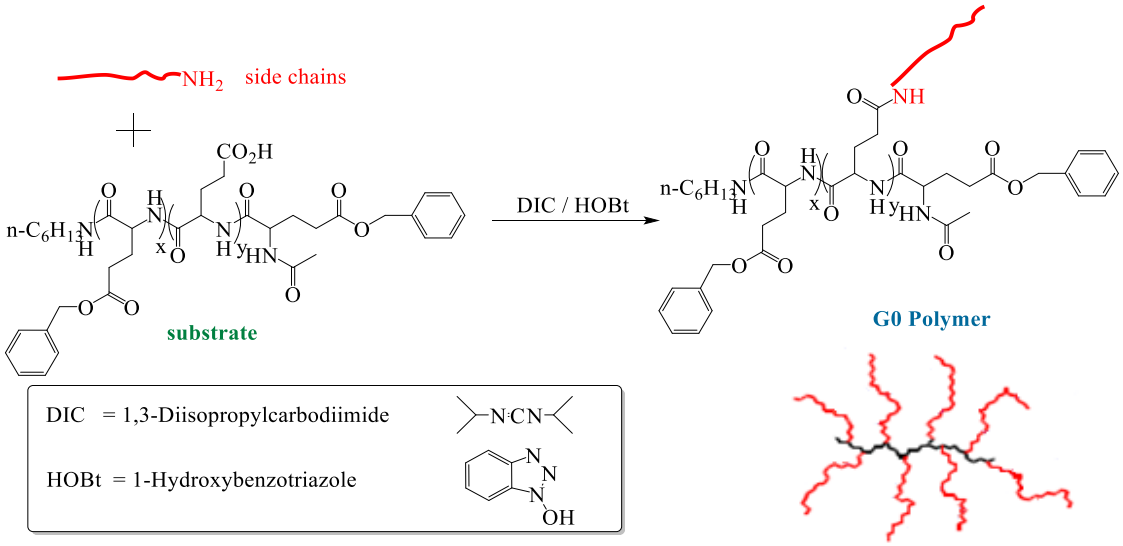

Scheme 4.4. Synthesis of a G0 polypeptide from PBG building blocks.

Different chain lengths and deprotection levels for the linear PBG substrate were used in the synthesis of G0PBG, while the PBG side chains had $M_n \approx 5000$ g/mol in all cases. Three well-defined (PDI ≤ 1.08) arborescent G0 (comb-branched) PBG were obtained in that manner: $G0PBG_{15}$ from a PBG substrate with $X_n = 15$ and 100% deprotection, $G0PBG_{29}$ from a PBG substrate with $X_n = 29$ and 31% deprotection, and $G0PBG_{65}$ from a PBG substrate with $X_n = 65$ and 31% deprotection. The corresponding characterization data are summarized in Table 4.3.

Table 4.3. Characteristics of arborescent G0PBG with different structures.

Sample	Deprotection level (%) of substrate	Molar ratio CO_2H : NH_2	M_n(g/mol)	PDI	G_y (%)	C_e (%)	f_n	b_d
$G0PBG_{15}$	100	1.1 : 1	65400	1.04	76	80	12	0.80
$G0PBG_{29}$	31	1.7 : 1	35300	1.08	87	54	5.4	0.19
$G0PBG_{65}$	31	1.7 : 1	51000	1.06	89	36	7.1	0.11

As shown in Table 4.3, the number-average branching functionality of the arborescent polypeptides, f_n, defined as the number of side chains added in the grafting reaction, increased with the deprotection level since more coupling sites were available. However, despite the identical deprotection levels of PBG_{29} and PBG_{65}, the branching functionality f_n achieved for $G0PBG_{29}$ was marginally lower. This may be due to increased steric crowding leading to less accessible carboxylic acid moieties in the shorter PBG_{29} substrate. The number-average branching density (b_d), defined as the number of side chains added in the grafting reaction divided by the number of repeating units in the linear substrate, clearly increased as the chain length of the substrate decreased and the deprotection level increased. As a result, a compact and dense structure is expected for $G0PBG_{15}$ (b_d = 0.80), as opposed to a loose and more porous structure for $G0PBG_{65}$ (b_d = 0.11) and an intermediate (semi-compact) structure for $G0PBG_{29}$ (b_d = 0.19).

The synthesis of the arborescent G0PBG samples with different branching densities (porosities) is illustrated with their SEC elution curves in Figure 4.3. It is clear that the elution volume of the graft polymers decreased as the branching functionality increased, while the breadth of the peaks remained constant. These different G0PBG structures will be compared in terms of their influence, when incorporated in the hydrophobic cores, to yield water-dispersible unimolecular micelles and to encapsulate and control the release rate of the drug.

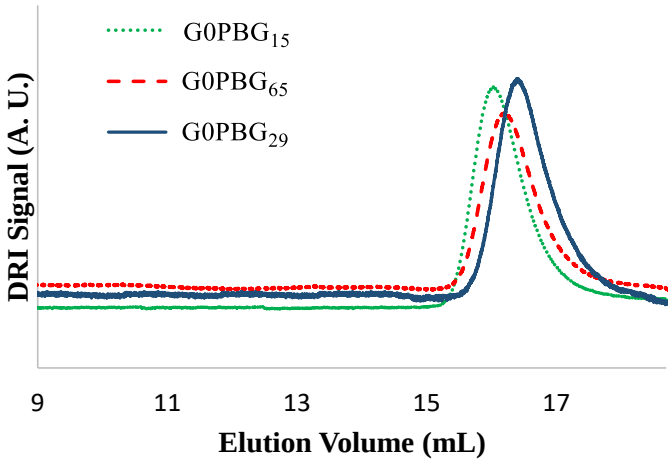

Figure 4.3. SEC traces for G0 arborescent PBG samples.

The G1 and G2 PBG arborescent substrates were synthesized and purified by the same method used for the G0 samples except that, in all cases, the deprotection level of the arborescent substrates used was ≈ 30%, and a 1:1.1 molar ratio of side chains (PBG-NH_2) to CO_2H groups was used to maximize the grafting yield and the coupling efficiency (Table 4.4). The unreacted side chain material was removed from the crude polymer by

preparative size exclusion chromatography (SEC). The absolute molecular weight of the arborescent PBG was determined by SEC-MALLS analysis in DMSO. The molecular weight of the polymers increased with the generation number, while a low polydispersity index (PDI $\leq$ 1.09) was maintained. The branching functionality also increased over successive generations, as more coupling sites were available after each grafting cycle. Sample G1PBG$_{15}$ showed the lowest G_y and C_e, which is attributed to the difficulty for the coupling sites to react in the compact and dense G0PBG$_{15}$ substrate as a result of increased crowding.

Table 4.4. Characteristics of upper generation PBG arborescent substrates.

Sample	M_n(g/mol)[a]	M_w/M_n[a]	G_y (%)[b]	C_e (%)[c]	f_n[d]
G1PBG$_{15}$	240,000	1.07	31	39	35
G1PBG$_{29}$	200,000	1.06	54	66	32
G1PBG$_{65}$	260,000	1.09	53	60	42
G2PBG$_{15}$	1.2×10^6	1.09	50	59	192
G2PBG$_{29}$	1.0×10^6	1.08	47	57	156
G2PBG$_{65}$	1.4×10^6	1.05	56	64	228

[a] Values from SEC-MALLS analysis in DMSO; [b] Grafting yield: fraction of side chains attached to the substrate; [c] Coupling efficiency: fraction of coupling sites on the substrate consumed in the reaction; [d] Branching functionality: number of branches added in the last grafting cycle.

4.4.4 Synthesis of Linear Amine-Terminated Poly(ethylene oxide)

Poly(ethylene oxide) with a primary amine terminus was used as hydrophilic shell material to demonstrate the synthesis of water-dispersible arborescent copolymer micelles. The anionic polymerization of ethylene oxide with a bifunctional initiator, 3-aminopropanol deprotonated with diphenylmethylpotassium (DPMK), was used to obtain linear PEO with a primary amine chain end as shown in Scheme 4.5.

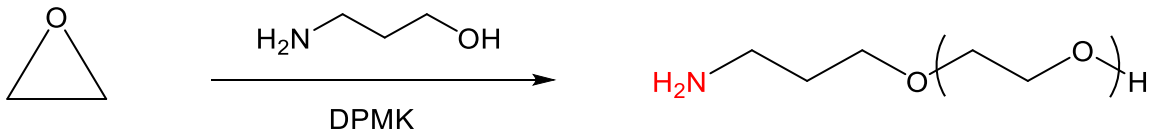

Scheme 4.5. Polymerization of ethylene oxide with 3-aminopropanol and DPMK.

The ^{1}H NMR spectrum obtained for the α-amino PEO sample synthesized is shown in Figure 4.4. The ratio of intensities for the -CH_2- protons next to the terminal amine (δ 3.1 ppm) and the four protons in the repeat units (δ 3.6 ppm) was used to determine the number-average degree of polymerization X_n = 228, which corresponds to M_n = 10,100 g/mol.

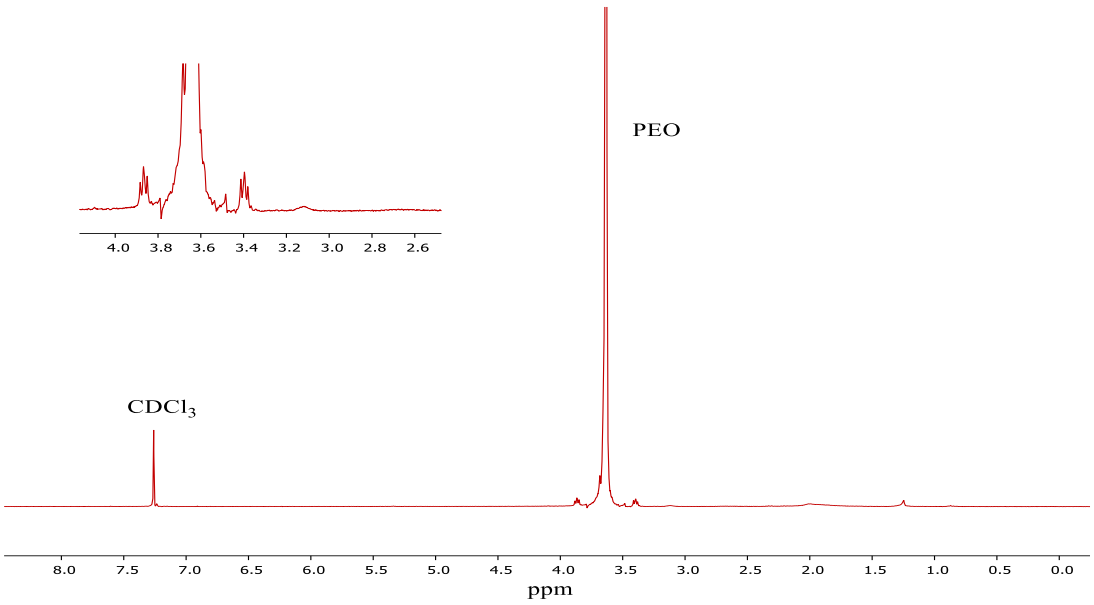

Figure 4.4. ^{1}H NMR spectrum for α-amino PEO in $CDCl_3$.

^{19}F NMR analysis served to determine the amine functionality level of PEO (f_{NH2}). The absence of primary amine end groups would lead to linear PEO chains being incapable of coupling with the substrate. A procedure developed by Ji et al.[28] was used to determine the primary amine functionality level of the PEO side chains. The terminal amine was reacted with 4-trifluoromethylbenzaldehyde (TFBA) to produce imine functionalities at the chain end of the polymer as shown in Scheme 4.6. ^{19}F NMR spectroscopy was then employed to observe the chemical shift of the fluorine atoms in the imine formed, to be compared with the signal for benzotrifluoride (BTF) serving as internal standard.

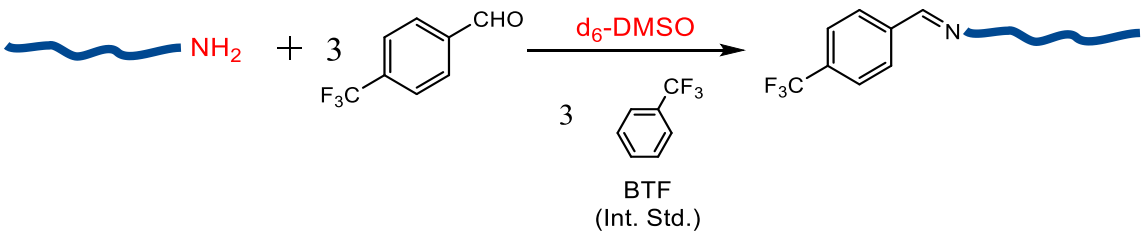

Scheme 4.6. Reaction of 4-trifluoromethylbenzaldehyde (TFBA) with the primary amines end group in the PEO side chains.

The ^{19}F NMR spectrum obtained for the linear PEO sample synthesized using the 3-aminopropanol/DPMK initiator system is shown in Figure 4.5. An amine functionality level f_{NH2} > 94% was obtained by that method. A detailed discussion of the method used to obtain the f_{NH2} value by ^{19}F NMR analysis was provided in Chapter 3.

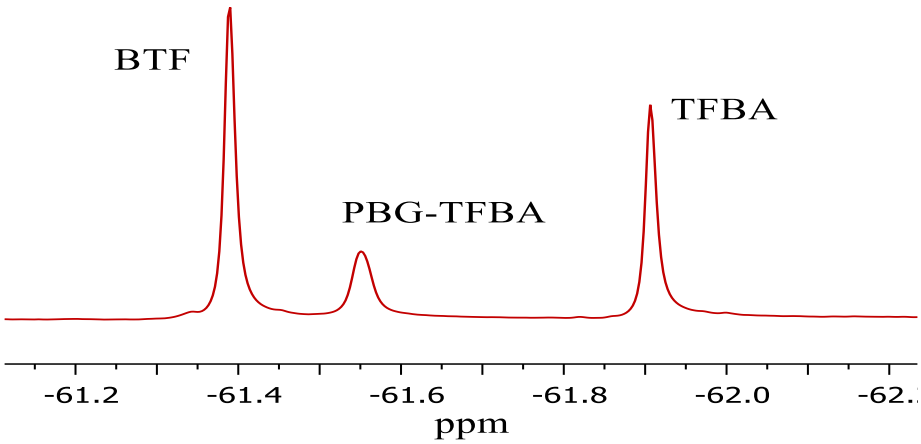

Figure 4.5. ^{19}F NMR spectrum for linear PEO synthesized using the 3-aminopropanol/DPMK initiator system, after treatment with 4-trifluoromethylbenzaldehyde (TFBA).

4.4.5 Synthesis of Randomly Grafted Arborescent Copolymers

Structural variables such as the size and the branching density (porosity) of arborescent copolymers can be designed to meet specific requirements for various applications. It was hypothesized that it should be possible to tailor the micellar properties of these materials by adjusting the length of the linear substrate used in the synthesis of the G0 polymer. Whitton and Gauthier previously reported the use of linear poly(ethylene oxide) with a molecular weight of 5000 (PEG_{110}), grafted either randomly or at the end of the chains on arborescent PBG substrates to generate arborescent copolymer micelles.[25] Unfortunately, the randomly grafted arborescent G1PBG-*g*-PEO_{110} copolymers obtained by that approach yielded large aggregated species in phosphate buffered saline (PBS), while G2PBG-*g*-PEO_{110} and G3PBG-*g*-PEO_{110} were both insoluble. The corresponding end-grafted samples PBG-*eg*-PEO_{110} displayed better dispersibility in PBS than the randomly grafted systems, albeit a small population of aggregates still existed in these samples. These results were nevertheless useful in demonstrating that the solubility of arborescent copolymers could be controlled through variations in their structure and composition. Therefore we hypothesized that by randomly grafting longer hydrophilic PEO chains (M_n =10,000 g/mol), the solubility of the copolymers in PBS would be enhanced to yield stable unimolecular micelles without aggregation. This would in turn affect the size and the properties of the micelles, and thereby provide control over the encapsulation and release behaviors of these unimolecular micelles.

In the current investigation, we expanded this approach by designing amphiphilic arborescent copolymers having poly(ethylene oxide) (PEO) chain segments with M_n =

10,100 g/mol randomly grafted onto arborescent PBG substrates of generations G1 and G2 with different G0PBG branching densities, to determine their influence on the dispersibility of the micelles in organic and aqueous environments, and on the encapsulation and release of a hydrophobic drug, doxorubicin. PBG of generations G1-G2 with three different G0PBG core branching densities were employed as substrates to generate a library of randomly grafted amphiphilic arborescent copolymers.

The synthesis of amphiphilic arborescent copolymers from amine-terminated PEO chains and the randomly carboxyl-functionalized PBG substrates (PBG-*rf*-CO_2H) with the different G0PBG cores was achieved using the optimized reaction conditions mentioned in Chapter 3. The coupling reagent *N*,*N*′-diisopropylcarbodiimide (DIC) and 1-hydroxybenzotriazole (HOBt) as coupling additive were used to activate the carboxyl groups. All the reactions were carried out in DMSO at 25 ˚C, using a 5:1 molar ratio of coupling agents (DIC/HOBt) to CO_2H groups on the substrate. The coupling of a randomly carboxyl-functionalized G1PBG substrate (G1PBG-*rf*-CO_2H) with amine-terminated PEO chains is illustrated in Scheme 4.7 as an example of the synthesis of an amphiphilic arborescent copolymer.

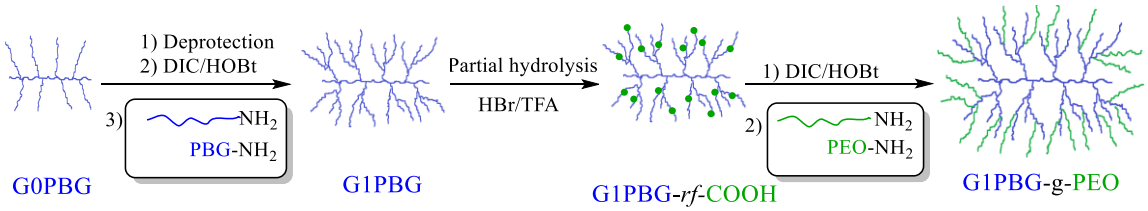

Scheme 4.7. Schematic representation of the synthesis of a randomly carboxyl-functionalized G1PBG substrate (G1PBG-*rf*-CO_2H) and a G1PBG randomly grafted arborescent copolymer.

The results obtained for grafting the different PBG substrates of generations G1 and G2 with PEO side chains are summarized in Table 4.5. The absolute molecular weight of the substrates and the arborescent copolymers was determined by SEC-MALLS analysis in DMSO. In all cases, the molecular weight of the copolymers increased relatively to the PBG substrates, while the polydispersity index remained low (PDI $\leq$ 1.09).

Table 4.5. Characteristics of randomly grafted PBG-*g*-PEO arborescent copolymers.

copolymer	PBG Substrate			Graft Copolymer			
	M_n (g/mol)[a]	%-CO_2H[b]	G_y[c]	M_n (g/mol)[a]	M_w/M_n[a]	f_n[d]	%-PEO[e]
G1PBG$_{15}$-*g*-PEO	240,000	31	27	1.2×10^6	1.07	96	80
G1PBG$_{29}$-*g*-PEO	200,000	31	27	1.0×10^6	1.09	80	80
G1PBG$_{65}$-*g*-PEO	260,000	33	29	1.5×10^6	1.08	124	82
G2PBG$_{15}$-*g*-PEO	1.2×10^6	31	13	3.4×10^6	1.08	220	65
G2PBG$_{29}$-*g*-PEO	1.0×10^6	32	15	3.2×10^6	1.09	220	69
G2PBG$_{65}$-*g*-PEO	1.4×10^6	30	13	3.9×10^6	1.06	250	64

[a] Values from SEC-MALLS analysis in DMSO; [b] Mole fraction of carboxyl groups in the substrate; [c] Grafting yield: fraction of side chains attached to the substrate; [d] Branching functionality: number of branches added in the last grafting cycle; [e] PEO weight fraction, from the difference in M_n of the copolymer and the substrate.

The grafting yield (G_y), defined as the fraction of linear chain segments becoming attached to the substrate, was determined from the weight fraction of each component in the copolymers, along with the known amounts of substrate and side chains used in each grafting reaction. The calculation of the grafting yield for sample G1PBG$_{15}$-*g*-PEO is provided in Equation 4.3 as an example. In this reaction 0.59 g of PEO side chains and 0.04 g of PBG substrate (corresponding to a NH_2/CO_2H ratio of 0.90) were used. Weight fractions for PEO and PBG of 0.80 and 0.20, respectively, were determined when comparing the molecular weights of the copolymer and the substrate. Multiplying the known mass of PBG used in the grafting reaction (0.04 g) by the weight fraction ratios

(0.8/0.2) yields a mass of 0.16 g PEO in the copolymer. Dividing this by the total mass used in the grafting reaction (0.59 g PEO), a grafting yield of 27% was obtained.[25]

$$G_y = \frac{mass\ PBG\ (g) \times \frac{Wt.\ Fraction\ PEO}{Wt.\ Fraction\ PBG}}{mass\ PEO\ (g)} = \frac{0.04 \times \frac{0.8}{0.2}}{0.59} = 0.27 \qquad (4.3)$$

Several factors could have contributed to the relatively low (13-29%) grafting yields in the synthesis of the amphiphilic arborescent copolymers. We assumed that partial deprotection of PBG would yield randomly distributed coupling sites within the substrates, but the deprotection of adjacent groups is also possible, which may lead to increased coupling site crowding. Some coupling sites are also necessarily located deeper within the PBG substrate, and thus less accessible in the grafting reaction. The grafting yield could therefore decline due to a combination of increased steric crowding and decreased accessibility of the carboxylic acid moieties. The grafting yield achieved for the G1PBG-*g*-PEO copolymers was higher than for the G2PBG-*g*-PEO copolymers, which is also expected due to the increased rigidity of the PBG substrates of higher generations.

The branching functionality f_n, defined as the number of PEO side chains added, was determined by dividing the increase in molecular weight observed for the grafted copolymer by the molecular weight of the PEO side chains. A calculation for sample $G1PBG_{15}$-*g*-PEO is provided in Equation 4.4 as an example. The weight fraction of PEO in the copolymers was determined by dividing the increase in molecular weight for the copolymers by their total molecular weight.

$$f_{\mathrm{n}} = \frac{M_n(G1PBG_{15} - g - PEO) - M_n(G1PBG_{15})}{M_n(PEO)} = \frac{1{,}200{,}000 - 240{,}000}{10{,}000} = 96 \quad (4.4)$$

All the copolymers synthesized were purified by preparative SEC. The SEC traces for the purified samples, corresponding to the data summarized in Table 4.5, are compared in Figure 4.6. As expected, a decrease in elution volume is observed as the generation number increases. Within each generation the elution volume decreased in the series PBG_{65}-*g*-PEO < PBG_{15}-*g*-PEO < PBG_{29}-*g*-PEO. The PBG_{65}-*g*-PEO showed the highest molecular weight, likely due to its more porous core structure minimizing steric crowding and facilitating the diffusion of the chains to the coupling sites in the grafting reaction.

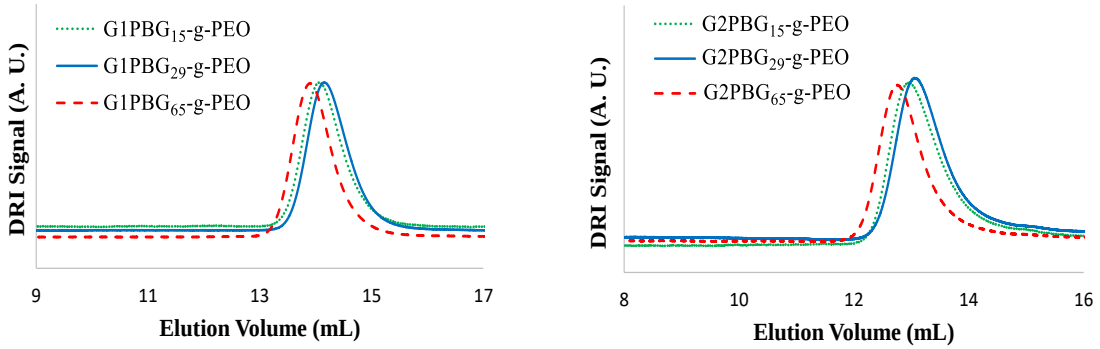

Figure 4.6. SEC traces for G1 (left) and G2 (right) arborescent copolymers.

4.4.6 Properties of Randomly Grafted Arborescent Copolymer Micelles

The different randomly grafted arborescent copolymers were evaluated for their potential to remain as unimolecular micelles in aqueous PBS solutions. The addition of hydrophilic PEO segments to the hydrophobic PBG core was proposed to stabilize the

micelles, without self-assembly typically observed for amphiphilic block copolymer micelles. The characteristics of the arborescent copolymers were evaluated by proton nuclear magnetic resonance (^{1}H NMR) spectroscopy, dynamic light scattering (DLS), transmission electron microscopy (TEM), and atomic force microscopy (AFM) to investigate the effects of the dendritic core structure and the PEO shell on the micelle properties.

The use of ^{1}H NMR spectroscopy to investigate the formation of micellar structures is illustrated in Figure 4.7. Complete disappearance of the peaks characteristic for PBG such as the benzylic methylene (2H at 4.9 ppm) and phenyl protons (5H at 7.3 ppm) is observed in D_2O, while these peaks are clearly visible in DMSO-d_6, which confirms that the G2PBG-*g*-PEO arborescent copolymer has a core–shell morphology in aqueous solutions with a collapsed hydrophobic PBG core and a hydrophilic PEO shell.

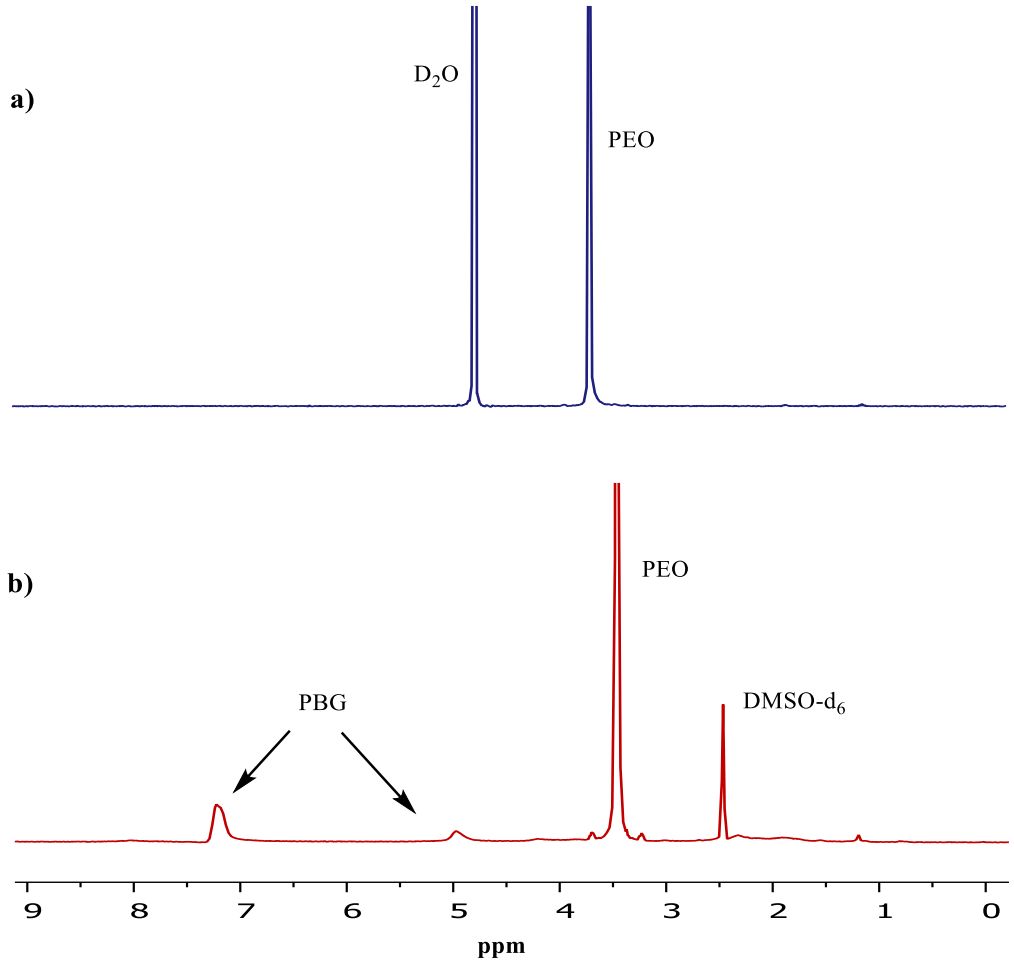

Figure 4.7. ^{1}H NMR spectra for G2PBG$_{29}$-*g*-PEO in (a) D$_2$O and (b) deuterated DMSO.

The hydrodynamic diameter of the copolymers, determined by DLS in DMF (good solvent for PBG and PEO) and in aqueous PBS buffer (solvent selective for PEO) followed the expected trends for increasing generation numbers (Table 4.6).

Table 4.6. Characteristics of randomly grafted PBG-*g*-PEO arborescent copolymers.

Copolymer	DMF				PBS			
	$D_{h,\ number}$	$D_{h,\ volume}$	$D_{h,\ intensity}$	PDI	$D_{h,\ number}$	$D_{h,\ volume}$	$D_{h,\ intensity}$	PDI
G1PBG$_{15}$-*g*-PEO	16 ± 1	18 ± 1	21 ± 1	0.18	16 ± 1	19 ± 1	22 ± 1	0.41
G1PBG$_{29}$-*g*-PEO	15 ± 1	18 ± 1	22 ± 1	0.16	17± 2	22 ± 2	27 ± 2	0.50
G1PBG$_{65}$-*g*-PEO	18 ± 1	22 ± 1	26 ± 1	0.09	19 ± 2	23 ± 2	28 ± 2	0.43
G2PBG$_{15}$-*g*-PEO	33 ± 2	36 ± 2	43 ± 2	0.06	35 ± 2	40 ± 3	47 ± 2	0.28
G2PBG$_{29}$-*g*-PEO	32 ± 2	36 ± 2	42 ± 2	0.03	34 ± 1	40 ± 1	46 ± 2	0.26
G2PBG$_{65}$-*g*-PEO	37 ± 1	45 ± 1	58 ± 2	0.07	39 ± 1	47 ± 1	58 ± 2	0.17

All experiments done in triplicate. The results are presented as the mean ± standard deviation.

The good agreement for the hydrodynamic diameters obtained in DMF and in PBS confirms that the randomly grafted arborescent copolymers formed unimolecular micelles, with mean number-average diameters between 16-18 nm and 32-37 nm for the G1 and G2 in DMF, respectively. As shown in Table 4.6, the unimolecular micelles are uniform in size since the values of the three average diameters (number, volume, and intensity) are similar. The copolymers should form unimolecular, non-aggregated solutions in DMF, a good solvent for both the PBG and PEO components. Analysis of the same copolymers in phosphate buffered saline (PBS) also yielded values for number-, volume-, and intensity-average diameters similar to those obtained in DMF, which suggests that all the arborescent

copolymers formed unimolecular micelles. It is nonetheless well-known that these values represent differently weighted means of the size distributions, and indeed size distribution analysis (Figure 4.8) shows that all the G1PBG-*g*-PEO copolymers exhibit a small quantity (16-34%) of aggregated structures with a diameter of 70−160 nm in their *intensity* distributions, while no aggregation is detected in neither the *number* nor the *volume* distributions. Size distribution analysis of the G2PBG-*g*-PEO copolymers likewise yielded a small quantity (17-32%) of aggregated structures with a diameter of 160−230 nm in the *intensity* distributions, while no aggregation was detected in neither the *number* nor the *volume* distributions (Figure 4.9). These results indicate that even though the vast majority of randomly grafted arborescent copolymer molecules exist as stable, isolated unimolecular micelles, a minute amount of aggregation occurs that is only detectable in the intensity-weighted distributions. Arborescent copolymers of the same generation yielded similar hydrodynamic diameters by DLS analysis even though their core structure was different. For example, when comparing the micelles formed by G2PBG$_{15}$-*g*-PEO and G2PBG$_{65}$-*g*-PEO, there is only a 4 nm difference in the number-average diameter, confirming that the core only has a minor influence on the overall micelle size. Since the hydrophobic PBG cores should collapse to minimize their unfavorable interactions with the aqueous solution (as determined by NMR analysis) and the G1 and G2 cores have similar molecular weight in each series, their contribution to the overall size of the micelles should be minimized in comparison to the more soluble PEO shell.

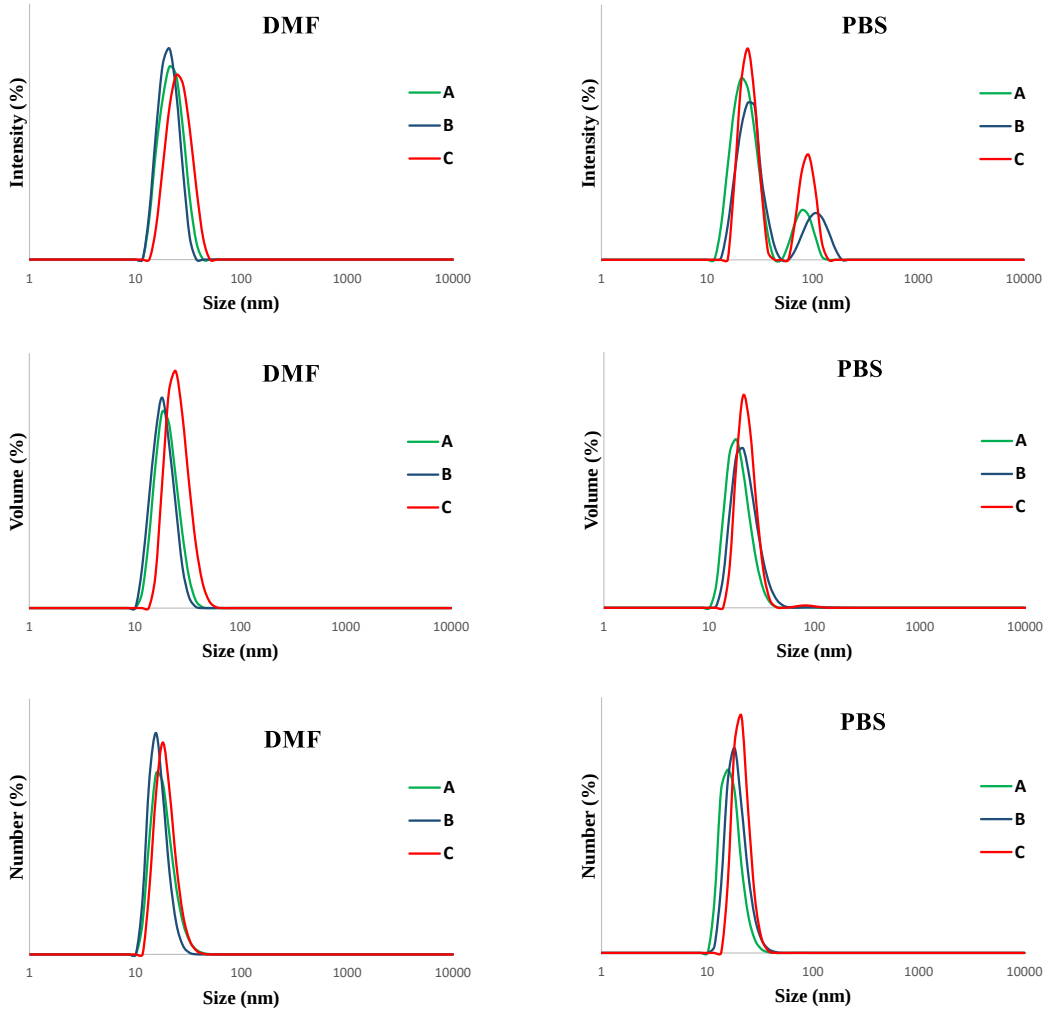

Figure 4.8. Hydrodynamic diameter distributions for randomly grafted arborescent copolymers determined by DLS in DMF (left) and in PBS (right): (A) G1PBG$_{15}$-*g*-PEO, (B) G1PBG$_{29}$-*g*-PEO, and (C) G1PBG$_{65}$-*g*-PEO.

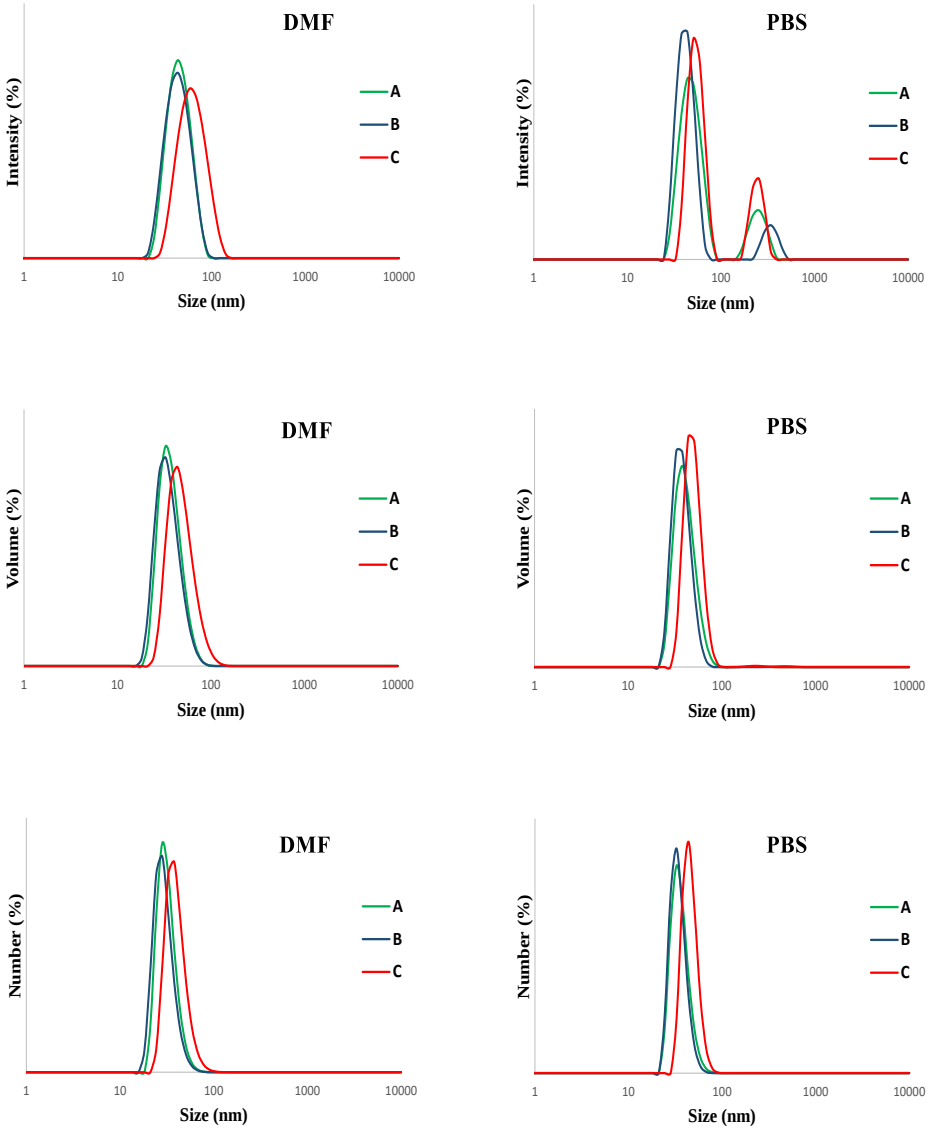

Figure 4.9. Hydrodynamic diameter distributions for randomly grafted arborescent copolymers determined by DLS in DMF (left) and in PBS (right): (A) G2PBG$_{15}$-*g*-PEO, (B) G2PBG$_{29}$-*g*-PEO, and (C) G2PBG$_{65}$-*g*-PEO.

The number-average diameters from DLS may also be used for comparison with other measurements providing number-average results (e.g. TEM and AFM analysis). The morphology and size of the unimolecular micelles were investigated by TEM, after staining

with phosphotungstic acid on a carbon-coated copper grid (negative staining was used to improve the contrast of the micelles), as well as by AFM (Figures 4.10 for G1 copolymers, Figure 4.11 for G2 copolymers). It can be seen that the unimolecular micelles have a fairly uniform size distribution and a spherical shape in all cases. The average micelle diameter measured by TEM was 15 ± 2, 14 ± 3 and 16 ± 2 nm for G1PBG$_{15}$-*g*-PEO, G1PBG$_{29}$-*g*-PEO and G1PBG$_{65}$-*g*-PEO, respectively. In contrast, the average micelle diameter was 29 ± 3, 30 ± 2 and 35 ± 3 nm for G2PBG$_{15}$-*g*-PEO, G2PBG$_{29}$-*g*-PEO and G2PBG$_{65}$-*g*-PEO, respectively. All the measurement were based on 15−30 particles within the same micrograph. The TEM measurements confirmed the trend seen in the DLS measurements in terms of increasing micelle size for higher generations. The diameter of these unimolecular micelles appears to be within the ideal size range for therapeutic nanocarriers to be used in cancer treatment.[30] The size of the micelles measured by TEM was somewhat smaller than by DLS analysis. Because TEM yields the diameter of the dry, somewhat flattened micelles on the TEM grid surface, while DLS measures their hydrodynamic (solvated) diameter, discrepancies are to be expected between these methods. The results obtained are therefore considered to be in good agreement.

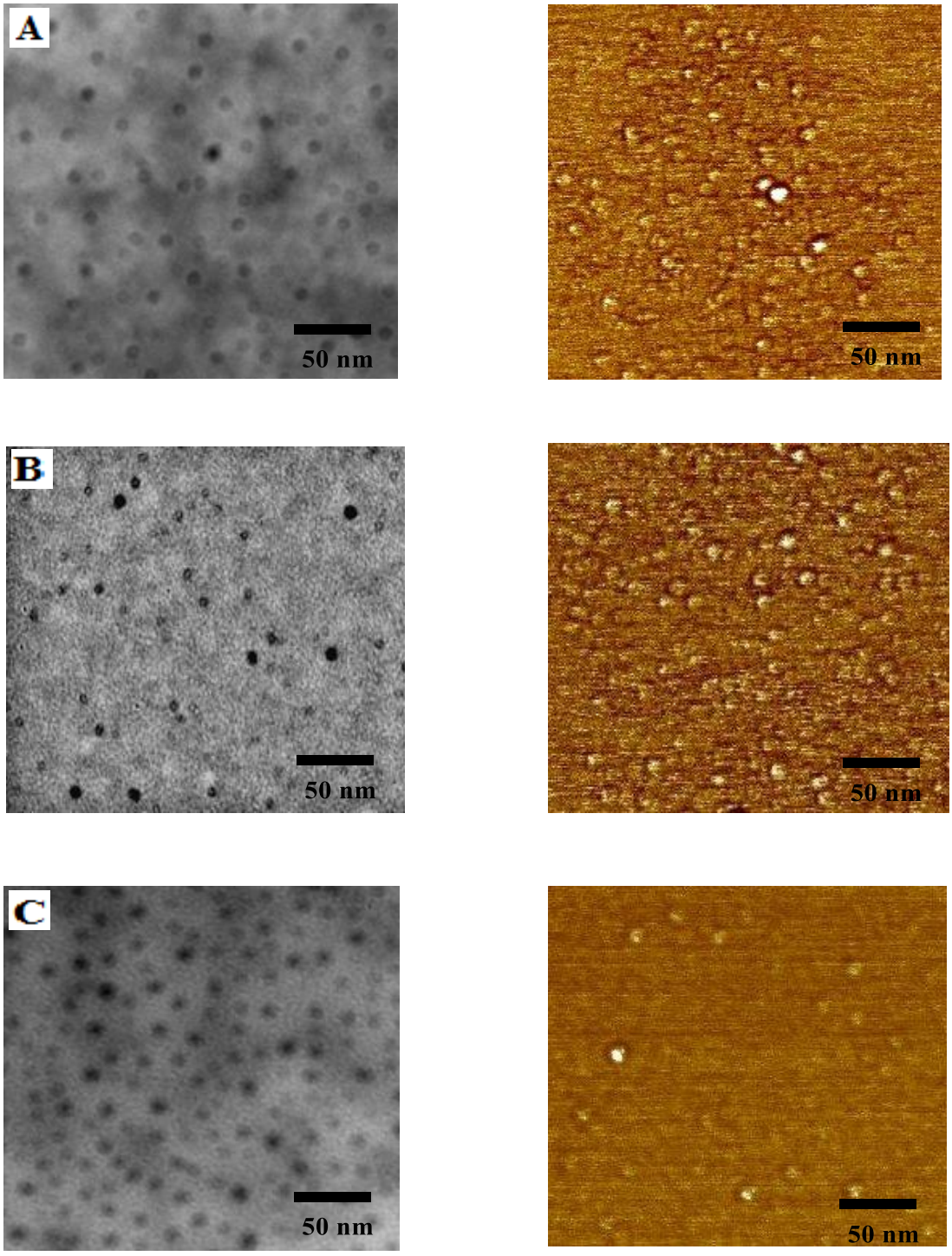

Figure 4.10. TEM (left) and AFM phase scan (right) for randomly grafted arborescent copolymers: (A) G1PBG$_{15}$-*g*-PEO, (B) G1PBG$_{29}$-*g*-PEO and (C) G1PBG$_{65}$-*g*-PEO.

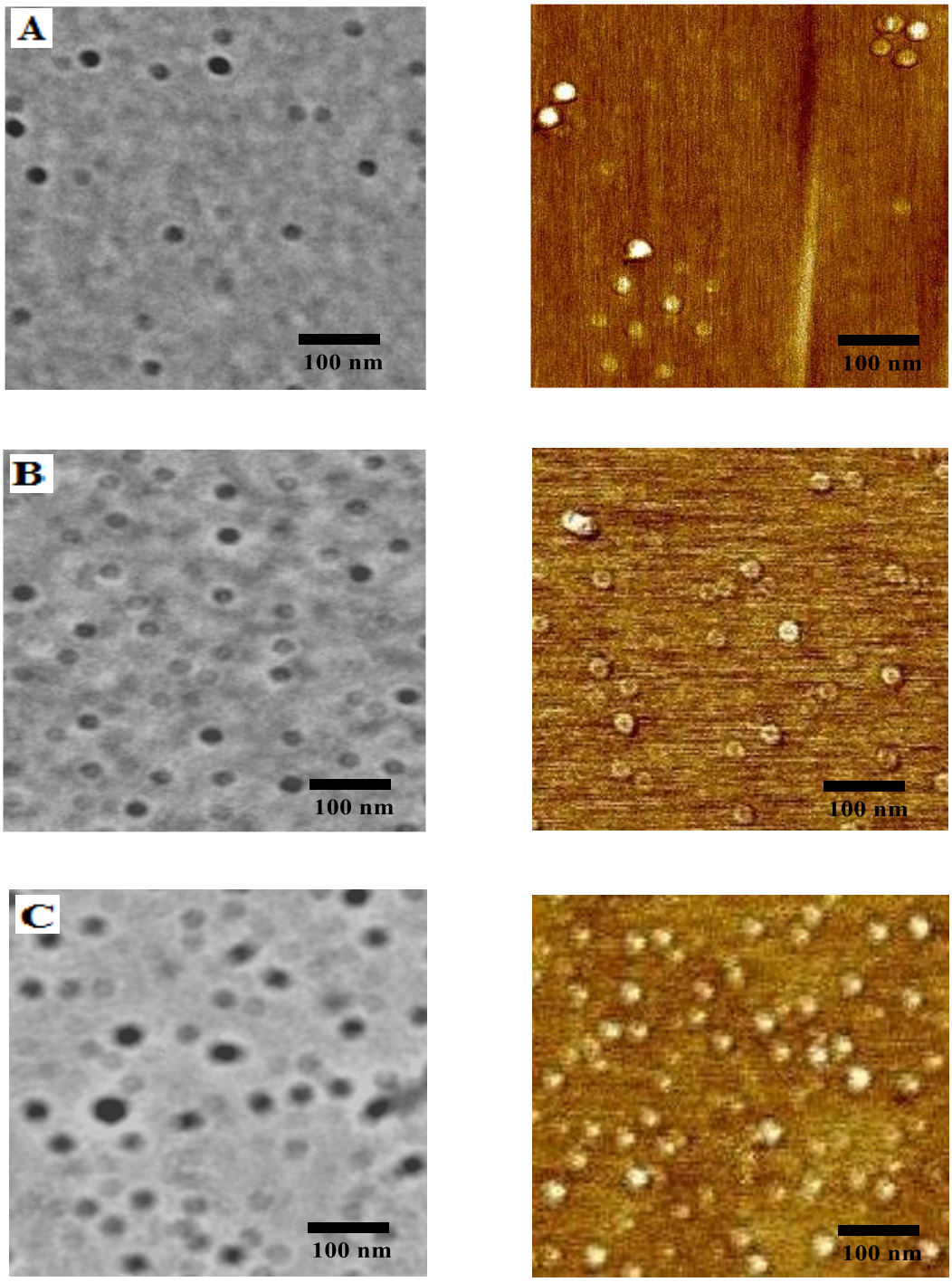

Figure 4.11. TEM (left) and AFM phase scan (right) for randomly grafted arborescent copolymers: (A) G2PBG$_{15}$-*g*-PEO, (B) G2PBG$_{29}$-*g*-PEO and (C) G2PBG$_{65}$-*g*-PEO.

4.4.7 Drug Loading and Micelle Characterization

Since the arborescent PBG-*g*-PEO copolymers have a hydrophobic PBG core and a hydrophilic PEG shell, these amphiphilic molecules could serve as nanocarriers to physically encapsulate hydrophobic guest molecules through hydrophobic interactions (Scheme 4.8).

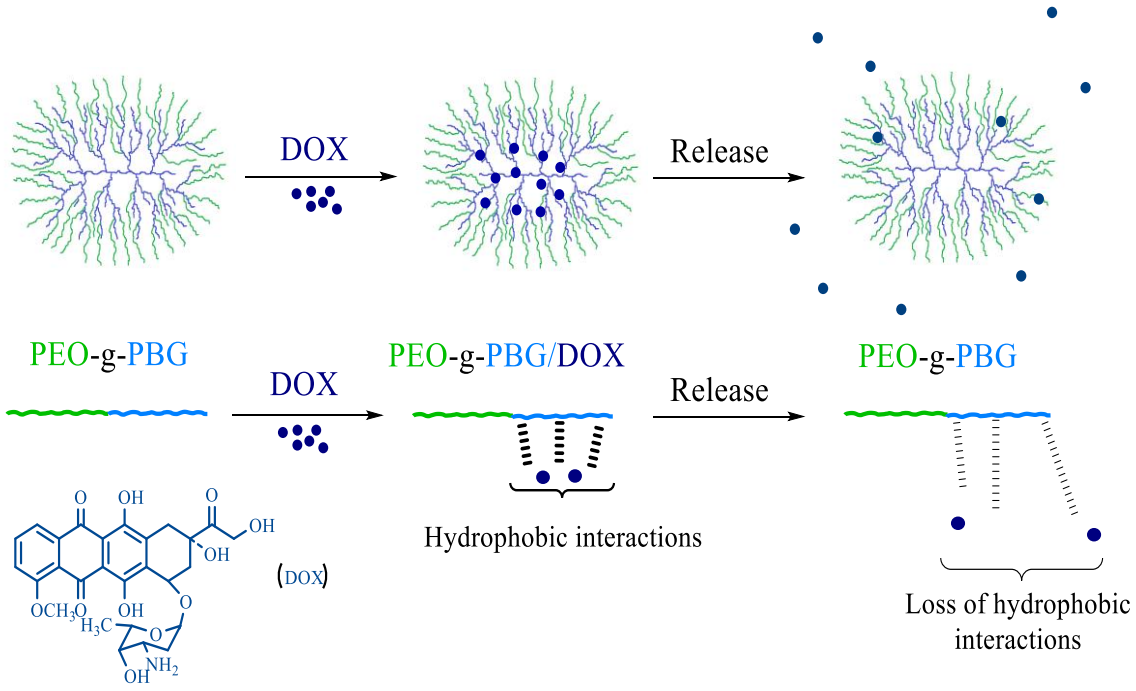

Scheme 4.8. Schematic representation of the encapsulation and release of DOX in the hydrophobic PBG core of G2PBG-*g*-PEO through hydrophobic interactions.

The ability to load the hydrophobic core of these unimolecular micelles with guest molecules was investigated to determine whether the differences in their core structure affected their ability to encapsulate and control the rate of release of the hydrophobic drug. Doxorubicin (DOX), an anticancer drug, was selected as a model drug to assess drug

loading and release *in vitro*. DOX·HCl was treated with triethylamine before encapsulation to obtain DOX in its free base (more hydrophobic) form. DOX was encapsulated within the hydrophobic core of G1PBG-*g*-PEO and G2PBG-*g*-PEO by a dialysis method. It was indeed determined that hydrophobic DOX could be solubilized in the amphiphilic arborescent copolymers, as shown in Figure 4.12. For example, the successful encapsulation of DOX within the hydrophobic core of G2PBG-*g*-PEO is indicated by the enhanced absorption around 490 nm of the DOX-loaded micellar solutions (G2PBG-*g*-PEO/DOX) as compared to the empty micelles (G2PBG-*g*-PEO). The encapsulation of DOX specifically within the hydrophobic core of the micelles is also suggested by the blue shift in the maximum absorption for G2PBG-*g*-PEO/DOX as compared to free DOX in PBS (λ_{max} = 483 nm), which is attributed to the hydrophobic microenvironment created by the PBG core of G2PBG-*g*-PEO.[31]

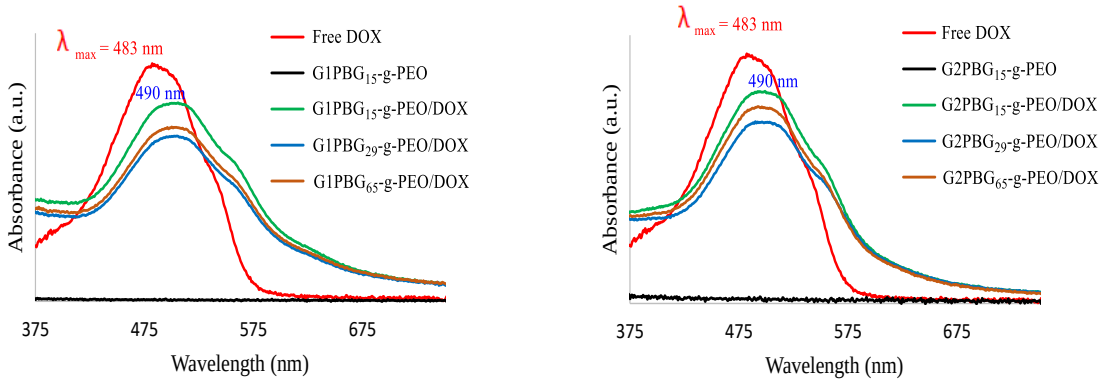

Figure 4.12. UV Absorption of free DOX, G1 (left) and free DOX, G2 (right) arborescent copolymers in PBS.

The existence of hydrophobic interactions was further confirmed by ^{1}H NMR analysis of the G2PBG$_{15}$-*g*-PEO/DOX unimolecular micelles in D_2O (Figure 4.13). The complete disappearance of both the PBG and DOX signals for G2PBG$_{15}$-*g*-PEO/DOX in D_2O (Figure 4.13c) in comparison to the characteristic signals observed of free DOX in D_2O at the same overall DOX concentration (Figure 4.13a) clearly confirms the restricted mobility of both the PBG and DOX components within the core of G2PBG$_{15}$-*g*-PEO. This again confirms the solubilization of DOX within the core of the micelles in aqueous solutions, but also the successful encapsulation of the DOX molecules.

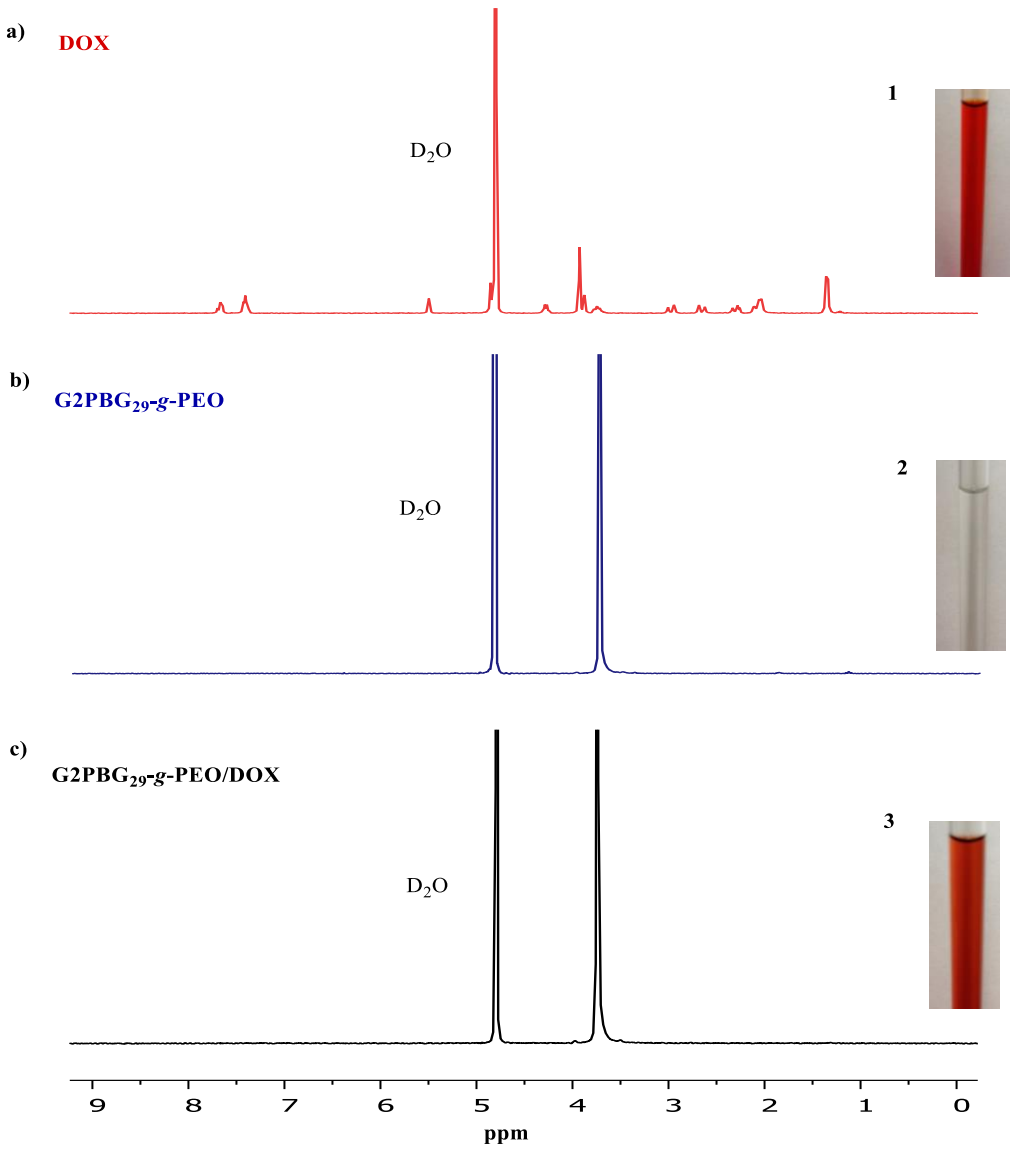

Figure 4.13. ^{1}H NMR spectra for (a) DOX in D_2O, (b) G2PBG$_{29}$-*g*-PEO in D_2O and (c) G2PBG$_{29}$-*g*-PEO/DOX in D_2O. The insets show the appearance of the (1) DOX, (2) G2PBG$_{29}$-*g*-PEO, and (3) G2PBG$_{29}$-*g*-PEO/DOX samples in D_2O.

The drug loading content (DLC) determined for the micelles ranged from 7.1–10.8 wt%, and the drug loading efficiency (DLE) from 42–65% for the different G1PBG and G2PBG copolymers (Table 4.7). Both the drug loading content (DLC) and the drug loading

efficiency (DLE) clearly increased with the generation number of the copolymers. However, for the same generation, the minor variations observed do not seem to correlate with parameters such as differences in branching density among the samples. Sample G2PBG$_{15}$-*g*-PEO/DOX nevertheless has slightly higher values of DLC (10.8%) and DLE (65%) as compared to the two other arborescent copolymers. Common sense dictates that larger particles should be capable of loading more drug. However it can be seen that, despite the lower molecular weight of G2PBG$_{15}$-*g*-PEO and its lower hydrodynamic diameter relatively to G2PBG$_{65}$-*g*-PEO, it has slightly higher DLC and DLE values. This could be related to the denser core of G2PBG$_{15}$-*g*-PEO micelles creating a more hydrophobic microenvironment for the drug. The size of all six DOX-loaded and empty micelles in PBS is compared in Table 4.7. It can be seen that for each arborescent copolymer, the size measured by DLS before and after drug loading is almost identical. Given that for a 10% drug loading, the diameter of a micelle is only expected to increase by ca. 3%, the very small increases observed seem to be reasonable.

Table 4.7. Characterization of DOX-loaded unimolecular micelles.

Copolymer	G2PBG-*g*-PEO		G2PBG-*g*-PEO/DOX			
	Size (nm)	PDI	Size (nm)	PDI	DLC (wt%)	DLE (%)
G1PBG$_{15}$-*g*-PEO/DOX	16	0.41	17	0.38	8.3 ± 0.3	50 ± 2
G1PBG$_{29}$-*g*-PEO/DOX	17	0.51	17	0.54	7.1 ± 0.2	42 ± 3
G1PBG$_{65}$-*g*-PEO/DOX	19	0.43	20	0.44	7.4 ± 0.2	44 ± 4
G2PBG$_{15}$-*g*-PEO/DOX	35	0.28	37	0.49	10.8 ± 0.2	65 ± 3
G2PBG$_{29}$-*g*-PEO/DOX	34	0.26	35	0.51	10.1 ± 0.2	60 ± 3
G2PBG$_{65}$-*g*-PEO/DOX	39	0.17	41	0.47	10.3 ± 0.3	62 ± 3

The data represent the mean ± standard deviation (n = 3).

As shown in Table 4.7, the drug loading content (DLC) and the drug loading efficiency (DLE) increased with the generation number of the copolymers, due to the higher PBG content of G2PBG-*eg*-PEO/DOX relatively to G1PBG-*eg*-PEO/DOX. The following release experiments mainly focused on G2PBG-*eg*-PEO/DOX systems, which had the highest DLC and DLE.

4.4.8 *In Vitro* Drug Release Kinetics

An *in vitro* drug release study was conducted using a dialysis method at 37 ˚C, in phosphate buffered saline (PBS) and at different pH values (7.4 and 5.5). The slightly acidic environment (pH 5.5) was used to simulate the pH of endosomal or lysosomal microenvironments. As shown in Figure 4.14, the results clearly demonstrate that the pH affected the DOX release rate from all three DOX-loaded unimolecular micelles

investigated. The release rate of DOX-loaded micelles was clearly slower at pH 7.4, with total release after 50 h reaching 12, 14.4 and 19.7 % for G2PBG$_{15}$-*g*-PEO/DOX (Figure 4.14a), G2PBG$_{29}$-*g*-PEO/DOX (Figure 4.14b) and G2PBG$_{65}$-*g*-PEO/DOX (Figure 4.14c), respectively, as compared with 17.7, 21.6 and 25.6% at pH 5.5. The relatively slower release at pH 7.4 is attributed to stronger hydrophobic interactions between the core of the nanocarriers and DOX. These results demonstrate that the DOX-loaded unimolecular micelles exhibit pH-dependent *in vitro* release behavior, whereby faster release of DOX takes place in an acidic environment (e.g., in endosomes/lysosomes) than at physiological pH (e.g., the bloodstream). The protonation of DOX in the acidic environment would also lead to higher aqueous solubility for DOX, since this would weaken the hydrophobic interactions between the DOX and the core of the micelles, and thus enhance DOX release.[32,33] This pH-dependent drug release behavior is highly desirable for drug delivery applications, as it should greatly increase the efficacy of cancer therapy while minimizing undesirable side effects.[34] For comparison, the releasing profile of free DOX is also presented (Figure 4.14e). Sustained release was observed for all the DOX-loaded micelles, in contrast to the burst release seen for free DOX in the absence of the copolymers.

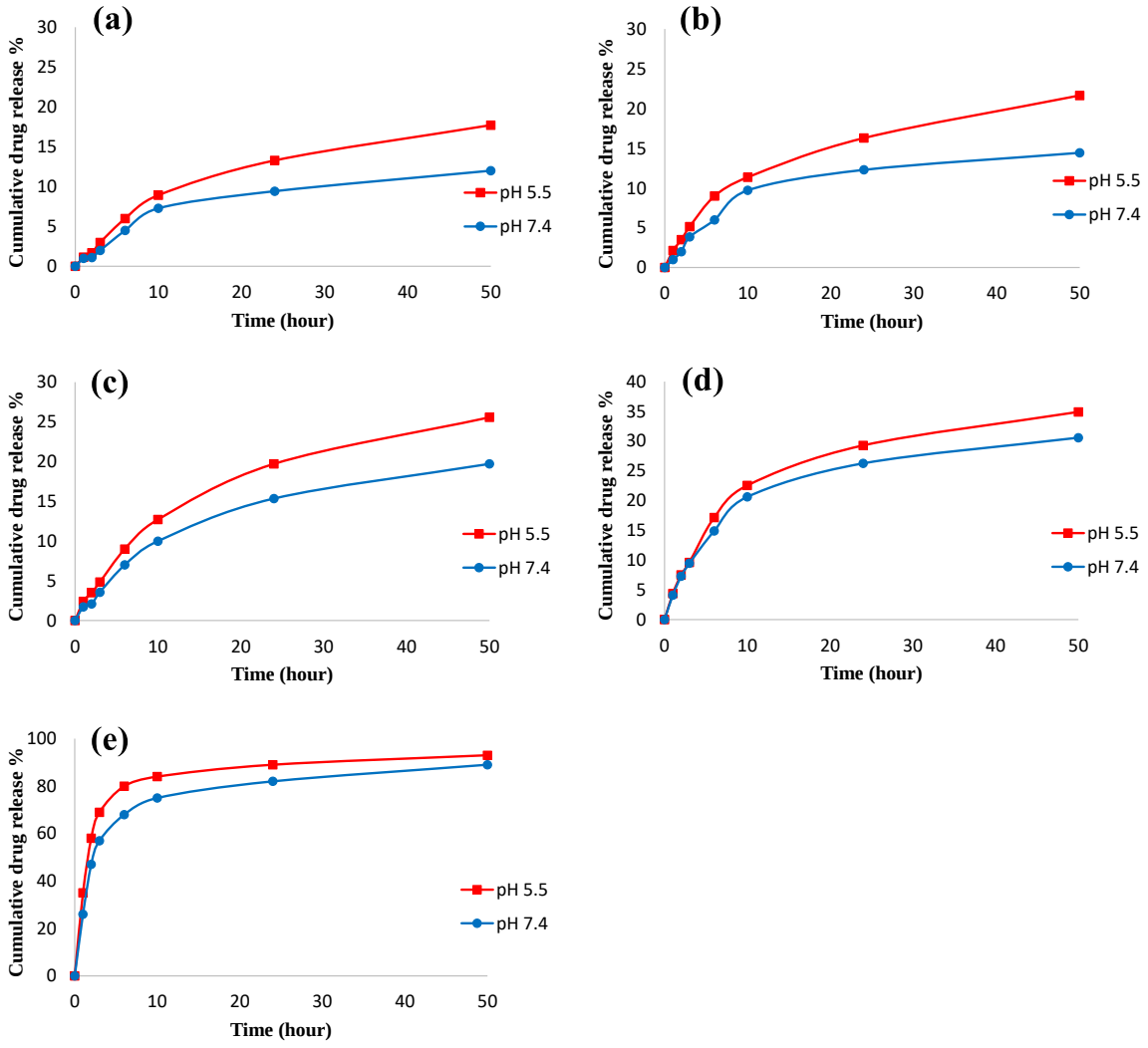

Figure 4.14. ***In vitro*** **DOX release profiles for (a) G2PBG$_{15}$-*g*-PEO/DOX, (b) G2PBG$_{29}$-*g*-PEO/DOX, (c) G2PBG$_{65}$-*g*-PEO/DOX, (d) G1PBG$_{29}$-*g*-PEO/DOX unimolecular micelles and (e) free DOX in PBS (pH 7.4 and 5.5) at 37 ˚C.**

The drug release mechanism from unimolecular arborescent micelles is expected to be passive diffusion. It is generally recognized that the smaller the mean particle diameter, the shorter the diffusion path for drug release, and thereby the faster the release rate. The

release rate of DOX at both pH was indeed slower for all the G2PBG-*g*-PEO/DOX systems as compared to G1PBG$_{29}$-*g*-PEO/DOX. For example, the total amount of drug released from G2PBG$_{29}$-*g*-PEO/DOX (Figure 4.14b) after 50 h reached 14.4 and 21.6 % at pH 7.4 and at pH 5.5, respectively, as compared with 30.5 and 34.9% from G1PBG$_{29}$-*g*-PEO/DOX (Figure 4.14d). This is obviously a consequence of the larger hydrodynamic diameter of G2PBG-*g*-PEO/DOX relatively to G1PBG-*g*-PEO/DOX, which increases the diffusion path for drug release, thus reducing the drug release rate. However since the G2PBG micelles used in the current investigation all had comparable diameters, no correlation between the micelle diameter and the release rate was attempted. Another parameter that might influence the release rate of the drug is structural rigidity, i.e. the branching density (b_d). As pointed out in Section 4.4.3, the branching density increased in the series G2PBG$_{65}$ < G2PBG$_{29}$ < G2PBG$_{15}$. Interestingly, the amount of drug released after 50 h was inversely related to the branching density of the PBG cores, namely G2PBG$_{15}$ < G2PBG$_{29}$ < G2PBG$_{65}$. The significant differences in release rate observed within this series of micelles is attributed to their different core b_d. Very compact and dense cores (G2PBG$_{15}$, b_d = 0.80) would indeed be expected to prevent the diffusion of the drug molecules out of the core more strongly, thus resulting in slower release. In contrast, a more porous core structure (e.g., G2PBG$_{65}$, b_d = 0.11) should facilitate the diffusion process. The results obtained therefore strongly suggest that the release rate of DOX can be controlled through variations in the branching density of the core for the randomly grafted arborescent copolymers.

An investigation of drug release over an extended time period (up to 30 days) was also carried out (Figure 4.15). It revealed that in all cases, the DOX release profiles displayed a

biphasic release pattern at both low and high pH, with an initial burst release followed by sustained release of the drug. At neutral pH (7.4) for example, 7% of the loaded DOX was released from G2PBG$_{65}$-*g*-PEO/DOX over the first 6 h, and only 19.7% after 50 h. Due to the random grafting of the PEO chains onto the PBG substrate, the burst release is attributed to the drug solubilized in the interfacial region of the micelles, which can diffuse more easily and faster into the release medium. The sustained release behavior of the unimolecular micelles again correlates with the branching density, with a larger cumulative release observed for the micelles with the lowest branching density (G2PBG$_{65}$-*g*-PEO/DOX). Even after one month the release of DOX from the micelles was incomplete (Figure 4.15). This could be due in part to strong hydrophobic interactions between the PBG core and the DOX molecules, which was indeed confirmed by analysis of the micelles left in the dialysis bag. A significant amount of DOX may also be physically trapped deeper within the hydrophobic PBG core of the micelles, which would make its diffusion out of the highly dense and branched PBG core more difficult. Such a hydrophobic environment can prevent the protonation of DOX, and thus decrease the diffusion capability of DOX. A similar explanation was suggested by Gauthier et al.[23] for the incomplete release of indomethacin from highly branched arborescent polystyrene-*g*-poly(2-vinylpyridine) copolymers, serving as non-biocompatible model systems with a structure similar to the unimolecular micelles used in the current investigation.

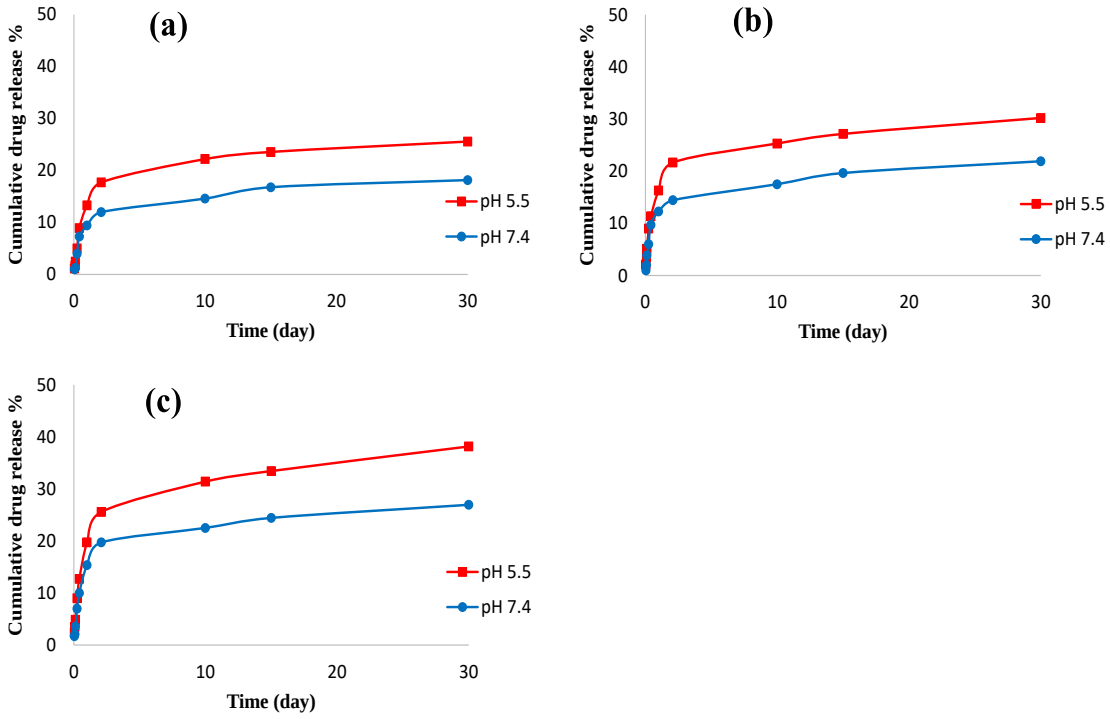

Figure 4.15. ***In vitro*** **DOX release profiles over a 30-day period for (a) G2PBG$_{15}$-*g*-PEO/DOX, (b) G2PBG$_{29}$-*g*-PEO/DOX and (c) G2PBG$_{65}$-*g*-PEO/DOX in PBS (pH 7.4 and 5.5) at 37 ˚C.**

4.5 Conclusions

A library of water-soluble amphiphilic arborescent copolymers PBG-*g*-PEO was successfully prepared. Poly(γ-benzyl L-glutamate) cores were generated by ring-opening polymerization of γ-benzyl L-glutamic acid *N*-carboxyanhydride (Glu-NCA) initiated with *n*-hexylamine. Cleavage of a fraction of the benzyl ester groups, and coupling with PBG chains to obtain a comb-branched (G0) PBG structure. Additional cycles of partial deprotection and grafting yielded G1 and G2 arborescent polypeptides. The PBG substrates serving as cores for the synthesis of amphiphilic arborescent copolymers also had randomly

distributed carboxylic acid functionalities. Side chains of poly(ethylene oxide) were grafted onto these functionalized arborescent PBG substrates to produce amphiphilic arborescent copolymers. Their aqueous solution behavior revealed that the copolymers existed mostly as unimolecular (non-aggregated) micellar species. An encapsulation study demonstrated that these well-defined, biocompatible copolymers could efficiently encapsulate hydrophobic DOX. Sustained, pH-responsive release of the encapsulated drug was observed.

The ability of these unimolecular micelles to encapsulate and release DOX was correlated with the generation number of the copolymers and the branching density (b_d) of the hydrophobic cores. Both the DLC and the DLE clearly increased with the generation number of the copolymers. For each generation, slightly higher values of DLE and DLC were obtained for the micelles with a denser core structure ($G1PBG_{15}$ and $G2PBG_{15}$), with a DLE of about 50% and 65%, respectively, and a DLC of about 8.3% and 10.8%, respectively. Both the DLE and DLC decreased slightly as the grafting density of the cores decreased. The release profiles indicated that the drug release rate could be controlled through the generation number of the copolymers and by modulating the grafting density, and thereby the porosity of the cores. Micelles with highly branched cores ($G2PBG_{15}$) reduced the diffusion rate of the drug, while a lower branching density ($G2PBG_{65}$) facilitated the diffusion process. The versatile encapsulation and release properties of these unimolecular micelles show that they could be useful as nanocarriers for a broad range of drug release applications.

Chapter 5 Influence of the Core Branching Density on Drug Release from Arborescent Poly(γ-benzyl L-glutamate) End-Grafted with Poly(ethylene oxide)

5.1 Overview

Amphiphilic dendritic copolymers of arborescent poly(γ-benzyl L-glutamate) of generations G1 and G2, grafted at their chain ends with poly(ethylene oxide) segments (PBG-*eg*-PEO) were synthesized, characterized and evaluated as nanocarriers for doxorubicin (DOX). The copolymers were designed with hydrophobic PBG cores having three different branching densities and were characterized using ^{1}H NMR spectroscopy, size exclusion chromatography (SEC), transmission electron microscopy (TEM) and atomic force microscopy (AFM). Dynamic light scattering (DLS) measurements revealed that these amphiphilic molecules behaved like unimolecular micelles without significant aggregation in aqueous media such as phosphate buffered saline (PBS), with diameters in the 13-29 nm range depending on the generation number and the core structure. Efficient encapsulation of DOX by these unimolecular micelles was demonstrated, with drug loading capacities of up to 11.2 wt%, drug loading efficiencies of up to 67%, and pH-responsive sustained drug release as determined by UV spectroscopy. The generation number of the copolymers and the branching density of the dendritic PBG core were found to influence the encapsulation and release properties of the micelles. Given the tailorable characteristics, good water dispersibility and biocompatibility of amphiphilic arborescent copolymers, these should be useful as robust nanocarriers for a broad range of therapeutic and diagnostic agents.

5.2 Introduction

Over the past two decades many new drug delivery systems have been developed to enhance the aqueous solubility of drugs, increase their circulation time in the bloodstream, and thereby increase their therapeutic efficacy.[1] Among different nanocarriers used for controlled drug delivery, polymeric micelles (e.g. amphiphilic block copolymer micelles, unimolecular micelles and cross-linked micelles) with tunable properties have shown great potential due to their excellent characteristics that brought them to the front line in the development of drug delivery systems.[2,3]

A considerable amount of research has been devoted to the design of polymeric micelles of different types, sizes, morphologies and stabilities for drug delivery applications. Among these, micelles formed by amphiphilic block copolymers were found very attractive due to their ability to solubilize hydrophobic or poorly water soluble drugs within their core, and thus enhance drug bioavailability.[4] Although the stability of amphiphilic block copolymer micelles has been improved significantly over the last few years, they are still sensitive to solvent composition and other parameters such as the concentration and temperature in many cases. For instance, once self-assembled micelles are injected into the body, they may dissociate due to dilution and lead to rapid release of physically encapsulated drugs, which reduces the efficacy of the treatment.[5] These unfavorable issues can be resolved by stabilizing polymeric micelles via crosslinking, either in the core or the corona, or by constructing unimolecular structures that are stable regardless of their environment.[6-8] Certain types of amphiphilic dendritic copolymers with covalently bonded core and shell components can behave like unimolecular micelles. In

contrast to conventional amphiphilic block copolymers forming micelles by aggregation only above their critical micelle concentration (CMC), dendritic unimolecular micelles do not dissociate upon dilution and show excellent colloidal stability in aqueous media, regardless of their concentration, while their size and morphology can be precisely controlled.[9] Dendritic polymers, defined as macromolecules with a tree-like multi-level branched architecture, can be divided into three main classes depending on the specific characteristics of their architecture: dendrimers, hyperbranched polymers, and dendrigraft polymers.[10-13] Due to their remarkable features, such as a compact globular topology with internal cavities and the presence of functional groups useful to fulfill different tasks simultaneously, amphiphilic dendritic polymers may be useful to replace block copolymers in drug delivery applications.[14,15] Among the three dendritic polymer classes, dendrigraft (or arborescent) polymers provide a good compromise between monodispersed dendrimers, generated by a tedious synthetic process, and highly polydisperse hyperbranched polymers obtained in one-step reactions. Dendrigraft polymers are typically obtained in a generation-based scheme analogous to dendrimers, but with cycles of polymerization and grafting reactions. The use of polymeric chain segments rather than small molecules as building blocks leads to very rapid growth, such that high molecular weights are obtained in only a few steps for these systems, while maintaining fairly narrow molecular weight distributions ($M_w/M_n < 1.1$).[16,17]

Amphiphilic arborescent copolymers can be synthesized by adding hydrophilic segments in the last grafting cycle. With proper design, these copolymers may behave like unimolecular micelles for which the size and porosity can be tailored via variations in the

length of the side chains and the grafting density. Whitton and Gauthier recently reported the synthesis of arborescent PBG substrates grafted either randomly or at their chain ends with poly(ethylene oxide) segments, to be evaluated as micellar species.[18] Unfortunately these copolymers formed a significant amount of large aggregated species in aqueous media, and their drug encapsulation and release properties were not explored.

This investigation focuses on the synthesis of arborescent poly(γ-benzyl L-glutamate) end-grafted with poly(ethylene oxide) segments (PBG-*eg*-PEO) designed to avoid aggregation, and their application as nanocarriers for doxorubicin (DOX) as a model hydrophobic drug. Micelles derived from PBG cores of generations G1 and G2 and three different branching densities were compared to determine the influence of these parameters on their dispersibility in aqueous media, and on the encapsulation and release of the hydrophobic drug.

5.3 Experimental Procedures

5.3.1 Characterization and Sample Preparation

5.3.1.1 Nuclear Magnetic Resonance (NMR) Spectroscopy

Proton nuclear magnetic resonance (^{1}H NMR) spectroscopy served to estimate the degree of polymerization of the linear PBG chains, to determine the deprotection level of the PBG substrates, and to investigate the ability of randomly grafted arborescent copolymers to form micelles. The instrument used was a Bruker 300 MHz spectrometer. Fluorine nuclear magnetic resonance (^{19}F NMR) spectroscopy was also performed on the

Bruker 300 MHz instrument to determine the chain end primary amine functionality, f_{NH2}, of the polymers used in the grafting reactions.

5.3.1.2 Size Exclusion Chromatography (SEC) Analysis

Analytical SEC was used for the characterization of the arborescent PBG substrates of generations G0-G2 and of the arborescent copolymers. The analytical SEC system was a Viscotek GPCmax unit equipped with a VE 2001 GPC Solvent/Sample Module, a Viscotek double detector array with refractive index and dual-angle light scattering detectors, and two Agilent Technologies PLgel 5 μm MIXED-C and PLgel 10 μm MIXED-B organic mixed bed columns, with dimensions of 7.5 mm (ID) × 300 mm (L). The system was operated at a flow rate of 0.5 mL/min at 70 ˚C, using dimethyl sulfoxide (DMSO) with LiBr (0.05 M) as the mobile phase. Analysis of the chromatograms was performed with the OmniSEC 4.6.1 software package.

Preparative SEC was carried out on a system consisting of a Waters M45 HPLC pump, a 2-mL sample injection loop, a Waters R401 differential refractometer detector, and a Jordi Gel DVB 1000 Å 250 mm × 22 mm preparative SEC column. *N*,*N*-Dimethylformamide (DMF) with 0.2 g/L LiCl served as the mobile phase. The concentration of the polymer solution injected was 25 mg/mL. The system was operated at a flow rate of 3 mL/min at room temperature (25 ˚C).

5.3.1.3 Dynamic Light Scattering (DLS) Measurements

Light scattering measurements were performed on a Zetasizer Nano ZS90 (Malvern Instruments) equipped with a 4 mW He–Ne laser operating at 633 nm and 25.0 ˚C, at a

scattering angle of 90°. The polymers were dispersed in phosphate buffered saline (PBS), DMF or water for at least 12 h before analysis. The concentration of the solutions was around 0.5 $mg \cdot mL^{-1}$, 0.2 $mg \cdot mL^{-1}$ and 0.1 $mg \cdot mL^{-1}$ for the G0, G1 and G2 copolymers, respectively. All the solutions were filtered with either PTFE or cellulose acetate membrane filters having a nominal pore size of 0.45 μm prior to the measurements. The light scattering data were analyzed with the Zetasizer 7.11 Software (Malvern Instruments). Each sample was measured in triplicate.

5.3.1.4 UV-visible (UV-vis) Spectroscopy

Absorption spectra were obtained on a Cary 100 Bio UV-Vis spectrophotometer with a spectral bandwidth (SBW) of 2 nm, operated with the Cary Varian UV Scan Application (v3.001339). The absorption peak at 483 nm was used to calculate the doxorubicin loading in the DOX-polymer samples. Absorbance measurements were performed in the 200–800 nm range and baseline correction was applied for PBS.

5.3.1.5 Transmission Electron Microscopy (TEM)

The dendritic micelles were imaged with a Philips CM10 electron microscope operated at 60 kV accelerating voltage. The images were recorded with an Advance Microscopy Techniques 11 megapixel digital camera and the Image Capture Software Engine version 5.42.558. The feature sizes and size distributions were measured with the open source processing program ImageJ (version 1.46r).[19] Either automatic selection or manual analysis of the features was used, depending on the contrast and the resolution of the images. In either case, a minimum of 15 measurements were taken for each sample to provide

adequate average size information. In some cases, contrast adjustment was necessary to improve visualization and help with the measurement of the features. The samples for TEM measurements were prepared by the following method: one drop of solution (0.05 $mg \cdot mL^{-1}$) was cast onto a 300 mesh Formvar® carbon-coated copper TEM grid (Electron Microscopy Sciences, FCF300-Cu) placed onto filter paper and excess solution was wicked off with filter paper. After 1 min, one drop of 2% (w/v) phosphotungstic acid was added to the grid and the excess staining solution was wicked off with filter paper. Finally the grid was transferred onto a new piece of filter paper in a Petri dish and left to dry overnight at room temperature.

5.3.1.6 Atomic Force Microscopy (AFM)

Muscovite mica discs were adhered onto steel substrates using double-sided adhesive tape to secure the sample to the magnetic spin coater. Immediately prior to film casting, a fresh surface was exposed by cleavage with a strip of Scotch® MultiTask tape. The polymer solutions were prepared at concentrations ranging from 0.01 to 0.05 $mg \cdot mL^{-1}$. A 20 μL aliquot of the solution was deposited on the mica substrate and spun at about 3000 revolutions per minute (rpm) for 60 s under ambient conditions. Atomic force microscopy (AFM) images were recorded in the tapping mode on a Nanoscope III instrument (Digital Instruments, model MMAFM-2, scan stage J) housed in a NanoCube acoustic isolation cabinet and mounted on a Halcyonics Micro 40 vibration isolation table. The measurements were performed using Si probes (VistaProbes, T300) having a spring constant of 40 N/m, a resonance frequency of 300 kHz, and the following characteristics: length 125 μm, width 40 μm, tip height 14 μm, and tip radius < 10 nm. The images were analyzed using the

Nanoscope v 1.40 software. The scan rate was typically between 0.7 and 1.2 Hz, at a scan angle of 0°, acquiring 512 samples/line.

5.3.2 Solvent and Reagent Purification

Dimethyl sulfoxide and *n*-hexylamine were purified by stirring overnight with CaH_2 and distillation under reduced pressure. *N,N'*-Dimethylformamide serving in the polymer synthesis (DMF; Aldrich, >99%) was purified by distillation under reduced pressure. Ethyl acetate (Fisher, 99.9%) was distilled from $LiAlH_4$ under nitrogen. γ-Benzyl L-glutamic acid (Bz-Glu; Bachem, >99%), diethyl ether (EMD Millipore OmniSolv), HBr solution (Aldrich, 33% in acetic acid), *N,N*'-diisopropylcarbodiimide (DIC; Aldrich, 99%), triphosgene (Aldrich, 98%), 1-ethyl-3-(3-dimethylaminopropyl)carbodiimide hydrochloride (EDC·HCl; Aldrich, 98%), $LiAlH_4$ (Aldrich, 95%), 1-hydroxybenzotriazole (HOBt; Fluka, water content ca. 15% w/w), tetrahydrofuran (THF, EMD Millipore OmniSolv), methanol (EMD Millipore OmniSolv), trifluoroacetic acid (TFA, Caledon, 99.9%), acetic anhydride (Caledon, 97%), deuterated DMSO (DMSO-d_6, Cambridge isotopes, 99.9% D), deuterated water (D_2O; Aldrich, 99.9 atom % D) and triethylamine (TEA, EMD) were used as received from the suppliers. Doxorubicin hydrochloride (DOX·HCl) was obtained from Sigma-Aldrich (USA). Dialysis bags Spectra/Por® 7 (MWCO 3.5 kDa) were purchased from Spectrum Laboratories Inc. (USA).

5.3.3 Synthesis

The synthesis of the monomer γ-benzyl L-glutamic acid *N*-carboxyanhydride (Glu-NCA), the PBG linear side chains, the linear PBG substrates with different lengths, the

partially and fully deprotected linear PBG substrates, the partially deprotected arborescent PBG cores of generations 0 (G0) and generation 1 (G1), linear poly(ethylene oxide) (PEO), and their characterization were accomplished according to the procedures described in Chapter 4.

The different linear PBG substrates are identified in the form PBG_x, where X denotes the experimental number of PBG repeating units in the chains. The arborescent G0PBG molecules obtained by coupling the amine-terminated PBG side chains with the different carboxyl-functionalized PBG substrates are likewise identified as $G0PBG_x$, where X denote the number of PBG repeating units that were used as substrate for the construction of G0PBG. For example, $G0PBG_{29}$ describes arborescent G0PBG derived from the PBG substrate with 29 repeating units. Similar sample notation is also used for the G1 and G2 samples.

Linear PBG substrates with different molecular weights and deprotection levels were used in the synthesis of arborescent G0PBG, while the PBG side chains (core building blocks) used in the subsequent reactions had $M_n \approx 5000$ g/mol. The three linear PBG substrates used had an increasing number of PBG repeating units (X_n = 15, 29 and 65, identified as PBG_{15}, PBG_{29} and PBG_{65}, respectively). Their deprotection level also varied from 31% (PBG_{29} and PBG_{65}) to 100% (PBG_{15}) of free glutamic acid moieties.

5.3.3.1 Synthesis of Glu(OtBu)$_2$-Poly(γ-benzyl L-glutamate) [(tBuO)$_2$-PBG)]

Linear $(tBuO)_2$-PBG serving as side chains for the last grafting cycle of the arborescent PBG core syntheses was obtained as described previously.[18] Briefly, γ-benzyl L-glutamic

acid *N*-carboxyanhydride (Glu-NCA; 9.2 g, 35.0 mmol) was dissolved in dry DMF (23 mL) at 40 ˚C. The *tert*-butyl diester of glutamic acid H-Glu(OtBu)-OtBu·HCl (414 mg, 1.39 mmol, for a target X_n = 25) was dissolved in dry DMF (2 mL), added as initiator to the monomer, and the reaction was allowed to proceed for 7 d at 40 ˚C. The reaction was cooled to room temperature and triethylamine (0.25 mL, 1.84 mmol) was added. After 5 min the linear polymer was recovered by precipitation in cold methanol, centrifugation and drying under vacuum overnight before characterization. Yield = 68%, M_w/M_n = 1.17. ^{1}H NMR (300 MHz, DMSO-d_6): δ: 8.01-7.7 (b, 1H), 7.26–7.20 (s, 5H), 5.01–4.88 (s, 2H), 4.30–3.85 (b, 1H), 2.30–1.68 (b, 4H), 1.31 (s, 0.75H), X_n = 24.0.

5.3.3.2 Synthesis of Chain End-Functionalized G1 and G2 Arborescent PBG Substrates

The chain end-functionalized arborescent PBG substrates were obtained by grafting glutamic acid-functionalized PBG linear chains in the last grafting cycle as described previously.[18] For example, the G1 polymer was synthesized from the partially deprotected G0PBG substrate (0.27 g, 0.438 mmol -CO_2H) and $(OtBu)_2$-PBG side chains (2.22 g, 0.398 mmol chains), dissolved in 22 mL of dry DMSO. The peptide coupling reagents DIC (0.377 mL, 2.41 mmol) and HOBt (0.325 g, 2.41 mmol) were then added to the reaction with TEA (0.28 mL, 1.99 mmol) as a base. The reaction was allowed to proceed for 36 h at room temperature before adding *n*-hexylamine (0.29 mL, 2.89 mmol), to deactivate residual activated carboxylic acid sites. After 3 h the product was precipitated in cold methanol and recovered by suction filtration. The product was dissolved in DMF, purified by preparative SEC, precipitated in methanol, recovered by suction filtration, and dried under vacuum

overnight before characterization. The G2 arborescent polymer was synthesized and purified as described for the G1 sample.

M_w/M_n = 1.07 (MALLS). ^{1}H NMR (300 MHz, DMSO-d_6) δ: 8.01-7.7 (b, 1H), 7.26–7.20 (s, 5H), 5.01–4.88 (s, 2H), 4.30–3.85 (b, 1H), 2.30–1.68 (b, 4H), 1.31 (s, 18H).

5.3.3.3 Deprotection of Chain End-Functionalized Arborescent PBG Substrates

The *tert*-butyl ester protecting groups were selectively removed to generate coupling sites only at the chain ends for further grafting reactions. As an example, the arborescent G1PBG substrate (0.3 g) was dissolved in trifluoroacetic acid (3 mL). After 10 min the polymer was precipitated in methanol, recovered by suction filtration, and dried under vacuum overnight before characterization. Yield: 0.23 g (77%). ^{1}H NMR (300 MHz, DMSO-d_6) δ: 8.01-7.7 (b, 1H), 7.26–7.20 (s, 5H), 5.01–4.88 (s, 2H), 4.30–3.85 (b, 1H), 2.30–1.68 (b, 4H).

5.3.3.4 Synthesis of Arborescent Copolymers

All the arborescent copolymers were synthesized and purified similarly to the reaction described for the arborescent PBG samples. The synthesis of G1PBG$_{15}$-*eg*-PEO is described below as an example. The deprotected chain end-functionalized arborescent G1PBG$_{15}$ substrate (0.120 g, 0.051 mmol -CO_2H) and the PEO serving as side chains (0.46 g, 0.046 mmol chains) were dissolved in 5 mL of dry DMSO. The peptide coupling reagents DIC (0.044 mL, 0.281 mmol) and HOBt (0.038 g, 0.281 mmol) were then added to the reaction with TEA (0.030 mL, 0.233 mmol) as a base. The reaction was allowed to proceed for 36 h at room temperature before adding *n*-hexylamine (0.034 mL, 0.338 mmol)

to deactivate residual activated carboxylic acid sites. After 3 h the product was precipitated in cold methanol and recovered by suction filtration. Unreacted PEO was removed from the G1PBG$_{15}$-*eg*-PEO crude polymer by preparative size exclusion chromatography (SEC) in DMF and the sample was recovered by precipitation in cold diethyl ether, suction filtration, and drying under vacuum. Grafting yield: 70%, M_n = 890,000, M_w/M_n = 1.06 (MALLS).

5.3.3.5 Preparation of DOX-loaded Unimolecular Micelles

DOX·HCl (2 mg) was first dissolved in 0.5 mL of DMSO and neutralized with two equivalents of TEA (4 μL) to obtain the drug in its free base (hydrophobic) form. The arborescent copolymer (10 mg) was dissolved in 1 mL of DMSO and stirred for 2 hours. Then the DOX solution was added and the mixture was stirred overnight in the dark. The organic solvent and the free drug were removed by dialysis (MWCO 3500) against deionized water (1 L) for 24 h with three changes of the dialysis medium, and the resulting solution was either lyophilized in the dark or used directly for the subsequent measurements. For the determination of the drug loading content (DLC) and the drug loading efficiency (DLE), the lyophilized DOX-loaded micelles (3 mg) were dissolved in deionized water and the absorbance was measured on a UV-Vis spectrometer at 483 nm. The DLC and DLE were calculated according to the following equations:

$$\mathrm{DLC} = \frac{\text{mass of drug in micelles}}{\text{mass of micelles and drug}} \times 100\% \tag{5.1}$$

$$\mathrm{DLE} = \frac{\text{mass of drug in micelles}}{\text{total mass of drug in feed}} \times 100\% \tag{5.2}$$

5.3.3.6 *In Vitro* DOX Release

To determine the DOX release profiles, a 3 mg sample of freeze-dried DOX-loaded micelles was dispersed in 1 mL of phosphate buffered saline (release medium, 10 mM phosphate, 137 mM NaCl and 2.7 mM KCl, pH 7.4 or 5.5; the pH was adjusted to 5.5 by addition of 6 M HCl) and transferred to a dialysis bag (MWCO 3500). The release experiment was initiated by placing the sealed dialysis bag into 3 mL of release medium at the same pH and 37 ˚C, with constant shaking at 100 rpm. At selected time intervals, the release medium was completely withdrawn and replaced with 3 mL of fresh medium. The amount of DOX released was calculated based on the absorbance measured on a UV-Vis spectrometer at 483 nm and a calibration curve. The drug release studies were performed in triplicate for each sample.

5.4 Results and Discussion

The structure of arborescent copolymers can be tailored to construct unimolecular micelles for various applications, and particularly for drug delivery. For example, the branching density (porosity) of the molecules can be varied by adjusting the length of the chains and the functionalization (deprotection) level in the arborescent PBG substrates, while their overall size and branching functionality can be controlled by using substrates of different generations. Linear PBG substrates with different molecular weights and deprotection levels were used in the current investigation for the synthesis of arborescent G0PBG, while the PBG side chains used in the subsequent reactions all had $M_n \approx 5000$ g/mol. The three linear PBG substrates used had an increasing number of PBG repeating

units (X_n = 15, 29 and 65, identified as PBG_{15}, PBG_{29} and PBG_{65}, respectively). The number of PBG units was controlled by varying the ratio of monomer (γ-benzyl L-glutamic acid *N*-carboxyanhydride, Glu-NCA) to initiator (*n*-hexylamine) used in the polymerization reaction. Their deprotection level also varied from 31 mol% (PBG_{29} and PBG_{65}) to 100 mol% (PBG_{15}) of free glutamic acid moieties. As a result, three well-defined (PDI < 1.09) comb-branched or arborescent G0PBG were obtained, but with a structure varying from compact and dense for $G0PBG_{15}$, to a loose and more porous structure for $G0PBG_{65}$, and an intermediate (semi-compact) structure for $G0PBG_{29}$. The different substrate lengths and deprotection levels of linear PBG were used initially in the synthesis of G0PBG in the hope that the topology (shape) of the molecules could be varied from spherical to rod-like, but TEM and AFM imaging indicated that all the molecules were spherical. This approach nevertheless allowed variations in the branching density (porosity) for the cores, which seems to correlate well with the release properties of the molecules as discussed in Section 5.4.5. A detailed discussion of the synthesis of these linear PBG substrates and the arborescent G0PBG serving as hydrophobic core components for the synthesis of arborescent copolymers was provided in Chapter 4, and hence will not be discussed further here.

The characterization data for the linear PBG and arborescent G0PBG substrates are provided in Tables 5.1 and 5.2, respectively. As seen in Table 5.2, the number-average branching density (b_d), defined as the number of side chains added in the grafting reaction divided by the number of repeating units on the linear chain substrate, increased as the chain length of the substrate decreased. $G0PBG_{15}$ had the highest branching density (b_d =

0.80) among the three PBG substrates, and therefore should have a more compact and dense core structure. In contrast, G0PBG$_{65}$ had the lowest branching density (b_d = 0.11) and should have a more porous core structure (G2PBG$_{65}$), while G2PBG$_{29}$-*eg*-PEO/DOX, with b_d = 0.19) is in-between.

Table 5.1. Characteristics of linear PBG substrates.

Sample	Target X_n	X_n(NMR)	M_n(NMR)	M_n^{app}(SEC)	PDI
PBG$_{15}$	15	15	3,600	3,880	1.11
PBG$_{29}$	30	29	6,600	6,900	1.10
PBG$_{65}$	68	65	14,500	15,700	1.12

Table 5.2. Characteristics of arborescent G0PBG with different branching densities (b_d).

Sample	Deprotection level (%) of substrate	Molar ratio CO_2H : NH_2	M_n(g/mol)	PDI	f_n	b_d
G0PBG$_{15}$	100	1.1 : 1	65400	1.04	12	0.80
G0PBG$_{29}$	31	1.7 : 1	35300	1.08	5.4	0.19
G0PBG$_{65}$	31	1.7 : 1	51000	1.06	7.1	0.11

5.4.1 Synthesis of Linear $(tBuO)_2$-PBG

Linear PBG with two *tert*-butyl ester protecting groups at one chain end, $(tBuO)_2$-PBG, was obtained by the ring-opening polymerization of Glu-NCA initiated by the HCl salt of glutamic acid di-*tert*-butyl ester.[18] The polymerization was carried out in DMF at 40 ˚C for 7 days (Scheme 5.1).

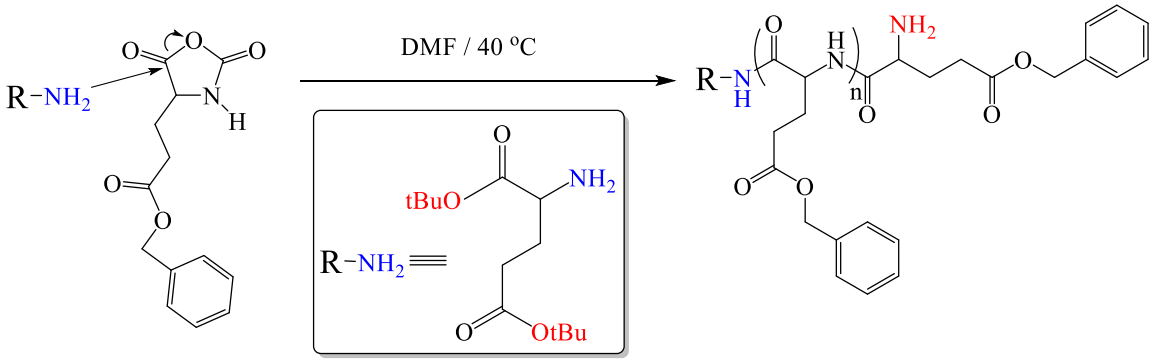

Scheme 5.1. Polymerization of γ-benzyl L-glutamic acid *N*-carboxyanhydride (Glu-NCA) using $Glu(OtBu)_2$·HCl as initiator.

The number-average degree of polymerization (X_n) of the $(tBuO)_2$-PBG sample was determined by ^{1}H NMR analysis as shown in Figure 5.1, by comparing the integrated peak intensities for the benzylic methylene protons in the repeating units (2H at 4.9 ppm) and the protons of the *tert*-butyl ester groups in the initiator fragment (18H at 1.3 ppm). The polymerization initiated by $Glu(OtBu)_2$·HCl yielded PBG with $X_n = 24$, in good agreement with the target $X_n = 25$.

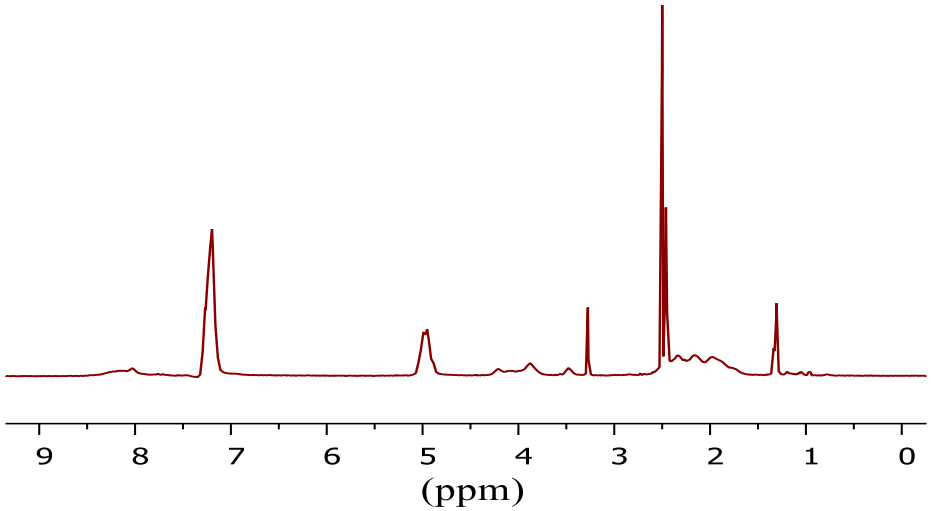

Figure 5.1. ^{1}H NMR spectrum for linear PBG with two *tert*-butyl ester protecting groups at one chain end $(tBuO)_2$-PBG.

5.4.2 Synthesis of Arborescent PBG Substrates with Carboxylic Acid Chain Ends

The PBG arborescent substrates serving as cores for the amphiphilic copolymer micelles were synthesized as described previously.[18] Three different PBG cores of generations G1 and G2 were employed as substrates to generate a library of chain end-grafted copolymers to be evaluated as nanocarriers for doxorubicin (DOX).

The chain end-functionalized substrates were obtained by grafting $(tBuO)_2$-PBG onto randomly deprotected arborescent PBG substrates of generations G0 and G1 as described in Chapter 3. The deprotection level of the arborescent PBG substrates was ca. 30%, and a 1 : 1.1 molar ratio of side chains NH_2 chain ends to CO_2H groups on the substrate was used to maximize the grafting yield and the coupling efficiency (Table 5.3). The unreacted side chains were removed from the crude polymer by preparative size exclusion

chromatography (SEC). The absolute molecular weight of the arborescent PBG samples was determined by SEC-MALLS analysis in DMSO. The molecular weight and the branching functionality (f_n) of the polymers increased with the generation number as expected, while maintaining a low polydispersity index (PDI ≤ 1.09). The lower grafting yield (G_y) and coupling efficiency (C_e) observed for sample $G1PBG_{15}$ are attributed to the dense structure of the $G0PBG_{15}$ substrate, making it difficult for the linear side chains to diffuse to the coupling sites.

Table 5.3. Characteristics of chain end-functionalized generation G1 and G2 arborescent PBG substrates.

Sample	M_n(g/mol)[a]	M_w/M_n[a]	G_y (%)[b]	C_e (%)[c]	f_n[d]
$G1PBG_{15}$	220,000	1.09	27	31	28
$G1PBG_{29}$	210,000	1.07	53	64	31
$G1PBG_{65}$	270,000	1.09	48	56	39
$G2PBG_{15}$	1.2×10^6	1.08	51	57	171
$G2PBG_{29}$	970,000	1.06	39	48	137
$G2PBG_{65}$	1.3×10^6	1.07	43	50	185

[a] Values from SEC-MALLS analysis in DMSO; [b] Grafting yield: fraction of side chains attached to the substrate; [c] Coupling efficiency: fraction of coupling sites on the substrate consumed in the reaction; [d] Branching functionality: number of branches added in the last grafting cycle.

The arborescent PBG substrates with *tert*-butyl ester-protected carboxylic acid groups at the chain end were then dissolved in trifluoroacetic acid (TFA), to selectively cleave the

tert-butyl ester protecting groups and generate two carboxylic acid groups at each chain end (PBG-*ef*-$(CO_2H)_2$). These chain end-functionalized arborescent PBG samples served as substrates in a subsequent grafting reaction with amine-terminated PEO chains to obtain the chain end-grafted amphiphilic arborescent copolymers PBG-*end-grafted*-PEO (PBG-*eg*-PEO) as shown in Scheme 5.2.

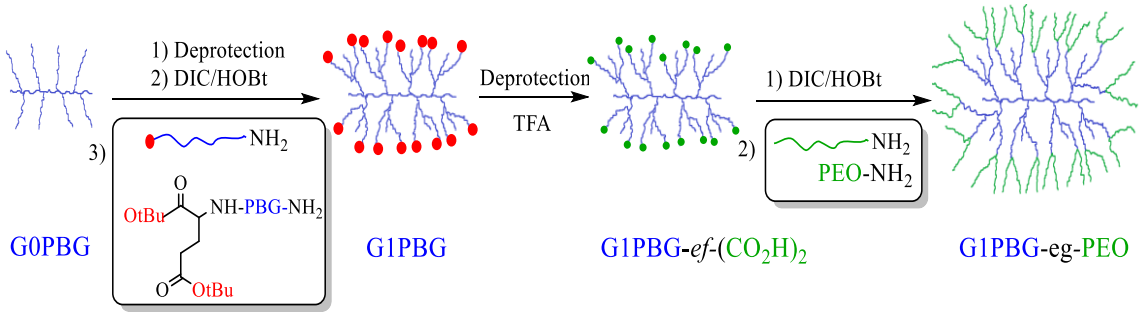

Scheme 5.2. Schematic representation of the synthesis of chain end carboxyl-functionalized G1PBG substrate (G1PBG-*ef*-$(CO_2H)_2$) and the chain end-grafted arborescent copolymer G1PBG-*eg*-PEO.

The mole fraction of *tert*-butyl ester groups in the arborescent substrates was determined by ^{1}H NMR analysis, as shown in Figure 5.2c, by comparing the integrated peak intensities for the methine protons in the repeating units (1H at 3.9 ppm) and the protons of the *tert*-butyl ester groups in the initiator fragment (18H at 1.3 ppm). A calculation of the mole fraction of *tert*-butyl ester groups before deprotection of the G1 PBG sample, $G1PBG_{15}$-*ef*-$(tBuO)_2$, is provided in Equation 5.3 as an example.

$$f_{tBu} = \frac{(\text{integral } tert-\text{butyl H})/18}{(\text{integral methine H})/1} = \frac{0.82/18}{1/1} = 0.045 \times 2 = 0.09 \qquad (5.3)$$

^{1}H NMR analysis was also used to confirm that complete deprotection of the *tert*-butyl ester groups was achieved before grafting PEO onto the PBG substrate. The complete disappearance of the *tert*-butyl protons at 1.3 ppm confirmed their complete removal (Figure 5.2b).

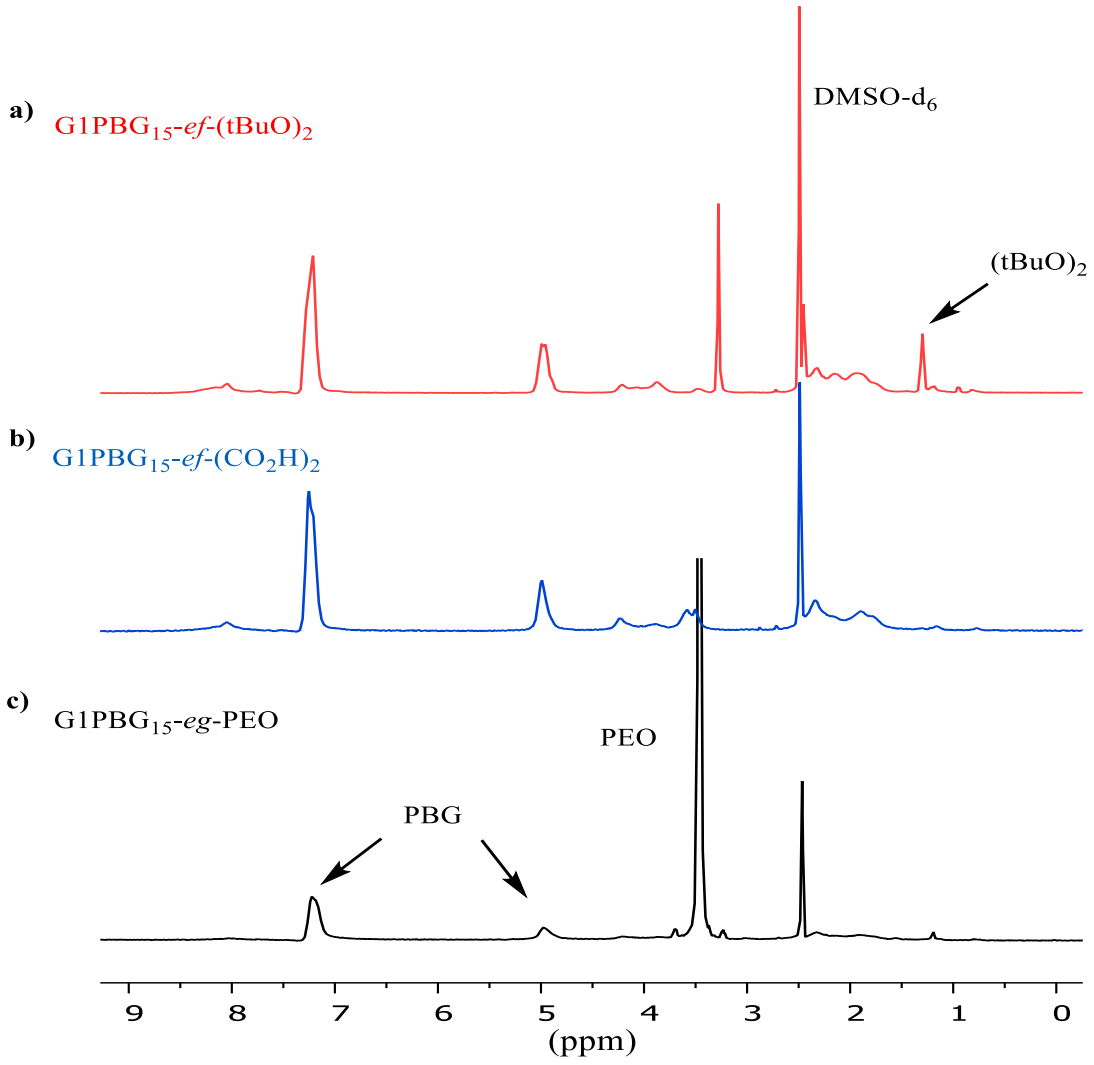

Figure 5.2. ^{1}H NMR spectra for G1PBG$_{15}$-*ef*-(tBuO)$_2$ (a) before and (b) after deprotection of the *tert*-butyl ester groups, and for G1PBG$_{15}$-*eg*-PEO (c) in DMSO-*d*$_6$.

The results obtained when coupling the six different G1 and G2 chain end-functionalized PBG-*ef*-$(CO_2H)_2$ substrates with PEO side chains to obtain the corresponding arborescent PBG-*end-grafted*-PEO (PBG-*eg*-PEO) copolymers are summarized in Table 5.4. The absolute molecular weight of the substrates and the arborescent copolymers was determined by SEC-MALLS analysis in DMSO. In all cases, the molecular weight of the copolymers increased with respect to the PBG substrates while maintaining a low polydispersity index (PDI ≤ 1.09).

Table 5.4. Characteristics of chain end-grafted PBG-*eg*-PEO arborescent copolymers.

copolymer	PBG Substrate			Graft Copolymer			
	M_n (g/mol)[a]	%-CO_2H[b]	G_y[c]	M_n (g/mol)[a]	M_w/M_n[a]	f_n[d]	%-PEO[e]
G1PBG$_{15}$-*eg*-PEO	220,000	9	70	890,000	1.06	67	75
G1PBG$_{29}$-*eg*-PEO	210,000	8	68	760,000	1.09	55	72
G1PBG$_{65}$-*eg*-PEO	270,000	9	63	1.0×10^6	1.05	73	73
G2PBG$_{15}$-*eg*-PEO	1.2×10^6	9	24	2.4×10^6	1.05	120	50
G2PBG$_{29}$-*eg*-PEO	970,000	9	31	2.3×10^6	1.09	133	57
G2PBG$_{65}$-*eg*-PEO	1.3×10^6	7	20	2.2×10^6	1.07	90	40

[a] Values from SEC-MALLS analysis in DMSO; [b] Mole fraction of carboxyl groups in the substrate; [c] Grafting yield: fraction of side chains attached to the substrate; [d] Branching functionality: number of branches added in the last grafting cycle; [e] PEO weight fraction from the difference in M_n of the copolymer and the substrate.

The grafting yield (G_y), defined as the fraction of linear chain segments becoming attached to the substrate, was calculated by the same method described in Chapter 4 for the randomly grafted systems. While a lower functionality level of CO_2H coupling sites was achieved for the chain end-functionalized PBG substrates (7–9 mol %) in comparison to the randomly functionalized PBG substrates (30–33 mol %), higher grafting yields were obtained under the same reaction conditions. For example, the PEO grafting yield for chain end grafting was 70, 68 and 63, for G1PBG$_{15}$-*eg*-PEO, G1PBG$_{29}$-*eg*-PEO and G1PBG$_{65}$-*eg*-PEO, respectively, significantly higher than for the randomly grafted systems (27, 24 and 29 for G1PBG$_{15}$-*g*-PEO, G1PBG$_{29}$-*g*-PEO and G1PBG$_{65}$-*g*-PEO, respectively, as provided in Chapter 4, Table 4.4). This can be explained by the better accessibility of the coupling sites in the chain end-functionalized PBG substrates in comparison to the randomly functionalized analogues. Despite the better accessibility of the coupling sites in the chain end-functionalized PBG substrates, arborescent copolymers with lower molar masses were obtained for the G1 and G2 polymers with different PBG core structures relatively to the randomly functionalized analogues. This means that a lower number of hydrophilic PEO segments were added in the last grafting cycle, and thus a lower branching functionality f_n was achieved. This is obviously a consequence of the lower functionality level of the chain end-functionalized PBG substrates.

The SEC traces obtained for the purified samples are compared in Figure 5.3, and the analysis results are summarized in Table 5.4. A decrease in elution volume is observed as the generation number increases. The elution volume increases in the G1 polymer series as G1PBG$_{65}$-*eg*-PEO < G1PBG$_{15}$-*eg*-PEO < G1PBG$_{29}$-*eg*-PEO, while for the G2 series it

increases as G2PBG$_{15}$-*eg*-PEO < G2PBG$_{29}$-*eg*-PEO < G2PBG$_{65}$-*eg*-PEO; the variations in absolute M_n within each series (Table 5.4) are small however, with average values of ca. $(9 \pm 1)\times10^5$ g/mol and $(2.3 \pm 0.1)\times10^6$ g/mol for the G1 and G2 copolymers, respectively.

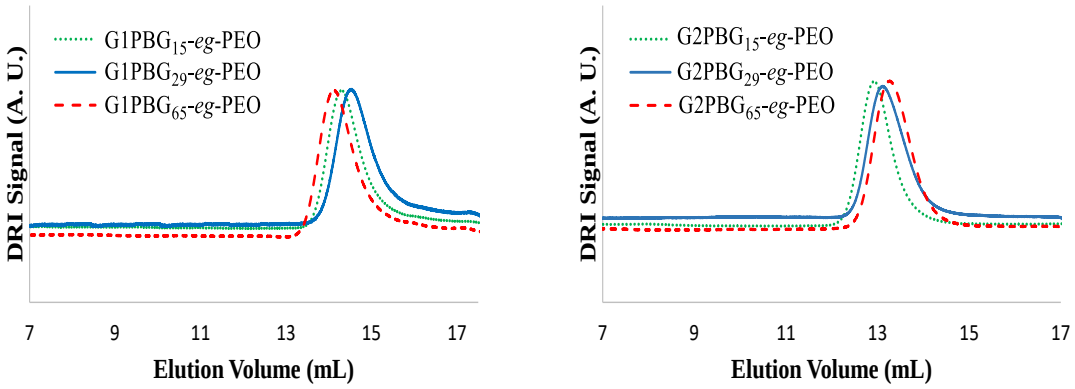

Figure 5.3. SEC traces for G1 (left) and G2 (right) arborescent copolymers.

5.4.3 Properties of Chain End-Grafted Arborescent Copolymer Micelles

Since the coupling sites for the chain end-functionalized PBG substrates are located closer to the periphery of the molecules, a better defined crew-cut core-shell morphology is expected for the amphiphilic copolymers. Consequently, the hydrophilic PEO shell should be able to shield the hydrophobic PBG core from intermolecular hydrophobic interactions and the aqueous environment more efficiently, leading to stable unimolecular micelles free of aggregation. The chain end-grafted arborescent copolymers were investigated using dynamic light scattering (DLS), transmission electron microscopy (TEM), and atomic force microscopy (AFM) measurements, to investigate the influence of the dendritic core structure on the micelle properties. The hydrodynamic diameter

determined by DLS followed the expected increasing trend from G1 to G2 molecules (Table 5.5). The addition of hydrophilic PEO segments strictly at the chain ends of the arborescent hydrophobic PBG core clearly facilitated the formation of unimolecular micelles without aggregates in aqueous solutions, in contrast to the randomly grafted copolymers investigated in Chapter 4.

Table 5.5. Characteristics of chain end-grafted arborescent PBG-*eg*-PEO copolymers.

copolymer	DMF				PBS			
	$D_{h,\ number}$	$D_{h,\ volume}$	$D_{h,\ intensity}$	PDI	$D_{h,\ number}$	$D_{h,\ volume}$	$D_{h,\ intensity}$	PDI
G1PBG$_{15}$-*eg*-PEO	11 ± 1	15 ± 1	17 ± 1	0.08	13 ± 2	17 ± 2	26 ± 2	0.19
G1PBG$_{29}$-*eg*-PEO	12 ± 1	13 ± 1	15 ± 1	0.10	14 ± 2	17 ± 2	22 ± 2	0.31
G1PBG$_{65}$-*eg*-PEO	14 ± 2	16 ± 2	18 ± 2	0.12	14± 2	16 ± 2	19 ± 3	0.27
G2PBG$_{15}$-*eg*-PEO	25 ± 2	27 ± 2	32 ± 2	0.04	29 ± 1	33 ± 1	37 ± 1	0.19
G2PBG$_{29}$-*eg*-PEO	25 ± 1	29 ± 1	35 ± 1	0.05	26 ± 1	31 ± 3	39 ± 1	0.27
G2PBG$_{65}$-*eg*-PEO	21 ± 1	23 ± 1	29 ± 1	0.09	22 ± 1	27 ± 1	31 ± 1	0.23

All experiments were carried out in triplicate, and the results are presented as the mean ± standard deviation for three measurements.

The good agreement in the hydrodynamic diameter of the copolymers determined by DLS analysis in both DMF (a good solvent for the core and shell component) and PBS solution (an aqueous environment, selective for the PEO shell) indeed suggests that unimolecular micelles were obtained with number-average mean diameters of 11-14 nm

and 21-29 nm for the G1 and G2 molecules, respectively (Table 5.5). Similar trends were also observed for the volume- and intensity-average diameters. The average hydrodynamic diameter of the end-grafted samples is clearly smaller than for the randomly grafted samples investigated in Chapter 4.

Size distribution analysis of the DLS results for the G1PBG-*eg*-PEO copolymers confirmed that the chain end-grafted copolymers formed exclusively stable unimolecular species without aggregation in DMF. Analysis of the same copolymers in phosphate buffered saline (PBS) solution yielded similar results, with number-average diameters comparable to those obtained in DMF in most cases. Interestingly, the G1PBG-*eg*-PEO copolymers also yielded a small amount (1−3 intensity %) of aggregates with a diameter around 5000 nm in the *intensity* distributions, while no aggregation was detected in the *number* nor in the *volume* distributions (Figure 5.4). This could be due to insignificant aggregation in the samples. The DLS measurements on all the G2PBG-*eg*-PEO samples yielded no detectable amounts of aggregates in DMF nor in PBS, as shown in Figure 5.5. The absence of significant amounts of aggregates in these systems clearly shows that the better defined crew-cut core-shell morphology of the chain end-grafted arborescent copolymers is a key factor in the formation of unimolecular micelles. In spite of the different hydrophobic G0PBG core structures used in the synthesis of the chain end-grafted G2 copolymers only small changes in hydrodynamic diameter were obtained, as determined by DLS analysis. This is attributed to the collapse of the hydrophobic PBG cores to minimize their exposure to the aqueous environment (as determined by ^{1}H NMR analysis), leading to a comparable contribution to the overall size of the micelles.

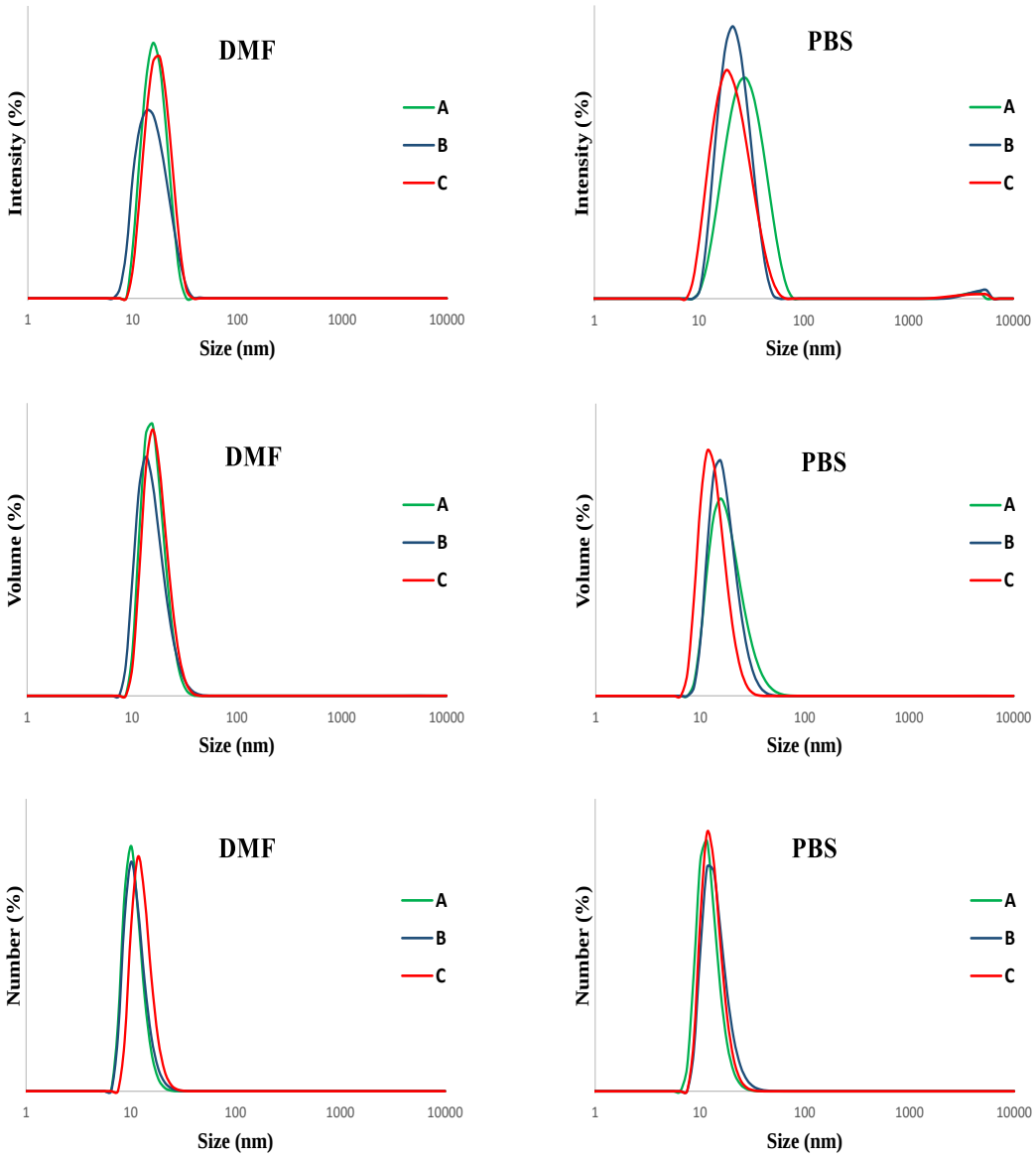

Figure 5.4. Hydrodynamic diameter distributions of the arborescent copolymers determined by DLS in DMF (left) and in PBS solution (right): (A) G1PBG$_{15}$-*eg*-PEO, (B) G1PBG$_{29}$-*eg*-PEO, and (C) G1PBG$_{65}$-*eg*-PEO.

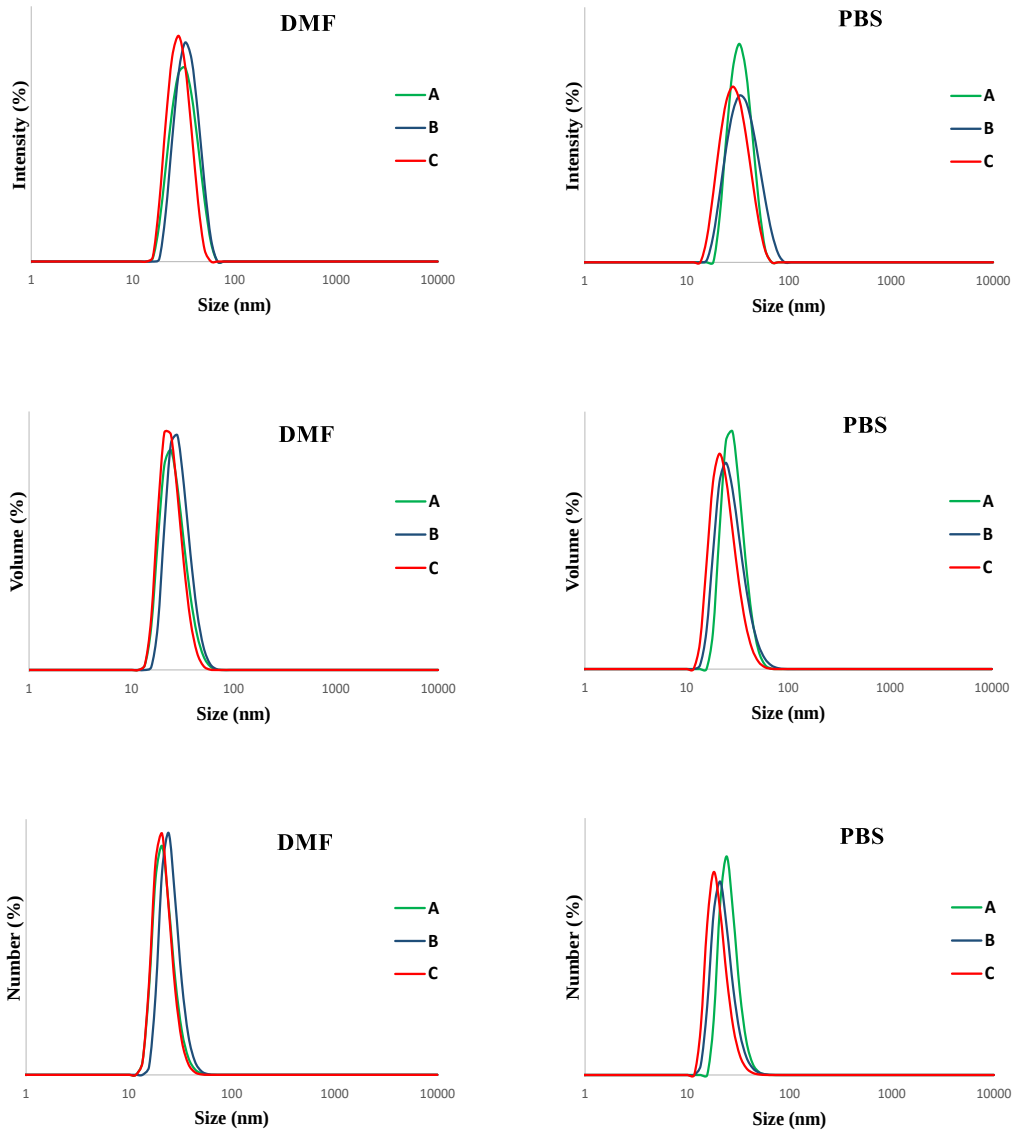

Figure 5.5. Hydrodynamic diameter distributions of the arborescent copolymers determined by DLS in DMF (left) and in PBS solution (right): (A) G2PBG$_{15}$-*eg*-PEO, (B) G2PBG$_{29}$-*eg*-PEO, and (C) G2PBG$_{65}$-*eg*-PEO.

The formation of micelles with a collapsed core structure was further confirmed by ^{1}H NMR spectroscopy as shown in Figure 5.6. For example, the analysis of G2PBG$_{15}$-*eg*-PEO in D_2O yielded no resonances for the phenyl (5H at 7.3) and benzylic methylene protons

(2H at 4.9 ppm), while these signals were present in DMSO-d_6, a good solvent for both the PBG core and PEO sides chains, indicating that the G2PBG core was collapsed in D_2O.

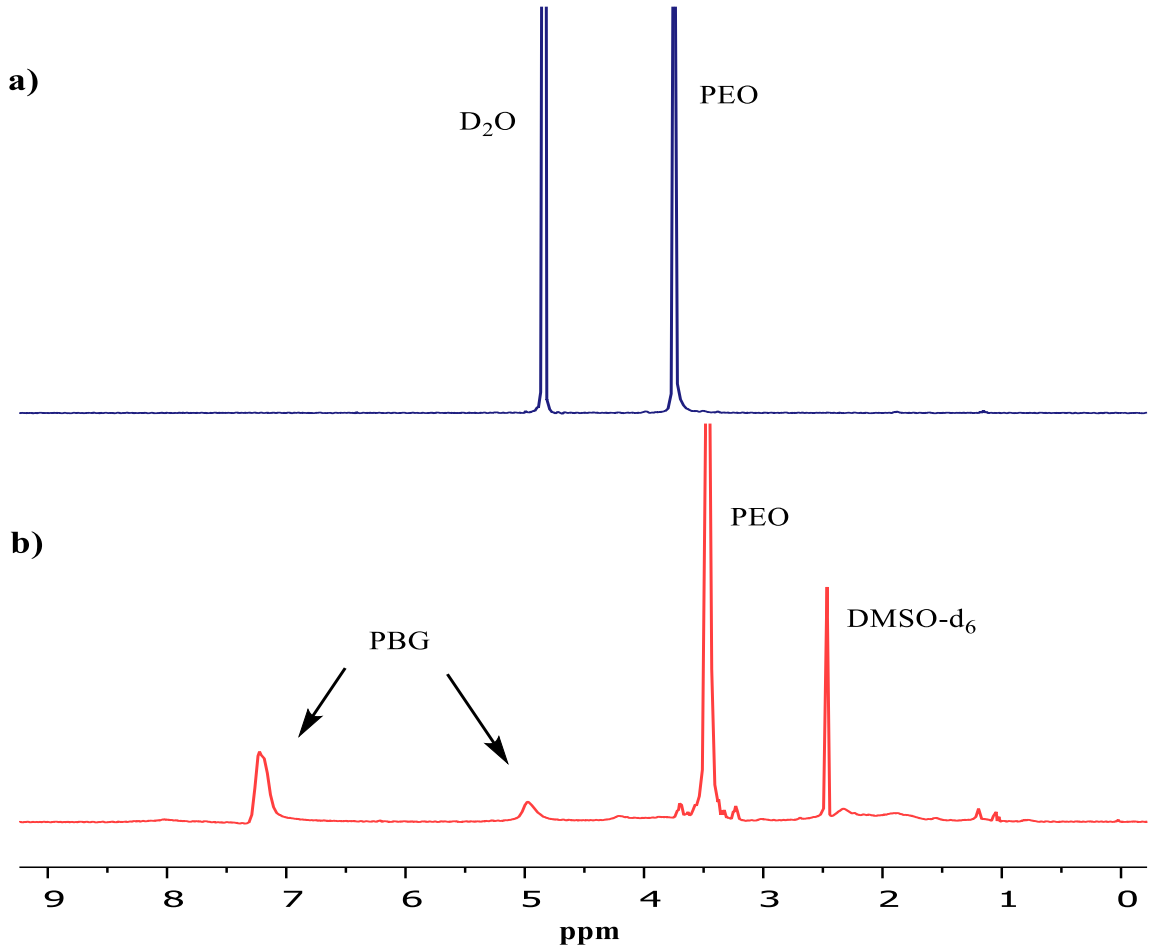

Figure 5.6. ^{1}H NMR spectra for G2PBG$_{15}$-*eg*-PEO in (a) D_2O and (b) deuterated DMSO.

Further analysis of the chain end-grafted copolymers by TEM (after staining with phosphotungstic acid) and by AFM revealed that all the samples had a uniform size distribution and a spherical shape (Figures 5.7 for G1 copolymers, Figure 5.8 for G2

copolymers). The average diameter measured by TEM for the G1 copolymers was 10 ± 2, 10 ± 3, and 13 ± 3 nm for G1PBG$_{15}$-*eg*-PEO, G1PBG$_{29}$-*eg*-PEO, and G1PBG$_{65}$-*eg*-PEO, respectively. For the G2 copolymers, the average diameter was 23 ± 3, 21 ± 5, and 18 ± 4 nm for G2PBG$_{15}$-*eg*-PEO, G2PBG$_{29}$-*eg*-PEO, and G2PBG$_{65}$-*eg*-PEO, respectively. The TEM measurements therefore confirm the trends observed by DLS of increasing micelle size with the generation number, but the diameter is smaller because the TEM analysis was performed in the dry state. Although it was expected that the different PBG linear substrates would yield micelles with different shapes, only spherical micelles were observed in both the AFM and TEM images (Figure 5.7 and Figure 5.8) for all the samples. While the exact reason for this is unknown, several factors may have contributed to the similar shape of the micelles including the branched structure of the copolymers, solvent effects and intramolecular hydrophobic interactions.[20-22]

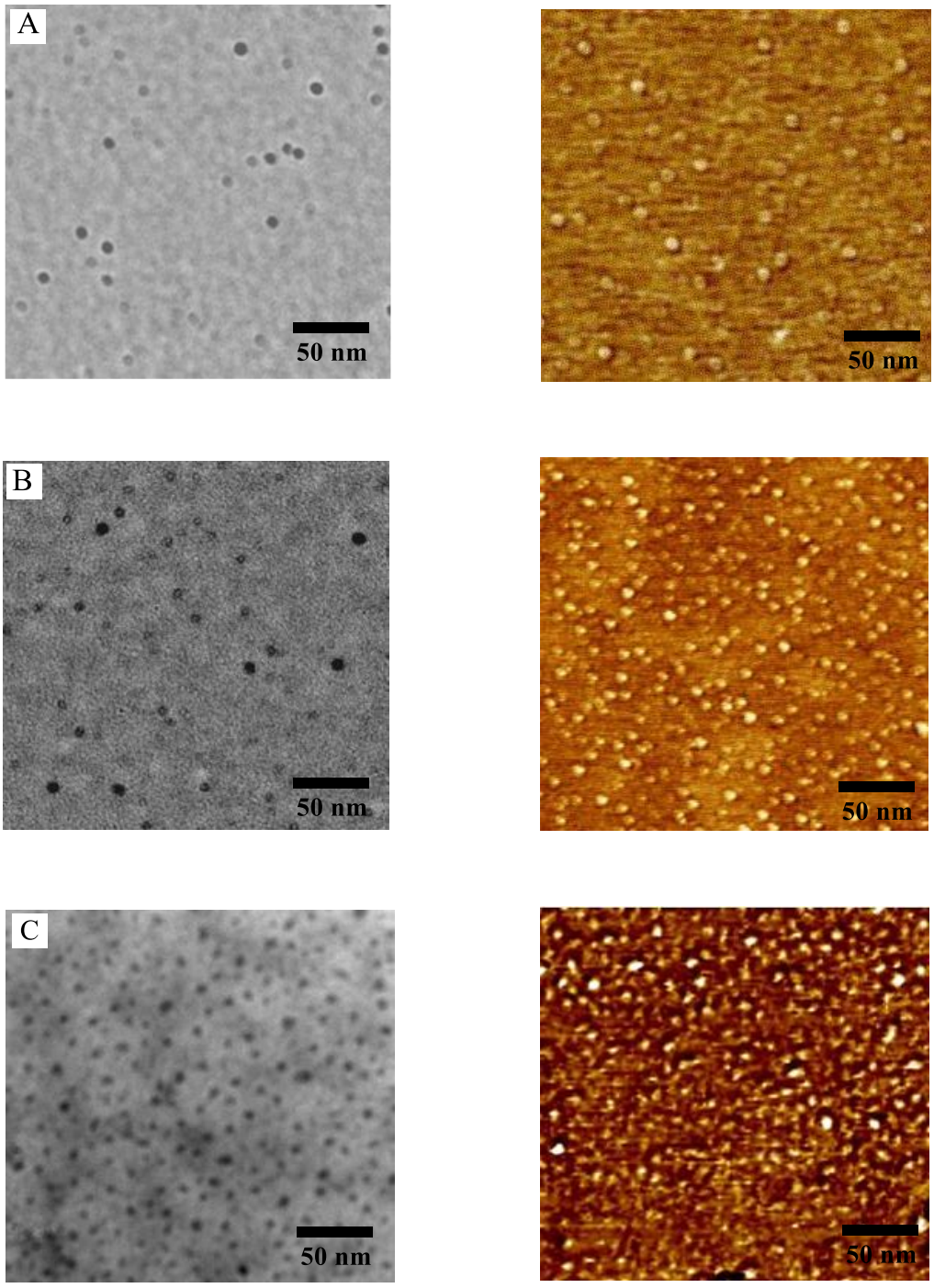

Figure 5.7. TEM (left) and AFM phase (right) images for chain end-grafted arborescent copolymers: (A) G1PBG$_{15}$-*eg*-PEO, (B) G1PBG$_{29}$-*eg*-PEO, and (C) G1PBG$_{65}$-*eg*-PEO.

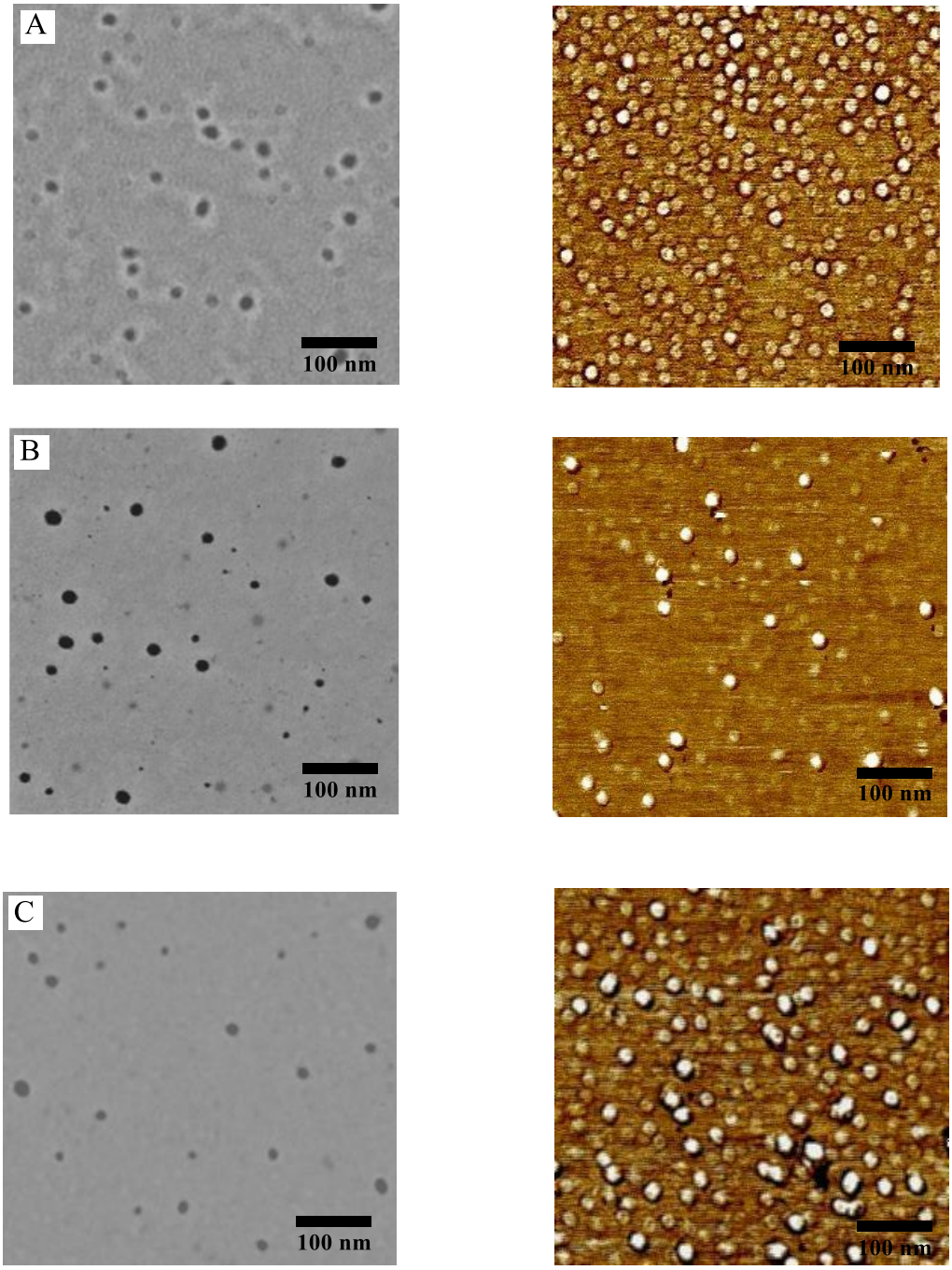

Figure 5.8. TEM (left) and AFM phase (right) images for chain end-grafted arborescent copolymers: (A) G2PBG$_{15}$-*eg*-PEO, (B) G2PBG$_{29}$-*eg*-PEO, and (C) G2PBG$_{65}$-*eg*-PEO.

5.4.4 Drug Loading and Micelle Characterization

The arborescent copolymers synthesized consist of an amphiphilic core–shell morphology with a hydrophobic arborescent poly(γ-benzyl L-glutamate) (PBG) core, creating a favorable microenvironment for the encapsulation of hydrophobic drugs via physical entrapment, and a hydrophilic shell of poly(ethylene oxide) (PEO) making these copolymers water-soluble (Scheme 5.3).

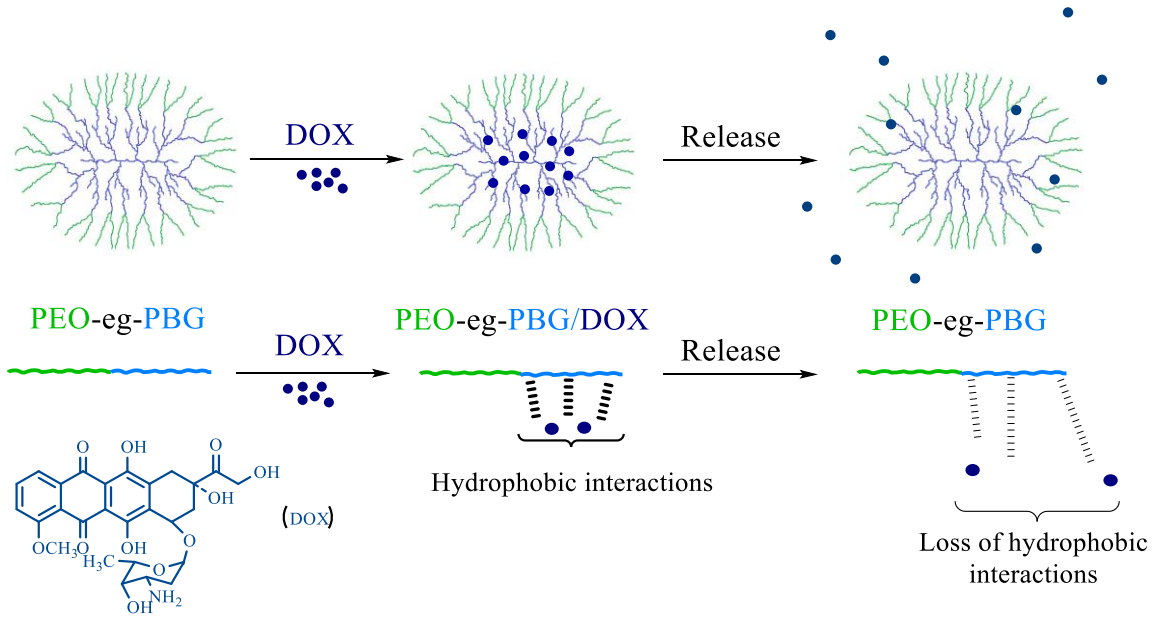

Scheme 5.3. Schematic representation of the encapsulation and release of DOX in the hydrophobic PBG core of G2PBG-*eg*-PEO through hydrophobic interactions.

In contrast to amphiphilic block copolymer micelles, unimolecular micelles are stable irrespective of their concentration or the solvency conditions used. Unimolecular micelles do not dissociate upon dilution in the human body, and thus should lead to more controlled drug release and increased treatment efficacy. To evaluate the encapsulation and release

properties of the synthesized arborescent copolymers, doxorubicin (DOX) was used as a model hydrophobic drug. The influence of differences in core structure on the ability to encapsulate and control the release of the hydrophobic drug was investigated.

To this end the hydrophilic doxorubicin hydrochloride (DOX·HCl) form of the drug was neutralized with two equivalents of triethylamine (TEA), to obtain the more hydrophobic DOX free base before encapsulation. The encapsulation study confirmed that, following purification by dialysis as described in Section 5.3.3.5, DOX could be solubilized in aqueous solutions of amphiphilic arborescent copolymers of generations G1 and G2. For example, the encapsulation of DOX within the hydrophobic core of G2PBG-*eg*-PEO yielded enhanced absorption around 490 nm for G2PBG-*eg*-PEO/DOX as compared to the blank micelles (Figure 5.9). The UV–vis spectra exhibited a bathochromic shift for the encapsulated drug (λ_{max} = 490 nm) as compared to free DOX (λ_{max} = 483 nm), attributed to hydrophobic interactions with the PBG core, which confirms successful DOX encapsulation within the micelles.

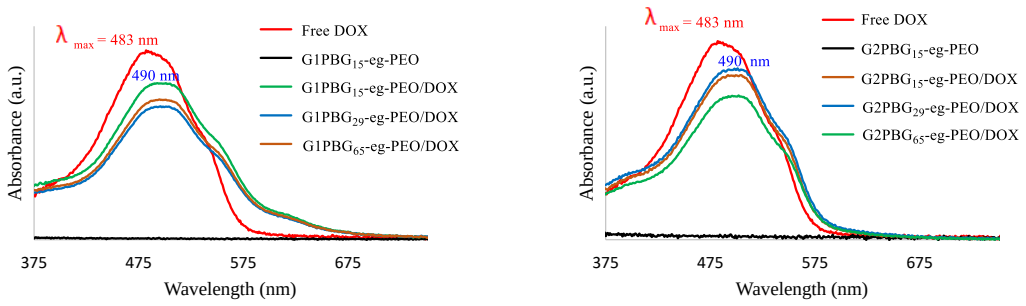

Figure 5.9. UV Absorption of free DOX, G1 (left) and free DOX, G2 (right) arborescent copolymers in PBS.

^{1}H NMR spectroscopy was also used to confirm the encapsulation of DOX as shown in Figure 5.10, by the complete disappearance of the PBG and DOX signals for G2PBG$_{15}$-*eg*-PEO/DOX in D_2O (Figure 5.10c), in comparison to the signal observed for free DOX in D_2O at the same overall concentration of 2 mg/mL (Figure 5.10a), indicating restricted mobility of the hydrophobic PBG core and the DOX molecules entrapped within the core of the nanocarriers.

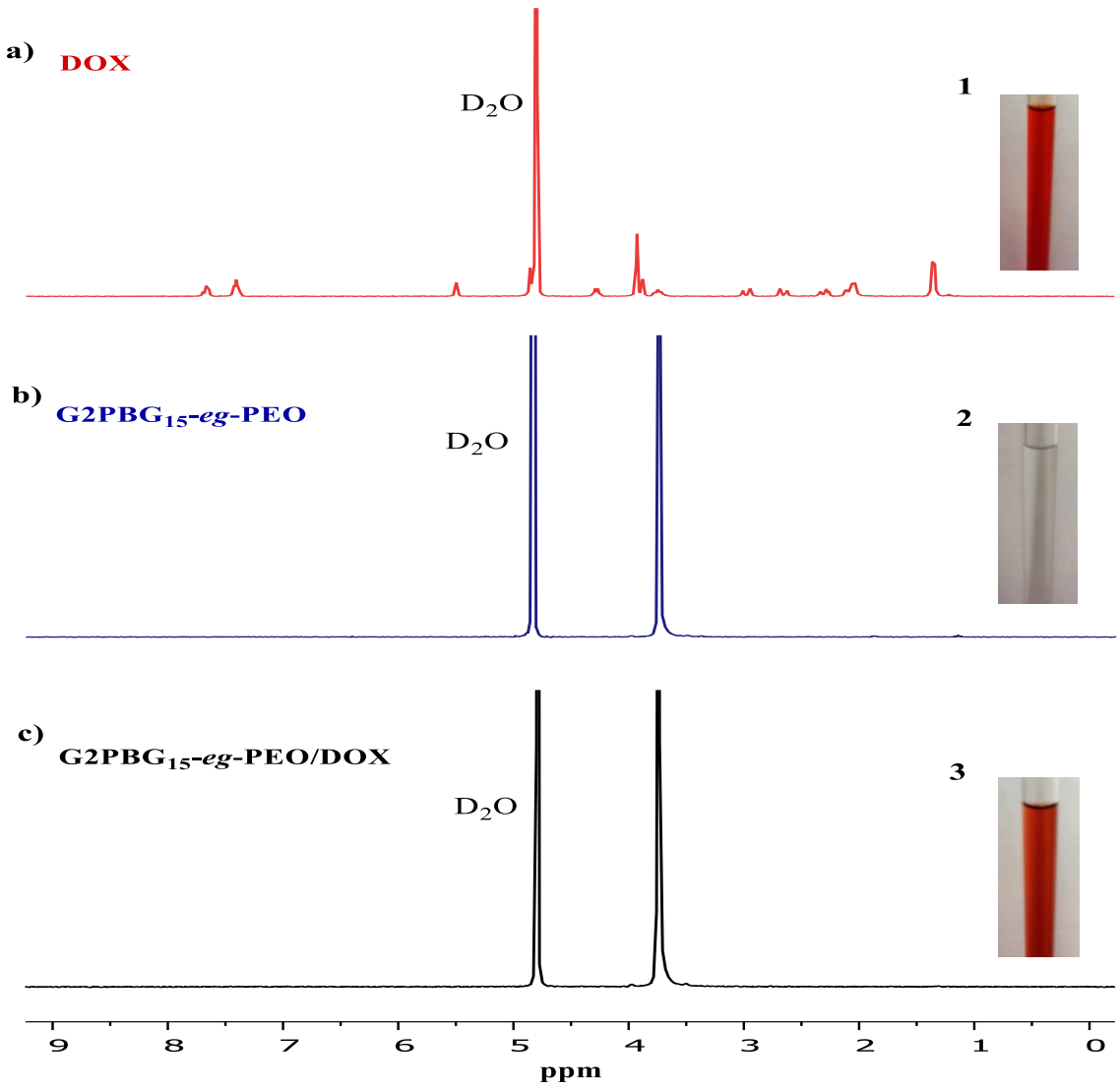

Figure 5.10. **^{1}H NMR spectra for (a) DOX in D_2O, (b) G2PBG$_{15}$-*eg*-PEO in D_2O and (c) G2PBG$_{15}$-*eg*-PEO/DOX in D_2O. The spectra show the appearance of the DOX signals upon encapsulation in G2PBG$_{15}$-*eg*-PEO.**

The physical encapsulation of hydrophobic drugs in micelles is mainly driven by hydrophobic interactions between the drug and the core of the micelles. By increasing the PBG content from a G1PBG to a G2PBG substrate in the synthesis of the unimolecular micelles, it should be possible to load more DOX in the micelles. Indeed, the DOX loading

capacity of the arborescent copolymers was higher for all the G2PBG-*eg*-PEO/DOX samples as compared to the G1PBG-*eg*-PEO/DOX systems (Table 5.6). For example, sample G2PBG$_{15}$-*eg*-PEO/DOX had higher values of DLC (11.2%) and DLE (67%) as compared to sample G1PBG$_{15}$-*eg*-PEO/DOX, with DLC and DLE values of 7.9% and 47%, respectively. This is attributed to the higher PBG content of G2PBG-*eg*-PEO/DOX relatively to G1PBG-*eg*-PEO/DOX, allowing for more DOX molecules to be physically encapsulated within the PBG core through hydrophobic interactions. Moreover, the DOX loading capacity of the arborescent copolymers varied slightly within the series G2PBG$_{15}$-*g*-PEO/DOX, G2PBG$_{65}$-*g*-PEO/DOX, G2PBG$_{29}$-*g*-PEO/DOX from 11.2 wt% to 10.4 wt% and 9.7 wt%, respectively. While these variations are minor, they could be related to variations in core size as seen in Table 5.6. Increasing the core size led to increased hydrophobicity for the G2PBG substrate for the synthesis of the unimolecular micelles, which enhanced their loading capacity for DOX.

Table 5.6. Characterization of DOX-loaded unimolecular micelles.

Copolymer	PBG		PBG-*eg*-PEO		PBG-*eg*-PEO/DOX			
	Size (nm)	PDI	Size (nm)	PDI	Size (nm)	PDI	DLC (wt%)	DLE (%)
G1PBG$_{15}$-eg-PEO/DOX	-	-	13	0.19	14	0.41	7.9 ± 0.3	47 ± 4
G1PBG$_{29}$-eg-PEO/DOX	-	-	14	0.31	14	0.32	7.5 ± 0.2	45 ± 4
G1PBG$_{65}$-eg-PEO/DOX	-	-	14	0.27	15	0.35	8.1 ± 0.2	49 ± 5
G2PBG$_{15}$-eg-PEO/DOX	14	0.18	29	0.19	31	0.28	11.2 ± 0.3	67 ± 4
G2PBG$_{29}$-eg-PEO/DOX	10	0.05	26	0.27	27	0.27	9.7 ± 0.2	58 ± 3
G2PBG$_{65}$-eg-PEO/DOX	12	0.04	22	0.23	24	0.29	10.4 ± 0.3	62 ± 4

Data represent the mean ± standard deviation (n = 3).

Examining the drug loading efficiency (DLE) to further investigate whether differences in core-shell morphology between the chain end-grafted and randomly grafted arborescent copolymers (Chapter 4) affect their ability to encapsulate the hydrophobic DOX, it was found that the DLE of all the arborescent copolymers with similar cores did not differ significantly. For example the end-grafted arborescent copolymers G2PBG$_{15}$-*eg*-PEO encapsulated DOX with a DLE of 67%, while the randomly grafted arborescent copolymers G2PBG$_{15}$-*g*-PEO had a DLE of 65%. The end-grafted copolymer had an insignificantly larger DLE, while its molar mass and hydrodynamic diameter were significantly lower (2.4×10^6 g.mol^{-1}, 29 nm, respectively) than for its randomly grafted

counterpart (3.4×10^6 g.mol^{-1}, 35 nm, respectively), which is attributed to the similarity of the core size and hydrophobicity in both copolymers. Similar trends were also observed for the other copolymers. These results further confirm that the branching density (b_d) of the hydrophobic core, and thus the core size and the hydrophobicity of the unimolecular micelles, is the main factor affecting their drug loading capacity rather than the overall size of the micelles.

The size of the DOX-loaded micelles in PBS was also investigated by DLS and found to be only slightly larger than the corresponding blank micelles (Table 5.6). For instance, the number-average diameter of G2PBG$_{15}$-*eg*-PEO increased from 29 to 31 nm upon loading with DOX. This size increase is of course small and close to the error limits of the DLS technique (ca. ± 1 nm), but is nevertheless consistent with the presence of entrapped DOX molecules. The following release experiments mainly focused on the G2PBG-*eg*-PEO/DOX systems, which had the highest DLC and DLE.

5.4.5 *In Vitro* Drug Release Kinetics

The *in vitro* drug release properties of the DOX-loaded micelles were investigated by dialysis at 37 ˚C in phosphate-buffered saline (PBS) at pH 7.4 (normal physiological conditions) and 5.5 (to mimic tumor cell environments). The release profile for the DOX-loaded micelles at the different pH are compared with the release profile for free DOX in Figure 5.11. It is clear that the pH significantly affected the release kinetics of DOX from all three DOX-loaded micelle systems. At pH 7.4 the DOX release was slower, with a cumulative release after 50 hours of only 14.5, 16.5 and 20.4% for G2PBG$_{15}$-*eg*-PEO/DOX

(Figure 5.11a), G2PBG$_{29}$-*eg*-PEO/DOX (Figure 5.11b), and G2PBG$_{65}$-*eg*-PEO/DOX (Figure 5.11c), respectively. However at pH 5.5, the cumulative release under the same conditions increased to 27.8, 28.6 and 39.4% for G2PBG$_{15}$-*eg*-PEO/DOX, G2PBG$_{29}$-*eg*-PEO/DOX, and G2PBG$_{65}$-*eg*-PEO/DOX, respectively. These results confirm that the DOX-loaded micelles show pH-dependent drug release profiles. This is presumably due to the protonation of DOX under acidic conditions, which increases its solubility and accelerates the diffusion rate of DOX. As a result, the hydrophobic interactions between DOX and the core of the micelles are weakened.[23,24] Such pH-dependent release behavior of DOX was pointed out to be highly beneficial in drug delivery for cancer therapy, as it would favor the release of DOX in cancer cells while limiting release in the blood stream.[25] As shown in Figure 5.11d, the release rate of DOX at both pH was faster for the G1PBG$_{29}$-*eg*-PEO/DOX system than for G2PBG$_{29}$-*eg*-PEO/DOX. For example, the total amount of drug released from G1PBG$_{29}$-*eg*-PEO/DOX after 50 h reached 33.2 and 50.4 % at pH 7.4 and at pH 5.5, respectively, as compared with 16.5 and 28.6% for G2PBG$_{29}$-*eg*-PEO/DOX (Figure 4.11b). This is attributed to the smaller hydrodynamic diameter of G1PBG$_{29}$-*eg*-PEO/DOX relatively to G2PBG$_{29}$-*eg*-PEO/DOX, decreasing the diffusion path for drug release and thus increasing the drug release rate. The release profile observed for free DOX is also provided in Figure 5.11e for comparison. The burst release of DOX is very obvious in that case when compared to all the DOX-loaded micelles.

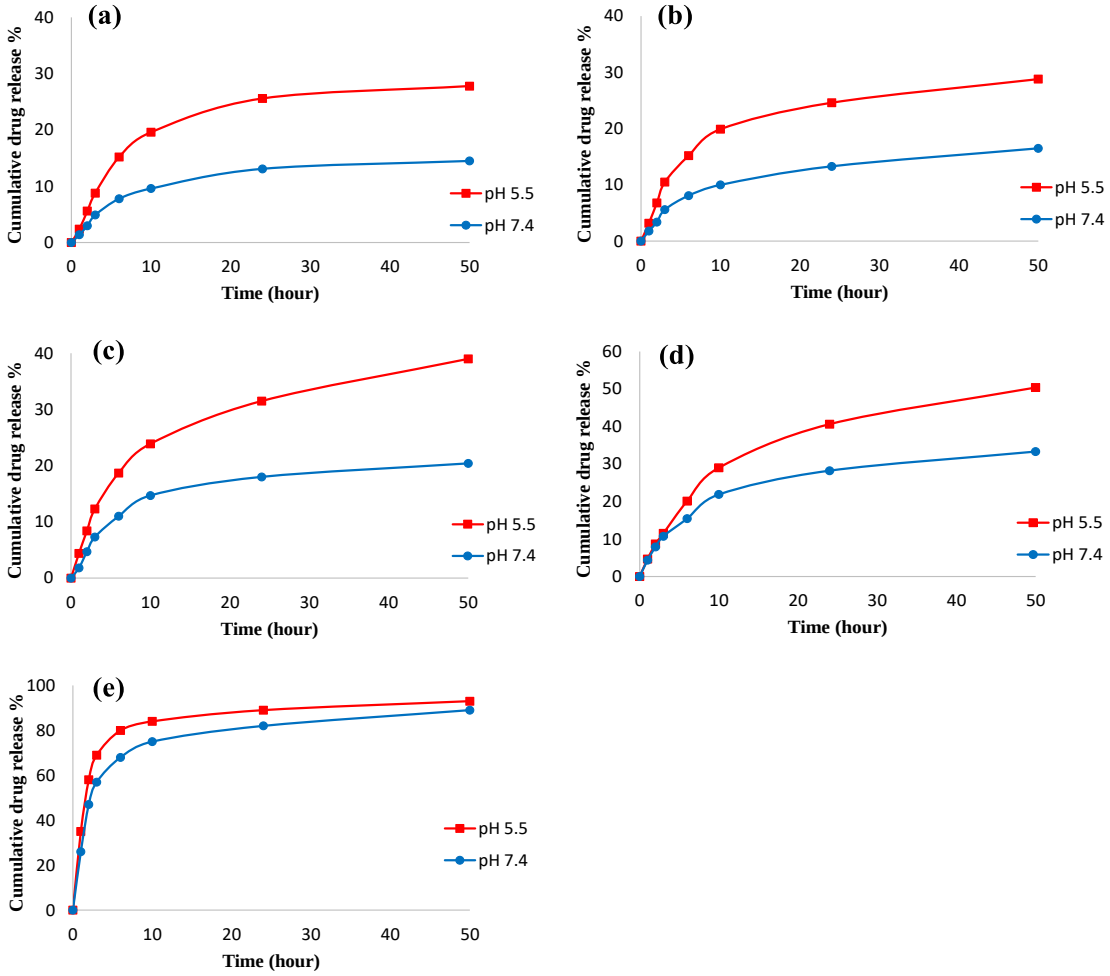

Figure 5.11. ***In vitro*** **DOX release profiles from (a) G2PBG$_{15}$-*eg*-PEO/DOX, (b) G2PBG$_{29}$-*eg*-PEO/DOX, (c) G2PBG$_{65}$-*eg*-PEO/DOX, (d) G1PBG$_{29}$-*eg*-PEO/DOX unimolecular micelles and (e) free DOX in PBS (pH 7.4 and 5.5) at 37 ˚C.**

As shown in Figure 5.11, faster DOX release was observed from G2PBG$_{65}$-*eg*-PEO/DOX as compared to the other two DOX-loaded micelles, which could be attributed to two factors. The most probable explanation for the difference is the micelle size. Since the drug release in these systems should be diffusion-controlled, faster drug release is expected from micelles with a smaller hydrodynamic diameter due to the shorter diffusion

path for drug release. G2PBG$_{65}$-*eg*-PEO/DOX has indeed the smallest hydrodynamic diameter (24 nm) and the fastest DOX release rate as compared to the other two DOX-loaded unimolecular micelles (31 and 27 nm for G2PBG$_{15}$-*eg*-PEO/DOX and G2PBG$_{29}$-*eg*-PEO/DOX, respectively). Another reason could be differences in core branching densities (b_d) among the micelles. G2PBG$_{65}$-*eg*-PEO/DOX has the lowest branching density (b_d = 0.11) among the three PBG core substrates, and therefore should have a more porous core structure allowing water molecules to penetrate more easily into it. Consequently the protonation rate of DOX should increase, resulting in its faster release. In contrast, G2PBG$_{15}$-*eg*-PEO/DOX has the highest branching density (b_d = 0.80) and a more compact core structure (G2PBG$_{15}$), while G2PBG$_{29}$-*eg*-PEO/DOX has an intermediate branching density (b_d = 0.19) which correlates with slower DOX release.

All the DOX-loaded micelles displayed a biphasic DOX release pattern at both pH, characterized by an initial burst release followed by slower and sustained release of the drug. The burst release could be due to DOX adsorbed in the interfacial core-shell region of the micelles, which can diffuse faster into the release medium. In all cases, the release profiles showed incomplete DOX release from the micelles even after one month, as shown in Figure 5.12, which is attributed to the dense and branched hydrophobic PBG core strongly interacting with DOX.

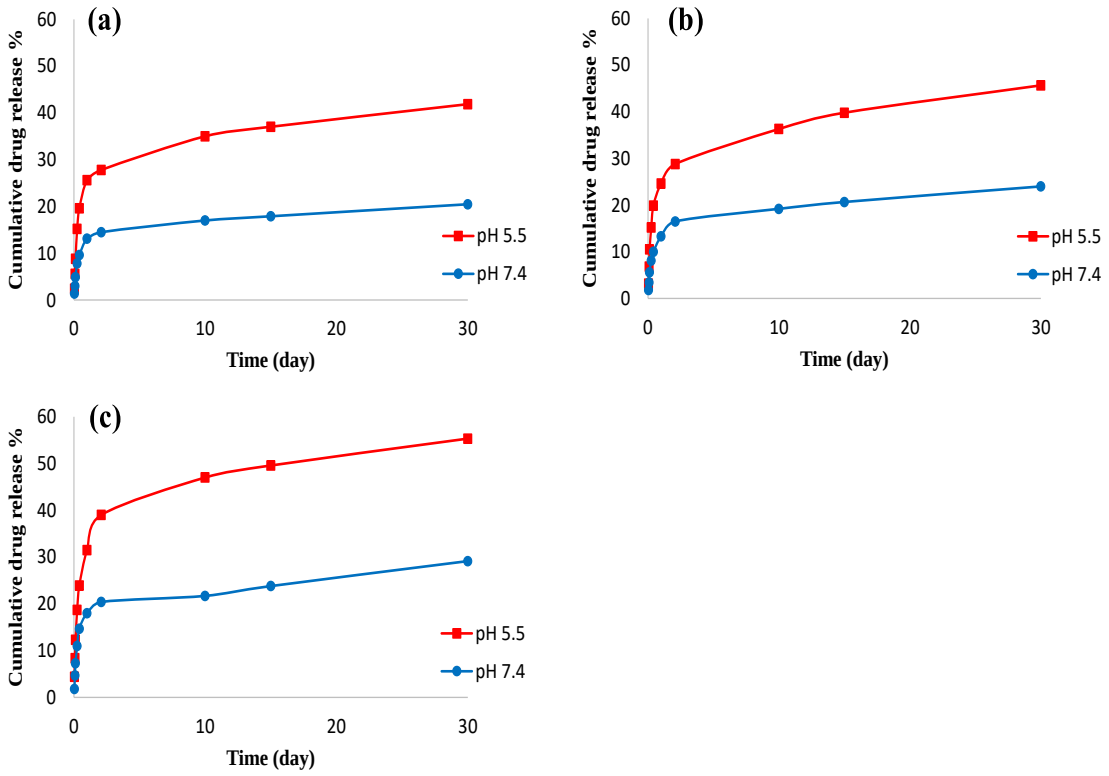

Figure 5.12. ***In vitro*** **DOX release profiles over 30 days from (a) G2PBG$_{15}$-*eg*-PEO/DOX, (b) G2PBG$_{29}$-*eg*-PEO/DOX and (c) G2PBG$_{65}$-*eg*-PEO/DOX micelles in PBS (pH 7.4 and 5.5) at 37 ˚C.**

All the DOX-loaded chain end-grafted arborescent copolymers exhibited faster DOX release rates in comparison with their randomly grafted counterparts (Chapter 4), as shown in Figure 5.13. The faster release rates observed in the current investigation are attributed to the smaller size and the unimolecular nature of the end-grafted copolymer micelles. The release rate of DOX was clearly influenced by the pH for both systems, but the chain end-grafted copolymers displayed enhanced pH responsiveness as compared to the randomly grafted systems. Since the chain end-grafted copolymers are expected to have a better-defined core-shell morphology, the hydrophilic PEO chains in the shell should be able to

shield the hydrophobic PBG core and the DOX from the aqueous environment more efficiently while minimizing the interfacial region, leading to better-defined pH responsiveness.

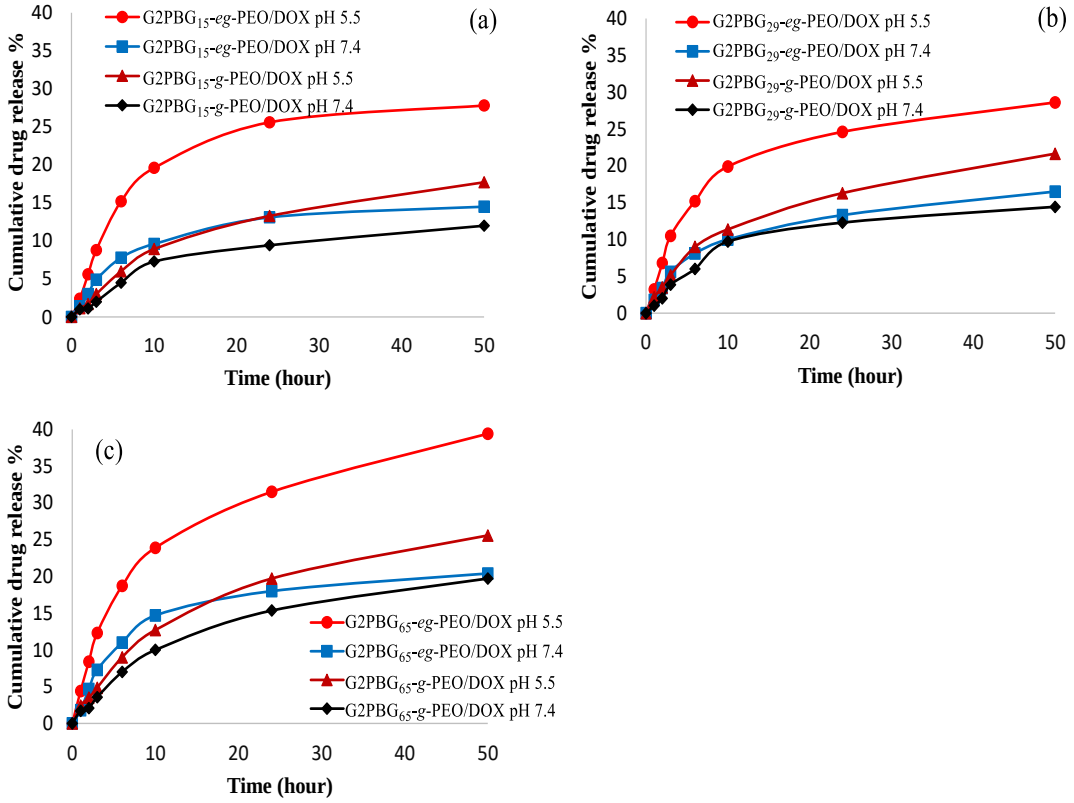

Figure 5.13. ***In vitro*** **DOX release profiles from (a) G2PBG$_{15}$-*eg*-PEO/DOX and G2PBG$_{15}$-*g*-PEO/DOX, (b) G2PBG$_{29}$-*eg*-PEO/DOX and G2PBG$_{29}$-*g*-PEO/DOX, (c) G2PBG$_{65}$-*eg*-PEO/DOX and G2PBG$_{65}$-*g*-PEO/DOX unimolecular micelles in PBS (pH 7.4 and 5.5) at 37 ˚C.**

The results obtained therefore demonstrate the advantages of using chain end-grafted arborescent copolymers in comparison to randomly grafted copolymers as nanocarriers for drug delivery: The end-grafted copolymers formed either insignificant (G1) or

undetectable (G2) amounts of aggregates in aqueous solutions, exhibited more sharply pH-dependent drug release profiles, but also a similar drug loading capacity for DOX even though their hydrodynamic diameter was smaller than their randomly grafted analogues.

5.5 Conclusions

In this study, a series of well-defined amphiphilic arborescent copolymers of generations G1 and G2 with three different poly(γ-benzyl L-glutamate) (G0PBG) core branching densities (b_d) were successfully synthesized and evaluated as drug delivery nanocarriers. The copolymers were obtained by end-grafting arborescent poly(γ-benzyl L-glutamate) (PBG) cores with different structures, of generations G1 and G2, with poly(ethylene oxide) (PEO) chain segments. These copolymers were characterized in solution by DLS, ^{1}H NMR and SEC-MALLS measurements, as well as by TEM and AFM in the dry state. All the copolymers investigated formed spherical unimolecular micelles with dimensions tailorable from 13 to 29 nm, depending on their generation number and core structure. The encapsulation ability of these unimolecular micelles was evaluated using doxorubicin (DOX) as a model hydrophobic drug, and drug loading contents of up to 11.2 wt% with pH-responsive sustainable drug release were observed by UV-vis spectroscopy.

Both the drug loading content (DLC) and the drug loading efficiency (DLE) increased with the generation number of the copolymers, due to the increase in PBG content from G1PBG to G2PBG in the micelles. The branching density of the dendritic G0PBG core was only found to have a minor influence on the overall unimolecular micelle diameter,

but it affected the drug loading content, the drug loading efficiency, and the drug release rate more significantly. Increasing the branching density of the G0PBG core, by increasing the deprotection level of the substrate, led to a larger core diameter and increased hydrophobicity for the G2BPG substrate for the synthesis of the unimolecular micelles, which enhanced their loading capacity for DOX. The release rate of DOX was also affected by the generation number and the hydrophobic core structure for the arborescent copolymers. Increasing the hydrodynamic diameter of the copolymers, by increasing the generation number, increased the diffusion path for drug release, thus reducing the drug release rate. In addition, the micelles with a denser core structure ($G2PBG_{15}$) exhibited the slowest release rate, while those with a more porous core structure ($G2PBG_{65}$) exhibited the fastest DOX release rate.

Considering their controllable molecular structure, good water solubility and drug loading capacity, and the desirable pH-dependent controlled release characteristics observed, unimolecular micelles based on amphiphilic arborescent copolymers appear to hold great potential as nanocarriers for drug delivery in cancer treatment.

Chapter 6 Encapsulation of Doxorubicin in Arborescent Polypeptide Micelles by Different Strategies: Preparation, Characterization and *In Vitro* Release Evaluation

6.1 Overview

Dendritic graft copolymers of generations G1 and G2, in the form of arborescent poly(γ-benzyl L-glutamate) grafted at their chain ends with poly(ethylene oxide) segments (PBG-*eg*-PEO), and the corresponding deprotected poly(L-glutamic acid)-*eg*-poly(ethylene oxide) (PGA-*eg*-PEO), were synthesized and evaluated as nanocarriers for the anticancer drug doxorubicin (DOX). These micelles had a spherical topology and a uniform size, with average diameters of 15 and 29 nm for G1PBG-*eg*-PEO and G2PBG-*eg*-PEO, respectively. Three different strategies were examined to load DOX in these carriers. The hydrophobic form of DOX could be physically entrapped within the poly(γ-benzyl L-glutamate) core. Doxorubicin hydrochloride (DOX·HCl) was also successfully loaded in the hydrophilic core of arborescent PGA-*eg*-PEO via either electrostatic interactions or conjugation through a pH-sensitive hydrazone bond. While a good drug loading capacity (7.6-14.1 wt%) was achieved in all cases, electrostatic interactions yielded the highest drug loading efficiency 66 and 83% for G1PGA-*eg*-PEO and G2PGA-*eg*-PEO, respectively. All the systems exhibited sustained and pH-sensitive drug release behavior, with a drug release rate increasing from physiological (pH 7.4) to acidic (pH 5.5) conditions. The hydrazone bond-conjugated systems had the best overall pH-responsive behavior however, due to the stability of the hydrazone bond at physiological pH eliminating burst release of the drug. The arborescent polymeric micelles would be useful as nanocarriers for drug delivery applications.

6.2 Introduction

Cancer is a group of more than 100 diseases characterized by the uncontrolled growth and spread of abnormal cells.[1] It is a leading cause of death worldwide, and chemotherapy remains one of the most effective methods for the treatment of cancer. Chemotherapy conventionally involves the use of small molecule drugs such as doxorubicin (DOX) to destroy rapidly dividing cancer cells via damage to their RNA or DNA. DOX is widely used in chemotherapy to treat many types of cancer that has spread such as lung, bladder and breast cancer.[2] Unfortunately, its therapeutic potential is limited by its cytotoxicity which lacks specificity to cancer cells, causing serious damage to healthy cells. One approach to reduce the side effects of DOX as well as to enhance its therapeutic effectiveness is to develop drug delivery systems. In recent years, various drug delivery systems have been developed with different designs for that purpose such as polymeric micelles, nanoparticles, dendrimers, liposomes and carbon nanotubes.[3] Such systems increase the solubility limit and action time of drugs, and most importantly facilitate their accumulation in tumors through the enhanced permeability and retention (EPR) effect.[4,5]

Among the many drug delivery systems investigated, polymer micelles based on amphiphilic diblock or triblock copolymers have attracted significant attention for biomedical applications due to their unique core-shell structure that can be used to encapsulate drugs within their hydrophobic core.[6-8] Unfortunately, self-assembled nanocarriers can become unstable and disassemble into free polymeric chains when subjected to pH or temperature variations, or upon dilution below their critical micelle concentration (CMC) in the bloodstream. In contrast, amphiphilic dendritic copolymers

can behave like unimolecular micelles and provide excellent *in vivo* stability irrespective of their surroundings, due to their covalently bonded core-shell structure.[9-12]

Dendritic polymers are a versatile class of macromolecules characterized by a highly branched tree-like architecture, incorporating multiple branching levels resulting from coupling reactions of either small molecule monomers (hyperbranched polymers and dendrimers) or macromolecular building blocks (dendrigraft polymers).[13-16] In aqueous media, amphiphilic dendritic polymers may either exist as unimolecular micelles or form multimolecular aggregates useful for a number of applications such as drug delivery.[9] Due to the vast array of architectures that can be obtained, dendrigraft (arborescent) polymers are an interesting alternative in the design of unimolecular micelles.[17-19] In contrast to the other dendritic polymer families, high molecular weight arborescent polymers can be obtained in relatively few steps, while maintaining fairly narrow molecular weight distributions ($M_w/M_n < 1.1$).[20] Furthermore, the properties of unimolecular arborescent micelles can be fine-tuned to suit certain needs, for example through the introduction of functional groups to attach drugs, imaging agents or targeting moieties, which makes them highly suited as nanocarriers for drug delivery.

Ideally, drug nanocarriers should not only solubilize hydrophobic anticancer drugs, but also protect them from inactivation in the biological milieu and from fast clearance processes (e.g. via urinary excretion). They should also possess functional groups to attach the drugs, and most of all, be biocompatible. There are certain requirements which the nanocarriers must meet to improve the efficacy of cancer therapy. These include a high drug loading efficiency, controlled drug release characteristics, and *in vivo* stability.

Polypeptides such as poly(glutamic acid), poly(L-lysine) and poly(aspartic acid) have attracted much interest as building blocks to construct nanostructures for biological applications, due to their remarkable characteristics including but not limited to good biocompatibility, biodegradability, economics, and the presence of versatile functional groups such as hydroxyl, carboxyl and amino groups that can serve for chemical modification.[21] In addition to these features making them excellent materials for drug delivery applications, polypeptides have the ability to form well-defined secondary structures (α-helices and β-sheets) contributing to their self-assembly, which leads to novel nanostructured materials. Poly(ethylene glycol) (PEG, also referred to as poly(ethylene oxide) or PEO), is the polymer most widely used to coat nanoparticulate carriers and minimize their interactions with components of biological fluids such as plasma proteins, and to avoid their recognition by the mononuclear phagocytic system (MPS) and subsequent clearance by the kidneys. In addition, PEG provides protection for cargoes that are sensitive to particular environments and prolongs the circulation time of polymeric micelles in the bloodstream.[22,23] As a result, various amphiphilic copolymers of different architectures, composed of hydrophobic polypeptide and hydrophilic PEG segments, have been studied for drug delivery applications.[24-26]

Three main strategies can be employed to load drugs into polymeric micelle cores: (i) physical entrapment, (ii) electrostatic interactions, and (iii) covalent conjugation. Depending on the polymer structure and the nature of the drug, each strategy has distinct advantages and disadvantages. In the literature, different types of PEO- or PEG-polypeptide copolymers such as poly(ethylene oxide)-*b*-poly(γ-benzyl L-glutamate) (PEO-

b-PBLG) diblock copolymers, PBLG-*b*-PEO-*b*-PBLG triblock copolymers, and poly(ethylene glycol)-*b*-poly(β-benzyl L-aspartate) block copolymers (PEG-*b*-PBLA) have been reported to encapsulate DOX via physical entrapment.[27,28] Hydrophilic DOX·HCl was also loaded via electrostatic interactions in poly(ethylene glycol)-*b*-poly(L-glutamic acid) (PEG-*b*-PLG) and poly(ethylene glycol)-*b*-poly(L-glutamic acid-*co*-L-phenylalanine) (PEG-*b*-P(Glu-*co*-Phe)).[29,30] Examples of the covalent conjugation of DOX to the hydrophobic segments of amphiphilic block copolymers include poly(ethylene glycol)-*b*-poly(β-benzyl L-aspartate) and the amphiphilic hyperbranched block copolymer Boltorn® H40-poly(β-benzyl L-aspartate)-*b*-poly(ethylene glycol) via pH-sensitive hydrazone linkages.[31,32] However despite the precise structure, controlled and high degree of size uniformity that could be achieved for unimolecular micelles constructed from arborescent polymer substrates,[33] their use as biocompatible drug nanocarriers through physical entrapment, electrostatic interactions, or covalent conjugation with drugs has yet to be explored.

The aim of this study was to load DOX into arborescent copolymer micelles by different strategies, so as to compare them in terms of loading efficiency, loading capacity, and drug release profiles. We report herein the synthesis of biocompatible arborescent polymeric micelles with poly(γ-benzyl L-glutamate) (PBG) and poly(ethylene oxide) segments. The arborescent poly(γ-benzyl L-glutamate) substrates were synthesized by ring-opening polymerization of γ-benzyl L-glutamic acid *N*-carboxyanhydride initiated with *n*-hexylamine, and successive grafting reactions via standard peptide coupling techniques. Amphiphilic unimolecular micelles of poly(benzyl L-glutamate)-*eg*-poly(ethylene oxide)

copolymers were obtained by grafting hydrophilic side chains of poly(ethylene oxide) at the end of the PBG chains on the hydrophobic arborescent substrates. The synthesized polymers were characterized by ^{1}H NMR spectroscopy, gel permeation chromatography (GPC), atomic force microscopy (AFM), dynamic light scattering (DLS), and transmission electron microscopy (TEM).

The encapsulation and release properties of these nanocarriers were investigated using doxorubicin (DOX) as a model anticancer drug, which was effectively encapsulated via three different methods. The hydrophobic form of DOX was physically entrapped within the core of the poly(γ-benzyl L-glutamate)-*eg*-poly(ethylene oxide) micelles. The nomenclature used to identify these samples is PBG-*eg*-PEO/DOX. Doxorubicin hydrochloride (DOX·HCl) was also loaded into the hydrophilic (deprotected) arborescent poly(L-glutamic acid)-*eg*-poly(ethylene oxide) copolymers via electrostatic interactions (PGA-*eg*-PEO-DOX). The conjugation of doxorubicin with poly(L-glutamic acid)-*eg*-poly(ethylene oxide) micelles via pH-sensitive hydrazone bonds was also achieved (PGA-*eg*-PEO-Hyd-DOX).

6.3 Experimental Procedures

6.3.1 Characterization and Sample Preparation

6.3.1.1 Nuclear Magnetic Resonance Spectroscopy

Proton nuclear magnetic resonance (^{1}H NMR) spectroscopy was used to estimate the degree of polymerization of linear poly(γ-benzyl L-glutamate) and to determine the

deprotection level of the PBG grafting substrates. The instrument used was a Bruker 300 MHz spectrometer. The concentration of the samples for the analysis ranged from 3–15 mg/mL and depending on the sample concentration, either 16 or 128 scans were used.

6.3.1.2 Size Exclusion Chromatography (SEC) Analysis

Analytical SEC served for the characterization of the arborescent PBG substrates of generations G0-G2 and of the copolymers. The analytical SEC system used was a Viscotek GPCmax unit with a VE 2001 GPC Solvent/Sample Module, a Viscotek double detector array with refractive index and dual-angle light scattering detectors, and two Agilent PLgel 5 µm MIXED-C and PLgel 10 µm MIXED-B organic mixed bed columns with dimensions of 7.5 mm (ID) × 300 mm (L). The system was operated at a flow rate of 0.5 mL/min at 70 ˚C, using dimethyl sulfoxide (DMSO) with LiBr (0.05 M) as the mobile phase. Data analysis was performed with the OmniSEC 4.6.1 software package.

Preparative SEC was carried out on a system consisting of a Waters M45 HPLC pump, a 2-mL sample injection loop, a Waters R401 differential refractometer detector, and a Jordi Gel DVB 1000 Å 250 mm × 22 mm preparative SEC column. *N*,*N*-Dimethylformamide (DMF) with 0.2 g/L LiCl was used as the mobile phase at a flow rate of 3 mL/min at room temperature. The concentration of polymer solution injected was 25 mg/mL.

6.3.1.3 Polymer Characterization

All the characterization techniques were previously described in Chapter 5. Briefly, light scattering measurements were performed on a Zetasizer Nano ZS90 (Malvern

Instruments) equipped with a 4 mW He–Ne laser operating at 633 nm and 25.0 ˚C, at a scattering angle of 90°. The samples were dissolved in phosphate buffered saline (PBS), DMF, or water at least 12 h before analysis.

Absorption spectra were obtained on a Cary 100 Bio UV-Vis spectrophotometer with a spectral bandwidth (SBW) of 2 nm, operated with the Cary Varian UV Scan Application (v3.001339). The absorption peak at 483 nm for doxorubicin and a molar extinction coefficient ε = 10,240 $M^{-1} \cdot cm^{-1}$ were used to calculate the doxorubicin loading in the polymer samples.

The dendritic micelles were imaged with a Philips CM10 electron microscope operated at 60 kV acceleration voltage. The feature sizes and size distributions were measured with the open source processing program ImageJ (version 1.46r).[34] Samples for the TEM measurements were prepared by the following method: One drop of solution (0.05 $mg \cdot mL^{-1}$) was cast onto a 300-mesh Formvar® carbon-coated copper TEM grid placed on filter paper and the excess solution was wicked off with filter paper. After 1 min, one drop of 2% (w/v) phosphotungstic acid was added to the grid and the excess staining solution was wicked off with filter paper. Finally, the grid was transferred onto a new piece of filter paper in a Petri dish and left to dry overnight at room temperature.

The Atomic Force Microscopy images were recorded in the tapping mode on a Nanoscope III instrument (Digital Instruments, model MMAFM-2, scan stage J). The polymer solutions were prepared at concentrations ranging from 0.01 to 0.05 $mg.mL^{-1}$. A 20 μL aliquot of solution was deposited on the mica substrate and spun at about 3000

revolutions per minute (rpm) for 60 s under ambient conditions. The images were analyzed using the Nanoscope v 1.40 software. The scan rate was typically between 0.7 and 1.2 Hz, at a scan angle of 0°, acquiring 512 samples/line.

6.3.2 Solvent and Reagent Purification

Dimethyl sulfoxide and *n*-hexylamine were purified by stirring overnight with CaH_2 and distillation under reduced pressure. *N*,*N*-Dimethylformamide serving in the polymer synthesis (DMF; Aldrich, >99%) was purified by distillation under reduced pressure. Anhydrous hydrazine was prepared by decomposition of hydrazine cyanurate using a procedure described elsewhere.[35] Ethyl acetate (Fisher, 99.9%) was distilled from $LiAlH_4$ under nitrogen. γ-Benzyl L-glutamic acid (Bz-Glu; Bachem, >99%), diethyl ether (EMD Millipore OmniSolv), HBr solution (Aldrich, 33% in acetic acid), 1-hydroxybenzotriazole (HOBt; Fluka, water content ca. 15% w/w), *N*,*N*'-diisopropylcarbodiimide (DIC; Aldrich, 99%), 1-ethyl-3-(3-dimethylaminopropyl)carbodiimide hydrochloride (EDC·HCl; Aldrich, 98%), tetrahydrofuran (THF, EMD Millipore OmniSolv), methanol (EMD Millipore OmniSolv), triphosgene (Aldrich, 98%), trifluoroacetic acid (TFA, Caledon, 99.9%), $LiAlH_4$ (Aldrich, 95%), acetic anhydride (Caledon, 97%), deuterated DMSO (DMSO-d_6, Cambridge isotopes, 99.9% D), deuterated H_2O (D_2O; Aldrich, 99.9 atom % D) and triethylamine (TEA, EMD) were used as received from the suppliers. Doxorubicin hydrochloride (DOX·HCl) was obtained from Sigma-Aldrich (USA). Dialysis bags Spectra/Por® 7 (MWCO: 3.5k Da) were purchased from Spectrum Laboratories Inc. (USA).

6.3.3 Synthesis

The synthesis of the monomer γ-benzyl L-glutamic acid *N*-carboxyanhydride (Glu-NCA), the PBG side chains, the PBG substrates, the partially deprotected arborescent poly(γ-benzyl L-glutamate) (PBG) cores of generations 0 (G0) and generation 1 (G1), linear poly(ethylene oxide), and arborescent PBG substrates of generations G1 and G2 functionalized with carboxyl groups at their chain ends was accomplished as described in Chapter 4.

6.3.3.1 Synthesis of Arborescent Poly(γ-benzyl L-glutamate)-*eg*-Poly(ethylene oxide) Copolymers (PBG-*eg*-PEO)

The procedure used for the synthesis of the chain end PEO-grafted arborescent copolymers was as described in Chapter 5, except that the reactions were carried out on a 3-fold larger scale. The synthesis of G1PBG-*eg*-PEO is described below as an example. The carboxyl chain end-functionalized arborescent G1PBG substrate (0.350 g, 0.132 mmol) and the PEO-NH_2 serving as side chains (1.210 g, 0.119 mmol) were dissolved in 15 mL of dry DMSO. The peptide coupling reagents DIC (0.103 mL, 0.670 mmol) and HOBt (0.089 g, 0.670 mmol) were then added, with TEA (0.071 mL, 0.532 mmol) as a base. The reaction was allowed to proceed for 36 h at room temperature before adding *n*-hexylamine (0.803 mL, 0.791 mmol), to deactivate residual activated carboxylic acid sites. After 3 h the product was precipitated in cold methanol and recovered by suction filtration. Unreacted PEO-NH_2 was removed from the G1PBG-*eg*-PEO crude polymer by preparative size exclusion chromatography (SEC) in DMF and the sample was recovered by

precipitation in cold diethyl ether, suction filtration, and drying under vacuum. Grafting yield = 70%, 230 mg, M_n = 790,000, M_w/M_n = 1.07 (MALLS).

6.3.3.2 Preparation of Arborescent Poly(γ-benzyl L-glutamate)-*eg*-Poly(ethylene oxide)/DOX (PBG-*eg*-PEO/DOX)

The physical entrapment of DOX into the hydrophobic core of PBG-*eg*-PEO was achieved for both generations of arborescent copolymers as follows: DOX·HCl was first neutralized with two equivalents of triethylamine (TEA) in DMSO to obtain the DOX free base (more hydrophobic) form. The arborescent copolymer (10.0 mg) was dissolved in 1.0 mL of DMSO which was stirred for 2 hours. Then 0.5 mL of DOX solution (in DMSO) at a concentration of 4.0 mg/mL was added to the polymer solution and the mixture was stirred overnight in the dark. The organic solvent and free drug were removed by dialysis (MWCO 3500) against deionized water (1 L) for 24 h (with three changes in the dialysis medium) before lyophilization in the dark to obtain the product, (PBG-*eg*-PEO/DOX).

6.3.3.3 Synthesis of Arborescent Poly(L-glutamic acid)-*eg*-Poly(ethylene oxide) Copolymers (PGA-*eg*-PEO)

The arborescent copolymers (PGA-*eg*-PEO) of generation G1 and G2 were synthesized and purified by the procedure described above, with an additional acidolysis step to deprotect the PBG core. The synthesis of G1PGA-*eg*-PEO is described below as an example. Briefly, the arborescent G1PBG-*eg*-PEO copolymer (90 mg, 0.41 mmol Bz-Glu units) was dissolved in a mixture of TFA (1.50 mL) to which 0.12 mL of 33% (w/w) HBr solution in acetic acid was added. The reaction was stirred for 3 hours at room temperature before the polymer was precipitated in diethyl ether. After drying under vacuum, the

precipitate was dialyzed against distilled water and freeze-dried, yielding a product with 100% deprotected glutamic acid moieties as a white solid. Yield = 29 mg.

6.3.3.4 Preparation of Arborescent Poly(L-glutamic acid)-*eg*-Poly(ethylene oxide)-DOX (PGA-*eg*-PEO-DOX)

The encapsulation of DOX into the hydrophilic core of PGA-*eg*-PEO via electrostatic interactions was achieved for both generations as follows: The arborescent copolymer (5.0 mg) was dissolved in 4.0 mL of deionized water and stirred for 10 min, and then the pH was adjusted to 7.4 with a few drops of 0.1 M NaOH. An aqueous solution of DOX·HCl (1.0 mL, 1 mg/mL) was added dropwise to the polymer solution and the mixture was stirred overnight in the dark. Excess drug was removed by dialysis (MWCO 3500) against deionized water (1 L) for 24 h (with three changes in the dialysis medium) before lyophilization in the dark to obtain the product, (PGA-*eg*-PEO-DOX).

6.3.3.5 Synthesis of Arborescent Poly(L-glutamate-hydrazide)-*eg*-Poly(ethylene oxide) Copolymers (PGA-*eg*-PEO-Hyd)

The benzyl ester group of the arborescent PBG-*eg*-PEO copolymers was substituted with a hydrazide (Hyd) functionality by an ester-amide exchange reaction as described previously.[36,37] For example, G1PBG-*eg*-PEO (83 mg, 0.39 mmol) was dissolved in 15 mL of anhydrous DMF, and anhydrous hydrazine (15.0 mg, 0.47 mmol) was added to the polymer solution under nitrogen atmosphere. The reaction was allowed to proceed for 24 h at 40 ˚C. The polymer was purified by dialysis against 0.25% ammonia solution for 48 h, and freeze-drying to obtain the product, G1PGA-*eg*-PEO-Hyd. The derivative G2PGA-*eg*-PEO-Hyd was synthesized by the same procedure.

In an attempt to reduce the hazards associated with preparing, handling and storing the anhydrous form of hydrazine, the benzyl ester group of the arborescent PBG-*eg*-PEO copolymers were also substituted with hydrazide (Hyd) functionalities using a hydrazine solution in THF. In this method, G1PBG-*eg*-PEO (28 mg, 0.13 mmol) was dissolved in 5 mL of anhydrous DMF, and hydrazine solution in THF (4 mL, 1.0 M) was added to the polymer solution under nitrogen atmosphere. The reaction was allowed to proceed for 6 days at 40 ˚C. The polymer was purified by dialysis against 0.25% ammonia solution for 48 h, and freeze-dried to obtain the product, G1PGA-*eg*-PEO-Hyd. While the ^{1}H NMR analysis confirmed complete disappearance of the peaks characteristic for PBG such as the benzylic methylene (2H at 4.9 ppm) and phenyl protons (5H at 7.3 ppm), FTIR analysis of the product was not attempted. Further investigation is needed to verify the lack of degradation or chain cleavage reactions under these conditions. Due to insufficient materials being available, DOX was only conjugated to the hydrazide groups of both generations of PGA-*eg*-PEO-Hyd obtained by the first method (using anhydrous hydrazine).

6.3.3.6 Synthesis of Arborescent Poly(L-glutamate-hydrazide-doxorubicin)-*eg*-Poly(ethylene oxide) Copolymers (PGA-*eg*-PEO-Hyd-DOX)

To conjugate DOX to the arborescent copolymer, G1PGA-*eg*-PEO-Hyd (20.0 mg, 3.45×10^{-3} mmol –hydrazide units) was dissolved in 3.00 mL of DMF, and an excess of DOX·HCl (4.00 mg, 6.90×10^{-3} mmol) was added. The solution was stirred at room temperature for 24 h in the dark. The product was then purified by dialysis against methanol for 24 h, dialysis against deionized water for 48 h to completely remove free DOX, and

freeze-drying to obtain the product, G1PGA-*eg*-PEO-Hyd-DOX. G2PGA-*eg*-PEO-Hyd-DOX was obtained by the same method.

6.3.3.7 Determination of the Drug Loading Content (DLC) and Drug Loading Efficiency (DLE)

For the determination of the drug loading content (DLC) and drug loading efficiency (DLE), the lyophilized DOX-loaded unimolecular micelles powder was dissolved in deionized water and the absorbance at 490 nm was measured with a UV-Vis spectrometer. The DLC and DLE were calculated according to the following equations:

$$\text{DLC} = \frac{\text{mass of drug in micelles}}{\text{mass of micelles and drug}} \times 100\% \quad (6.1)$$

$$\text{DLE} = \frac{\text{mass of drug in micelles}}{\text{total mass of drug in feed}} \times 100\% \quad (6.2)$$

6.3.3.8 *In Vitro* Release of DOX

In a typical experiment to determine the DOX release profiles, 3.0 mg of the freeze-dried DOX-loaded unimolecular micelles powder was dispersed in 1.0 mL of phosphate buffered saline (PBS) for 20 min (release medium; 10 mM phosphate, 137 mM NaCl and 2.7 mM KCl, pH 7.4 and 5.5; the pH was adjusted to by the addition of 6 M HCl) and transferred into a dialysis bag (MWCO 3500). The release experiment was initiated by placing the sealed dialysis bag into 3.0 mL of release medium at 37 ˚C with constant shaking at 100 rpm (New Brunswick Scientific Innova 4000 Incubator Shaker). At selected time intervals, all the release medium was withdrawn and the same volume of fresh

medium was added. The amount of DOX released was calculated using the molar extinction coefficient of DOX at 483 nm, ε = 10,240 $M^{-1} \cdot cm^{-1}$, and the absorbance of the DOX solution. The drug release studies were performed in triplicate for each sample.

6.4 Results and Discussion

6.4.1 Synthesis and Characterization of Arborescent Poly(γ-benzyl L-glutamate)-*eg*-Poly(ethylene oxide) Copolymers (PBG-*eg*-PEO)

Amphiphilic dendritic copolymers with distinct core and shell phases that are covalently bound have recently attracted much attention for drug delivery due to their excellent *in vivo* stability. In the current investigation, arborescent PBG substrates of generations G1 and G2 serving as cores for the construction of amphiphilic copolymers were synthesized with carboxylic acid termini using standard peptide coupling techniques as described in Chapter 5. The synthesis of the chain end-functionalized arborescent PBG substrates, and their subsequent coupling with amine-terminated PEO chains is represented in Scheme 6.1, using G1PBG-*eg*-PEO as an example. In this case, two carboxylic acid functional groups were generated at the end of each chain of the arborescent G1PBG substrate (G1PBG-*ef*-$(CO_2H)_2$) using trifluoroacetic acid (TFA) to deprotect the *tert*-butyl ester groups at the chain end, before coupling with the amine-terminated PEO chains to obtain the amphiphilic copolymers. Copolymer G2PBG-*eg*-PEO was synthesized by the same procedure.

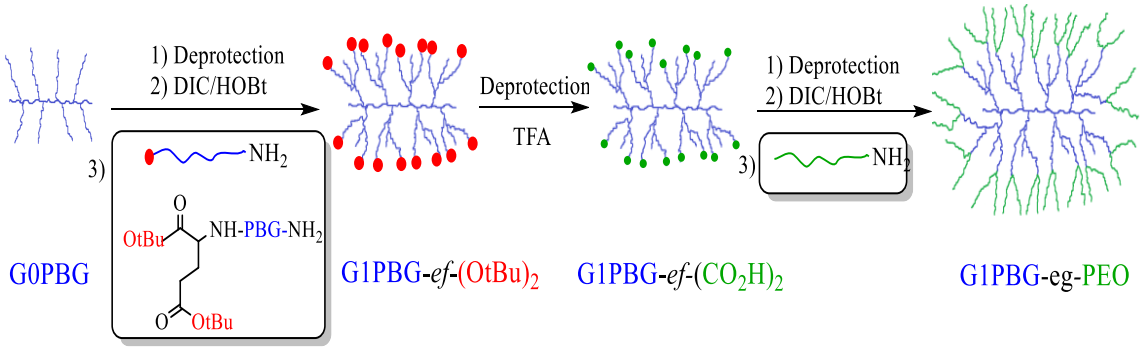

Scheme 6.1. Schematic representation of the synthesis of a chain end carboxyl-functionalized G1PBG substrate (G1PBG-*ef*-$(CO_2H)_2$) and the copolymer G1PBG-*eg*-PEO.

The synthesis of the G1PBG-*ef*-$(CO_2H)_2$ substrate was confirmed by ^{1}H NMR analysis of the purified polymers, as shown in Figure 6.1. For the G0PBG substrate (Figure 6.1a), the peaks at 7.3 and 5.0 ppm are ascribed to the protons of the benzyl and methylene groups of the PBG chains. Grafting linear PBG with two *tert*-butyl ester protecting groups at the chain ends $(tBuO)_2$-PBG onto the randomly deprotected arborescent G0PBG substrate yielded arborescent PBG with the *tert*-butyl ester protecting groups at the periphery of generation G1 molecule (G1PBG-*ef*-$(tBuO)_2$). The grafting reaction was carried out in dry DMSO at room temperature, in the presence of DIC and HOBt to activate the carboxylic groups on the G0PBG substrate. In the ^{1}H NMR spectrum of G1PBG-*ef*-$(tBuO)_2$ (Figure 6.1b), an additional peak is observed at 1.3 ppm due to the (18H) protons of the *tert*-butyl ester groups in the grafted PBG-$(tBuO)_2$ chains. This clearly confirms the formation of arborescent G1PBG-*ef*-$(tBuO)_2$. Similar spectra were obtained for the synthesis of G2PBG-*ef*-$(tBuO)_2$. Deprotection of the *tert*-butyl ester protecting groups before the

grafting reaction of PEO was likewise confirmed by ^{1}H NMR analysis, by the complete disappearance of the *tert*-butyl protons at 1.3 ppm (Figure 6.1c).

The core–shell amphiphilic arborescent PBG-*eg*-PEO copolymers were obtained by coupling amine-terminated PEO chains with the arborescent PBG core substrates (PBG-*ef*-$(CO_2H)_2$). The ^{1}H NMR spectrum obtained for copolymer G1PBG-*eg*-PEO, after complete removal of unreacted PEO-NH_2 chains, is provided in Figure 6.1d. The large peak from 3.60-3.72 ppm is assigned to the methylene protons of the PEO chains. These results indicate the successful formation of the amphiphilic arborescent PBG-*eg*-PEO copolymers with a hydrophobic dendritic PBG core and a hydrophilic PEO shell.

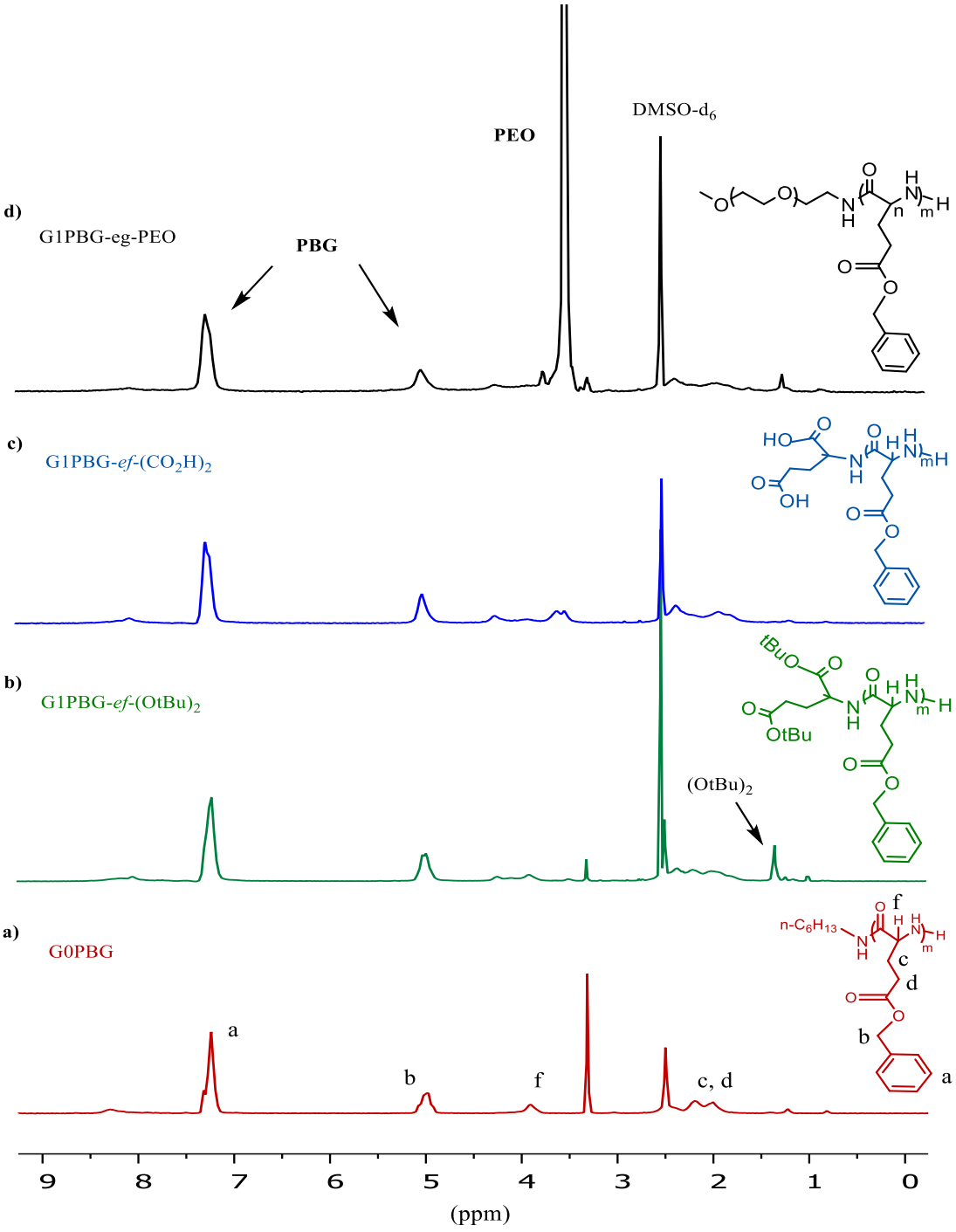

Figure 6.1. **^{1}H NMR spectra for (a) G0PBG, G1PBG-*ef*-(tBuO)$_2$ sample before (b) and after deprotection (c) of the *tert*-butyl ester protecting groups, and (d) G1PBG-*eg*-PEO in DMSO-*d*$_6$.**

The results obtained upon grafting the PBG-*ef*-$(CO_2H)_2$ substrates of generations G1 and G2 with amine-terminated PEO chains are summarized in Table 6.1. The absolute molecular weights of the substrates and the arborescent copolymers were determined by SEC-MALLS analysis in DMSO. The molecular weight of the copolymers increased relatively to the corresponding PBG substrates, while a low polydispersity index was maintained (PDI ≤ 1.08).

Table 6.1. Characteristics of chain end-grafted PBG-*eg*-PEO arborescent copolymers.

copolymer	PBG Substrate			Graft Copolymer			
	M_n (g/mol)	mol% [a] -CO_2H	G_y [b]	M_n (g/mol)	M_w/M_n	f_n [c]	%-PBG [d]
G1PBG-*eg*-PEO	220,000	8	70	790,000	1.07	57	29
G2PBG-*eg*-PEO	1.0×10^6	9	35	2.4×10^6	1.08	140	42

[a] Mole fraction of carboxyl groups in the PBG-*ef*-$(CO_2H)_2$ substrate; [b] Grafting yield: fraction of side chains attached to the substrate; [c] Branching functionality: number of branches added in the last grafting cycle; [d] PBG weight fraction from the difference in M_n of the copolymer and the substrate.

The arborescent G1PBG-*eg*-PEO and G2PBG-*eg*-PEO copolymers were expected to behave like unimolecular micelles in aqueous solutions because of their amphiphilic character and their globular topology. The hydrophilic PEO chains formed a shell stabilizing the micelles, whereas PBG constituted the hydrophobic core. The characteristics of the arborescent copolymer were evaluated by size exclusion chromatography (SEC),

dynamic light scattering (DLS), transmission electron microscopy (TEM), and atomic force microscopy (AFM) as shown in Figure 6.2 for G1PBG-*eg*-PEO, and Figure 6.3 for G2PBG-*eg*-PEO.

The hydrodynamic diameter of the arborescent copolymers is consistent with the formation of unimolecular micelles, as the number-average diameter in phosphate buffered saline (PBS) is 15 and 29 nm for the G1 and G2, respectively, and comparable to the diameter measured in DMF (14 and 27 nm for the G1 and G2 copolymers, respectively) which is a good solvent for both the PEO and PBG components. As shown in Figures 6.2 and 6.3, the micelles are uniform in size, with a single size population and similar values for the number, volume, and intensity DLS distributions, and the absence of a second (aggregated) size population even in the intensity-weighted distributions.

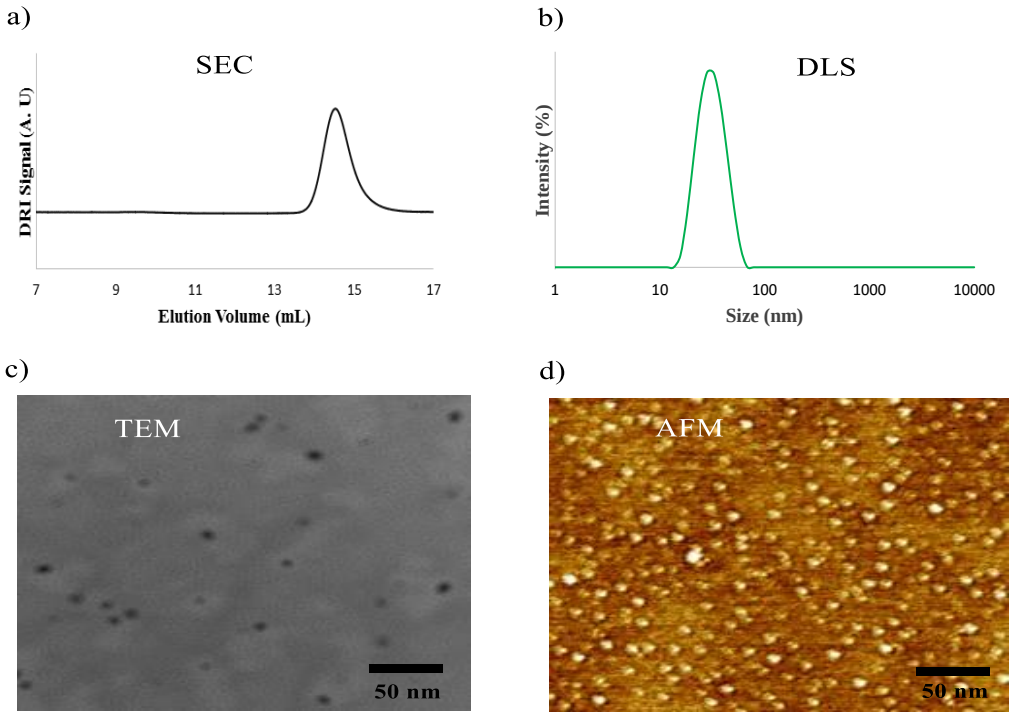

Figure 6.2. Characterization of G1PBG-*eg*-PEO: (a) SEC trace, (b) DLS intensity distributions, (c) TEM image, and AFM (d) phase scan.

The size and morphology of the unimolecular micelles were further evaluated by TEM and AFM imaging (Figure 6.2 for the G1 copolymer, Figure 6.3 for the G2 copolymer). The TEM and AFM images likewise indicated that the size distribution of the micelles was uniform, with average diameters comparable to those measured by DLS analysis (Table 6.2).

Table 6.2. The average diameters of arborescent PBG-*eg*-PEO copolymers by different techniques.

copolymer	DLS				TEM	AFM
	$D_{h,\ number}$	$D_{h,\ volume}$	$D_{h,\ intensity}$	PDI	D_h	D_h
G1PBG-eg-PEO	15 ± 2	18 ± 2	22 ± 2	0.25	13 ± 3	13 ± 2
G2PBG-eg-PEO	29 ± 2	33 ± 2	41 ± 3	0.29	22 ± 3	26 ± 3

These measurements confirmed the trends seen in the DLS measurement, such as the increase in micelle size with the generation number. The small difference in the average size determined by DLS, TEM and AFM analysis can be explained by shrinkage of the micelles during TEM and AFM sample preparation.

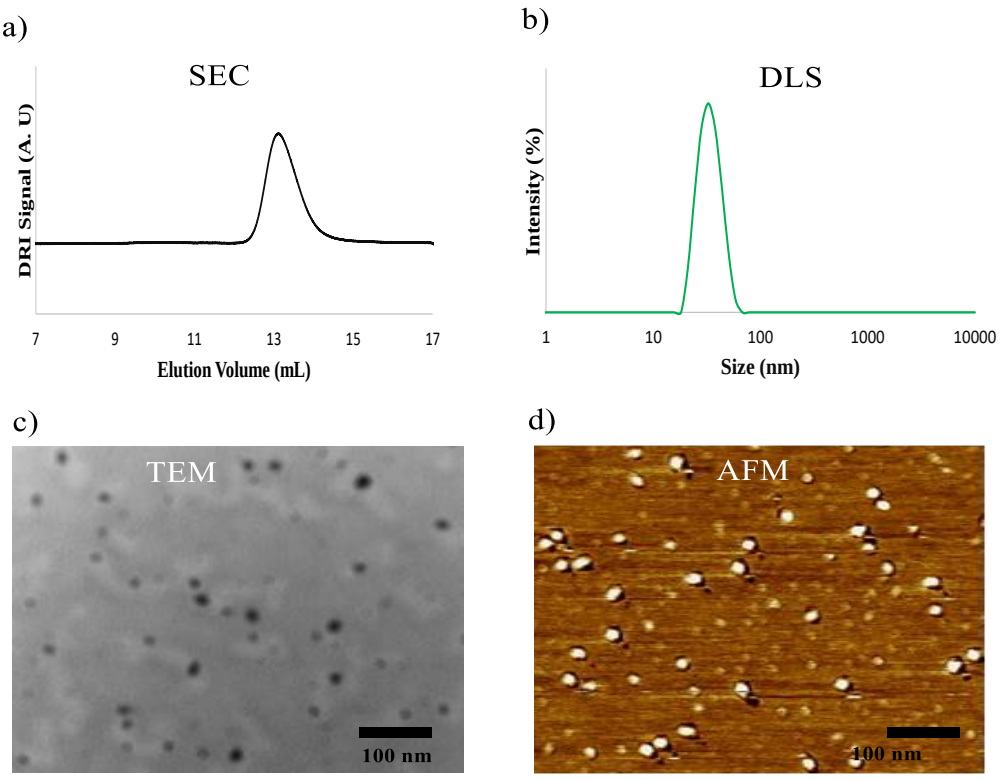

Figure 6.3. Characterization of G2PBG-*eg*-PEO: (a) SEC trace, (b) DLS intensity distributions, (c) TEM image, and AFM (d) phase scan.

Given the size range of the G1PBG-*eg*-PEO and G2PBG-*eg*-PEO micelles determined by DLS analysis, they should be suitable as nanocarriers for drug delivery through passive tumor targeting via the enhanced permeability and retention effect. The size of these micelles (diameter below 50 nm) should minimize clearance by filtration in the spleen, but should also be large enough (diameter greater than 5.0 nm) to prevent fast renal clearance. This, again, gives the unimolecular micelles a better chance of accumulation in the tumor and thus to increase their overall therapeutic efficacy.[38]

6.4.2 Encapsulation via Physical Entrapment

In contrast to dendrimer-based amphiphilic copolymers, arborescent copolymers are obtained as high molecular weight materials with a larger core, in fewer synthetic steps, which makes them very attractive as nanocarriers for drug encapsulation. The PBG segments in the arborescent core, and the PEO segments in the shell should endow arborescent copolymers with both good biocompatibility and biodegradability.[24]

The ability of these unimolecular micelles to encapsulate hydrophobic guest molecules within their hydrophobic core was investigated using doxorubicin (DOX) as a model anticancer drug. While three different encapsulation strategies were explored for DOX, simple physical entrapment via hydrophobic interactions between DOX and the PBG core was first considered. To this end, the hydrophilic doxorubicin hydrochloride (DOX·HCl) was neutralized with triethylamine (TEA) to obtain the more hydrophobic free base DOX form before encapsulation in a common solvent (DMSO) and purification by dialysis (Scheme 6.2).

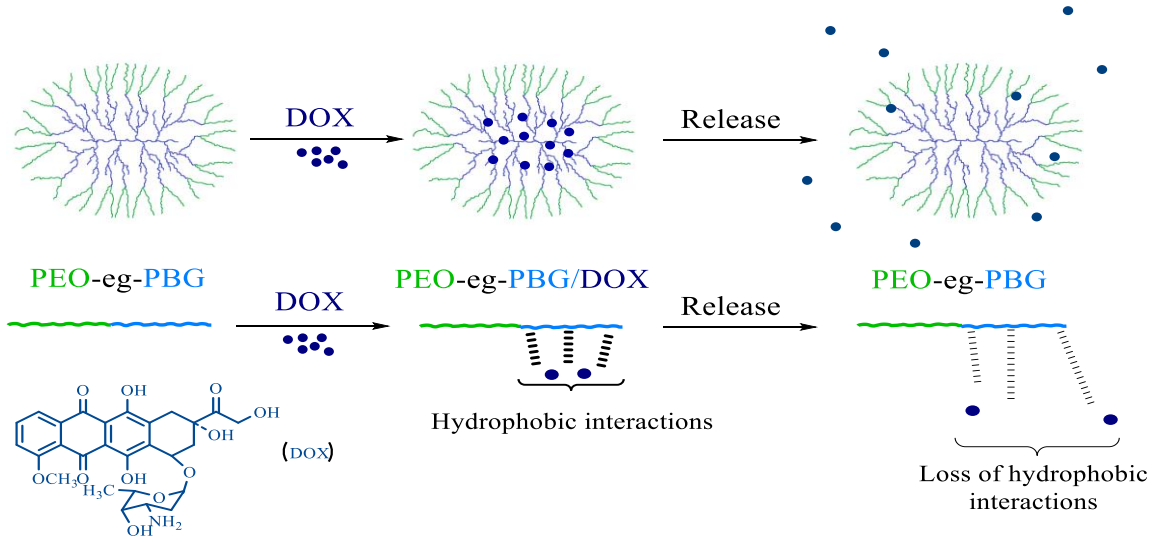

Scheme 6.2. Schematic representation of the encapsulation and release of DOX in G2PBG-*eg*-PEO/DOX through hydrophobic interactions.

UV-vis analysis confirmed that hydrophobic DOX could indeed be solubilized in the amphiphilic arborescent PBG-*eg*-PEO copolymers of both generations, as indicated by the enhanced absorption around 490 nm for the DOX-loaded micellar solutions as compared to the empty micelles (Figure 6.4). The red-orange coloration of the PBG-*eg*-PEO/DOX dispersions also provided direct visual evidence for the encapsulation of DOX into PBG-*eg*-PEO (Figure 6.4).

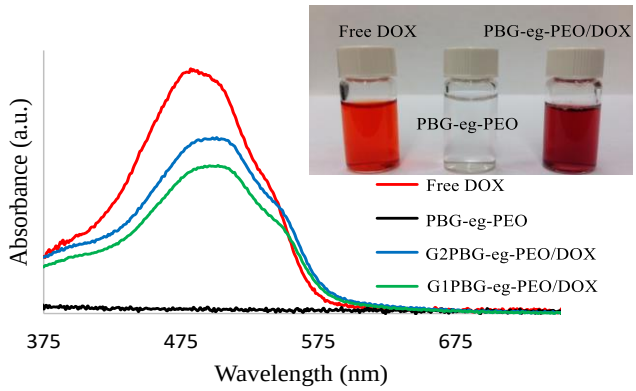

Figure 6.4. UV absorption spectra for DOX·HCl, PBG-*eg*-PEO, G1PBG-*eg*-PEO/DOX and G2PBG-*eg*-PEO/DOX in PBS. The inset shows the appearance of PBS solutions of DOX·HCl, PBG-*eg*-PEO and PBG-*eg*-PEO/DOX.

The amount of drug encapsulated into G1PBG-*eg*-PEO and G2PBG-*eg*-PEO micelles was quantified by UV-visible spectrometry (Table 6.3). Both the drug loading content (DLC) and the drug loading efficiency (DLE) were slightly higher for G2PBG-*eg*-PEO/DOX than for G1PBG-*eg*-PEO/DOX, due to the higher PBG content of G2PBG-*eg*-PEO/DOX relatively to G1PBG-*eg*-PEO/DOX.

Table 6.3. Characterization of unimolecular micelles loaded via hydrophobic interactions.

Copolymer	PBG-*eg*-PEO		PBG-*eg*-PEO/DOX			
	Size (nm)	PDI	Size (nm)	PDI	DLC (wt%)	DLE (%)
G1PBG-*eg*-PEO/DOX	15	0.22	18	0.35	7.6 ± 0.2	40 ± 3
G2PBG-*eg*-PEO/DOX	29	0.26	34	0.37	9.5 ± 0.2	47 ± 4

Data represent the mean ± standard deviation (n = 3).

The encapsulation results clearly show that the DLC and DLE increased with the PBG content of the micelles. Such a difference suggests that the hydrophobic interactions between the drug and the core of the micelles is the main driving force for physical entrapment. The size of the DOX-loaded micelles and the empty micelles in PBS is also compared in Table 6.3. The small (3-5 nm) size increase observed upon drug loading is consistent with the modest DLC of the micelles (less than 10% by weight).

6.4.3 Encapsulation via Electrostatic Interactions

The DOX-loaded arborescent copolymers, poly(L-glutamic acid)-*eg*-poly(ethylene oxide)-DOX (PGA-*eg*-PEO-DOX), of generations G1 and G2 were prepared as shown in Scheme 6.3. The G1PGA-*eg*-PEO and G2PGA-*eg*-PEO copolymers were first synthesized to allow DOX loading via electrostatic interactions between the carboxylic acid groups of the PGA segments and the amine group on DOX.

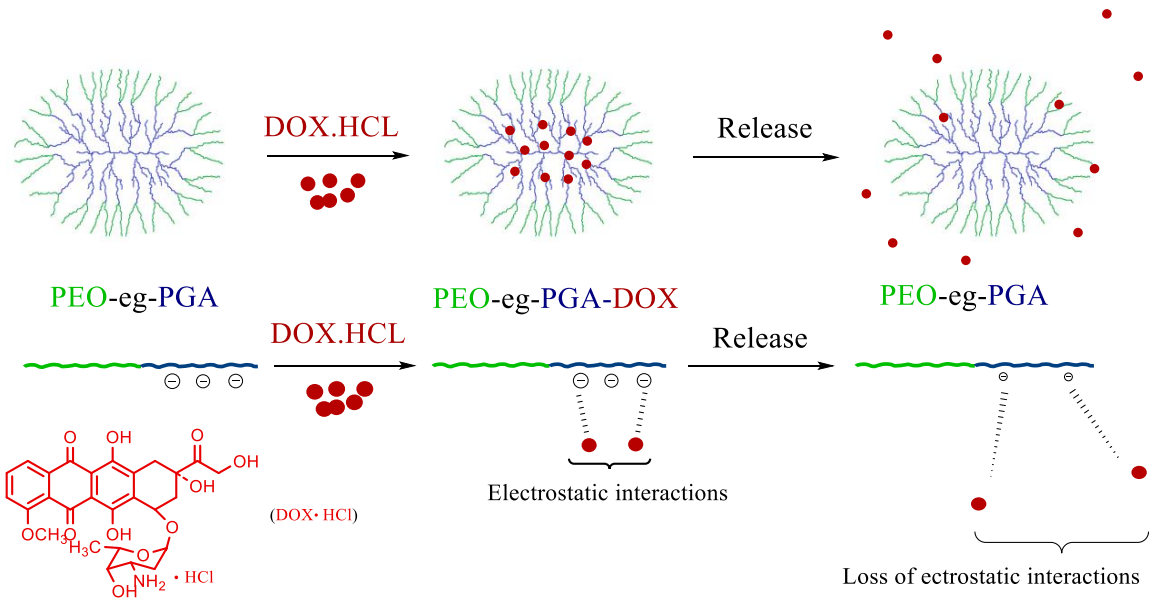

Scheme 6.3. Schematic representation of the encapsulation and release of DOX·HCl in the hydrophilic PGA core of G2PGA-*eg*-PEO via electrostatic interactions.

The arborescent G1PGA-*eg*-PEO and G2PGA-*eg*-PEO copolymers were prepared by complete deprotection of the benzyl ester groups of G1PBG-*eg*-PEO and G1PBG-*eg*-PEO, respectively, using 33% (w/w) HBr solution in acetic acid. The synthesis of arborescent G1PGA-*eg*-PEO is provided in Scheme 6.4 as an example.

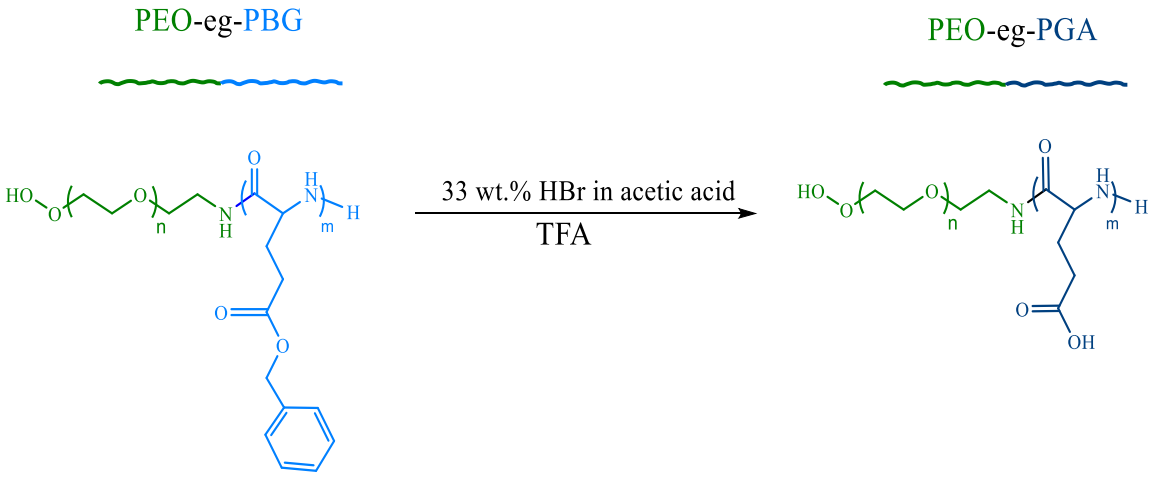

Scheme 6.4. Synthesis of arborescent G1PGA-*eg*-PEO copolymer.

^{1}H NMR spectra for copolymers G1PBG-*eg*-PEO and G1PGA-*eg*-PEO are shown in Figure 6.5. The disappearance of the benzylic methylene protons (2H at 4.9 ppm) and phenyl protons (5H at 7.3 ppm) confirms the complete deprotection of the γ-benzyl groups in the PBG core. The ^{1}H NMR spectra therefore prove that the arborescent copolymer was successfully synthesized.

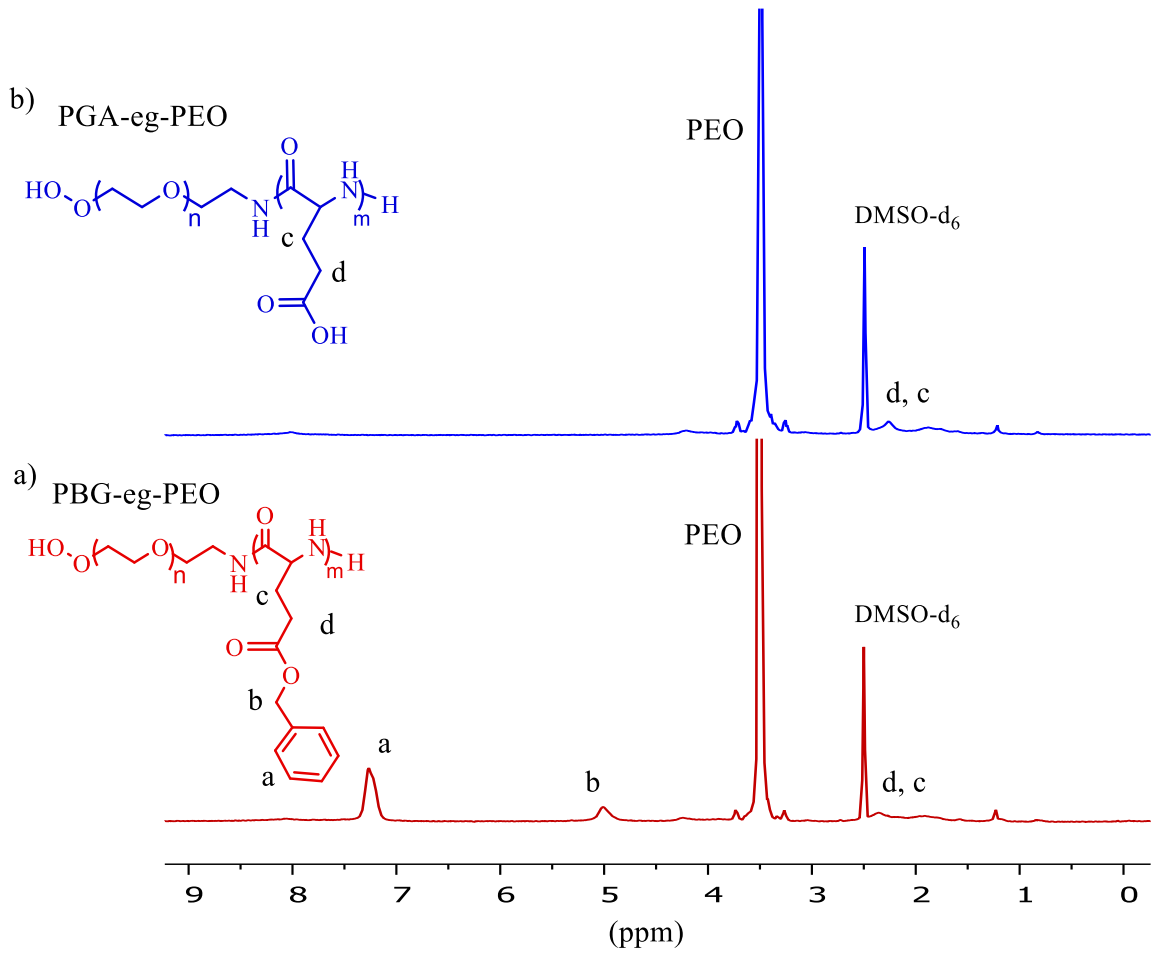

Figure 6.5. **^{1}H NMR spectra for (a) PBG-*eg*-PEO and (d) PGA-*eg*-PEO in DMSO-*d*$_6$.**

The hydrophilic doxorubicin hydrochloride (DOX·HCl), which is a weak amphipathic base (pKa = 8.2),[39] can be loaded into anionic polymers such as poly(L-glutamic acid) (PGA) through electrostatic interactions in aqueous media. The electrostatic interactions make the use of organic solvents unnecessary, which is a significant advantage when compared to the physical entrapment strategy. This is also important because organic solvents are not only toxic, but they may accelerate the decomposition of drugs.[40] Since

DOX·HCl is a weak amphipathic base, most of the amino groups in the sugar moiety are protonated under normal physiological conditions. DOX·HCl was loaded into the PGA-*eg*-PEO copolymers of both generations by first converting the carboxylic acid moieties of PGA-*eg*-PEO to carboxylates by adjusting the pH with NaOH. Aqueous solutions of the copolymer and the drug were combined and stirred overnight at a pK below the pKa of DOX, and then free drug was removed by dialysis. The encapsulation of cationic DOX within the anionic arborescent PGA core was investigated by UV-Vis spectrometry, using the maximum absorbance of free DOX at 483 nm; the empty micelles showed no significant absorption around that wavelength (Figure 6.6). After DOX was loaded the colorless PGA-*eg*-PEO solution became orange (PGA-*eg*-PEO-DOX), indicating the successful encapsulation of DOX.

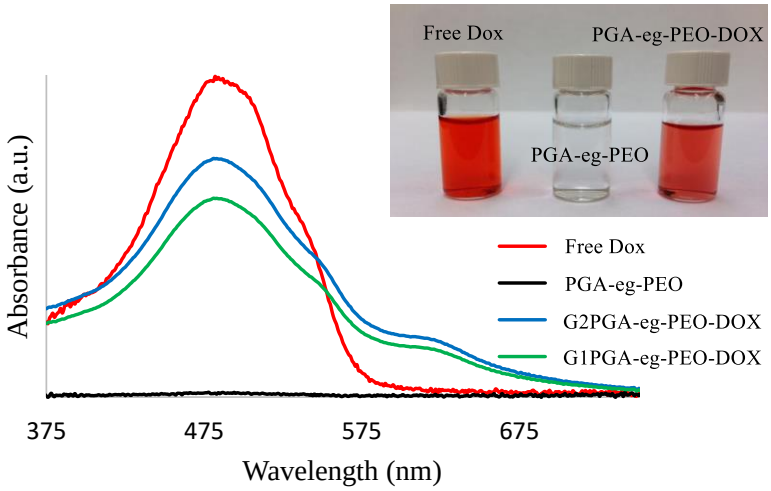

Figure 6.6. UV absorption spectra for DOX·HCl, PGA-*eg*-PEO, G1PGA-*eg*-PEO-DOX and G2PGA-*eg*-PEO-DOX in PBS. The inset shows the appearance of PBS solutions of DOX·HCl, PGA-*eg*-PEO and PGA-*eg*-PEO-DOX.

The DLC and DLE determined by spectrophotometry, listed in Table 6.4, increased with the generation number of the copolymers. Electrostatic interactions therefore allowed more DOX·HCl to be loaded into the unimolecular micelles, similarly to the physical entrapment approach examined previously. The DLC were 11 and 14 wt%, and the corresponding DLE were 66 and 83% for G1PGA-*eg*-PEO-DOX and G2PGA-*eg*-PEO-DOX, respectively. This is likely because the arborescent copolymers of the higher generation number have a higher PBG content (42% by weight) and thus a larger number of coupling sites (carboxyl groups) available for DOX·HCl to bind.

Table 6.4. Characterization of unimolecular micelles loaded via electrostatic interactions.

Copolymer	PGA-*eg*-PEO		PGA-*eg*-PEO-DOX			
	Size (nm)	PDI	Size (nm)	PDI	DLC (wt%)	DLE (%)
G1PGA-*eg*-PEO-DOX	17	0.48	16	0.29	11.2 ± 0.4	66 ± 5
G2PGA-*eg*-PEO-DOX	34	0.60	32	0.35	14.1 ± 0.3	83 ± 4

Data represent the mean ± standard deviation (n = 3).

Using the drug loading efficiency (DLE) for comparison of the physical and electrostatic entrapment strategies used to prepare the drug-loaded micelles, it is clear that a higher DLE was achieved with the second strategy. For example, G2PGA-*eg*-PEO-DOX had a DLE of 83%, while a DLE of 47% was achieved for G2PBG-*eg*-PEO/DOX.

The higher DLC and DLE achieved with the electrostatic interaction strategy is mainly attributed to ionic bonding between the cationic DOX·HCl and the carboxylic acid groups in the core of nanocarriers, although other contributions due to hydrophobic interactions or hydrogen bonding cannot be excluded. Under normal physiological conditions (pH 7.4) the carboxylic acid groups of PGA-*eg*-PEO (pKa = 5.6)[41] should be deprotonated, forming anionic carboxylates, while most of the amino groups in the sugar moiety of DOX (pKa = 8.3) should be protonated, forming cationic ammonium groups. This is the main reason for postulating that electrostatic interactions should dominate between the DOX and PGA components.

6.4.4 Encapsulation via pH-Sensitive Hydrazone Bond Conjugation

As mentioned earlier, three main strategies can be employed to load drugs into polymeric micelles: (i) physical entrapment, (ii) electrostatic interactions, and (iii) covalent conjugation. The first two strategies are simple, but are unlikely to ensure optimal control over the drug release rate because the drug is not covalently attached to the nanocarrier. The latter strategy, in contrast, provides the option of enhanced stimuli-responsive drug release, which should increase the therapeutic efficiency and reduce toxicity by ensuring drug release at a target site. Different stimuli have been considered for that purpose including sensitivity to specific enzymes, pH, temperature, and light.[42] For instance, the pH around tumor tissues tends to be lower (5.4 to 6.5) relatively to physiological pH (7.4).[43] Therefore, much attention has been paid to polymer–drug conjugates with acid-cleavable bonds such as hydrazone derivatives.[31]

In the current investigation, we also constructed pH-sensitive copolymers in which DOX was conjugated to the core of the micelles via a cleavable hydrazone bond (samples denoted as PGA-*eg*-PEO-Hyd-DOX). The influence of covalent drug conjugation on the drug loading capacity and the drug release rate was investigated and compared with the analogous PBG-*eg*-PEO/DOX and PGA-*eg*-PEO-DOX systems. A schematic illustration of the formation of pH-sensitive micelles is presented in Scheme 6.5.

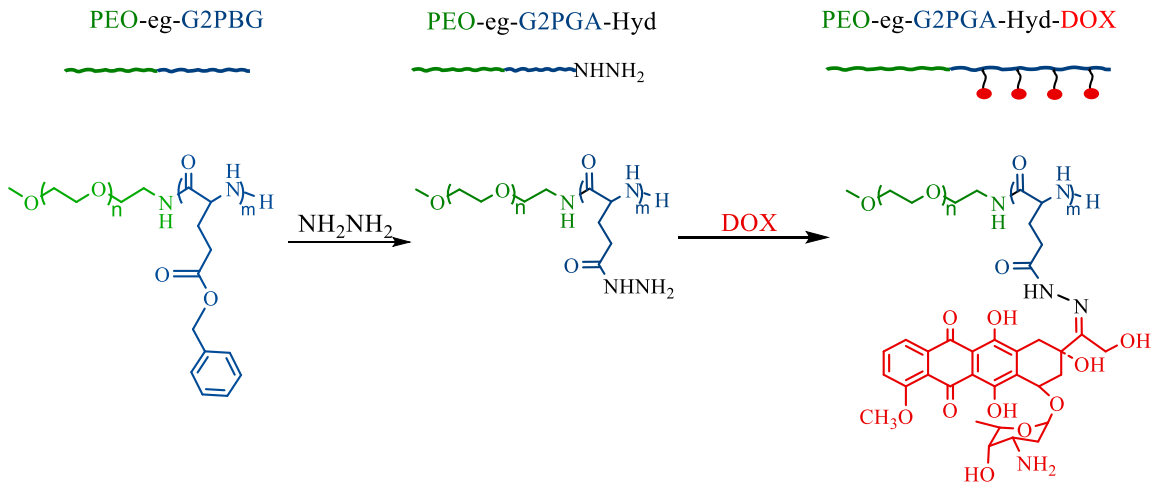

Scheme 6.5. Formation of pH-sensitive PGA-*eg*-PEO-Hyd-DOX micelles.

As shown in Scheme 6.5, the benzyl groups of PBG-*eg*-PEO were substituted with hydrazide groups by an ester-amide exchange aminolysis reaction to obtain PGA-*eg*-PEO-Hyd. The DOX was then conjugated to the hydrazide groups of PGA-*eg*-PEO-Hyd to obtain the final product, PGA-*eg*-PEO-Hyd-DOX.[36,37]

The PBG-*eg*-PEO, PGA-*eg*-PEO-Hyd and PGA-*eg*-PEO-Hyd-DOX arborescent copolymers were characterized by ^{1}H NMR spectroscopy as shown in Figure 6.7. As

observed for PGA-*eg*-PEO-Hyd (Figure 6.7b), the disappearance of the benzylic methylene protons (2H at 4.9 ppm) and phenyl protons (5H at 7.3 ppm) confirms that the benzyl esters residues were replaced completely with hydrazide groups. A new signal (2H at 4.4 ppm) corresponds to the amino protons in the hydrazide group, further confirming the successful synthesis of PGA-*eg*-PEO-Hyd. In addition to the peaks characteristic for PEO, the conjugation of DOX onto PGA-*eg*-PEO-Hyd was confirmed by the appearance of aromatic protons for DOX at 7.95 and 7.69 ppm, and its methyl groups at 1.16 and at 4.00 ppm. The disappearance of the hydrazide protons of PGA-*eg*-PEO-Hyd (2H at 4.4 ppm) in the spectrum of the final product (Figure 6.7c) also indicates the depletion of hydrazide groups during the conjugation process.

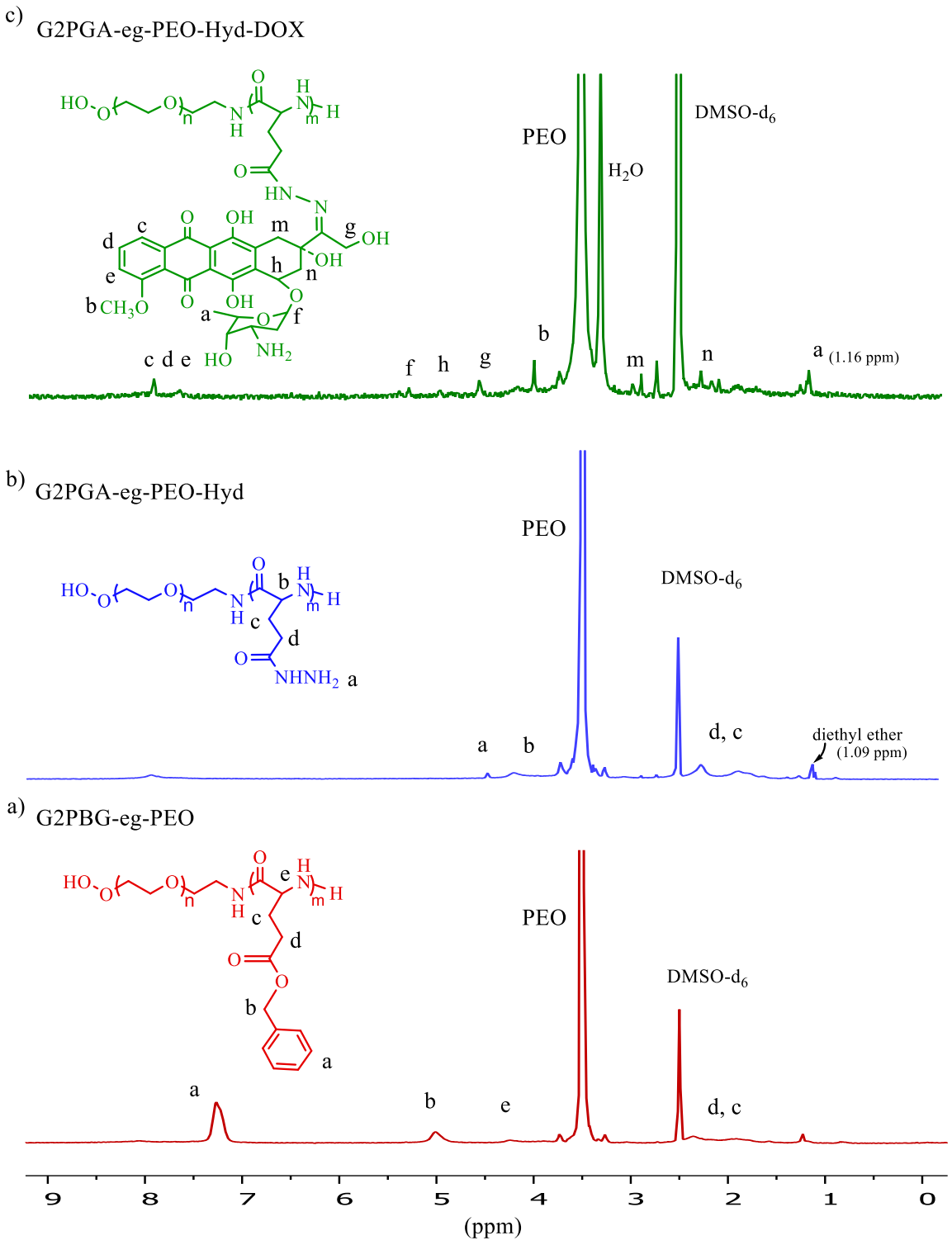

Figure 6.7. ^{1}H NMR spectra for (a) PBG-*eg*-PEO, (b) PGA-*eg*-PEO-Hyd and (c) PGA-*eg*-PEO-Hyd-DOX in DMSO-*d*$_6$.

This result was further verified by comparing the FTIR spectra for the PBG-*eg*-PEO and PGA-*eg*-PEO-Hyd arborescent copolymers before and after reaction with hydrazine and DOX, respectively (Figure 6.8). After the reaction with hydrazine a new peak, attributed to the stretching vibrations of amino (NH_2) groups, was detected around 1465 cm^{-1} (Figure 6.8c). The disappearance of the ester C=O stretch vibration (1735 cm^{-1}) also indicated the complete removal of the benzyl ester groups in the PBG core and the conjugation of the hydrazide (Figure 6.8b). The disappearance in Figure 6.8d of the peak at 1730 cm^{-1} for the carbonyl stretching of free DOX (Figure 6.8a) is also consistent with the formation of a hydrazone bond between the ketone and hydrazine (PGA-*eg*-PEO-Hyd-DOX). Finally the intensity of the peak at 1465 cm^{-1} decreased, which suggests partial consumption of NH_2 in the formation of hydrazone bonds. These results clearly confirm the successful covalent conjugation of DOX to the core of the micelles via a hydrazone bond.

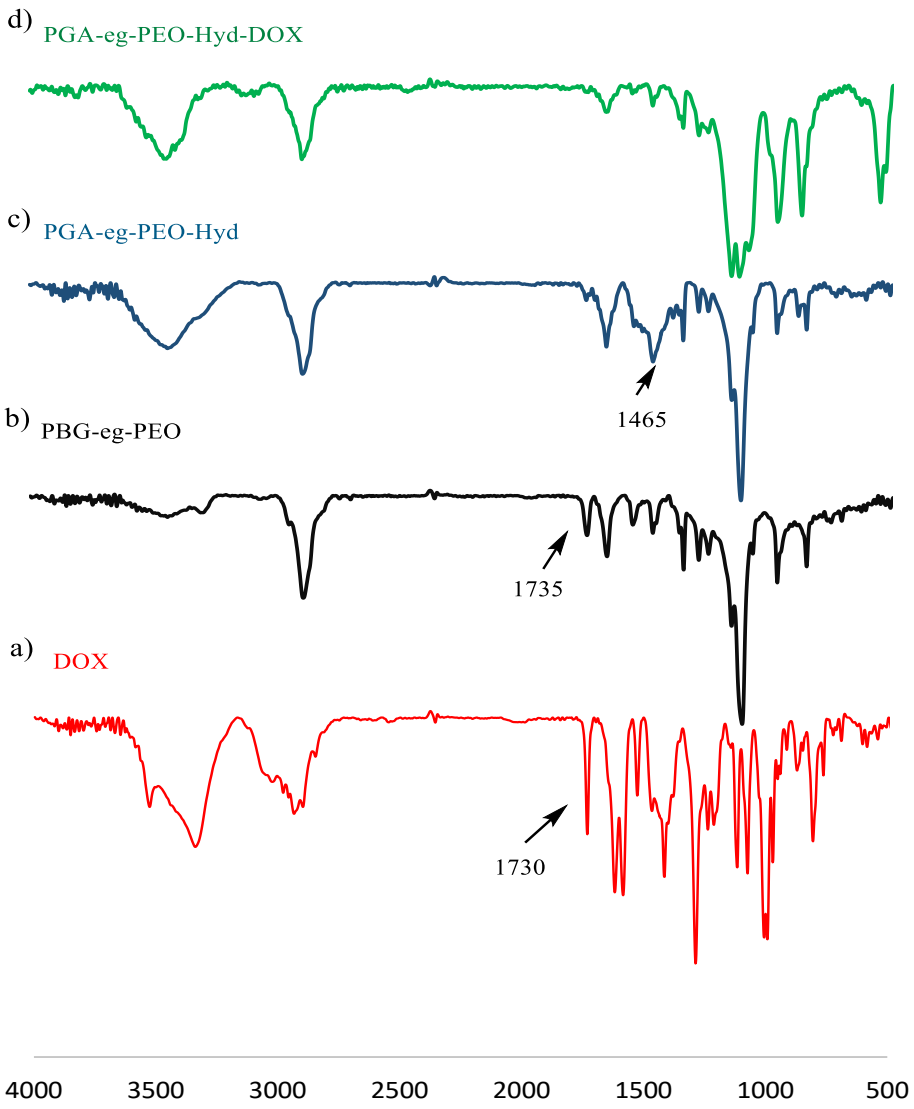

Figure 6.8. FT-IR spectra for (a) free DOX, (b) PBG-*eg*-PEO, (c) PGA-*eg*-PEO-Hyd and (d) PGA-*eg*-PEO-Hyd-DOX.

The UV-vis absorption spectra for DOX·HCl, PGA-*eg*-PEO-Hyd, and PGA-*eg*-PEO-Hyd-DOX of both generations are compared in Figure 6.9. Successful conjugation is indicated by the enhanced absorption around 490 nm of the DOX-loaded micellar solutions (G1PGA-*eg*-PEO-Hyd-DOX and G2PGA-*eg*-PEO-Hyd-DOX) as compared to the empty

micelles PGA-*eg*-PEO-Hyd. As before, the PGA-*eg*-PEO-Hyd solutions were colorless but became red-orange after DOX conjugation (PGA-*eg*-PEO-Hyd-DOX), as seen in the inset of Figure 6.9.

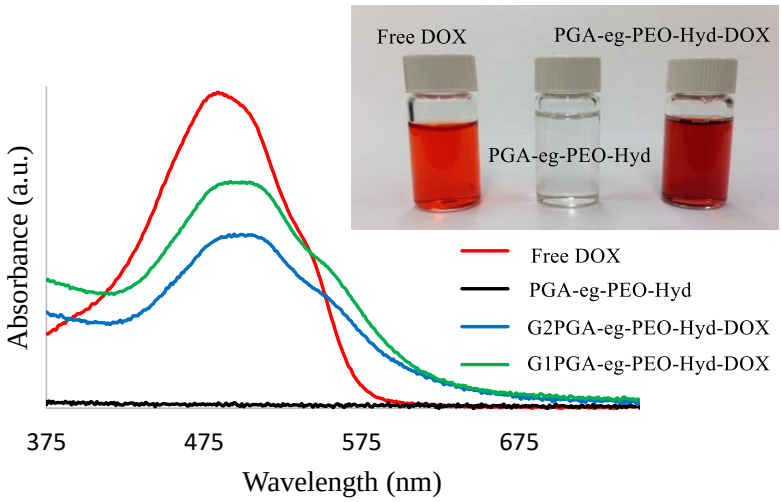

Figure 6.9. UV absorption spectra for DOX·HCl, PGA-*eg*-PEO-Hyd, G1PGA-*eg*-PEO-Hyd-DOX and G2PGA-*eg*-PEO-Hyd-DOX in PBS. The inset shows the appearance of PBS solutions of DOX·HCl, PGA-*eg*-PEO-Hyd and PGA-*eg*-PEO-Hyd-DOX.

The amount of drug covalently conjugated to the G1PGA-*eg*-PEO-Hyd and G2PGA-*eg*-PEO-Hyd micelles was determined by UV-Visible spectrometry (Table 6.5). The DLC were determined to be 7.7 and 10.3 wt%, and the corresponding DLE were 46 and 62% for G1PGA-*eg*-PEO-Hyd-DOX and G2PGA-*eg*-PEO-Hyd-DOX, respectively. Similarly to the two previous systems, G2PGA-*eg*-PEO-Hyd-DOX had higher values of DLC and DLE as compared to G1PGA-*eg*-PEO-Hyd-DOX. This is due to the higher PBG content (42%

by weight) and therefore, a large number of coupling sites (hydrazide groups) available for conjugation on the relatively larger G2PGA-*eg*-PEO-Hyd-DOX micelle.

Table 6.5. Characterization of unimolecular micelles loaded via pH-sensitive hydrazone bond conjugation.

Copolymer	PBG-*eg*-PEO		PGA-*eg*-PEO-Hyd-DOX			
	Size (nm)	PDI	Size (nm)	PDI	DLC (wt%)	DLE (%)
G1PGA-*eg*-PEO-Hyd-DOX	15	0.22	17	0.38	7.7 ± 0.4	46 ± 5
G2PGA-*eg*-PEO-Hyd-DOX	29	0.26	35	0.34	10.0 ± 0.3	62 ± 4

Data represent the mean ± standard deviation (n = 3).

6.4.5 *In Vitro* Drug Release Study

To demonstrate the influence of DOX encapsulation via electrostatic interactions (PGA-*eg*-PEO-DOX), covalent conjugation (PGA-*eg*-PEO-Hyd-DOX) and physical entrapment (PBG-*eg*-PEO/DOX) on the drug release rate from the unimolecular micelles, an *in vitro* drug release study was conducted by dialysis at 37 ˚C. The drug release profile was assessed under both simulated physiological conditions (PBS, pH 7.4) and acidic conditions (PBS, pH 5.5), corresponding to the endosomal and lysosomal microenvironments, respectively. For all the systems investigated, the DOX release rate was affected by the pH, with slower DOX release at pH 7.4. For G1PBG-*eg*-PEO/DOX and G2PBG-*eg*-PEO/DOX (Figure 6.10a), the total release after 50 h reached 30 and 17.5 %, respectively, as compared with 48 and 26% at pH 5.5. As before, the faster release at

pH 5.5 is attributed to the protonation of DOX in the acidic environment increasing its aqueous solubility.[44,45] While G2PBG-*eg*-PEO/DOX had a higher DLC and DLE than G1PBG-*eg*-PEO/DOX, the release rate of DOX at both pH was much slower for G2PBG-*eg*-PEO/DOX as compared to G1PBG-*eg*-PEO/DOX. This is attributed to the larger hydrodynamic diameter of G2PBG-*eg*-PEO/DOX relatively to G1PBG-*eg*-PEO/DOX, increasing the diffusion path for drug release, and thus reducing the drug release rate. Another parameter that might influence the release rate of the drug is the PBG content for the arborescent copolymers. As pointed out in Table 6.1, the PBG content increased with generation number. The micelles with a higher PBG content (G2PBG-eg-PEO/DOX, 42% by weight) exhibited slower release rate, while those with a lower PBG content (G1PBG-eg-PEO/DOX, 29% by weight) exhibited the faster DOX release rate.

In an attempt to achieve better control over the DOX release rate, the PGA-*eg*-PEO-DOX samples were prepared in which DOX was loaded via electrostatic interactions. The *in vitro* drug release profiles for both generations of PGA-*eg*-PEO-DOX in PBS at different pH at 37 ˚C are compared in Figure 6.10b. The total amount of drug released after 50 h at pH 7.4 reached 13 and 27 % for G1PGA-*eg*-PEO-DOX and G2PGA-*eg*-PEO-DOX, respectively, as compared with 56 and 38% at pH 5.5. As discussed earlier, since electrostatic interactions exist between DOX and the carboxylic acid groups of the copolymers at pH 7.4, the release rate should be decreased. However at pH 5.5 most of the carboxyl groups should be protonated, which would weaken the electrostatic interactions between PGA-*eg*-PEO and DOX, and thereby accelerate drug release.

The release rate of DOX from PGA-*eg*-PEO-DOX was clearly influenced by pH for both generations, but G1PGA-*eg*-PEO-DOX displayed better defined pH-responsive behavior as compared to G2PGA-*eg*-PEO-DOX. For example, approximately four times the amount of loaded DOX was released from G1PGA-*eg*-PEO-DOX after 50 h at pH 5.5 in comparison to pH 7.4, while only a small incremental amount of DOX was released from G2PGA-*eg*-PEO-DOX at pH 5.5 vs. pH 7.4. The relatively low pH responsiveness of G2PGA-*eg*-PEO-DOX is attributed to the larger size of its hydrophobic core. DOX bonded to the core of the micelles via electrostatic interactions should be nevertheless more sensitive to changes in pH. Such electrostatic interactions will be weakened under acidic conditions, and thus increase the DOX release rate. This also explains why the difference in release rate of DOX from G1PGA-*eg*-PEO-DOX is larger at the different pH as compared to G2PGA-*eg*-PEO-DOX.

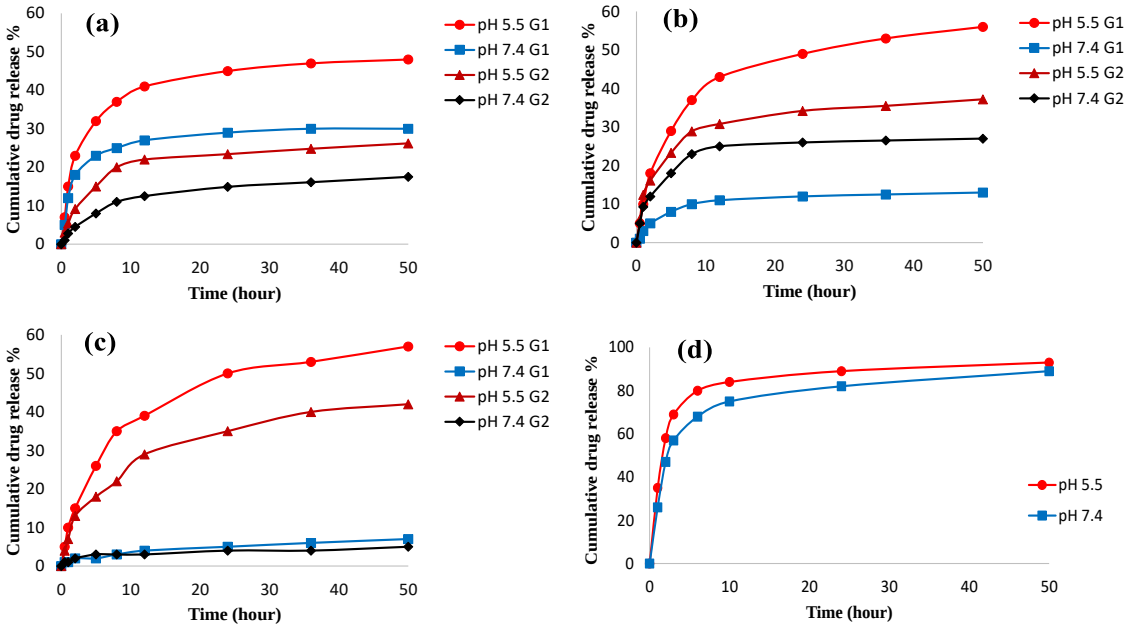

Figure 6.10. ***In vitro*** **DOX release profiles from (a) PBG-*eg*-PEO/DOX, (b) PGA-*eg*-PEO-DOX, (c) PGA-*eg*-PEO-Hyd-DOX micelles, and (d) free DOX in PBS (pH 7.4 and 5.5) at 37 ˚C.**

To combine the sustained release characteristics of the above two systems and reduce the occurrence of burst (premature) DOX release, pH-sensitive arborescent copolymers (PGA-*eg*-PEO-Hyd-DOX), in which the DOX was covalently conjugated to the core of the micelles via a cleavable hydrazone bond, were also synthesized. Since the hydrazone linkage between DOX and the copolymers is subject to hydrolysis under acidic conditions, the DOX release rate should increase in acidic environments (e.g. the tumor extracellular environment) and may provide a system with better pH-responsive behavior. The results indeed clearly show that both generations of PGA-*eg*-PEO-Hyd-DOX were very stable at pH 7.4, but exhibited much faster DOX release at pH 5.5. At pH 7.4 after 50 h, for example,

only 7 and 5% of the total drug was released from G1PGA-*eg*-PEO-Hyd-DOX and G2PGA-*eg*-PEO-Hyd-DOX, respectively, as compared with 57 and 42% at pH 5.5. This suggests that the hydrazone linkage would remain stable in the bloodstream and thereby eliminate burst drug release, while controlling the DOX release rate from PGA-*eg*-PEO-Hyd-DOX once exposed to the acidic environment of the endosomal intracellular compartments (Figure 6.10c). Furthermore, similarly to the PBG-*eg*-PEO/DOX systems, the release rate of DOX from PGA-*eg*-PEO-Hyd-DOX at pH 5.5 decreased for the G2 copolymer, while the release rate of DOX from PGA-*eg*-PEO-Hyd-DOX at pH 7.4 remained relatively unaffected. This pH-dependent release behavior is highly desirable for drug delivery applications, as it should greatly increase the efficacy of cancer therapy while minimizing undesirable side effects. For comparison, the release profiles for free DOX are also presented (Figure 6.10d). Sustained release was observed for all the DOX-loaded micelles, in contrast to the sharp burst release seen for free DOX in the absence of the copolymers.

6.5 Conclusions

Amphiphilic arborescent copolymers of generations G1 and G2 with poly(γ-benzyl L-glutamate) (PBG) in the core and poly(ethylene oxide) (PEO) chain segments in the shell were synthesized and evaluated as nanocarriers for drug delivery applications. The copolymers were characterized using ^{1}H NMR, DLS, SEC-MALLS, TEM and AFM measurements. These results demonstrated that these copolymers formed exclusively stable, non-aggregated (unimolecular) micelles. The size distribution of these micelles was

narrow, with average diameters of ca. 15 and 29 nm for G1PBG-*eg*-PEO and G2PBG-*eg*-PEO, respectively.

Three different strategies were used to load DOX into these unimolecular micelles. The hydrophobic form of DOX was physically entrapped within the core of the micelles to obtain G1PBG-*eg*-PEO/DOX and G2PBG-*eg*-PEO/DOX, with a DLE of 40 and 47%, respectively. Physical entrapment was easy to achieve, but the DOX release profiles showed an initial burst which is undesirable for controlled release. In the second strategy, DOX·HCl was loaded into the hydrophilic G1PGA-*eg*-PEO and G2PGA-*eg*-PEO copolymers via electrostatic interactions between the cationic DOX and the anionic nanocarriers to obtain G1PGA-*eg*-PEO-DOX and G2PGA-*eg*-PEO-DOX, with a DLE of up to 66 and 83%, respectively. This strategy yielded the highest drug loading capacity for both generations. The use of electrostatic interactions also avoided the use of organic solvents, which is a significant advantage when compared to physical entrapment. The release rate of DOX from PGA-*eg*-PEO-DOX was clearly influenced by pH for both generations, but G1PGA-*eg*-PEO-DOX showed better-defined pH-responsive behavior as compared to G2PGA-*eg*-PEO-DOX. Finally, to further reduce initial burst (premature) DOX release, the DOX was covalently conjugated to the core of G1PBG-*eg*-PEO and G2PBG-*eg*-PEO via an acid-cleavable hydrazone bond to obtain G1PGA-*eg*-PEO-DOX and G2PGA-*eg*-PEO-DOX, with a DLE of 46 and 62%, respectively. The conjugated system had an intermediate drug loading capacity as compared to the other systems, but displayed the best pH-sensitive release profile. The PGA-*eg*-PEO-Hyd-DOX system therefore has obvious advantages over the other two systems, namely enhanced pH-

sensitivity and sustained drug release behavior. This sustained and pH-sensitive release behavior is very promising for drug delivery applications, as it would facilitate maintaining an adequate drug concentration for longer times and thus improve patient compliance, while the pH-sensitive release behavior should minimize undesirable side effects and increase the efficacy of cancer therapy.

Chapter 7 Concluding Remarks and Suggestions for Future Work

7.1 Original Contributions to Knowledge

The main goals of this Ph.D. research work were to synthesize amphiphilic arborescent copolymers designed to serve as nanocarriers for drug delivery applications, to study their aqueous solution behavior, and for the first time, to investigate the ability of these biocompatible copolymers to encapsulate and control the release rate of a hydrophobic drug (doxorubicin) in aqueous media. Previously, Whitton and Gauthier reported the use of linear poly(ethylene oxide) with a molecular weight of 5000 (PEG_{110}), grafted either randomly or at the end of the chains on arborescent PBG substrates, to generate arborescent copolymer micelles. Unfortunately, the randomly grafted arborescent G1PBG-*g*-PEO_{110} copolymers obtained by that approach yielded large aggregated species in phosphate buffered saline (PBS), while G2PBG-*g*-PEO_{110} and G3PBG-*g*-PEO_{110} were both insoluble. The corresponding end-grafted samples PBG-*eg*-PEO_{110} displayed better dispersibility in PBS than the randomly grafted systems, albeit a small population of aggregates still existed in these samples. In the current investigation, we expanded this approach by designing amphiphilic arborescent copolymers having poly(ethylene oxide) (PEO) chain segments with M_n = 10,100 g/mol grafted onto arborescent PBG substrates of generations G1 and G2 with different G0PBG branching densities, to determine their influence on the dispersibility of the micelles in organic and aqueous environments, and on the encapsulation and release of a hydrophobic drug, doxorubicin. The poly(γ-benzyl L-glutamate) building blocks were generated by ring-opening polymerization of γ-benzyl L-glutamic acid *N*-carboxyanhydride (Glu-NCA) initiated with *n*-hexylamine. Partial or full deprotection of the benzyl ester groups followed by coupling with PBG chains yielded a

comb-branched (arborescent polymer generation zero or G0) PBG structure. Additional cycles of deprotection and grafting yielded G1 and G2 arborescent polypeptides. It was demonstrated that the efficiency of the polypeptide coupling reactions used to synthesize arborescent polypeptides could be optimized beyond the conditions previously used by varying the solvent, temperature, reaction time, and reactant stoichiometry used. Utilizing the optimized reaction conditions, namely reactions carried out in DMSO at 25 ˚C for at least 36 h, using a 1.1:1 ratio of CO_2H:NH_2 and 5:1 molar ratio of coupling agents (DIC/HOBt) to CO_2H groups on the substrate, well-defined (PDI < 1.04) G0 arborescent or comb-branched polypeptides were obtained with a grafting yield and coupling efficiency reaching 67% and 74%, respectively. These optimized reaction conditions were also used to synthesize arborescent PBG of the upper generations (G1–G2).

Two classes of amphiphilic arborescent copolymers, namely randomly grafted arborescent poly(γ-benzyl L-glutamate)-*g*-poly(ethylene oxide) (PBG-*g*-PEO) and chain end-grafted arborescent poly(γ-benzyl L-glutamate)-*eg*-poly(ethylene oxide) (PBG-*eg*-PEO) were then synthesized. For each series of compounds, the influence of the generation number and the branching density of the G0PBG substrate on unimolecular micelle properties such as the drug loading capacity and the release kinetics was investigated. Consequently, for each system, three G0PBG cores with different branching densities varying from a compact and dense to a loose and more porous structure were synthesized as the molecular weight of the linear substrate was varied. All the amphiphilic arborescent copolymers provided opportunities to tailor their dimensions, from 13 to 39 nm, by the generation number and the branching density of the G0PBG cores. The size distribution of

these unimolecular micelles was found to be quite uniform. The aqueous solution behavior for all PBG-*g*-PEO revealed that these amphiphilic copolymers behave like unimolecular micelles in many cases, whereas all PBG-*eg*-PEO formed spontaneously stable unimolecular micelles with insignificant amounts of aggregation, if any. An encapsulation study demonstrated that these well-defined, biocompatible copolymers could efficiently physically encapsulate the hydrophobic (free base) form of DOX. Sustained, pH-responsive release of the encapsulated drug was observed.

The ability of these unimolecular micelles to encapsulate and release DOX correlated with the generation number of the copolymers and the branching density of the hydrophobic cores in each system. Both the drug loading content (DLC) and the drug loading efficiency (DLE) increased with the generation number of the copolymers as a result of increasing the PBG content in the micelles. For each generation, slightly higher values of DLC and DLE were obtained for the micelles with a denser core structure. Both the DLE and DLC decreased slightly as the grafting density of the cores decreased. The release profiles indicated that the drug release rate could be modulated through the generation number of the copolymers as well as by controlling the grafting density, and thereby the porosity of the cores. Increasing the hydrodynamic diameter of the copolymers, by increasing the generation number, increased the diffusion path for drug release, and thus reduced the drug release rate. In addition, micelles with highly branched cores reduced the diffusion rate of the drug, while a lower branching density facilitated the diffusion process. All the DOX-loaded unimolecular micelles clearly showed biphasic DOX release patterns at both pH investigated (5.5 and 7.4), characterized by an initial burst release followed by

slow and sustained release of the drug. The results obtained demonstrate important advantages of the end-grafted arborescent copolymers relatively to randomly grafted arborescent copolymers as nanocarriers for drug delivery applications: The end-grafted copolymers exhibited better drug release profiles and a similar drug loading capacity for hydrophobic DOX, even though the hydrodynamic diameter of these copolymers was smaller than their randomly grafted analogues.

Furthermore, three different strategies were examined to load DOX into G1PBG-*eg*-PEO and G2PBG-*eg*-PEO. The DOX was either physically entrapped (PBG-*eg*-PEO/DOX), loaded via electrostatic interactions (PGA-*eg*-PEO-DOX) or covalently conjugated to the unimolecular micelles via pH-sensitive hydrazone bond (PGA-*eg*-PEO-Hyd-DOX). While physical entrapment was easy to achieve, the DOX release profiles showed an initial burst release which is not ideal for controlled release applications. All the systems showed a good drug loading capacity, but encapsulation via electrostatic interactions showed the highest DLC and DLE for both generations. In addition, the use of electrostatic interactions in this procedure avoided the use of organic solvents, which is a significant advantage when compared to physical entrapment. All these systems exhibited sustained and pH-sensitive drug release behavior, that is, the drug release rate was slow at physiological pH (7.4) but increased at pH 5.5. The conjugated system PGA-*eg*-PEO-Hyd-DOX had an intermediate drug loading capacity as compared to the other systems, but it displayed the best pH-sensitive release profile of DOX for both generations of PGA-*eg*-PEO-Hyd-DOX arborescent copolymers investigated. Therefore the PGA-*eg*-PEO-Hyd-

DOX system appears to have obvious advantages over the other two systems, that is, enhanced pH-sensitivity and a sustained drug release behavior.

7.2 Suggestions for Future Work

The work presented in this Thesis is the first investigation to examine the ability of the biocompatible arborescent PBG-*g*-PEO and PBG-*eg*-PEO copolymers as nanocarriers to encapsulate and control the release rate of doxorubicin (DOX) as model drugs. While these unimolecular micelles have already showed controlled and sustained drug release rates, it would certainly be interesting to evaluate the cytotoxicity and cellular uptake of these systems both *in vitro* and *in vivo*.

7.2.1 Cytotoxicity and Cellular Uptake

The characteristics of arborescent copolymers such as the size, branching density, and porosity can be tailored via systematic variations in the side chains length, substrate length, and branching functionality, leading to an extremely versatile range of nanostructures. These different structures can affect the manner in which these materials interact with biological environments (uptake processes), and ultimately determine their potential for cytotoxicity. The size and shape of nanocarriers are key parameters that dominate their properties, and hence they may also affect cellular uptake and toxicity. It is indeed known that the shape of nanocarriers can influence their circulation time, uptake and intracellular interactions.[1,2] For example, worm-like nanoparticles have been shown to circulate for a prolonged duration after injection in mice as compared to their spherical counterparts.[2] In

contrast, spherical gold nanoparticles displayed higher cellular uptake than the rod-shaped particles in vitro.[3] The size of the nanocarriers is another factor that significantly influences uptake processes. For example, the uptake of gold nanoparticles in HeLa cells varied with their size.[4] Therefore, understanding the relation between cellular uptake and toxicity of the arborescent nanocarriers in biological systems would represent a big step in designing nanocarriers that are efficient but also have minimal toxicity for biomedical applications.

7.2.2 Active Targeting Strategies for Enhanced Treatment Selectivity

In the current research, we designed the nanocarriers to take advantage of the so-called 'passive targeting strategy'. In this strategy, the drug-loaded nanocarriers can passively accumulate in tumors through the enhanced permeability and retention (EPR) effect.[5,6] The nanocarriers are large enough to escape premature elimination in the kidneys *via* glomerular filtration, but small enough to participate in the EPR effect to passively accumulate in tumor tissues.[7] Blood vessels surrounding tumor tissues are leaky in comparison to normal blood vessels, and thus drug-loaded nanocarriers can effectively travel across the fenestrations to reach tumor tissues and accumulate in them, thereby exerting their therapeutic effect as the drug is being released. In contrast, free small drugs will diffuse non-specifically to most tissues. Due to passive targeting of drug-loaded nanocarriers to tumor tissues, the undesirable side-effects of the drugs will be minimized as normal cells will be less affected. However, these nanoparticles do not interact with cancer cells directly and sometimes have a limited tumor penetration ability. By contrast, an 'active targeting strategy' can be achieved by introducing on the nanocarriers ligands such as antibodies, peptides, or aptamers to interact with overexpressed receptors on the

tumor cells, which enables the systems to specifically target tumor sites while sparing the rest of the body.[8] This strategy increases the interactions between nanocarriers and the cells, thus enhancing drug internalization, which might reduce the severe adverse effects of the therapy. It would therefore be highly advantageous if the periphery of the arborescent nanocarriers were functionalized with a specific targeting molecule capable of actively binding to an area of interest.

The targeting ligands need to be conjugated to the surface of the nanocarriers for cancer cell targeting via receptor-mediated endocytosis. One targeting compound that received much attention is folic acid, as folate receptors are frequently over-expressed on the surface of human tumors including ovarian, brain, breast, colon, renal and lung cancers.[9] Folate is a stable, non-immunogenic molecule (M = 441 Da), which specifically binds to folate receptors. Therefore it would be interesting to design folate-conjugated arborescent poly(benzyl L-glutamate)-*eg*-poly(ethylene oxide) PBG-*eg*-PEO nanocarriers, to assess how efficiently these systems penetrate tumors both *in vitro* and *in vivo*.

The folate-conjugated PBG-*eg*-PEO nanocarriers could be obtained by coupling the folate to the terminal –OH groups of the PEO corona chains of the nanocarriers using an esterification reaction. Steglich esterification is a widely used method under mild conditions to condense carboxylic acids with alcohols to form esters.[10] The reaction usually utilizes *N,N'*-dicyclohexylcarbodiimide (DCC) as a coupling reagent and 4-dimethylaminopyridine (DMAP) as a catalyst. The primary alcohols present at the end of the PEO chains can be coupled with the carboxylic groups of folic acid, and the resulting folate-conjugated PBG-*g*-PEO can be used to prepare doxorubicin-loaded nanocarriers.

Following this strategy, we expect that doxorubicin will enter the cells mainly via folate receptor-mediated endocytosis, which will enhance the local concentration of doxorubicin surrounding cancer cells and thus increase therapeutic efficacy in cancer therapy.

7.2.3 Synergistic Co-Delivery of Doxorubicin and Paclitaxel

The use of single chemotherapeutic drug has shown some limitations in cancer treatment due to toxicity at high drug dosage, the development of drug resistance, and the heterogeneity of cancer.[11,12] Combination therapy of two or more drugs has been invested to overcome these limitations. Co-delivery is a promising strategy to reduce toxicity and to achieve synergistic effects for cancer therapy.

In recent years, doxorubicin (DOX) and paclitaxel (PTX) have emerged as the most commonly used chemotherapeutic drugs in clinical tests against various solid tumors. They are drugs with distinct solubility characteristics, have different mechanisms of action and non-overlapping toxicities. Therefore, these combinations may exhibit synergistic effects in cancer therapy.[11] Indeed, the combination of DOX and PTX has been used as the first-line treatment for metastatic breast cancer and the clinical studies showed increased tumor regression rates as compared to the individual drugs.[13,14]

In the present research DOX was covalently conjugated to the poly(benzyl L-glutamate)-*eg*-poly(ethylene oxide) PBG-*eg*-PEO unimolecular micelles via a pH-sensitive hydrazone bond (PGA-*eg*-PEO-Hyd-DOX). It would be of great interest if PTX could also be physically encapsulated by PGA-*eg*-PEO-Hyd-DOX to obtain nanocarriers with both doxorubicin and paclitaxel in the nanoparticles (PGA-*eg*-PEO-Hyd-DOX/PTX).

In this way, doxorubicin and paclitaxel combined could improve therapeutic efficacy, and reduce toxicity and frequency of drug administration in tumor therapy.

References

Chapter 1

1. Teertstra, S. J. and Gauthier, M., *Progress in Polymer Science*, **2004**, 29, 277-327.

2. Lukowiak, M. C., Thota, B. N. S. and Haag, R., *Biotechnology Advances*, **2015**, 33, 1327-1341.

3. Gauthier, M. and Moeller, M., *Macromolecules*, **1991**, 24, 4548-4553.

4. Tomalia, D. A., Hedstrand, D. M. and Ferritto, M. S., *Macromolecules*, **1991**, 24, 1435-1438.

5. Njikang, G. N., Gauthier, M. and Li, J., *Polymer*, **2008**, 49, 5474-5481.

6. Njikang, G., Gauthier, M. and Li, J., *Polymer*, **2008**, 49, 1276-1284.

7. Whitton, G. and Gauthier, M., *Journal of Polymer Science Part A: Polymer Chemistry*, **2016**, 54, 1197-1209.

Chapter 2

1. Pérez-Herrero, E. and Fernández-Medarde, A., *European Journal of Pharmaceutics and Biopharmaceutics*, **2015**, 93, 52-79.

2. *World Cancer Report 2014*, [2014]. edn., IARC Press, Lyon, France, 2014.

3. Soni, G. and Yadav, K. S., *Materials Science and Engineering: C*, **2015**, 47, 156-164.

4. Sun, T., Zhang, Y. S., Pang, B., Hyun, D. C., Yang, M. and Xia, Y., *Angewandte Chemie International Edition*, **2014**, 53, 12320-12364.

5. Egusquiaguirre, S. P., Igartua, M., Hernandez, R. M. and Pedraz, J. L., *Clinical & Translational Oncology*, **2012**, 14, 83-93.

6. Maeda, H., Wu, J., Sawa, T., Matsumura, Y. and Hori, K., *Journal of Controlled Release*, **2000**, 65, 271-284.

7. Prabhakar, U., Maeda, H., Jain, R. K., Sevick-Muraca, E. M., Zamboni, W., Farokhzad, O. C., Barry, S. T., Gabizon, A., Grodzinski, P. and Blakey, D. C., *Cancer Research*, **2013**, 73, 2412-2417.

8. Peer, D., Karp, J. M., Hong, S., Farokhzad, O. C., Margalit, R. and Langer, R., *Nature Nanotechnology*, **2007**, 2, 751-760.

9. *AIDS Patient Care*, **1995**, 9, 306.

10. Bourzac, K., *Nature*, **2012**, 491, S58-S60.

11. Barenholz, Y., *Journal of Controlled Release*, **2012**, 160, 117-134.

12. Montero, A. J., Adams, B., Diaz-Montero, C. M. and Glück, S., *Expert Review of Clinical Pharmacology*, **2011**, 4, 329-334.

13. Oerlemans, C., Bult, W., Bos, M., Storm, G., Nijsen, J. F. and Hennink, W. E., *Pharmaceutical Research*, **2010**, 27, 2569-2589.

14. Lao, J., Madani, J., Puertolas, T., Alvarez, M., Hernandez, A., Pazo-Cid, R., Artal, A. and Anton Torres, A., *Journal of Drug Delivery*, **2013**, 12, 456409.

15. Kato, K., Chin, K., Yoshikawa, T., Yamaguchi, K., Tsuji, Y., Esaki, T., Sakai, K., Kimura, M., Hamaguchi, T., Shimada, Y., Matsumura, Y. and Ikeda, R., *Investigational New Drugs*, **2012**, 30, 1621-1627.

16. Hrkach, J., Von Hoff, D., Ali, M. M., Andrianova, E., Auer, J., Campbell, T., De Witt, D., Figa, M., Figueiredo, M., Horhota, A., Low, S., McDonnell, K., Peeke, E., Retnarajan, B., Sabnis, A., Schnipper, E., Song, J. J., Song, Y. H., Summa, J., Tompsett, D., Troiano, G., Van Geen Hoven, T., Wright, J., LoRusso, P., Kantoff, P. W., Bander, N. H., Sweeney, C., Farokhzad, O. C., Langer, R. and Zale, S., *Science Translational Medicine*, **2012**, 4, 128-139.

17. Lee, J. L., Ahn, J. H., Park, S. H., Lim, H. Y., Kwon, J. H., Ahn, S., Song, C., Hong, J. H., Kim, C. S. and Ahn, H., *Investigational New Drugs*, **2012**, 30, 1984-1990.

18. Potera, C., *Genetic Engineering & Biotechnology News*, **2011**, 31, 45-47.

19. Zhao, P. and Astruc, D., *ChemMedChem*, **2012**, 7, 952-972.

20. Kumari, P., Ghosh, B. and Biswas, S., *Journal of Drug Targeting*, **2016**, 24, 179-191.

21. Guo, S. and Huang, L., *Biotechnology Advances*, **2014**, 32, 778-788.

22. Ahmad, Z., Shah, A., Siddiq, M. and Kraatz, H.-B., *RSC Advances*, **2014**, 4, 17028-17038.

23. Movassaghian, S., Merkel, O. M. and Torchilin, V. P., *Wiley Interdisciplinary Reviews: Nanomedicine and Nanobiotechnology*, **2015**, 7, 691-707.

24. Masood, F., *Materials Science and Engineering: C*, **2016**, 60, 569-578.

25. Cabral, H. and Kataoka, K., *Journal of Controlled Release*, **2014**, 190, 465-476.

26. Gulzar, A., Gai, S., Yang, P., Li, C., Ansari, M. B. and Lin, J., *Journal of Materials Chemistry B*, **2015**, 3, 8599-8622.

27. Vauthier, C. and Bouchemal, K., *Pharmaceutical Research*, **2009**, 26, 1025-1058.

28. Li, Y., Maciel, D., Rodrigues, J., Shi, X. and Tomás, H., *Chemical Reviews*, **2015**, 115, 8564-8608.

29. Xu, H., Yao, Q., Cai, C., Gou, J., Zhang, Y., Zhong, H. and Tang, X., *Journal of Controlled Release*, **2015**, 199, 84-97.

30. Li, M., Song, W., Tang, Z., Lv, S., Lin, L., Sun, H., Li, Q., Yang, Y., Hong, H. and Chen, X., *ACS Applied Materials & Interfaces*, **2013**, 5, 1781-1792.

31. Lv, S., Li, M., Tang, Z., Song, W., Sun, H., Liu, H. and Chen, X., *Acta Biomaterialia*, **2013**, 9, 9330-9342.

32. Kataoka, K., Matsumoto, T., Yokoyama, M., Okano, T., Sakurai, Y., Fukushima, S., Okamoto, K. and Kwon, G. S., *Journal of Controlled Release*, **2000**, 64, 143-153.

33. Matsumura, Y., *Japanese Journal of Clinical Oncology*, **2014**, 44, 515-525.

34. Liang, H.-F., Chen, S.-C., Chen, M.-C., Lee, P.-W., Chen, C.-T. and Sung, H.-W., *Bioconjugate Chemistry*, **2006**, 17, 291-299.

35. Cheng, J. and Deming, T. J., *Topics in Current Chemistry*, **2012**, 310, 1-26.

36. Vayaboury, W., Giani, O., Cottet, H., Deratani, A. and Schué, F., *Macromolecular Rapid Communications*, **2004**, 25, 1221-1224.

37. Knop, K., Hoogenboom, R., Fischer, D. and Schubert, U. S., *Angewandte Chemie International Edition*, **2010**, 49, 6288-6308.

38. Yokoyama, M., *Expert Opinion on Drug Delivery*, **2010**, 7, 145-158.

39. Piskin, Kaitian, X., Denkbas, E. B. and Kucukyavuz, Z., *Journal of Biomaterials Science Polymer Edition*, **1995**, 7, 359-373.

40. Zhang, X., Jackson, J. K. and Burt, H. M., *International Journal of Pharmaceutics*, **1996**, 132, 195-206.

41. Lv, Y., Yang, B., Jiang, T., Li, Y. M., He, F. and Zhuo, R. X., *Colloids and surfaces B: Biointerfaces*, **2014**, 115, 253-259.

42. Hamaguchi, T., Kato, K., Yasui, H., Morizane, C., Ikeda, M., Ueno, H., Muro, K., Yamada, Y., Okusaka, T., Shirao, K., Shimada, Y., Nakahama, H. and Matsumura, Y., *British Journal of Cancer*, **2007**, 97, 170-176.

43. Ahn, H. K., Jung, M., Sym, S. J., Shin, D. B., Kang, S. M., Kyung, S. Y., Park, J.-W., Jeong, S. H. and Cho, E. K., *Cancer Chemotherapy and Pharmacology*, **2014**, 74, 277-282.

44. Hamaguchi, T., Doi, T., Eguchi-Nakajima, T., Kato, K., Yamada, Y., Shimada, Y., Fuse, N., Ohtsu, A., Matsumoto, S.-i., Takanashi, M. and Matsumura, Y., *Clinical Cancer Research*, **2010**, 16, 5058-5066.

45. Danson, S., Ferry, D., Alakhov, V., Margison, J., Kerr, D., Jowle, D., Brampton, M., Halbert, G. and Ranson, M., *British Journal of Cancer*, **2004**, 90, 2085-2091.

46. Matsumura, Y., Hamaguchi, T., Ura, T., Muro, K., Yamada, Y., Shimada, Y., Shirao, K., Okusaka, T., Ueno, H., Ikeda, M. and Watanabe, N., *British Journal of Cancer*, **2004**, 91, 1775-1781.

47. Lukowiak, M. C., Thota, B. N. S. and Haag, R., *Biotechnology Advances*, **2015**, 33, 1327-1341.

48. Larson, N. and Ghandehari, H., *Chemistry of Materials*, **2012**, 24, 840-853.

49. Mura, S., Nicolas, J. and Couvreur, P., *Nature Materials*, **2013**, 12, 991-1003.

50. Khandare, J., Calderon, M., Dagia, N. M. and Haag, R., *Chemical Society Reviews*, **2012**, 41, 2824-2848.

51. Madaan, K., Kumar, S., Poonia, N., Lather, V. and Pandita, D., *Journal of Pharmacy & Bioallied Sciences*, **2014**, 6, 139-150.

52. Tomalia, D. A., Christensen, J. B. and Boas, U., *Dendrimers, Dendrons, and Dendritic Polymers*, Cambridge University Press, **2012**.

53. Talelli, M., Barz, M., Rijcken, C. J. F., Kiessling, F., Hennink, W. E. and Lammers, T., *Nano Today*, **2015**, 10, 93-117.

54. Wang, H., Tang, L., Tu, C., Song, Z., Yin, Q., Yin, L., Zhang, Z. and Cheng, J., *Biomacromolecules*, **2013**, 14, 3706-3712.

55. Jiménez-Pardo, I., González-Pastor, R., Lancelot, A., Claveria-Gimeno, R., Velázquez-Campoy, A., Abian, O., Ros, M. B. and Sierra, T., *Macromolecular Bioscience*, **2015**, 15, 1381-1391.

56. Aggarwal, S. L. and Sweeting, O. J., *Chemical Reviews*, **1957**, 57, 665-742.

57. White, J. L., Dharod, K. C. and Clark, E. S., *Journal of Applied Polymer Science*, **1974**, 18, 2539-2568.

58. Vögtle, F., Richardt, G. and Werner, N., in *Dendrimer Chemistry*, Wiley-VCH Verlag GmbH & Co. KGaA, **2009**, pp. 1-24.

59. Gauthier, M., *Journal of Polymer Science Part A: Polymer Chemistry*, **2007**, 45, 3803-3810.

60. Teertstra, S. J. and Gauthier, M., *Progress in Polymer Science*, **2004**, 29, 277-327.

61. Tomalia, D. A., Jørn B. Christensen, and Boas., U., *Dendrimers, Dendrons, and Dendritic Polymers*, Cambridge University Press, **2012**.

62. Gauthier, M., Tichagwa, L., Downey, J. S. and Gao, S., *Macromolecules*, **1996**, 29, 519-527.

63. Jikei, M. and Kakimoto, M.A., *Progress in Polymer Science*, **2001**, 26, 1233-1285.

64. Kim, Y. H., *Journal of Polymer Science Part A: Polymer Chemistry*, **1998**, 36, 1685-1698.

65. Gauthier, M. and Möeller, M., *Macromolecules*, **1991**, 24, 4548-4553.

66. Tomalia, D. A., Hedstrand, D. M. and Ferritto, M. S., *Macromolecules*, **1991**, 24, 1435-1438.

67. Kaminskas, L. M. and Porter, C. J. H., *Advanced Drug Delivery Reviews*, **2011**, 63, 890-900.

68. Paolino, M., Ennen, F., Lamponi, S., Cernescu, M., Voit, B., Cappelli, A., Appelhans, D. and Komber, H., *Macromolecules*, **2013**, 46, 3215-3227.

69. Kannan, R. M., Nance, E., Kannan, S. and Tomalia, D. A., *Journal of Internal Medicine*, **2014**, 276, 579-617.

70. Menjoge, A. R., Kannan, R. M. and Tomalia, D. A., *Drug Discovery Today*, **2010**, 15, 171-185.

71. Wu, W., Wang, W. and Li, J., *Progress in Polymer Science*, **2015**, 46, 55-85.

72. Sowinska, M. and Urbanczyk-Lipkowska, Z., *New Journal of Chemistry*, **2014**, 38, 2168-2203.

73. Wu, L.-p., Ficker, M., Christensen, J. B., Trohopoulos, P. N. and Moghimi, S. M., *Bioconjugate Chemistry*, **2015**, 26, 1198-1211.

74. Kurniasih, I. N., Keilitz, J. and Haag, R., *Chemical Society Reviews*, **2015**, 44, 4145-4164.

75. Kurtoglu, Y. E., Mishra, M. K., Kannan, S. and Kannan, R. M., *International Journal of Pharmaceutics*, **2010**, 384, 189-194.

76. Bhattacharya, P., Geitner, N. K., Sarupria, S. and Ke, P. C., *Physical Chemistry Chemical Physics*, **2013**, 15, 4477-4490.

77. Dong, R., Zhou, Y. and Zhu, X., *Accounts of Chemical Research*, **2014**, 47, 2006-2016.

78. Zheng, Y., Li, S., Weng, Z. and Gao, C., *Chemical Society Reviews*, **2015**, 44, 4091-4130.

79. Svenson, S., *Chemical Society Reviews*, **2015**, 44, 4131-4144.

80. Wang, D., Zhao, T., Zhu, X., Yan, D. and Wang, W., *Chemical Society Reviews*, **2015**, 44, 4023-4071.

81. Bugno, J., Hsu, H.-j. and Hong, S., *Biomaterials Science*, **2015**, 3, 1025-1034.

82. Amir, R. J., Albertazzi, L., Willis, J., Khan, A., Kang, T. and Hawker, C. J., *Angewandte Chemie International Edition*, **2011**, 50, 3425-3429.

83. Hu, Q.-Y., Berti, F. and Adamo, R., *Chemical Society Reviews*, **2016**, 45, 1691-1719.

84. Buhleier, E., Wehner, W. and Vögtle, F., *Synthesis*, **1978**, 2, 155-158.

85. Tomalia, D. A., Baker, H., Dewald, J., Hall, M., Kallos, G., Martin, S., Roeck, J., Ryder, J. and Smith, P., *Polymer Journal*, **1985**, 17, 117-132.

86. Newkome, G. R., Yao, Z., Baker, G. R. and Gupta, V. K., *The Journal of Organic Chemistry*, **1985**, 50, 2003-2004.

87. Hawker, C. J. and Fréchet, J. M. J., *Journal of the American Chemical Society*, **1990**, 112, 7638-7647.

88. Dengiz, C., Breiten, B., Gisselbrecht, J.-P., Boudon, C., Trapp, N., Schweizer, W. B. and Diederich, F., *Journal of Organic Chemistry*, **2015**, 80, 882-896.

89. Walter, M. V. and Malkoch, M., *Chemical Society Reviews*, **2012**, 41, 4593-4609.

90. Wong, C.-H. and Zimmerman, S. C., *Chemical Communications*, **2013**, 49, 1679-1695.

91. Zeng, F. and Zimmerman, S. C., *Journal of the American Chemical Society*, **1996**, 118, 5326-5327.

92. Wu, P., Feldman, A. K., Nugent, A. K., Hawker, C. J., Scheel, A., Voit, B., Pyun, J., Fréchet, J. M. J., Sharpless, K. B. and Fokin, V. V., *Angewandte Chemie International Edition*, **2004**, 43, 3928-3932.

93. Kolb, H. C., Finn, M. G. and Sharpless, K. B., *Angewandte Chemie International Edition*, **2001**, 40, 2004-2021.

94. Gonzaga, F., Sadowski, L. P., Rambarran, T., Grande, J., Adronov, A. and Brook, M. A., *Journal of Polymer Science Part A: Polymer Chemistry*, **2013**, 51, 1272-1277.

95. Lowe, A. B., *Polymer Chemistry*, **2014**, 5, 4820-4870.

96. Montañez, M. I., Campos, L. M., Antoni, P., Hed, Y., Walter, M. V., Krull, B. T., Khan, A., Hult, A., Hawker, C. J. and Malkoch, M., *Macromolecules*, **2010**, 43, 6004-6013.

97. Kottari, N., Chabre, Y. M., Shiao, T. C., Rej, R. and Roy, R., *Chemical Communications*, **2014**, 50, 1983-1985.

98. Sharma, R., Zhang, I., Abbassi, L., Rej, R., Maysinger, D. and Roy, R., *Polymer Chemistry*, **2015**, 6, 1436-1444.

99. Leiro, V., Garcia, J. P., Tomás, H. and Pêgo, A. P., *Bioconjugate Chemistry*, **2015**, 26, 1182-1197.

100. Morgan, M. T., Nakanishi, Y., Kroll, D. J., Griset, A. P., Carnahan, M. A., Wathier, M., Oberlies, N. H., Manikumar, G., Wani, M. C. and Grinstaff, M. W., *Cancer Research*, **2006**, 66, 11913-11921.

101. Majoros, I. J., Williams, C. R., Becker, A. and Baker, J. R., *Wiley Interdisciplinary Reviews: Nanomedicine and Nanobiotechnology*, **2009**, 1, 502-510.

102. Porsch, C., Zhang, Y., Ducani, C., Vilaplana, F., Nordstierna, L., Nyström, A. M. and Malmström, E., *Biomacromolecules*, **2014**, 15, 2235-2245.

103. Khandare, J. J., Jayant, S., Singh, A., Chandna, P., Wang, Y., Vorsa, N. and Minko, T., *Bioconjugate Chemistry*, **2006**, 17, 1464-1472.

104. Flory, P. J., *Journal of the American Chemical Society*, **1952**, 74, 2718–2723.

105. Gunatillake, P. A., Odian, G. and Tomalia, D. A., *Macromolecules*, **1988**, 21, 1556-1562.

106. Hanselmann, R., Hölter, D. and Frey, H., *Macromolecules*, **1998**, 31, 3790-3801.

107. Bharathi, P. and Moore, J. S., *Macromolecules*, **2000**, 33, 3212-3218.

108. Schallausky, F., Erber, M., Komber, H. and Lederer, A., *Macromolecular Chemistry and Physics*, **2008**, 209, 2331-2338.

109. Kim, Y. H. and Webster, O. W., *Journal of the American Chemical Society*, **1990**, 112, 4592-4593.

110. Pérignon, N., Mingotaud, A.-F., Marty, J.-D., Rico-Lattes, I. and Mingotaud, C., *Chemistry of Materials*, **2004**, 16, 4856-4858.

111. Frechet, J. M., Henmi, M., Gitsov, I., Aoshima, S., Leduc, M. R. and Grubbs, R. B., *Science*, **1995**, 269, 1080-1083.

112. Seleci, M., Seleci, D. A., Ciftci, M., Odaci Demirkol, D., Stahl, F., Timur, S., Scheper, T. and Yagci, Y., *Langmuir*, **2015**, 31, 4542-4551.

113. Zhu, L., Tu, C., Zhu, B., Su, Y., Pang, Y., Yan, D., Wu, J. and Zhu, X., *Polymer Chemistry*, **2011**, 2, 1761-1768.

114. Saiyin, W., Wang, D., Li, L., Zhu, L., Liu, B., Sheng, L., Li, Y., Zhu, B., Mao, L., Li, G. and Zhu, X., *Molecular Pharmaceutics*, **2014**, 11, 1662-1675.

115. Zhuang, Y., Su, Y., Peng, Y., Wang, D., Deng, H., Xi, X., Zhu, X. and Lu, Y., *Biomacromolecules*, **2014**, 15, 1408-1418.

116. Gao, C. and Yan, D., *Progress in Polymer Science*, **2004**, 29, 183-275.

117. Hirao, A., Sugiyama, K., Matsuo, A., Tsunoda, Y. and Watanabe, T., *Polymer International*, **2008**, 57, 554-570.

118. Li, J. and Gauthier, M., *Macromolecules*, **2001**, 34, 8918-8924.

119. Yuan, Z. and Gauthier, M., *Macromolecules*, **2005**, 38, 4124-4132.

120. Hempenius, M. A., Michelberger, W. and Möller, M., *Macromolecules*, **1997**, 30, 5602-5605.

121. Kee, R. A. and Gauthier, M., *Macromolecules*, **2002**, 35, 6526-6532.

122. Kee, R. A. and Gauthier, M., *Journal of Polymer Science Part A: Polymer Chemistry*, **2008**, 46, 2335-2346.

123. Whitton, G. and Gauthier, M., *Journal of Polymer Science Part A: Polymer Chemistry*, **2013**, 51, 5270-5279.

124. Whitton, G. and Gauthier, M., *Journal of Polymer Science Part A: Polymer Chemistry*, **2016**, 54, 1197-1209.

125. Alsehli, M. and Gauthier, M., *Materials Research Society Symposium Proceedings*, **2016**, 1819.

126. Njikang, G. N., Gauthier, M. and Li, J., *Polymer*, **2008**, 49, 1276-1284.

127. Njikang, G. N., Gauthier, M. and Li, J., *Polymer*, **2008**, 49, 5474-5481.

128. Huang, C. K., Lo, C. L., Chen, H. H. and Hsiue, G. H., *Advanced Functional Materials*, **2007**, 17, 2291-2297.

129. Gyawali, D., Zhou, S., Tran, R. T., Zhang, Y., Liu, C., Bai, X. and Yang, J., *Advanced Healthcare Materials*, **2014**, 3, 182-186.

130. Chen, G., Wang, L., Cordie, T., Vokoun, C., Eliceiri, K. W. and Gong, S., *Biomaterials*, **2015**, 47, 41-50.

131. Chytil, P., Koziolová, E., Janoušková, O., Kostka, L., Ulbrich, K. and Etrych, T., *Macromolecular Bioscience*, **2015**, 15, 839-850.

132. Six, J.-L. and Gnanou, Y., *Macromolecular Symposia*, **1995**, 95, 137-150.

133. Feng, X., Taton, D., Ibarboure, E., Chaikof, E. L. and Gnanou, Y., *Journal of the American Chemical Society*, **2008**, 130, 11662-11676.

134. Feng, X.-S., Taton, D., Chaikof, E. L. and Gnanou, Y., *Journal of the American Chemical Society*, **2005**, 127, 10956-10966.

135. Gnanou, Y. and Taton, D., *Macromolecular Symposia*, **2001**, 174, 333-341.

136. Feng, X., Pinaud, J., Chaikof, E. L., Taton, D. and Gnanou, Y., *Journal of Polymer Science Part A: Polymer Chemistry*, **2011**, 49, 2839-2849.

137. Libera, M., Formanek, P., Schellkopf, L., Trzebicka, B., Dworak, A. and Stamm, M., *Journal of Polymer Science Part A: Polymer Chemistry*, **2014**, 52, 3488-3497.

138. He, H., Wang, Y., Wen, H. and Jia, X., *RSC Advances*, **2014**, 4, 3643-3652.

139. Cao, W., Zhou, J., Mann, A., Wang, Y. and Zhu, L., *Biomacromolecules*, **2011**, 12, 2697-2707.

140. Puskas, J. E. and Grasmüller, M., *Macromolecular Symposia*, **1998**, 132, 117-126.

141. Puskas, J. E. and Kwon, Y., *Polymers for Advanced Technologies*, **2006**, 17, 615-620.

142. Puskas, J. E. and Hoerr, R. A., *Macromolecular Symposia*, **2010**, 291-292, 326-329.

Chapter 3

1. Tomalia, D. A. and Fréchet, J. M. J., *Journal of Polymer Science Part A: Polymer Chemistry*, **2002**, 40, 2719-2728.

2. Teertstra, S. J. and Gauthier, M., *Progress in Polymer Science*, **2004**, 29, 277-327.

3. Lukowiak, M. C., Thota, B. N. S. and Haag, R., *Biotechnology Advances*, **2015**, 33, 1327-1341.

4. Dong, R., Zhou, Y. and Zhu, X., *Accounts of Chemical Research*, **2014**, 47, 2006-2016.

5. Tomalia, D. A., Jørn B. Christensen, and Boas., U., *Dendrimers, Dendrons, and Dendritic Polymers*, Cambridge University Press, **2012**.

6. Gauthier, M. and Möeller, M., *Macromolecules*, **1991**, 24, 4548-4553.

7. Tomalia, D. A., Hedstrand, D. M. and Ferritto, M. S., *Macromolecules*, **1991**, 24, 1435-1438.

8. Deming, T. J., *Progress in Polymer Science*, **2007**, 32, 858-875.

9. Valeur, E. and Bradley, M., *Chemical Society Reviews*, **2009**, 38, 606-631.

10. El-Faham, A. and Albericio, F., *Chemical Reviews*, **2011**, 111, 6557-6602.

11. Al-Warhi, T. I., Al-Hazimi, H. M. A. and El-Faham, A., *Journal of Saudi Chemical Society*, **2012**, 16, 97-116.

12. Sheehan, J. C. and Hess, G. P., *Journal of the American Chemical Society*, **1955**, 77, 1067-1068.

13. Rebek, J. and Feitler, D., *Journal of the American Chemical Society*, **1974**, 96, 1606-1607.

14. König, W. and Geiger, R., *Chemische Berichte*, **1970**, 103, 788-798.

15. Carpino, L. A., *Journal of the American Chemical Society*, **1993**, 115, 4397-4398.

16. Carpino, L. A. and El-Faham, A., *Tetrahedron*, **1999**, 55, 6813-6830.

17. Whitton, G. and Gauthier, M., *Journal of Polymer Science Part A: Polymer Chemistry*, **2013**, 51, 5270-5279.

18. Poché, D. S., Moore, M. J. and Bowles, J. L., *Synthetic Communications*, **1999**, 29, 843-854.

19. Ji, S., Hoye, T. R. and Macosko, C. W., *Macromolecules*, **2005**, 38, 4679-4686.

20. Leuchs, H., *Berichte der Deutschen Chemischen Gesellschaft*, **1906**, 39, 857-861.

21. Farthing, A. C. and Reynolds, R. J., *Nature*, **1950**, 165, 647.

22. Daly, W. H. and Poché, D., *Tetrahedron Letters*, **1988**, 29, 5859-5862.

23. Kricheldorf, H. R., *Angewandte Chemie International Edition*, **2006**, 45, 5752-5784.

24. Blout, E. R. and Karlson, R. H., *Journal of the American Chemical Society*, **1956**, 78, 941-946.

25. Mitchell, J. C., Woodward, A. E. and Doty, P., *Journal of the American Chemical Society*, **1957**, 79, 3955-3960.

26. Habraken, G. J. M., Wilsens, K. H. R. M., Koning, C. E. and Heise, A., *Polymer Chemistry*, **2011**, 2, 1322-1330.

27. Vayaboury, W., Giani, O., Cottet, H., Deratani, A. and Schué, F., *Macromolecular Rapid Communications*, **2004**, 25, 1221-1224.

28. Habraken, G. J. M., Peeters, M., Dietz, C. H. J. T., Koning, C. E. and Heise, A., *Polymer Chemistry*, **2010**, 1, 514-524.

29. Neises, B. and Steglich, W., *Angewandte Chemie International Edition*, **1978**, 17, 522-524.

Chapter 4

1. Ahmad, Z., Shah, A., Siddiq, M. and Kraatz, H.-B., *RSC Advances*, **2014**, 4, 17028-17038.

2. Gaucher, G., Dufresne, M.-H., Sant, V. P., Kang, N., Maysinger, D. and Leroux, J.-C., *Journal of Controlled Release*, **2005**, 109, 169-188.

3. Kataoka, K., Harada, A. and Nagasaki, Y., *Advanced Drug Delivery Reviews*, **2012**, 64, 37-48.

4. Rösler, A., Vandermeulen, G. W. M. and Klok, H.-A., *Advanced Drug Delivery Reviews*, **2012**, 64, 270-279.

5. Chytil, P., Koziolova, E., Janouskova, O., Kostka, L., Ulbrich, K. and Etrych, T., *Macromolecular Bioscience*, **2015**, 15, 839-850.

6. Gong, J., Chen, M., Zheng, Y., Wang, S. and Wang, Y., *Journal of Controlled Release*, **2012**, 159, 312-323.

7. Khandare, J., Calderon, M., Dagia, N. M. and Haag, R., *Chemical Society Reviews*, **2012**, 41, 2824-2848.

8. Kurniasih, I. N., Keilitz, J. and Haag, R., *Chemical Society Reviews*, **2015**, 44, 4145-4164.

9. Lukowiak, M. C., Thota, B. N. S. and Haag, R., *Biotechnology Advances*, **2015**, 33, 1327-1341.

10. Paolino, M., Ennen, F., Lamponi, S., Cernescu, M., Voit, B., Cappelli, A., Appelhans, D. and Komber, H., *Macromolecules*, **2013**, 46, 3215-3227.

11. Kannan, R. M., Nance, E., Kannan, S. and Tomalia, D. A., *Journal of Internal Medicine*, **2014**, 276, 579-617.

12. Wu, W., Wang, W. and Li, J., *Progress in Polymer Science*, **2015**, 46, 55-85.

13. Sowinska, M. and Urbanczyk-Lipkowska, Z., *New Journal of Chemistry*, **2014**, 38, 2168-2203.

14. Wu, L.-p., Ficker, M., Christensen, J. B., Trohopoulos, P. N. and Moghimi, S. M., *Bioconjugate Chemistry*, **2015**, 26, 1198-1211.

15. Kurtoglu, Y. E., Mishra, M. K., Kannan, S. and Kannan, R. M., *International Journal of Pharmaceutics*, **2010**, 384, 189-194.

16. Tomalia, D. A., Jørn B. Christensen, and Boas., U., *Dendrimers, Dendrons, and Dendritic Polymers*, Cambridge University Press, **2012**.

17. Sun, T., Zhang, Y. S., Pang, B., Hyun, D. C., Yang, M. and Xia, Y., *Angewandte Chemie International Edition*, **2014**, 53, 12320-12364.

18. Svenson, S., *Chemical Society Reviews*, **2015**, 44, 4131-4144.

19. Gauthier, M. and Möeller, M., *Macromolecules*, **1991**, 24, 4548-4553.

20. Tomalia, D. A., Hedstrand, D. M. and Ferritto, M. S., *Macromolecules*, **1991**, 24, 1435-1438.

21. Gauthier, M., *Journal of Polymer Science Part A: Polymer Chemistry*, **2007**, 45, 3803-3810.

22. Njikang, G. N., Gauthier, M. and Li, J., *Polymer*, **2008**, 49, 1276-1284.

23. Njikang, G. N., Gauthier, M. and Li, J., *Polymer*, **2008**, 49, 5474-5481.

24. Whitton, G. and Gauthier, M., *Journal of Polymer Science Part A: Polymer Chemistry*, **2013**, 51, 5270-5279.

25. Whitton, G. and Gauthier, M., *Journal of Polymer Science Part A: Polymer Chemistry*, **2016**, 54, 1197-1209.

26. Abràmoff, M. D., Magalhães, P. J. and Ram, S. J., *Biophotonics International*, **2004**, 11, 36-42.

27. Poché, D. S., Moore, M. J. and Bowles, J. L., *Synthetic Communications*, **1999**, 29, 843-854.

28. Ji, S., Hoye, T. R. and Macosko, C. W., *Macromolecules*, **2005**, 38, 4679-4686.

29. Normant, H. and Angelo, B., *Bulletin de la Societe Chimique de France*, **1960**, 354-359.

30. Chow, E. K.-H. and Ho, D., *Science Translational Medicine*, **2013**, 5, 216rv214-216rv214.

31. Xu, Z., Liu, S., Liu, H., Yang, C., Kang, Y. and Wang, M., *Chemical Communications*, **2015**, 51, 15768-15771.

32. Pouton, C. W., Wagstaff, K. M., Roth, D. M., Moseley, G. W. and Jans, D. A., *Advanced Drug Delivery Reviews*, **2007**, 59, 698-717.

33. Prabaharan, M., Grailer, J. J., Pilla, S., Steeber, D. A. and Gong, S., *Biomaterials*, **2009**, 30, 3009-3019.

34. Bareford, L. M. and Swaan, P. W., *Advanced Drug Delivery Reviews*, **2007**, 59, 748-758.

Chapter 5

1. Chow, E. K.-H. and Ho, D., *Science Translational Medicine*, **2013**, 5, 216rv214-216rv214.

2. Movassaghian, S., Merkel, O. M. and Torchilin, V. P., *Wiley Interdisciplinary Reviews: Nanomedicine and Nanobiotechnology*, **2015**, 7, 691-707.

3. Ahmad, Z., Shah, A., Siddiq, M. and Kraatz, H.-B., *RSC Advances*, **2014**, 4, 17028-17038.

4. Kataoka, K., Harada, A. and Nagasaki, Y., *Advanced Drug Delivery Reviews*, **2001**, 47, 113-131.

5. Kurniasih, I. N., Keilitz, J. and Haag, R., *Chemical Society Reviews*, **2015**, 44, 4145-4164.

6. Kim, J. O., Sahay, G., Kabanov, A. V. and Bronich, T. K., *Biomacromolecules*, **2010**, 11, 919-926.

7. Lee, S. J., Min, K. H., Lee, H. J., Koo, A. N., Rim, H. P., Jeon, B. J., Jeong, S. Y., Heo, J. S. and Lee, S. C., *Biomacromolecules*, **2011**, 12, 1224-1233.

8. Wang, Y. and Grayson, S. M., *Advanced Drug Delivery Reviews*, **2012**, 64, 852-865.

9. Kikuchi, A. and Nose, T., *Macromolecules*, **1996**, 29, 6770-6777.

10. Vögtle, F., Richardt, G. and Werner, N., in *Dendrimer Chemistry*, Wiley-VCH Verlag GmbH & Co. KGaA, **2009**, 1-24.

11. Gauthier, M., *Journal of Polymer Science Part A: Polymer Chemistry*, **2007**, 45, 3803-3810.

12. Teertstra, S. J. and Gauthier, M., *Progress in Polymer Science*, **2004**, 29, 277-327.

13. Tomalia, D. A., Jørn B. Christensen, and Boas., U., *Dendrimers, Dendrons, and Dendritic Polymers*, Cambridge University Press, **2012**.

14. Lukowiak, M. C., Thota, B. N. S. and Haag, R., *Biotechnology Advances*, **2015**, 33, 1327-1341.

15. Gauthier, M., Tichagwa, L., Downey, J. S. and Gao, S., *Macromolecules*, **1996**, 29, 519-527.

16. Gauthier, M. and Möeller, M., *Macromolecules*, **1991**, 24, 4548-4553.

17. Tomalia, D. A., Hedstrand, D. M. and Ferritto, M. S., *Macromolecules*, **1991**, 24, 1435-1438.

18. Whitton, G. and Gauthier, M., *Journal of Polymer Science Part A: Polymer Chemistry*, **2016**, 54, 1197-1209.

19. Abràmoff, M. D., Magalhães, P. J. and Ram, S. J., *Biophotonics international*, **2004**, 11, 36-42.

20. Guo, J., Hong, H., Chen, G., Shi, S., Nayak, T. R., Theuer, C. P., Barnhart, T. E., Cai, W. and Gong, S., *ACS Applied Materials & Interfaces*, **2014**, 6, 21769-21779.

21. Sheiko, S. S., Borisov, O. V., Prokhorova, S. A. and Möller, M., *The European Physical Journal*, **2004**, 13, 125-131.

22. Han, D., Tong, X. and Zhao, Y., *Macromolecules*, **2011**, 44, 5531-5536.

23. Pouton, C. W., Wagstaff, K. M., Roth, D. M., Moseley, G. W. and Jans, D. A., *Advanced Drug Delivery Reviews*, **2007**, 59, 698-717.

24. Prabaharan, M., Grailer, J. J., Pilla, S., Steeber, D. A. and Gong, S., *Biomaterials*, **2009**, 30, 3009-3019.

25. Bareford, L. M. and Swaan, P. W., *Advanced Drug Delivery Reviews*, **2007**, 59, 748-758.

Chapter 6

1. Pérez-Herrero, E. and Fernández-Medarde, A., *European Journal of Pharmaceutics and Biopharmaceutics*, **2015**, 93, 52-79.

2. Laginha, K. M., Verwoert, S., Charrois, G. J. R. and Allen, T. M., *Clinical Cancer Research*, **2005**, 11, 6944-6949.

3. Sun, T., Zhang, Y. S., Pang, B., Hyun, D. C., Yang, M. and Xia, Y., *Angewandte Chemie International Edition*, **2014**, 53, 12320-12364.

4. Maeda, H., Wu, J., Sawa, T., Matsumura, Y. and Hori, K., *Journal of Controlled Release*, **2000**, 65, 271-284.

5. Prabhakar, U., Maeda, H., Jain, R. K., Sevick-Muraca, E. M., Zamboni, W., Farokhzad, O. C., Barry, S. T., Gabizon, A., Grodzinski, P. and Blakey, D. C., *Cancer Research*, **2013**, 73, 2412-2417.

6. Oerlemans, C., Bult, W., Bos, M., Storm, G., Nijsen, J. F. W. and Hennink, W. E., *Pharmaceutical Research*, **2010**, 27, 2569-2589.

7. Torchilin, V. P., *Pharmaceutical Research*, **2007**, 24, 1-16.

8. Yokoyama, M., *Expert Opinion on Drug Delivery*, **2010**, 7, 145-158.

9. Lukowiak, M. C., Thota, B. N. S. and Haag, R., *Biotechnology Advances*, **2015**, 33, 1327-1341.

10. Kurniasih, I. N., Keilitz, J. and Haag, R., *Chemical Society Reviews*, **2015**, 44, 4145-4164.

11. Khandare, J., Calderon, M., Dagia, N. M. and Haag, R., *Chemical Society Reviews*, **2012**, 41, 2824-2848.

12. Xiao, Y., Hong, H., Javadi, A., Engle, J. W., Xu, W., Yang, Y., Zhang, Y., Barnhart, T. E., Cai, W. and Gong, S., *Biomaterials*, **2012**, 33, 3071-3082.

13. Gauthier, M. and Möeller, M., *Macromolecules*, **1991**, 24, 4548-4553.

14. Tomalia, D. A., Hedstrand, D. M. and Ferritto, M. S., *Macromolecules*, **1991**, 24, 1435-1438.

15. Tomalia, D. A., Christensen, J. B. and Boas, U., *Dendrimers, Dendrons, and Dendritic Polymers*, Cambridge University Press, **2012**.

16. Kim, Y. H., *Journal of Polymer Science Part A: Polymer Chemistry*, **1998**, 36, 1685-1698.

17. Njikang, G. N., Gauthier, M. and Li, J., *Polymer*, **2008**, 49, 5474-5481.

18. Njikang, G. N., Gauthier, M. and Li, J., *Polymer*, **2008**, 49, 1276-1284.

19. Whitton, G. and Gauthier, M., *Journal of Polymer Science Part A: Polymer Chemistry*, **2016**, 54, 1197-1209.

20. Teertstra, S. J. and Gauthier, M., *Progress in Polymer Science*, **2004**, 29, 277-327.

21. Xu, H., Yao, Q., Cai, C., Gou, J., Zhang, Y., Zhong, H. and Tang, X., *Journal of Controlled Release*, **2015**, 199, 84-97.

22. Knop, K., Hoogenboom, R., Fischer, D. and Schubert, U. S., *Angewandte Chemie International Edition*, **2010**, 49, 6288-6308.

23. Masood, F., *Materials Science and Engineering: C*, **2016**, 60, 569-578.

24. Osada, K., Christie, R. J. and Kataoka, K., *Journal of the Royal Society Interface*, **2009**, 6, 325-339.

25. Osada, K. and Kataoka, K., in *Peptide Hybrid Polymers*, eds. H.-A. Klok and H. Schlaad, Springer Berlin Heidelberg, Berlin, Heidelberg, **2006**, 113-153.

26. Yilong, C., *Current Pharmaceutical Biotechnology*, **2016**, 17, 212-226.

27. Kakkar, D., Mazzaferro, S., Thevenot, J., Schatz, C., Bhatt, A., Dwarakanath, B. S., Singh, H., Mishra, A. K. and Lecommandoux, S., *Macromolecular Bioscience*, **2015**, 15, 124-137.

28. Kataoka, K., Matsumoto, T., Yokoyama, M., Okano, T., Sakurai, Y., Fukushima, S., Okamoto, K. and Kwon, G. S., *Journal of Controlled Release*, **2000**, 64, 143-153.

29. Li, M., Song, W., Tang, Z., Lv, S., Lin, L., Sun, H., Li, Q., Yang, Y., Hong, H. and Chen, X., *ACS Applied Materials & Interfaces*, **2013**, 5, 1781-1792.

30. Lv, S., Li, M., Tang, Z., Song, W., Sun, H., Liu, H. and Chen, X., *Acta Biomaterialia*, **2013**, 9, 9330-9342.

31. Bae, Y., Nishiyama, N., Fukushima, S., Koyama, H., Yasuhiro, M. and Kataoka, K., *Bioconjugate Chemistry*, **2005**, 16, 122-130.

32. Prabaharan, M., Grailer, J. J., Pilla, S., Steeber, D. A. and Gong, S., *Biomaterials*, **2009**, 30, 5757-5766.

33. Gauthier, M., *Journal of Polymer Science Part A: Polymer Chemistry*, **2007**, 45, 3803-3810.

34. Abràmoff, M. D., Magalhães, P. J. and Ram, S. J., *Biophotonics International*, **2004**, 11, 36-42.

35. Nachbaur, E. and Leiseder, G., *Monatshefte für Chemie*, **1971**, 102, 1718-1723.

36. Bae, Y., Jang, W. D., Nishiyama, N., Fukushima, S. and Kataoka, K., *Molecular Biosystems*, **2005**, 1, 242-250.

37. Yang, X., Grailer, J. J., Rowland, I. J., Javadi, A., Hurley, S. A., Matson, V. Z., Steeber, D. A. and Gong, S., *ACS Nano*, **2010**, 4, 6805-6817.

38. Petros, R. A. and DeSimone, J. M., *Nature Reviews Drug Discovery*, **2010**, 9, 615-627.

39. Sturgeon, R. J. and Schulman, S. G., *Journal of Pharmaceutical Sciences*, **1977**, 66, 958-961.

40. Grodowska, K. and Parczewski, A., *Acta Poloniae Pharmaceutica*, **2010**, 67, 3-12.

41. Fisher, S. and Kunin, R., *Journal of Physical Chemistry*, **1956**, 60, 1030-1032.

42. Mura, S., Nicolas, J. and Couvreur, P., *Nature Materials*, **2013**, 12, 991-1003.

43. Gulzar, A., Gai, S., Yang, P., Li, C., Ansari, M. B. and Lin, J., *Journal of Materials Chemistry B*, **2015**, 3, 8599-8622.

44. Pouton, C. W., Wagstaff, K. M., Roth, D. M., Moseley, G. W. and Jans, D. A., *Advanced Drug Delivery Reviews*, **2007**, 59, 698-717.

45. Prabaharan, M., Grailer, J. J., Pilla, S., Steeber, D. A. and Gong, S., *Biomaterials*, **2009**, 30, 3009-3019.

Chapter 7

1. Albanese, A., Tang, P. S. and Chan, W. C., *Annual Review of Biomedical Engineering*, **2012**, 14, 1-16.

2. Geng, Y., Dalhaimer, P., Cai, S., Tsai, R., Tewari, M., Minko, T. and Discher, D., *Nature Nanotechnology*, **2007**, 2, 249-255.

3. Chithrani, B. D., Ghazani, A. A. and Chan, W. C. W., *Nano Letters*, **2006**, 6, 662-668.

4. Chithrani, B. D. and Chan, W. C. W., *Nano Letters*, **2007**, 7, 1542-1550.

5. Maeda, H., Wu, J., Sawa, T., Matsumura, Y. and Hori, K., *Journal of Controlled Release*, **2000**, 65, 271-284.

6. Prabhakar, U., Maeda, H., Jain, R. K., Sevick-Muraca, E. M., Zamboni, W., Farokhzad, O. C., Barry, S. T., Gabizon, A., Grodzinski, P. and Blakey, D. C., *Cancer Research*, **2013**, 73, 2412-2417.

7. Peer, D., Karp, J. M., Hong, S., Farokhzad, O. C., Margalit, R. and Langer, R., *Nature Nanotechnology*, **2007**, 2, 751-760.

8. Bertrand, N., Wu, J., Xu, X., Kamaly, N. and Farokhzad, O. C., *Advanced Drug Delivery Reviews*, **2014**, 66, 2-25.

9. Hilgenbrink, A. R. and Low, P. S., *Journal of Pharmaceutical Sciences*, **2005**, 94, 2135-2146.

10. Neises, B. and Steglich, W., *Angewandte Chemie International Edition*, **1978**, 17, 522-524.

11. Wang, H., Zhao, Y., Wu, Y., Hu, Y.-l., Nan, K., Nie, G. and Chen, H., *Biomaterials*, **2011**, 32, 8281-8290.

12. Lehar, J., Krueger, A. S., Avery, W., Heilbut, A. M., Johansen, L. M., Price, E. R., Rickles, R. J., Short, G. F., 3rd, Staunton, J. E., Jin, X., Lee, M. S., Zimmermann, G. R. and Borisy, A. A., *Nature Biotechnology*, **2009**, 27, 659-666.

13. Ahmed, F., Pakunlu, R. I., Brannan, A., Bates, F., Minko, T. and Discher, D. E., *Journal of Controlled Release*, **2006**, 116, 150-158.

14. Gustafson, D. L., Merz, A. L. and Long, M. E., *Cancer Letters*, **2005**, 220, 161-169.